The Mechanics of Ship Collisions

Shengming Zhang
January 1999

DTU

The Mechanics of Ship Collisions

by

Shengming Zhang
Department of Naval Architecture
and Offshore Engineering
Technical University of Denmark

January 1999

Preface and Acknowledgements

This thesis is submitted as partial fulfilment of the requirements for the Danish Ph.D. degree. The work was carried out at the Department of Naval Architecture and Offshore Engineering, the Technical University of Denmark from July 1996 to January 1999, under the successful supervision of Professor Preben Terndrup Pedersen.

My sincere thanks to my supervisor, Professor Preben Terndrup Pedersen, for his invaluable guidance and inspiration throughout the study. I also wish to thank my Chinese supervisor, Professor Yousheng Wu, for his kind support.

I am grateful to Professor J. Juncher Jensen for his help and his valuable discussions. Thanks to Dr Bo C. Simonsen and Associate Professor P. Friis Hansen for their valuable discussions. Thanks to Associate Professor Jan Baatrup for assisting with the computers and to the Department Secretaries Marianne and Linda and Technical Assistants Hugo and Peter for their kind help. Great thanks to Mr. M. Birk-Sørensen for his help and to all my colleagues of the Department for their help, kindness and friendliness!

Special thanks to my wife, Ling Wang, for her family support!

Shengming Zhang
January 1999

This page is intentionally left blank.

Abstract

Mathematical models for ship collisions are studied in this thesis. Collision energy losses, collision forces and structural damages are determined. The analysis procedures are divided into two parts: the external dynamics and the internal mechanics. By combining the outer analysis and the inner analysis, a number of examples for full-scale ship collisions are analysed. Finally, a method relating the absorbed energy and the destroyed material volume is developed and verified.

In the external dynamics, analytical methods are developed for the collision energy loss and the impact impulse in arbitrary ship-ship collisions, in ship impacts with floating objects, in ship collisions with rigid walls and in ship collisions with offshore platforms. The involved ships may be any kinds of vessels with no limitations on ship size, impact velocity, impact location or striking angle. Collisions involving glancing blows are also included. The energy loss to be dissipated by destroying the ship structures is given in closed-form expressions. Thus, the calculation of the collision energy is simple and fast and it can be used for probabilistic analyses of ship collisions. A comparison of the present method with reported simulation results shows that good agreement has been achieved.
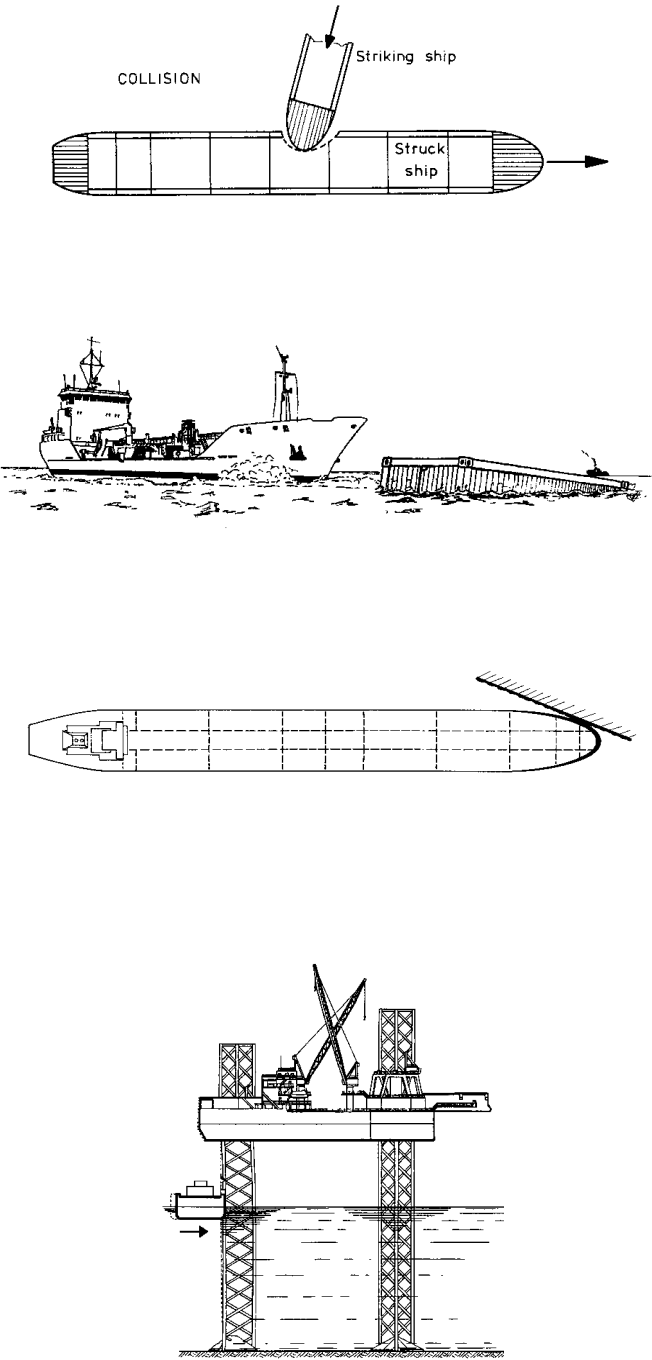
In the internal mechanics, a series of damage analyses for basic structural elements is carried out using upper-bound methods. Large plastic deformation of the shell plating subjected to various loadings is developed. Folding and crushing of frames are studied and analysis of denting and crushing of intersections is performed. Theoretical models for cutting of bare plates are established, where the critical rupture strain enters the solutions for the cutting force and the absorbed energy. Finally, folding and crushing of stiffened decks and bottoms are studied. These basic analysis methods are verified by existing experimental results and numerical solutions.
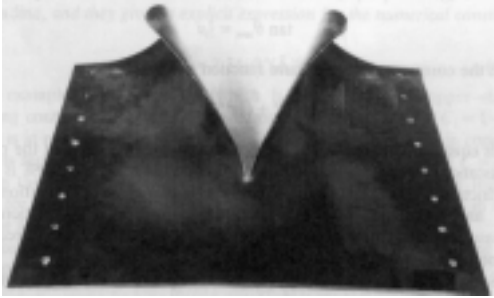
By combining the external and the internal analyses, calculation examples of full-scale ship collisions are carried out. The first example treats the impact strength of high-speed craft colliding with floating objects, and dropped objects impacting plates are studied. The existing minimum thickness requirement of aluminium craft and FRP single-skin craft is converted into critical impact energy or critical object mass. Secondly, collisions where Ro-Ro vessels are struck by other ships are analysed. Conventional and bulbous striking bows are considered. The present calculation results are compared with existing results and it is found that the agreement is acceptable for such complex problem. The third analysis example concerns collisions where unidirectional double-hull tankers are struck by other ships. Comparison with tests shows that the agreement is good. The last example is collision analyses where double-hull oil tankers struck by other ships are presented. It is shown that the double hull tanker has a high capability to prevent oil outflow.

Finally, simple expressions relating the absorbed energy and the destroyed material volume are developed. This approach overcomes a major drawback of Minorsky's well-known method since it takes into account the structural arrangement, the materials properties and the damage modes. The validity of the method is verified against a large number of the existing experimental results and numerical simulations. The procedure is illustrated by analyses of full-scale grounding accidents and bottom raking damage to oil tankers. The proposed method is used to translate grounding damage distribution from conventional vessels to new types of ships such as high-speed vessels and is also used to investigate the effect of ship size on damage distributions in ship grounding and collisions. The results show that a larger ship suffers higher probability of larger relative damage length than that of a smaller ship in grounding but the result for ship collisions is just opposite to the conclusion for ship grounding.

An illustrative summary of the present thesis is presented in the following tables.

Summary of the Research on the Mechanics of Ship Collisions

Illustration of Collision	**Formulation**
1. Outer Mechanics	Collision energy loss:

$$E_\xi = \frac{1}{2} \frac{1}{D_\xi + \mu D_\eta} \dot{\xi}(0)^2$$

$$E_\eta = \frac{1}{2} \frac{1}{K_\xi / \mu + K_\eta} \dot{\eta}(0)^2$$

$$E = \frac{k_{11}}{k_{11} + k_s}(E_0 - E_s - E_p)$$

2. Basic Failure Patterns	Collision Resistance
2.1. Plate tension	
	$$F_1 = 0.385\sigma_0 tA\delta\left(\frac{1}{a_1 a_2} + \frac{1}{b_1 b_2}\right)$$
2.2. Plate cutting	
	$$F_2 = 1.59\sigma_0 t^{1.5} l^{0.5} \varepsilon^{0.25} g(\theta, \mu)$$ $$g(\theta, \mu) = \frac{1}{(\cos\theta)^{0.5}}\left(1 + \frac{1}{2}\frac{\mu}{\tan\theta}\right)$$
2.3. Concertina tearing	
	$$F_3 = 6.77\sigma_0 t^{1.67} b^{0.33}$$
2.4. Plate folding	
	$$F_4 = 4.33\sigma_0 t^{1.67} b^{0.33}$$
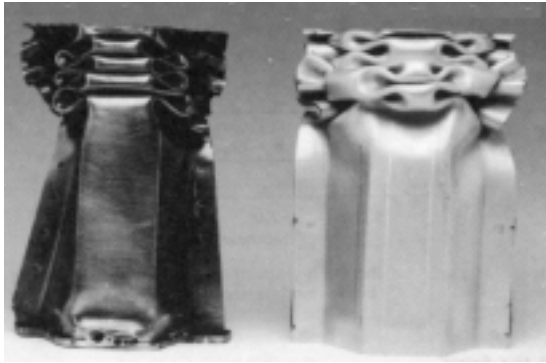
2.5. Axial crushing	
	$$F_5 = n \cdot 3.26\sigma_0 t^{1.67} c^{0.33}$$ $$n = n_L + 1.2 n_T + 2.1 n_X$$
2.6. Intersection denting	
	$$F_6 = 3.29\sigma_0 t^{1.5} c^{0.5} + 4.16\sigma_0 t^2$$
2.7. Deck crushing	
	$$F_7 = n_T \cdot 3.92\sigma_0 t^{1.67} c^{0.33}$$ $$+ 4.33\sigma_0 t_d^{1.67} b^{0.33}$$
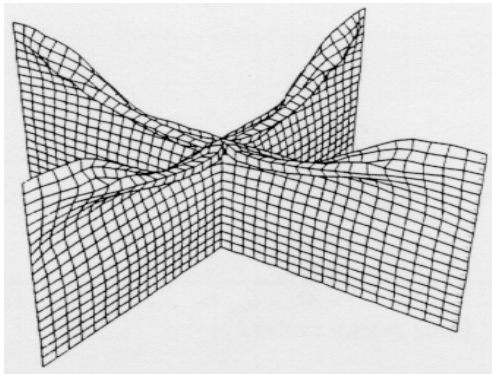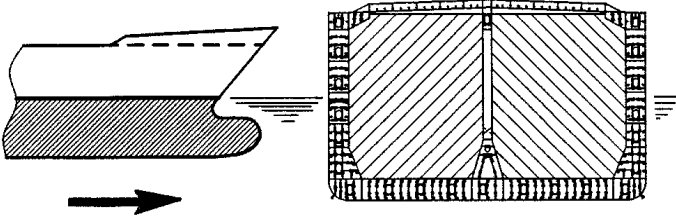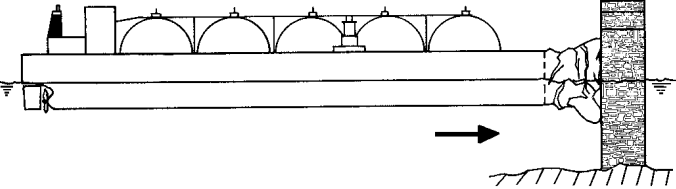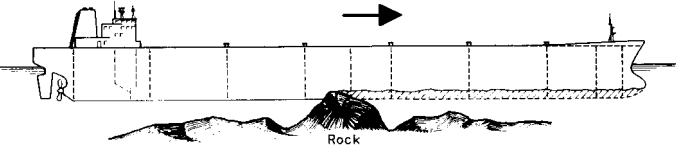
The Revised Minorsky Methods for Damage Prediction in Ship Collisions and Grounding

Damage Case	**Prediction Method**
1. Side collision	$E_1 = 0.77\sigma_0\varepsilon_c R_{T1}$ $+\ 3.50(\dfrac{t}{d})^{0.67}\sigma_0 R_{T2}$
2. Bow crushing	$E_2 = 3.50(\dfrac{t}{d})^{0.67}\sigma_0 R_T$
3. Grounding	$E_3 = 3.21(\dfrac{t}{l})^{0.6}\sigma_0 R_T$

Relationship of Non-dimensional Damage Size between Different Ships in Collisions and Grounding.

Case	Formulation
1. **Grounding:** high-speed craft and conventional ships	$$\frac{(L_{dam}/L)_1}{(L_{dam}/L)_2} = \frac{M_1}{M_2} \cdot (\frac{V_1}{V_2})^2 \cdot \frac{L_2}{L_1} \cdot \frac{F_2}{F_1}$$ $$\frac{F_2}{F_1} = \frac{\sigma_2}{\sigma_1} \cdot \frac{t_{eq2}}{t_{eq1}} \cdot (\frac{t_2}{t_1})^{0.6} \cdot (\frac{T_2}{T_1})^{0.4}$$
2. **Grounding:** different sizes of oil tankers	$$\frac{(L_{dam}/L)_1}{(L_{dam}/L)_2} = (\frac{\sigma_2}{\sigma_1})^{0.2} \cdot (\frac{L_1}{L_2})^{1.133}$$
3. **Side collision:** different sizes of struck ships	$$\frac{(L_{dam}/L)_1}{(L_{dam}/L)_2} = (\frac{\sigma_2}{\sigma_1})^{0.25} \cdot (\frac{L_1}{L_2})^{0.417}$$ $$\cdot (\frac{L_2^{3.33} + 0.6 L_0^{3.33}}{L_1^{3.33} + 0.6 L_0^{3.33}})^{0.5}$$

This page is intentionally left blank.

Dansk Resumé

Matematiske modeller for skibskollisioner undersøges i denne afhandling.

Kollisionsenergitab, kollisionskræfter og konstruktionsskader bestemmes. Analysemetoderne er delt i to: ekstern dynamik og intern mekanik. Ved en kombination af den ydre og den indre analyse undersøges et antal eksempler på skibskollisioner. Til sidst udvikles og efterprøves en metode, som forbinder den absorberede energi og den ødelagte materialemængde.

I den eksterne dynamik udvikles metoder til analyse af kollisionsenergitab og impuls i vilkårlige kollisioner mellem skibe, mellem skibe og flydende genstande, mellem skibe og stive vægge og mellem skibe og boreplatforme. De involverede skibe kan være alle slags skibe uden begrænsninger med hensyn til skibsstørrelse, hastighed, kontaktpunkt eller kontaktvinkel. Kollisioner, som indebærer strejfende kontakter, medtages også. Det energitab, der optages ved ødelæggelsen af skibskonstruktionerne, gives i lukkede udtryk. Således er beregningen af kollisionsenergien enkel og hurtig, og den kan bruges til probabilistiske analyser af skibskollisioner. En sammenligning af nærværende metode med rapporterede simuleringsresultater viser, at en god overensstemmelse er opnået.

I den interne mekanik udføres en række skadeanalyser for basale konstruktionselementer ved hjælp af øvre-grænsemetoder. Der udvikles udtryk for omfattende plastisk deformation af yder-klædningen, som er udsat for forskellige typer af belastninger. Sammenfoldning og knusning af spanterne undersøges. Teoretiske modeller for opskæring af bare plader opstilles, hvor den kritiske brudtøjning indgår i løsningerne for skærekraften og den absorberede energi. Endelig undersøges sammenfoldning og knusning af afstivet dæk og bund. Disse grundlæggende analysemetoder efterprøves mod eksisterende forsøgsresultater og numeriske løsninger.

Ved at kombinere de eksterne og interne analyser udføres beregningseksempler på skibs-kollisioner i naturlig størrelse. Det første eksempel drejer sig om højhastighedsfartøjers slag-styrke i kollision med flydende genstande, og nedkastede genstandes indvirkning på pladerne undersøges. Det eksisterende minimumstykkelseskrav til aluminiumsskibe og FRP enkeltklæd-ningsfartøjer konverteres til kritisk slagenergi og kritisk genstandsmasse. For det andet analyse-res kollisioner, hvor Ro-Ro skibe rammes af andre skibe. Konventionelle og bulbformede stødgivende bove betragtes. Nærværende beregningsresultater sammenlignes med eksisterende resultater, og der viser sig at være tilfredsstillende overensstemmelse for sådan et kompliceret problem. Det tredie analyseeksempel vedrører kollisioner, hvor dobbeltskrogstankskibe rammes af andre skibe. Sammenligning med forsøg viser, at der er god overensstemmelse. Det påvises, at dobbeltskrogstankskibet har en høj evne til at forhindre olieudslip.

Endelig udvikles enkle udtryk, der forbinder den absorberede energi og den ødelagte materialemængde. Denne fremgangsmåde overvinder en stor ulempe ved Minorskys velkendte metode, idet den tager hensyn til konstruktionen, materialeegenskaberne og skademåderne. Metodens gyldighed efterprøves mod et stort antal eksisterende forsøgsresultater og numeriske simuleringer. Fremgangsmåden illustreres ved analyser af grundstødninger i naturlig størrelse og bundskader på olietankskibe. Den foreslåede metode bruges til at overføre fordelingen af grundstødningsskader fra konventionelle skibe til nye skibstyper, som for eksempel højhastig-hedsskibe, og endvidere til at undersøge virkningen af skibsstørrelse på skadedistributionen under grundstødning og kollisioner. Resultaterne viser, at et større skib har øget sandsynlighed for større relativ skadelængde end et mindre skib under grundstødning, men resultatet for skibskollisioner er lige modsat konklusionen for skibsgrundstødninger.

Et illustrerende resumé af nærværende afhandling gives i de følgende tabeller.

Contents

Chapter 5.
Absorbed Energy versus Damaged Material Volume

Chapter 1

Introduction and Objective

1.1   Background and Objective

In this thesis, studies on the mechanics of ship collisions are presented.

In recent years, there has been a growing demand for reducing ocean pollution and vessel losses due to accidents, such as collisions and grounding. Especially, the environmental damage caused by the 'Exxon Valdez' accident forced the USA to make the law of The Oil Pollution Act 1990 (OPA-90). The tragic losses of several Ro-Ro passenger ships: the 'European Gateway' (1982), the 'Herald of Free Enterprise' (1987), and particularly the catastrophe of the 'Estonia' (1994) with the loss of more than 800 lives, led to a reassessment of the safety of passenger ships in many countries.

Fig. 1.1 shows the damage in a collision accident where a 100,000 dwt single hull tanker was struck by a 23,000 dwt container ship in 1992. Heavy side damage was caused by the collision. Consequently, 10,000 t oil was spilt and a fire disaster followed.

Fig. 1.2 shows a grounding accident. In February 1996, the "Sea Empress", a 147,000 dwt tanker, grounded at Millford Haven harbour in UK. About 65,000 tons of crude oil was spilt into the sea.

Collision and grounding contribute significantly to ship structural damage. According to the statistics of Lloyd's Register (1995), ship collisions and grounding are responsible for nearly half of all ship losses. A new study on shuttle tankers (Hu, 1998) shows that collision and grounding accidents are responsible for 70% of all polluting events caused by shuttle tankers. From these statistical results it can be concluded that collisions and grounding are one of the major risks to the safety of ships.

Fig. 1.1. Damage to a 100,000 dwt tanker struck by a 22,600 dwt container ship (1992).

Fig. 1.2. The grounding accident of a 147,000 dwt tanker (1996).

To deal with such a problem, at least three complicated tasks should be studied. The first is to derive procedures for calculation of the probability of ship collisions in a given area, which is complicated by the fact that it must include the human element. The result of such analyses is joint probability distribution for various collision scenarios (Pedersen et al., 1996).

For each collision scenario the subsequent analysis is to determine the collision energy to be dissipated by the destroying of the ship and the resulting structural damage.

The capacity of computers and software has made it possible to treat collision events as integrated formulations, where the equations of motion are solved for the ship structures and the surrounding water by application of general purpose numerical methods like the finite element method. This approach has the potential for producing accurate results but its application is very expensive both in terms of man-power and computer time. An alternative to the integrated formulation is to separate the problem into external dynamics and internal mechanics. The external dynamics describes the rigid body motion of the ships and the collision energy to be dissipated in the structures. The internal mechanics is concerned with the local processes of structural deformation and damage. Apart from reducing the above-mentioned modelling cost, this latter approach also provides better insight into the overall physics of the considered events.

As in case of other impact problems from classical mechanics, the external dynamics can be solved by two different approaches:

- Numerical: Solution of the equations of motion for two ships as an initial value problem.

- Analytical: Consideration of the conservation of momentum.

Due to the requirement of rapid evaluation, the analytical approach is adopted in the present thesis. Minorsky's publication (1959) included the first attempt to divide the collision problem into an internal and an external part. For the external dynamics it was assumed that the struck ship is stationary and the striking ship moves in a nearly perpendicular direction. The loss in energy due to structural plastic deformations is then expressed in a closed form. Although several authors have presented attempts to generalise Minorsky's approach to include arbitrary impact angles, positions and velocities of the two involved ships, there still seems to be a general lack of either accuracy or generality of the published formulas.

Thus, the first objective of this thesis is to develop analytical formulas which express the energy to be dissipated in the involved ships for a given collision. The colliding ships may be any types of ships with no limitations on ship size, impact velocity and striking angle. The developed formulas are compared with results of numerical simulations. Ship-

ship collisions as well as ship collisions with rigid walls, offshore platforms and floating objects are studied as an integral part.

When the collision energy to be absorbed by deformation of the involved ship structures is known, the next step is to determine the resulting damage to the ship structures. A study of observed failure modes reveals that the primary energy absorbing deformation mechanisms to be captured by the internal mechanics model are:

The struck ship:
- Cutting or crushing of horizontal decks and bottom.
- Membrane deformation of shell plating and longitudinal members.
- Failure of transverse frames in a global mode or in a local denting mode.

The striking ship:
- Crushing of longitudinal plate intersections in the bow.

Therefore, the second objective of this thesis is to develop simplified methods for calculating and predicting the damage to the struck ship due to collisions, and it is assumed that the bow of the striking ship is rigid. The emphasis is placed on the struck ship. The simplified method is based on the upper-bound theorem. By combining the external dynamics and the internal mechanics, analysis examples for full-scale ship collisions are performed.

Minorsky's well-known empirical formula, which relates the absorbed energy to the destroyed material volume, has been widely used in analysis of high energy collisions and grounding for nearly 40 years. The advantage of the method is its apparent simplicity. Obviously, its drawback is that the absorbed energy does not depend on the arrangement of the structure, the materials properties, and the damage mode.

Thus, the other purpose of the present thesis is to establish a new simple relation between the absorbed energy and the destroyed material volume, which can be used as a design tool for analysis of ship collisions and grounding. The developed expressions reflect the structural arrangement, the materials properties and the different damage patterns. This method is validated against a large number of existing experimental results and numerical simulation results. It may be considered as an alternative approach to the Minorsky method. This method is used to investigate the effect of ship size on damage distributions in ship grounding and collisions.

1.2   Outline of the Present Thesis

In Chapter 2, an analytical procedure for calculating the collision energy loss and the impact impulse of ship collisions is developed. The analysis is restricted to ship motions in the plane of the water surface. The collision energy for dissipation by structural deformation of the involved structures is given in closed-form expressions. The derived general energy expressions are extended to the cases of ship collision with rigid walls,

ship collision with floating objects and ship impact with flexible offshore platforms. Numerical illustrative examples are presented.

In Chapter 3, the internal mechanics of basic structural damage is presented. The method is based on the upper-bound theorem. It includes plastic deformation of shell plating, folding and crushing of frames, denting and crushing of intersections, cutting of bare plates and crushing of stiffened decks and bottoms. The derived formulas are checked with existing experimental and numerical results.

In Chapter 4, analysis examples of full-scale ship collisions are presented. The examples include high-speed craft impacts with floating objects, Ro-Ro vessel collisions, advanced double hull tanker collisions and oil tanker collisions.

Chapter 5 presents methods relating the absorbed energy and the destroyed material volume. The proposed approaches overcome the major drawback of Minorsky's empirical method. The method can be used as a design tool for analysing ship collisions and grounding. Applications of the method are given.

Chapter 6 gives conclusions.

This page is intentionally left blank.

Chapter 2

External Dynamics of Ship Collisions

2.1   Introduction

The purpose of this chapter is to develop an analytical procedure for calculating the impact impulses and the collision energy to be dissipated by destroying ship structures. The analysis is restricted to ship motions in the plane of the water surface.

In 1982, Petersen studied a procedure for time simulation of the outer dynamics in ship collisions. The hydrodynamic forces acting on the ship's hull during the collision were calculated by a strip theory. The involved ships were treated as essentially stiff bodies with all deformations taking place in the contact area. The structural responses in the contact area were modelled as non-linear springs. Also Woisin (1988) made an external analysis of ship-ship collisions and estimated the loss of kinetic energy. In this case the collision was assumed to be entirely plastic. A similar analysis procedure was developed by Pawlowski (1995) and Hanhirova (1995). Again the ships were supposed to be completely rough, i.e. no sliding was allowed in the contact area.

In the first part of the present chapter, an analytical method for the energy loss and the impact impulse is developed for arbitrary ship-ship collisions. At the start of the calculation, the ships are supposed to have surge motion and sway motion, and the subsequent sliding and rebounding in the plane of the water surface during the collision are analysed. The energy loss for dissipation by structural deformations of the involved structures is expressed in closed-form expressions. The derived general energy expressions are extended to the case of ship collisions with rigid walls and to collision between ships and flexible offshore platforms. The procedure is based on rigid body mechanics, where it is assumed that there is negligible strain energy for deformation outside the contact region and that the contact region is local and small. This implies that the collision can be considered as instantaneous as each body is assumed to exert an impulsive force on the other at the point of contact. The model includes friction between the impacting surfaces so that situations with glancing blows can be identified.

Numerical examples of ship-ship collisions in different impact locations and at different impact angles are performed. Comparison with existing results obtained by simulations in the time domain shows that good agreement is achieved. This agreement with time domain simulation results verifies that the applied rigid body mechanics procedure is sufficiently accurate for analysis of ship-ship collisions. The external mechanics involved in a collision between a supply vessel and a flexible platform is also analysed. The results show that the effect of the flexibility of the platform is significant for the amount of energy released for the crushing of the ship.

2.2   Ship – Ship Collisions

2.2.1   The Analytical Theory

Let us consider a striking ship (A), which sails at a forward speed of V_{ax} and a speed of V_{ay} in the sway direction and collides with a struck ship (B), sailing at a forward speed of V_{b1} and a sway speed of V_{b2}. An XYZ-coordinate system is fixed to the sea bottom. The Z-axis points in a direction out of the water surface, the X-axis lies in the symmetry plane of the striking ship pointing towards the bow, and the origin of the XYZ-system is placed so that the midship section is in the YZ-plane at the moment $t = 0$. The origin of a $\xi \eta$ - system is located at the impact point C, the ξ - direction is normal to the impact surface, the angle between the X-axis and the η -axis is α, and the angle between the X-axis and the 1-axis is β (Fig. 2.1).
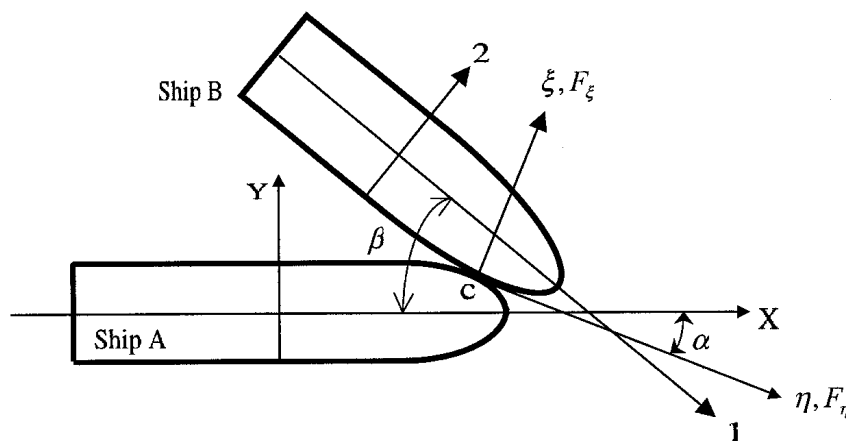
Fig. 2.1. The coordinate system used for analysis of ship-ship collisions.

Motions of the Striking Ship

The equations of motion of the striking ship (A) due to the impact force components F_ξ in the ξ- direction and F_η in the η- direction can be expressed as

$$M_a(1+m_{ax})\dot{v}_{ax} = -F_\xi \sin\alpha - F_\eta \cos\alpha \tag{2.1}$$

$$M_a(1+m_{ay})\dot{v}_{ay} = -F_\xi \cos\alpha + F_\eta \sin\alpha \tag{2.2}$$

$$M_a R_a^2(1+j_a)\dot{\omega}_a = F_\xi[y_c \sin\alpha - (x_c - x_a)\cos\alpha]$$
$$+ F_\eta[y_c \cos\alpha + (x_c - x_a)\sin\alpha] \tag{2.3}$$

Here M_a is the mass of the striking ship, $(\dot{v}_{ax}, \dot{v}_{ay}, \dot{\omega}_a)$ denote the accelerations during the collisions of the striking ship in the X- and Y-directions and the rotation around the centre of gravity, respectively. The radius of the ship mass inertia around the centre of gravity is R_a, the coordinate of the centre of gravity of the striking ship is $(x_a, 0)$, the coordinate of the impact point is (x_c, y_c), the added mass coefficient for the surge motion is m_{ax}, the added mass coefficient for the sway motion is m_{ay} and the added mass coefficient of moment for the rotation around the centre of the gravity is j_a.

From Eqs. (2.1) to (2.3) the accelerations at the centre of gravity of the striking ship are expressed as

$$\dot{v}_{ax} = -\frac{\sin\alpha}{M_a(1+m_{ax})}F_\xi - \frac{\cos\alpha}{M_a(1+m_{ax})}F_\eta$$

$$\dot{v}_{ay} = -\frac{\cos\alpha}{M_a(1+m_{ay})}F_\xi + \frac{\sin\alpha}{M_a(1+m_{ay})}F_\eta$$

$$\dot{\omega}_a = \frac{y_c \sin\alpha - (x_c - x_a)\cos\alpha}{M_a R_a^2(1+j_a)}F_\xi + \frac{y_c \cos\alpha + (x_c - x_a)\sin\alpha}{M_a R_a^2(1+j_a)}F_\eta$$

The acceleration at the impact point C of the striking ship in the ξ-direction can be expressed as

$$\ddot{\xi}_a = (\dot{v}_{ax} - \dot{\omega}_a y_c)\sin\alpha + [\dot{v}_{ay} + \dot{\omega}_a(x_c - x_a)]\cos\alpha$$

$$= -\frac{F_\xi}{M_a}\left\{\frac{1}{1+m_{ax}}\sin^2\alpha + \frac{1}{1+m_{ay}}\cos^2\alpha + \frac{1}{1+j_a}\cdot\frac{[y_c \sin\alpha - (x_c - x_a)\cos\alpha]^2}{R_a^2}\right\}$$

$$-\frac{F_\eta}{M_a}\{[\frac{1}{1+m_{ax}}-\frac{1}{1+m_{ay}}]\sin\alpha\cos\alpha+\frac{1}{1+j_a}\cdot\frac{[y_c\sin\alpha-(x_c-x_a)\cos\alpha][y_c\cos\alpha+(x_c-x_a)\sin\alpha]}{R_a^2}\}$$

Similarly, the acceleration of the striking ship at the impact point C in the $\eta-$ direction can be written as

$$\ddot{\eta}_a=[\dot{v}_{ax}-\dot{\omega}_a\,y_c]\cos\alpha-[\dot{v}_{ay}+\dot{\omega}_a(x_c-x_a)]\sin\alpha$$

$$=-\frac{F_\xi}{M_a}\{[\frac{1}{1+m_{ax}}-\frac{1}{1+m_{ay}}]\sin\alpha\cos\alpha+\frac{1}{1+j_a}\cdot\frac{[y_c\sin\alpha-(x_c-x_a)\cos\alpha][y_c\cos\alpha+(x_c-x_a)\sin\alpha]}{R_a^2}\}$$

$$-\frac{F_\eta}{M_a}\{\frac{1}{1+m_{ax}}\cos^2\alpha+\frac{1}{1+m_{ay}}\sin^2\alpha+\frac{1}{1+j_a}\cdot\frac{[y_c\cos\alpha+(x_c-x_a)\sin\alpha]^2}{R_a^2}\},$$

Motions of the Struck Ship

The motions of the struck ship can be expressed as

$$M_b(1+m_{b1})\dot{v}_{b1}=-F_\xi\sin(\beta-\alpha)+F_\eta\cos(\beta-\alpha) \tag{2.4}$$

$$M_b(1+m_{b2})\dot{v}_{b2}=F_\xi\cos(\beta-\alpha)+F_\eta\sin(\beta-\alpha) \tag{2.5}$$

$$M_bR_b^2(1+j_b)\dot{\omega}_b=-F_\xi[(y_c-y_b)\sin\alpha-(x_c-x_b)\cos\alpha]$$
$$-F_\eta[(y_c-y_b)\cos\alpha+(x_c-x_b)\sin\alpha] \tag{2.6}$$

where the mass of the struck ship is M_b, the radius of inertia of the struck ship around the centre of gravity is R_b, and the coordinate of the centre of gravity of the struck ship is (x_b, y_b). The added mass coefficient for the surge motion is m_{b1}, the added mass coefficient for the sway motion is m_{b2}, the added mass coefficient of moment for the rotation around the centre of gravity is j_b.

From Eqs. (2.4) to (2.6) the accelerations of the struck ship at the impact point C in the ξ-direction and in the $\eta-$ direction are expressed as

$$\ddot{\xi}_b=\dot{v}_{b1}\sin(\beta-\alpha)+\dot{v}_{b2}\cos(\beta-\alpha)-\dot{\omega}_b[(y_c-y_b)\sin\alpha-(x_c-x_b)\cos\alpha]$$

$$=\frac{F_\xi}{M_b}\{\frac{1}{1+m_{b1}}\sin^2(\beta-\alpha)+\frac{1}{1+m_{b2}}\cos^2(\beta-\alpha)+\frac{1}{1+j_b}\cdot\frac{[(y_c-y_b)\sin\alpha-(x_c-x_b)\cos\alpha]^2}{R_b^2}\}$$

$$+\frac{F_\eta}{M_b}\{-\frac{1}{1+m_{b1}}\sin(\beta-\alpha)\cos(\beta-\alpha)+\frac{1}{1+m_{b2}}\sin(\beta-\alpha)\cos(\beta-\alpha)$$

$$+\frac{1}{1+j_b}\cdot\frac{[(y_c-y_b)\sin\alpha-(x_c-x_b)\cos\alpha][(y_c-y_b)\cos\alpha+(x_c-x_b)\sin\alpha]}{R_b^2}\},$$

$$\ddot{\eta}_b=-[\dot{v}_{bx}-\dot{\omega}_b(y_c-y_b)]\cos\alpha+[\dot{v}_{by}+\dot{\omega}_b(x_c-x_b)]\sin\alpha$$

$$=\frac{F_\xi}{M_b}\{-\frac{1}{1+m_{b1}}\sin(\beta-\alpha)\cos(\beta-\alpha)+\frac{1}{1+m_{b2}}\sin(\beta-\alpha)\cos(\beta-\alpha)$$

$$+\frac{1}{1+j_b}\cdot\frac{[(y_c-y_b)\sin\alpha-(x_c-x_b)\cos\alpha][(y_c-y_b)\cos\alpha+(x_c-x_b)\sin\alpha]}{R_b^2}\}$$

$$+\frac{F_\eta}{M_b}\{\frac{1}{1+m_{b1}}\cos^2(\beta-\alpha)+\frac{1}{1+m_{b2}}\sin^2(\beta-\alpha)+\frac{1}{1+j_b}\cdot\frac{((y_c-y_b)\cos\alpha+(x_c-x_b)\sin\alpha)^2}{R_b^2}\},$$

Relative Motions of the Striking Ship and the Struck Ship

The relative accelerations of the striking ship and the struck ship at the impact point C are found to be

$$\ddot{\xi}=\ddot{\xi}_a-\ddot{\xi}_b=-\left[\frac{D_{a\xi}}{M_a}+\frac{D_{b\xi}}{M_b}\right]\cdot F_\xi-\left[\frac{D_{a\eta}}{M_a}+\frac{D_{b\eta}}{M_b}\right]\cdot F_\eta \tag{2.7}$$

$$\ddot{\eta}=\ddot{\eta}_a-\ddot{\eta}_b=-\left[\frac{K_{a\xi}}{M_a}+\frac{K_{b\xi}}{M_b}\right]\cdot F_\xi-\left[\frac{K_{a\eta}}{M_a}+\frac{K_{b\eta}}{M_b}\right]\cdot F_\eta \tag{2.8}$$

where

$$D_{a\xi}=\frac{1}{1+m_{ax}}\sin^2\alpha+\frac{1}{1+m_{ay}}\cos^2\alpha+\frac{1}{1+j_a}\cdot\frac{[y_c\sin\alpha-(x_c-x_a)\cos\alpha]^2}{R_a^2},$$

$$D_{a\eta}=\frac{1}{1+m_{ax}}\sin\alpha\cos\alpha-\frac{1}{1+m_{ay}}\sin\alpha\cos\alpha$$

$$+\frac{1}{1+j_a}\cdot\frac{[y_c\sin\alpha-(x_c-x_a)\cos\alpha][y_c\cos\alpha+(x_c-x_a)\sin\alpha]}{R_a^2},$$

$$D_{b\xi}=\frac{1}{1+m_{b1}}\sin^2(\beta-\alpha)+\frac{1}{1+m_{b2}}\cos^2(\beta-\alpha)+\frac{1}{1+j_b}\cdot\frac{[(y_c-y_b)\sin\alpha-(x_c-x_b)\cos\alpha]^2}{R_b^2},$$

$$D_{b\eta} = -\frac{1}{1+m_{b1}}\sin(\beta-\alpha)\cos(\beta-\alpha) + \frac{1}{1+m_{b2}}\sin(\beta-\alpha)\cos(\beta-\alpha)$$
$$+ \frac{1}{1+j_b} \cdot \frac{[(y_c-y_b)\sin\alpha - (x_c-x_b)\cos\alpha][(y_c-y_b)\cos\alpha + (x_c-x_b)\sin\alpha]}{R_b^2},$$

$$K_{a\xi} = \frac{1}{1+m_{ax}}\sin\alpha\cos\alpha - \frac{1}{1+m_{ay}}\sin\alpha\cos\alpha$$
$$+ \frac{1}{1+j_a} \cdot \frac{[y_c\sin\alpha - (x_c-x_a)\cos\alpha][y_c\cos\alpha + (x_c-x_a)\sin\alpha]}{R_a^2},$$

$$K_{a\eta} = \frac{1}{1+m_{ax}}\cos^2\alpha + \frac{1}{1+m_{ay}}\sin^2\alpha + \frac{1}{1+j_a} \cdot \frac{[y_c\cos\alpha + (x_c-x_a)\sin\alpha]^2}{R_a^2},$$

$$K_{b\xi} = -\frac{1}{1+m_{b1}}\sin(\beta-\alpha)\cos(\beta-\alpha) + \frac{1}{1+m_{b2}}\sin(\beta-\alpha)\cos(\beta-\alpha)$$
$$+ \frac{1}{1+j_b} \cdot \frac{[(y_c-y_b)\sin\alpha - (x_c-x_b)\cos\alpha][(y_c-y_b)\cos\alpha + (x_c-x_b)\sin\alpha]}{R_b^2},$$

$$K_{b\eta} = \frac{1}{1+m_{b1}}\cos^2(\beta-\alpha) + \frac{1}{1+m_{b2}}\sin^2(\beta-\alpha) + \frac{1}{1+j_b} \cdot \frac{[(y_c-y_b)\cos\alpha + (x_c-x_b)\sin\alpha]^2}{R_b^2},$$

The simplified forms for Eqs. (2.7) and (2.8) are as follows:

$$\ddot{\xi} = -D_\xi \cdot F_\xi - D_\eta \cdot F_\eta \tag{2.9}$$

$$\ddot{\eta} = -K_\xi \cdot F_\xi - K_\eta \cdot F_\eta \tag{2.10}$$

where

$$D_\xi = \frac{D_{a\xi}}{M_a} + \frac{D_{b\xi}}{M_b}, \quad D_\eta = \frac{D_{a\eta}}{M_a} + \frac{D_{b\eta}}{M_b}$$

$$K_\xi = \frac{K_{a\xi}}{M_a} + \frac{K_{b\xi}}{M_b}, \quad K_\eta = \frac{K_{a\eta}}{M_a} + \frac{K_{b\eta}}{M_b}$$

Relative Velocities before and after Collisions

To solve Eqs.(2.9) and (2.10), we need to know the relative velocities of the two ships before the collision and after the collision. At the beginning of the collision, $t = 0$, the

relative velocities of the striking ship and the struck ship at impact point C in the ξ – direction and the η – direction can be determined from the initial velocities of the two ships, that is

$$\dot{\xi}(0) = \dot{\xi}_a(0) - \dot{\xi}_b(0) = V_{ax}\sin\alpha + V_{ay}\cos\alpha + V_{b1}\sin(\beta - \alpha) - V_{b2}\cos(\beta - \alpha) \quad (2.11)$$

$$\dot{\eta}(0) = \dot{\eta}_a(0) - \dot{\eta}_b(0) = V_{ax}\cos\alpha - V_{ay}\sin\alpha - V_{b1}\cos(\beta - \alpha) - V_{b2}\sin(\beta - \alpha) \quad (2.12)$$

where V_{ax} is the surge speed of the striking ship (A), V_{ay} is the sway speed of the striking ship, V_{b1} is the surge speed of the struck ship (B), and V_{b2} is the sway speed of the struck ship.

At the end of the collision, $t = T$, we assume that the ships may rebound from each other in the ξ-direction, that is

$$\dot{\xi}(T) = \dot{\xi}_a(T) - \dot{\xi}_b(T) = -e \cdot \dot{\xi}(0) \tag{2.13}$$

Here e $(0 \le e \le 1)$ is the coefficient of restitution. For an entirely plastic collision $e = 0$, and for a perfectly elastic collision $e = 1$. For the case where the two ships are locked together after a collision, the relative velocities can be written as

$$\dot{\xi}(T) = 0$$

$$\dot{\eta}(T) = 0 \tag{2.14}$$

In the following sections we shall discuss the case of glancing blows. That is the two ships slide against each other during a collision.

Determination of the Impact Impulse

By integration of Eqs.(2.9) and (2.10) with respect to time and by use of Eqs.(2.11) to (2.14), the impact impulse in the ξ - direction and in the η - direction can be obtained as

$$I_{\xi 0} = \int_0^T F_\xi \, dt = \frac{K_\eta \, \dot{\xi}(0)(1+e) - D_\eta \, \dot{\eta}(0)}{D_\xi \cdot K_\eta - D_\eta \cdot K_\xi}$$

$$I_{\eta 0} = \int_0^T F_\eta \, dt = \frac{D_\xi \, \dot{\eta}(0) - K_\xi \, \dot{\xi}(0)(1+e)}{D_\xi \cdot K_\eta - D_\eta \cdot K_\xi}$$

Thus, the ratio of the impact impulses is expressed as

$$\mu = \frac{I_{\eta 0}}{I_{\xi 0}} = \frac{D_\xi \dot{\eta}(0) - K_\xi \dot{\xi}(0)(1+e)}{K_\eta \dot{\xi}(0)(1+e) - D_\eta \dot{\eta}(0)} \tag{2.15}$$

If the collision angle is small or very large, the ships may glance against each other. Therefore, it is necessary to consider an impact with friction. The coefficient of friction between the ships is assumed to be μ_0. Then we have

If $|\mu_0| \geq |\mu|$, the two ships stick together. If $|\mu_0| < |\mu|$, the two ships slide against each other.

In order to determine the energy to be dissipated by crushing of the ship structures, we further make the assumption that the ratio between the parallel component F_η of the collision force and the perpendicular component F_ξ is constant during the collision. That is $F_\eta = \mu \cdot F_\xi$. Then Eqs. (2.9) and (2.10) can be reduced to

$$\ddot{\xi} = -(D_\xi + \mu D_\eta) \cdot F_\xi \tag{2.16}$$

$$\ddot{\eta} = -(\frac{1}{\mu} K_\xi + K_\eta) \cdot F_\eta \tag{2.17}$$

Energy Released for Crushing of Ship Structures

Before determining the energy to be dissipated by crushing, we must know the relative velocity $\dot{\eta}(T)$ at the end of the collision for the case of sliding. Integrating Eq. (2.17) (now $\mu = \mu_0$) with respect to time, we get the glancing speed at the end of the collision:

$$\dot{\eta}(T) = \dot{\eta}(0) - \frac{K_\xi + \mu_0 K_\eta}{D_\xi + \mu_0 D_\eta} \cdot \dot{\xi}(0)(1+e) \tag{2.18}$$

By use of the transformations $\ddot{\xi} = \dfrac{d\dot{\xi}}{d\xi}\dfrac{d\xi}{dt} = \dot{\xi}\dfrac{d\dot{\xi}}{d\xi}$ and $\ddot{\eta} = \dfrac{d\dot{\eta}}{d\eta}\dfrac{d\eta}{dt} = \dot{\eta}\dfrac{d\dot{\eta}}{d\eta}$, Eqs. (2.16) and (2.17) become

$$\dot{\xi}\,d\dot{\xi} = -(D_\xi + \mu D_\eta) \cdot F_\xi d\xi \tag{2.19}$$

$$\dot{\eta}\, d\dot{\eta} = -(\frac{1}{\mu}K_\xi + K_\eta) \cdot F_\eta\, d\eta \tag{2.20}$$

Integrating Eqs. (2.19) and (2.20) and using the conditions given above, we obtain the results of the energy released for crushing of ship structures and the impact impulses for the ship sticking case and sliding case.

Sticking case: The energy released in the ξ - direction E_ξ can be expressed as

$$E_\xi = \int_0^{\xi_{max}} F_\xi\, d\xi = \frac{1}{2} \frac{1}{D_\xi + \mu \cdot D_\eta} \dot{\xi}(0)^2 \tag{2.21}$$

The energy released in the η - direction E_η can be expressed as

$$E_\eta = \int_0^{\eta_{max}} F_\eta\, d\eta = \frac{1}{2} \frac{1}{\frac{1}{\mu} \cdot K_\xi + K_\eta} \dot{\eta}(0)^2 \tag{2.22}$$

where ξ_{max} and η_{max} are the penetrations in the ξ - direction and in the η - direction at the end of the collision. The total released energy is the sum of the energy released in the ξ - direction and in the η - direction: $E_{total} = E_\xi + E_\eta$.

The components of the impact impulse in the ξ - direction and in the η - direction can be calculated from

$$I_\xi = \int_0^T F_\xi\, dt = \frac{1}{D_\xi + \mu \cdot D_\eta} \dot{\xi}(0) \tag{2.23}$$

$$I_\eta = \int_0^T F_\eta\, dt = \frac{1}{\frac{1}{\mu} K_\xi + K_\eta} \dot{\eta}(0) \tag{2.24}$$

Sliding case: In this case, the released energy can be expressed as

$$E_\xi = \int_0^{\xi_{max}} F_\xi\, d\xi = \frac{1}{2} \frac{1}{D_\xi + \mu_0 \cdot D_\eta} \dot{\xi}(0)^2 (1 - e^2) \tag{2.25}$$

$$E_\eta = \int_0^{\eta_{max}} F_\eta\, d\eta = \frac{1}{2} \frac{1}{\frac{1}{\mu_0} \cdot K_\xi + K_\eta} (\dot{\eta}(0)^2 - \dot{\eta}(T)^2) \tag{2.26}$$

The components of the impact impulse in the glancing case are

$$I_\xi = \int_0^T F_\xi \, dt = \frac{1}{D_\xi + \mu_0 \cdot D_\eta} \dot{\xi}(0)(1+e) \tag{2.27}$$

$$I_\eta = \int_0^T F_\eta \, dt = \frac{1}{\frac{1}{\mu_0} K_\xi + K_\eta} (\dot{\eta}(0) - \dot{\eta}(T)) \tag{2.28}$$

Velocities at the End of Collisions

At the end of a collision, the two ships still undergo translational and rotational motions. The equations of conservation of momentum for the striking ship are expressed as

$$M_a(1 + m_{ax})(v_{ax} - V_{ax}) = -I_x$$
$$M_a(1 + m_{ay})(v_{ay} - V_{ay}) = -I_y$$
$$M_a R_a^2 (1 + j_a) \cdot \omega_a = -I_x y_c + I_y (x_c - x_a)$$

where I_x and I_y are the components of the impact impulses in the x – direction and the y – direction, respectively.

Similarly, the equations of conservation of momentum for the struck ship can be expressed as

$$M_b(1 + m_{b1})(v_{b1} - V_{b1}) = I_1$$
$$M_b(1 + m_{b2})(v_{b2} - V_{b2}) = I_2$$
$$M_b R_b^2 (1 + j_b) \cdot \omega_b = -I_x(y_c - y_b) + I_y(x_c - x_b)$$

where I_1 and I_2 are the components of the impact impulse in the 1 – direction and the 2 – direction, respectively.

By application of the transformations

$$I_x = I_\xi \sin\alpha + I_\eta \cos\alpha$$
$$I_y = I_\xi \cos\alpha - I_\eta \sin\alpha$$
$$I_1 = I_\xi \sin(\beta - \alpha) - I_\eta \cos(\beta - \alpha)$$
$$I_2 = -I_\xi \cos(\beta - \alpha) - I_\eta \sin(\beta - \alpha)$$

the expressions for the velocities of the striking ship at the end of the collision are found to be

$$v_{ax} = V_{ax} - \frac{I_\xi \sin\alpha + I_\eta \cos\alpha}{M_a(1+m_{ax})}$$

$$v_{ay} = V_{ay} - \frac{I_\xi \cos\alpha - I_\eta \sin\alpha}{M_a(1+m_{ay})}$$ (2.29)

$$\omega_a = -\frac{I_\xi[y_c \cdot \sin\alpha - (x_c - x_a)\cos\alpha] + I_\eta[y_c \cdot \cos\alpha + (x_c - x_a)\sin\alpha]}{M_a R_a^2(1+j_a)}$$

The velocities of the struck ship at the end of the collision are

$$v_{b1} = V_{b1} - \frac{I_\xi \sin(\beta-\alpha) - I_\eta \cos(\beta-\alpha)}{M_b(1+m_{b1})}$$

$$v_{b2} = V_{b2} + \frac{I_\xi \cos(\beta-\alpha) + I_\eta \sin(\beta-\alpha)}{M_b(1+m_{b2})}$$ (2.30)

$$\omega_b = \frac{I_\xi[(y_c - y_b)\sin\alpha - (x_c - x_b)\cos\alpha] + I_\eta[(y_c - y_b)\cos\alpha + (x_c - x_b)\sin\alpha]}{M_b R_b^2(1+j_b)}$$

2.2.2 Verification

Added Mass Coefficients

The added mass coefficients m_{ax}, m_{ay}, j_a and m_{b1}, m_{b2}, j_b, taking into account the interaction effects between the ships and the surrounding water, depend on the hull form of the ships and the impact duration etc. For simplicity, Minorsky (1959) proposed to use a constant value of the added mass coefficients of ships for the sway motion:

$$m_{ay} = 0.4$$

Motora et al. (1978) conducted a series of model tests and a hydrodynamic analysis on the added mass coefficient for the sway motion. They found that the added mass coefficient varies during the collision, the value is in the range of $m_{ay} = 0.4 \sim 1.3$. The longer the duration, the larger the value of the coefficient. However, if the collision duration is very short, the value of $m_{ay} = 0.4$ assumed by Minorsky may be correct. In Petersen and Pedersen (1981), it is shown that the added mass coefficient for the sway motion can be estimated from

$$m_{ay} = \{m(\infty) + k[m(0) - m(\infty)]\}$$

where $m(\infty)$ and $m(0)$ are the threshold values of the added mass coefficient for the sway motion when the frequency of the collision approaches infinity or zero, respectively. The value of the factor k is a function of the duration of the collision and the ship draught.

The added mass coefficient m_{ax} related to the forward motion is small compared with the mass of the ship. It is found to be

$$m_{ax} = 0.02 \quad to \quad 0.07$$

The added mass coefficient for the yaw motion of the ship, j_a, is (Pedersen et al., 1993):

$$j_a = 0.21$$

For simplicity, in the examples of the present calculations, the added mass coefficients are taken to be

$$m_{ax} = m_{b1} = 0.05 \text{ (for the surge motion)}$$
$$m_{ay} = m_{b2} = 0.85 \text{ (for the sway motion)}$$
$$j_a = j_b = 0.21 \text{ (for the yaw motion)}$$

The radius of inertia of the ship can be approximated by the following expression (Pianc, 1984): $R = (0.19C_b + 0.11)L$, where C_b is the block coefficient and L is the ship length. In the examples of the present calculations, the radius of inertia is taken to be a quarter of the ship length: $R_a = L_a / 4$ and $R_b = L_b / 4$.

Comparison with Existing Results

The first example is taken from Petersen (1982) and Hanhirova (1995). The results presented by Petersen were calculated by time simulations and the results obtained by Hanhirova were calculated by an analytical method. The case was a collision between two similar ships. The main dimensions of the ships are given in Table 2.1.

Firstly, we use the same assumption as used by Petersen. That is an entirely plastic collision where the two ships are locked together after the collision. The present calculation results and the existing results are presented in Table 2.2 where d is the impact location measured from the centre of the struck ship. From Table 2.2 it is seen that good agreement is achieved except in case No. 4. We cannot explain the difference in case No. 4, except that the high value given by Petersen for this case does not seem reasonable.

Table 2.1. Main dimensions of the validation ships.

Length	116.0m
Breadth	19.0m
Draught	6.9m
Displacement	10 340t
Radius of the ship inertia	29.0m

Table 2.2. Comparison of results for the energy loss in collisions.

Parameters ($[V] = m/s$)					$E_\xi(MJ)$			$E_\eta(MJ)$		
Case	Va	Vb	$\alpha = \beta$	d	Present	Petersen (1982)	Hanhirova (1995)	Present	Petersen (1982)	Hanhirova (1995)
1	4.5	0	90	0	70.1	69.6	54.4	0.0	0.0	0.0
2	4.5	4.5	90	0	70.1	64.1	54.4	21.4	24.7	41.5
3	4.5	4.5	60	0	35.3	29.8	28.3	0.2	5.2	15.8
4	4.5	4.5	30	0	7.4	71.9	4.0	0.0	49.3	7.2
5	4.5	4.5	120	0	64.9	60.5	41.7	90.4	93.1	115.0
6	4.5	4.5	120	L/3	42.9	49.2	74.1	85.4	90.7	102.0
7	4.5	4.5	120	L/6	60.0	64.9	60.6	92.3	91.6	110.0
8	4.5	4.5	120	-L/3	30.8	26.3	74.1	68.0	86.7	102.0
13	4.5	0	120	0	50.1	54.0	40.9	15.0	9.8	14.0
14	4.5	2.25	120	0	57.5	60.3	42.8	45.1	40.7	51.5
15	4.5	9.5	120	0	81.4	50.7	28.6	245.3	258.0	347.0

Secondly, we consider the ships sliding against each other. The coefficient of friction between the two ships is assumed to be $\mu_0 = 0.6$, and the calculation results are presented in Table 2.3. The results show that when the ships slide against each other, the energy to be dissipated by the crushing structures is decreased in comparison with the case where the ships are locked together.

Table 2.3. Comparison of results obtained by the present method for the energy loss in the cases of ships being locked together or sliding against each other.

Parameters ($[V] = m/s$)					$E_\xi(MJ)$		$E_\eta(MJ)$		$\dot{\eta}(T)(m/s)$	
Case	Va	Vb	$\alpha = \beta$	d	Plastic	$\mu_0 = 0.6$	Plastic	$\mu_0 = 0.6$	Plastic	$\mu_0 = 0.6$
1	4.5	0	90	0	70.1	70.1	0.0	0.0	0.0	0.00
2	4.5	4.5	90	0	70.1	70.1	21.4	21.4	0.0	0.00
3	4.5	4.5	60	0	35.3	35.3	0.2	0.2	0.0	0.00
4	4.5	4.5	30	0	7.4	7.4	0.0	0.0	0.0	0.00
5	4.5	4.5	120	0	64.9	53.6	90.4	84.1	0.0	-3.44
6	4.5	4.5	120	L/3	42.9	28.9	85.4	54.4	0.0	-5.48
7	4.5	4.5	120	L/6	60.0	45.6	92.3	77.8	0.0	-4.34
8	4.5	4.5	120	-L/3	30.8	24.9	68.0	44.2	0.0	-4.76
13	4.5	0	120	0	50.1	50.1	15.0	15.0	0.0	0.00
14	4.5	2.25	120	0	57.5	53.6	45.1	43.9	0.0	-1.19
15	4.5	9.5	120	0	81.4	53.6	245.3	166.6	0.0	-8.44

2.2.3 Calculation Examples

Example 1. Collision between Two Similar Supply Vessels

Two similar supply vessels sailing at the same forward speed of V=4.5 m/s, collide at different impact angles and in different locations. The dimensions of the vessels and the collision situation are presented in Table 2.4. The impact positions along the struck ship and the calculated energy losses are shown in Table 2.5. Fig. 2.2 shows the ratio of the energy loss and the total kinetic energy of the two ships before the collision. The coefficient of friction is assumed to be $\mu_0 = 0.6$.

From the results it is observed that the impact angle and the impact location have significant influence on the energy loss, which is larger if the collision occurs in the forward part of the struck ship. This means that the fore part of a ship is exposed to high risk of damage. It should be noted that this result may partly explains the observed distribution of more damages in the forward part of the ship's hull, see IMO A265A.

Table 2.4. Dimensions of the supply vessel.

Length	82.5 m
Breadth	18.8 m
Draught	7.6 m
Displacement	4000.0 t
Va = Vb	4.5 m/s
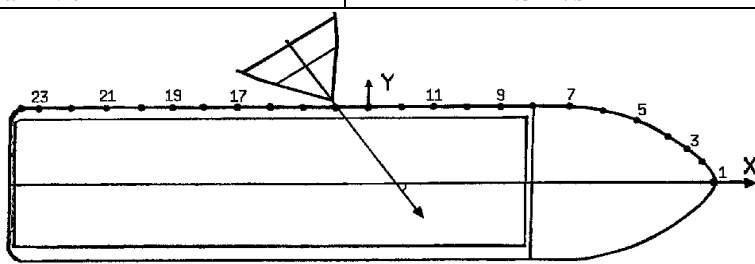
Table 2.5. Energy losses in collisions between two similar supply vessels ($\mu_0 = 0.6$).

Impact point	x_c (m)	y_c (m)	Angle $\alpha°$	Total energy loss (MJ)				
				$\beta = 30°$	$\beta = 60°$	$\beta = 90°$	$\beta = 120°$	$\beta = 150°$
1(bow)	40.0	0.0	90.0	0.98	5.35	15.87	37.82	67.07
2	38.5	2.6	45.0	1.55	6.88	18.10	39.03	69.45
3	36.6	4.1	37.5	1.63	7.26	19.21	41.16	69.77
4	34.6	5.6	32.5	1.71	7.67	20.40	43.43	66.92
5	30.8	7.5	21.7	1.86	8.42	22.51	47.06	50.47
6	27.0	9.0	14.4	2.01	9.20	24.74	50.17	38.82
7	23.1	9.4	7.3	2.16	9.98	26.89	48.92	26.82
8	19.3	9.4	0.0	2.30	10.78	29.09	42.36	16.02
9	15.4	9.4	0.0	2.44	11.61	31.29	46.88	17.14
10	11.6	9.4	0.0	2.56	12.39	33.26	50.58	18.02
11	7.7	9.4	0.0	2.67	13.07	34.80	53.09	18.64
12	3.9	9.4	0.0	2.74	13.53	35.54	53.85	18.88
13	0.0	9.4	0.0	2.76	13.70	35.26	52.79	18.74

14	-3.9	9.4	0.0	2.64	13.51	33.92	50.10	18.21
15	-7.7	9.4	0.0	2.57	12.98	31.79	46.36	17.39
16	-11.6	9.4	0.0	2.56	12.17	29.10	41.91	16.32
17	-15.4	9.4	0.0	2.43	11.22	26.34	37.41	15.14
18	-19.3	9.4	0.0	2.28	10.18	23.62	32.97	13.88
19	-23.1	9.4	0.0	2.12	9.19	21.26	29.00	12.66
20	-27.0	9.4	0.0	1.95	8.24	19.14	25.38	11.46
21	-30.8	9.4	0.0	1.80	7.43	17.38	22.30	10.38
22	-34.6	9.4	0.0	1.65	6.72	15.73	19.63	9.38
23	-38.5	9.4	0.0	1.51	6.09	14.18	17.28	8.46
24(stern)	-40.0	9.4	0.0	1.45	5.88	13.62	16.48	8.14
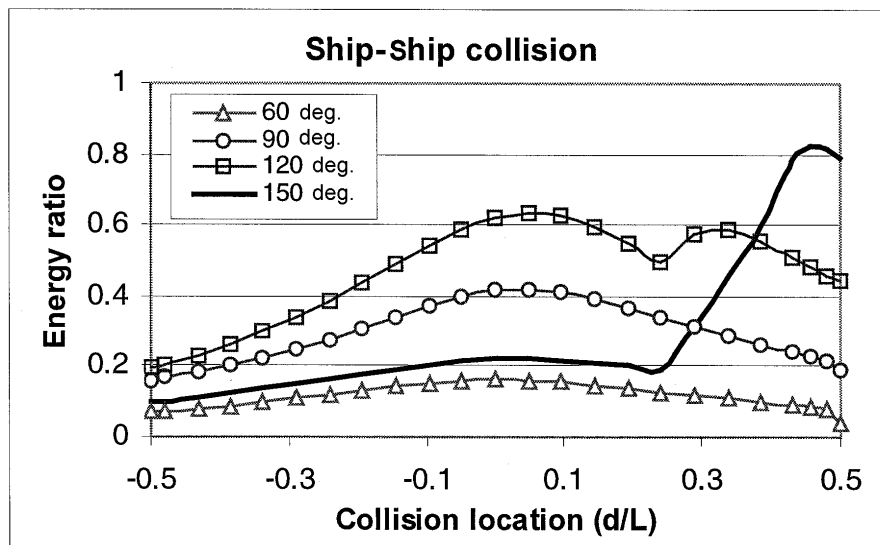
Fig.2.2. Collision of two supply vessels. The energy ratio is defined as the ratio between the energy loss and the total kinetic energy of the two ships before the collision, the collision location is the ratio between the distance d measured from the centre of the struck ship and the struck ship length L, the collision angles are $\beta = 60^0, 90^0, 120^0, 150^0$.

Example 2.   Collision between Two Similar Container Vessels

In this example, we consider two identical container ships sailing at the same forward speed of V = 4.5 m/s and colliding at different impact angles and in different locations. The dimensions of the ships are presented in Table 2.6. The impact position and the calculated results for energy losses are shown in Table 2.7 and also in Fig. 2.3. It is seen that the results are similar to the previous example.

Table 2.6. Main particulars of the container ships.

Length	185.93 m
Breadth	25.91 m
Draught	8.40 m
Displacement	25,205.73 t
Va = Vb	4.50 m/s

Table 2.7. Energy losses in collisions between two container ships ($\mu_0 = 0.6$).

Impact Point	x_c (m)	Deck width (m)	Angle α°	Energy loss (MJ)				
				$\beta = 30^\circ$	$\beta = 60^\circ$	$\beta = 90^\circ$	$\beta = 120^\circ$	$\beta = 150^\circ$
1(bow)	93.0	0.0	90.0	6.20	33.72	100.0	238.4	422.7
2	88.3	8.4	24.4	9.87	43.41	113.4	239.7	268.4
3	83.7	11.7	18.4	10.32	45.51	118.8	239.2	215.3
4	79.0	14.6	15.0	10.79	47.74	124.6	241.2	191.5
5	74.4	16.7	13.9	11.26	49.99	130.5	251.1	190.8
6	65.1	19.2	12.7	12.21	54.76	143.0	275.3	198.4
7	55.8	20.9	10.2	13.20	59.98	156.8	293.9	188.5
8	46.5	24.2	7.7	14.22	65.73	172.7	313.6	176.3
9	37.2	25.9	2.6	15.22	71.53	188.7	305.9	130.7
10	27.9	25.9	0.0	16.11	77.08	203.6	306.4	110.9
11	18.6	25.9	0.0	16.81	81.87	215.7	327.2	115.8
12	9.3	25.9	0.0	17.26	85.18	222.9	337.9	118.4
13	0.0	25.9	0.0	17.42	86.37	223.4	336.5	118.4
14	-9.3	25.9	0.0	17.26	85.09	216.6	323.3	115.8
15	-18.6	25.9	0.0	16.81	81.50	203.8	301.0	111.0
16	-27.9	25.9	0.0	16.11	76.17	187.3	273.2	104.4
17	-37.2	25.9	0.0	15.22	69.89	169.7	243.4	96.8
18	-46.5	25.9	0.0	14.21	63.36	152.8	214.1	88.7
19	-55.8	25.0	355.0	13.20	57.18	138.2	152.7	48.8
20	-65.1	24.2	352.0	12.10	51.63	120.9	114.0	29.3
21	-74.4	22.5	350.0	11.05	46.85	103.7	88.6	18.2
22	-79.0	20.9	350.0	10.56	44.79	97.3	83.0	17.4
23	-83.7	19.2	350.0	10.09	42.86	91.2	77.7	16.5
24	-88.3	16.7	350.0	9.65	41.10	85.8	72.9	15.7
25(stern)	-93.0	15.0	350.0	9.24	39.28	80.5	68.4	15.0
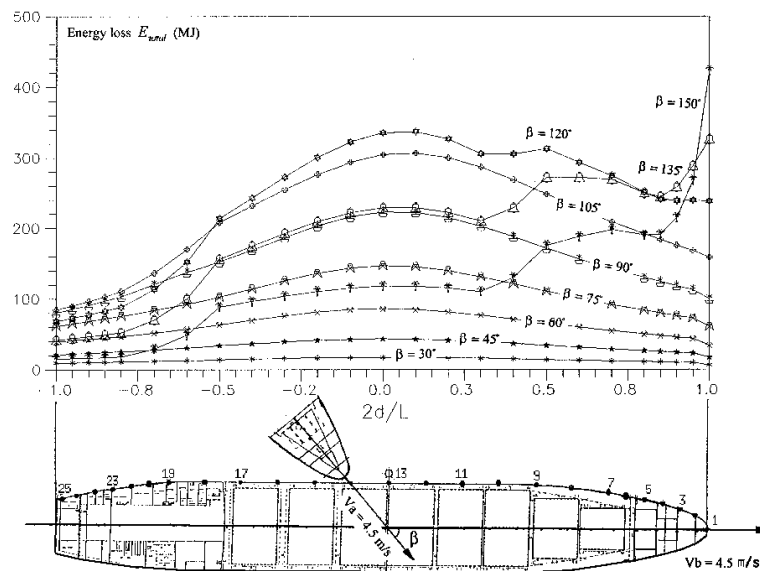
Fig. 2.3. Energy losses in collisions between two similar container ships.

Example 3. Collision between a Ship and a Floating Container

Fig. 2.4 shows a ship which sails at a forward speed of $V = 4.5$ m/s and collides with a floating container. The dimensions of the ship and the container are presented in Table 2.8. The coordinates of the impact point C are (x_c, y_c)=(65.08m, 3.16m) and the impact surface angle is $\alpha = 8°$. The calculation results for the energy loss of the collision are shown in Table 2.9. Two cases are calculated. One is a sticking case and the other is a sliding case. In the sliding case, the friction between the ship and the container is assumed to be $\mu_0 = 0.6$. The results indicate that the energy loss in the sticking case is much higher than in the sliding case. As regards the sliding collision, the floating container slides away after the collision.

Table 2.8. Dimensions of the ship and the floating container.

Parameters	The ship	The container
L (m)	185.93	6.06
B (m)	25.91	2.44
T (m)	8.40	2.59
M (t)	25,205.73	38.27

Fig.2.4. A ship collision with a floating container.

Table 2.9. Energy losses in collisions between the ship and the container.

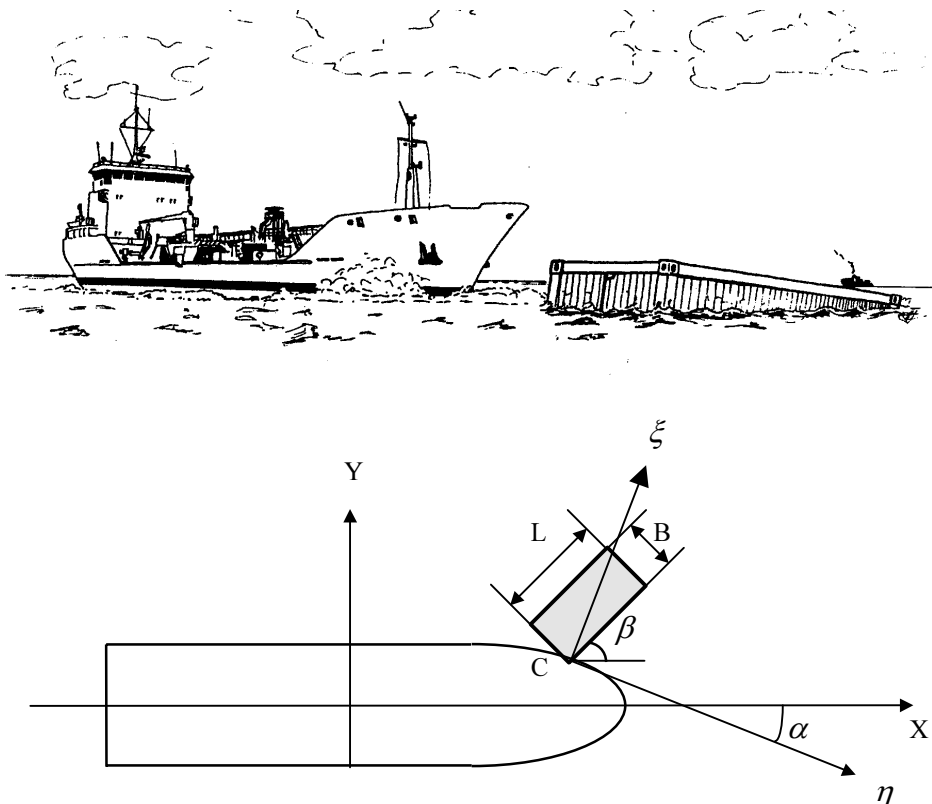| Angle $\beta°$	$E_\xi(kJ)$		$E_\eta(kJ)$		$E_{tot}(kJ)$		$\dot{\eta}(T)(m/s)$	
	Plastic	$\mu_0=0.6$	Plastic	$\mu_0=0.6$	Plastic	$\mu_0=0.6$	Plastic	$\mu_0=0.6$
0	35.80	6.47	511.42	55.36	547.23	61.83	0.0	4.47
10	40.96	8.39	466.26	71.38	507.16	79.77	0.0	4.42
20	41.39	10.98	401.40	91.79	442.79	102.77	0.0	4.27
30	36.72	13.58	328.96	109.81	365.68	123.39	0.0	3.98
40	29.91	14.52	266.55	112.66	294.46	127.18	0.0	3.64
50	16.71	12.92	228.12	97.88	244.83	110.79	0.0	3.45
60	4.56	10.18	220.89	77.28	225.44	87.46	0.0	3.47

Example 4.   Collision between a Ship and a Floating Log

Here we assume that a ship (shown in Table 2.8) sailing at a forward speed of $V = 4.5$ m/s collides with a floating log as shown in Fig. 2.5. The parameters of the floating log are presented in Table 2.10. The coordinate of the impact point is (x_c, y_c)=(65.08, 3.16) and the impact surface angle is $\alpha = 8°$. The calculated results for the energy losses in the collisions are shown in Table 2.11.

The results show that the energy losses in the sliding case are much smaller than in the sticking case. When the impact angle is $\beta = 65°$, the energy loss is maximum in the glancing case. It is also seen that the energy loss (E_ξ) in the direction normal to the impact surface are much smaller than the energy loss (E_η) in the direction parallel to the impact surface. In this example, $E_\eta \approx 8E_\xi$ for the glancing case. The reason is that the angle α of the impact surface is relatively small.

Table 2.10. The dimensions of the floating log.

Length	Diameter	Mass
25.0 m	0.7 m	4.9 t

Table 2.11. Energy losses in collisions between a ship and a floating log.

Angle $\beta°$	$E(kJ)$		$E_\eta(kJ)$		$E_{tot}(kJ)$		$\dot{\eta}(T)(m/s)$	
	Plastic	$\mu_0=0.6$	Plastic	$\mu_0=0.6$	Plastic	$\mu_0=0.6$	Plastic	$\mu_0=0.6$
0	1.08	0.34	56.02	2.90	57.09	3.25	0.0	4.40
10	2.20	0.39	62.00	3.34	64.21	3.74	0.0	4.47
20	3.45	0.47	65.45	4.03	68.90	4.50	0.0	4.52
30	4.41	0.59	63.18	5.07	67.59	5.66	0.0	4.55
40	4.69	0.76	54.40	6.55	59.09	7.31	0.0	4.51
50	4.24	0.99	42.48	8.32	46.73	9.30	0.0	4.36
60	3.35	1.18	31.70	9.65	35.04	10.83	0.0	4.05
70	2.29	1.22	24.14	9.50	26.43	10.72	0.0	3.69
80	1.22	1.05	20.07	8.03	21.29	9.08	0.0	3.49
90	0.20	0.83	19.12	6.29	19.33	7.11	0.0	3.49
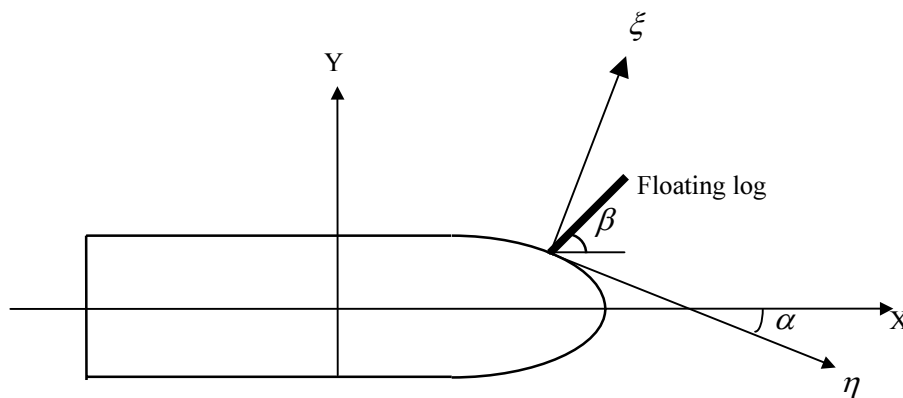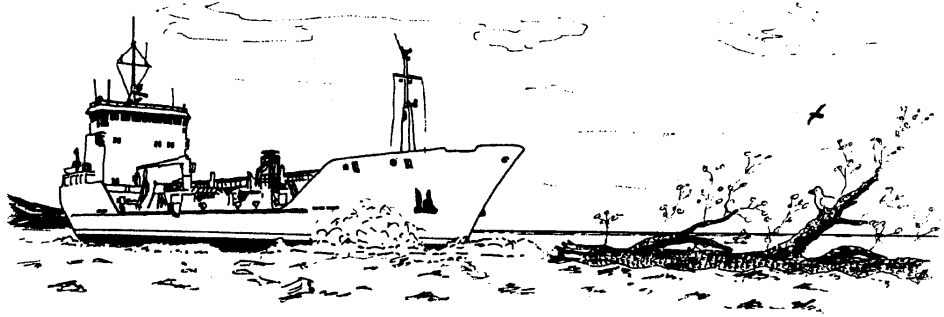
Fig.2.5. A ship collision with a floating log.

2.2.4 Simplified Formulation

When the bow of the striking ship impacts the parallel side of the struck ship directly, the two ships can be simplified as slender beams, as shown in Fig. 2.6. For such collisions, we have the simplified relations:

$$\beta = \alpha$$

$$x_c - x_a = \frac{L_a}{2}$$

$$y_c = 0$$

$$x_c - x_b = d \cdot \cos\alpha - \frac{B}{2} \cdot \sin\alpha$$

$$y_c - y_b = -d \cdot \sin\alpha - \frac{B}{2} \cdot \cos\alpha$$

$$R_a = \frac{L_a}{4}, \qquad R_b = \frac{L_b}{4},$$
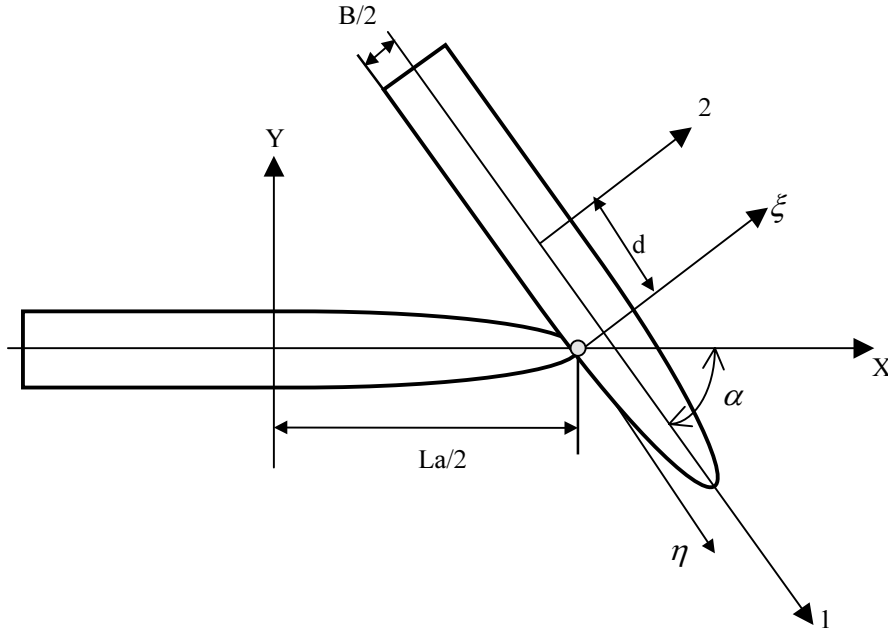
Fig. 2.6. Simplified collision case between two ships.

Therefore, the coefficients $D_{a\xi}$, $D_{a\eta}$, $D_{b\xi}$, D_b , $K_{a\xi}$, $K_{a\eta}$, K_b and $K_{b\eta}$ become

$$D_{a\xi} = \frac{1}{1+m_{ax}}\sin^2\alpha + \frac{1}{1+m_{ay}}\cos^2\alpha + \frac{4}{1+j_a}\cos^2\alpha,$$

$$D_{a\eta} = (\frac{1}{1+m_{ax}} - \frac{1}{1+m_{ay}} - \frac{4}{1+j_a})\sin\alpha\cos\alpha,$$

$$D_{b\xi} = \frac{1}{1+m_{b2}} + \frac{16}{1+j_b}\cdot(\frac{d}{L_b})^2,$$

$$D_{b\eta} = \frac{8}{1+j_b}\cdot(\frac{B\cdot d}{L_b{}^2}),$$

$$K_{a\xi} = (\frac{1}{1+m_{ax}} - \frac{1}{1+m_{ay}} - \frac{4}{1+j_a})\sin\alpha\cos\alpha,$$

$$K_{a\eta} = \frac{1}{1+m_{ax}}\cos^2\alpha + \frac{1}{1+m_{ay}}\sin^2\alpha + \frac{4}{1+j_a}\sin^2\alpha,$$

$$K_{b\xi} = \frac{8}{1+j_b}\cdot(\frac{B\cdot d}{L_b{}^2}),$$

$$K_{b\eta} = \frac{1}{1+m_{b1}} + \frac{4}{1+j_b}\cdot(\frac{B}{L_b})^2,$$

The energy losses in the sticking case are then simplified as

$$E_\xi = \frac{1}{2} \frac{\dfrac{M_a}{D_a}}{1 + \dfrac{M_a}{D_a} \cdot \dfrac{D_b}{M_b}} \dot{\xi}(0)^2 \tag{2.31}$$

$$E_\eta = \frac{1}{2} \frac{\dfrac{M_a}{K_a}}{1 + \dfrac{M_a}{K_a} \cdot \dfrac{K_b}{M_b}} \dot{\eta}(0)^2 \tag{2.32}$$

The related impact impulses are expressed as

$$I_\xi = \int_0^{T_1} F_\xi \, dt = \frac{\dfrac{M_a}{D_a}}{1 + \dfrac{M_a}{D_a} \cdot \dfrac{D_b}{M_b}} \dot{\xi}(0) \tag{2.33}$$

$$I_\eta = \int_0^{T_2} F_\eta \, dt = \frac{\dfrac{M_a}{K_a}}{1 + \dfrac{M_a}{K_a} \cdot \dfrac{K_b}{M_b}} \dot{\eta}(0) \tag{2.34}$$

where

$$D_a = \frac{1}{1 + m_{ax}} (\sin\alpha + \mu \cdot \cos\alpha) \sin\alpha + \left(\frac{1}{1 + m_{ay}} + \frac{4}{1 + j_a}\right)(\cos\alpha - \mu \cdot \sin\alpha) \cos\alpha,$$

$$D_b = \frac{1}{1 + m_{b2}} + \frac{16}{1 + j_b} \cdot \left(\frac{d}{L_b}\right)^2 + \mu \cdot \frac{8}{1 + j_b} \cdot \left(\frac{B \cdot d}{L_b^2}\right),$$

$$K_a = \frac{1}{1 + m_{ax}} (\cos\alpha + \frac{1}{\mu} \cdot \sin\alpha) \cos\alpha + \left(\frac{1}{1 + m_{ay}} + \frac{4}{1 + j_a}\right)(\sin\alpha - \frac{1}{\mu} \cdot \cos\alpha) \sin\alpha,$$

$$K_b = \frac{1}{1 + m_{b1}} + \frac{4}{1 + j_b} \cdot \left(\frac{B}{L_b}\right)^2 + \frac{1}{\mu} \cdot \frac{8}{1 + j_b} \cdot \left(\frac{B \cdot d}{L_b^2}\right),$$

$$\mu = \frac{D_\xi \dot{\eta}(0) - K_\xi \dot{\xi}(0)(1 + e)}{K_\eta \dot{\xi}(0)(1 + e) - D_\eta \dot{\eta}(0)}$$

2.3 Ship Collision with a Rigid Wall

When a ship collides with a rigid wall, the rigid wall can be treated as a fixed object, that is the mass $M_b \to \infty$. The analysis procedure is similar to the case of ship-ship collisions. Here we only list the related formulas.
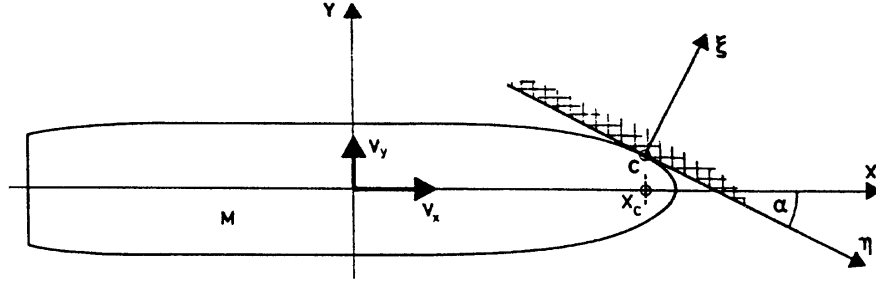
Fig. 2.7. Ship collision with a rigid wall.

2.3.1 The Formulation

Sticking case ($|\mu_0| \geq |\mu|$), the energy loss can be expressed as

$$E_\xi = \int_0^{\xi_{max}} F_\xi d\xi = \frac{1}{2} \cdot \frac{M_a}{D_{a\xi} + \mu \cdot D_{a\eta}} \dot{\xi}(0)^2 \tag{2.35}$$

$$E_\eta = \int_0^{\eta_{max}} F_\eta d\eta = \frac{1}{2} \cdot \frac{M_a}{\frac{1}{\mu} K_{a\xi} + K_{a\eta}} \dot{\eta}(0)^2 \tag{2.36}$$

and the impact impulse is

$$I_\xi = \int_0^T F_\xi dt = \frac{M_a}{D_{a\xi} + \mu \cdot D_{a\eta}} \cdot \dot{\xi}(0) \tag{2.37}$$

$$I_\eta = \int_0^T F_\eta dt = \frac{M_a}{\frac{1}{\mu} D_{a\xi} + D_{a\eta}} \dot{\xi}(0) \tag{2.38}$$

where

$$\dot{\xi}(0) = V_{ax} \sin\alpha + V_{ay} \cos\alpha$$

$$\dot{\eta}(0) = V_{ax} \cos\alpha - V_{ay} \sin\alpha$$

$$\dot{\xi}(T) = -e \cdot \dot{\xi}(0)$$

$$\dot{\eta}(T) = \dot{\eta}(0) - \frac{K_{a\xi} + \mu_0 \cdot K_{a\eta}}{D_{a\xi} + \mu_0 \cdot D_{a\eta}} \cdot \dot{\xi}(0)(1 + e)$$

V_{ax} and V_{ay} are the surge velocity and the sway velocity of the ship

$$\mu = \frac{D_{a\xi}\,\dot{\eta}(0) - K_{a\xi}\,\dot{\xi}(0)(1+e)}{K_{a\eta}\,\dot{\xi}(0)(1+e) - D_{a\eta}\,\dot{\eta}(0)}$$

Sliding case ($|\mu_0| < |\mu|$), the energy loss can be expressed as

$$E_\xi = \int_0^{\xi_{max}} F_\xi d\xi = \frac{1}{2} \cdot \frac{M_a}{D_{a\xi} + \mu_0 \cdot D_{a\eta}} \cdot \dot{\xi}(0)^2(1+e^2) \tag{2.39}$$

$$E_\eta = \int_0^{\eta_{max}} F_\eta d\eta = \frac{1}{2} \cdot \frac{M_a}{\dfrac{1}{\mu_0} K_{a\xi} + K_{a\eta}} \cdot \dot{\eta}(0)^2(1+e^2) \tag{2.40}$$

and the impact impulse is

$$I_\xi = \int_0^T F_\xi dt = \frac{M_a}{D_{a\xi} + \mu_0 \cdot D_{a\eta}} \cdot \dot{\xi}(0)(1+e) \tag{2.41}$$

$$I_\eta = \int_0^T F_\eta dt = \frac{M_a}{\dfrac{1}{\mu_0} D_{a\xi} + D_{a\eta}} \cdot \dot{\xi}(0)(1+e) \tag{2.42}$$

Ship Velocities at the End of the Collision

The velocities of the colliding ship at the end of the collision can be calculated from

$$v_{ax} = V_{ax} - \frac{I_\xi \sin\alpha + I_\eta \cos\alpha}{M_a(1+m_{ax})}$$

$$v_{ay} = V_{ay} - \frac{I_\xi \cos\alpha - I_\eta \sin\alpha}{M_a(1+m_{ay})} \tag{2.43}$$

$$\omega_a = -\frac{I_\xi[y_c \cdot \sin\alpha - (x_c - x_a)\cos\alpha] + I_\eta[y_c \cdot \cos\alpha + (x_c - x_a)\sin\alpha]}{M_a R_a^2(1+j_a)}$$

2.3.2   Calculation Examples

A Slender Rod Impacting a Surface

Here we consider an example from Brach (1993) using a slender rod (free in air) impacting a surface. The problem is illustrated in Fig. 2.8. The physical parameters are presented in Table 2.12. A comparison of the present results with Brach's results is given in Table 2.13. In the example, the initial velocity of the rod in the normal direction of the surface is $\dot{\xi}(0) = 1.0$ m/s. The initial rotational velocity of the rod is zero and the initial velocities in the direction parallel to the surface are $\dot{\eta}(0) = 0.0$ m/s, -0.2 m/s, -0.6m/s, and 1.0 m/s, respectively. The coefficients of restitution are $e = 0.5$ and 0.05, respectively.

The comparison shows that the present results and Brach's results agree quite well.

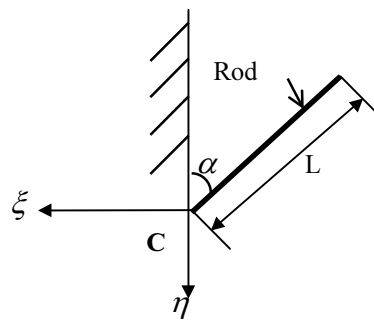*Fig. 2.8. Diagram of a slender rod striking a massive plane at the point C.*

Table 2.12. Physical parameters of the slender rod.

Mass	M=1.0 kg
Length (m)	L=1.0 m
Moment of inertia	$I = \dfrac{1}{12}ML^2$
Impact angle $\alpha°$	45 deg.
Initial velocities (m/s)	$\dot{\xi}(0) = 1.0, \quad \omega(0) = 0;$ $\dot{\eta}(0) = -0.2, \ -0.6, \ 0, \ 1.0$

Table 2.13. Comparison of the present results with Brach's results.

Initial velocity $\dot{\eta}(0)$	Coefficient of restitution $e = -\dfrac{\dot{\xi}(T)}{\dot{\xi}(0)}$	Impulse ratio μ	Normal impulse I_ξ (Nm)		$\dfrac{Energy\ loss}{Initial\ energy} \cdot 100\%$	
			Present	Brach	Present	Brach
0.0	$e = 0.5$	0.600#	0.938	0.938	46.9	46.9
	$e = 0.05$	0.600#	0.656	0.656	62.3	62.3
-0.2	$e = 0.5$	0.507#	0.862	0.862	33.1	33.3
	$e = 0.05$	0.462#	0.581	0.580	47.9	47.9
-0.6	$e = 0.5$	0.263#	0.712	0.732	17.9	17.9
	$e = 0.05$	0.043#	0.431	0.569	29.3	29.3
1.0	$e = 0.5$	0.905#	1.313	1.395	92.2	92.1
	$e = 0.05$	0.988#	1.031	1.031	99.9	99.6

Critical value which just causes the glancing to stop.

Example 1. A Ro-Ro Ship Collision with a Rigid Wall

Ship damage is often caused by accidents during berthing of the vessel. Furthermore, the design of fender systems, harbour quays and bridge piers must be based on the statistical distribution of the impact momentum and the energy associated with ship impacts. Therefore, let us consider an incident where a Ro-Ro ship approaches a rigid wall at a forward speed of 2.78 m/s. The main dimensions of the Ro-Ro ship are shown in Table 2.14. The coefficients of friction between the ship and the rigid wall are assumed to be $\mu_0 = 0.3$ and $\mu_0 = 0.6$, respectively. The calculated results for the energy loss are presented in Table 2.15. Fig. 2.9 shows the ratio between the total energy loss and the total kinetic energy for the ship before the collision. The results show that the larger the friction, the more energy will be lost to crushing of the ship structure. When the collision angle is smaller than $50°$ ($\mu_0 = 0.6$), the ship will slide against the wall. When the collision angle is greater than $50°$ ($\mu_0 = 0.6$), the kinetic energy of the ship will be lost. On the other hand, if the collision angle is smaller than $30°$, only a relatively small amount of the total kinetic energy will be lost.

Table 2.14. Main dimensions of the RoRo ship.

Length	157.0 m
Breadth	24.6 m
Draught	7.25 m
Displacement	16,224 t

Table 2.15. The results of the Ro-Ro ship collision with a wall (V=2.78 m/s).

| Angle $\alpha°$	E_ξ (MJ)		E_η (MJ)		E_{total} (MJ)		$\dot{\eta}(T)$ (m/s)	
	$\mu_0 = 0.3$	$\mu_0 = 0.6$	$\mu_0 = 0.3$	$\mu_0 = 0.6$	$\mu_0 = 0.3$	$\mu_0 = 0.6$	$\mu_0 = 0.3$	$\mu_0 = 0.6$
10	0.52	0.54	1.77	3.67	2.29	4.21	2.76	2.72
20	2.25	2.46	3.82	8.20	6.07	10.66	2.77	2.67
30	5.65	6.55	6.34	14.05	11.99	20.60	2.79	2.56
40	11.55	14.33	9.49	21.19	21.05	35.51	2.76	2.27
50	21.24	28.34	13.06	26.45	34.30	54.79	2.58	1.53
60	36.03	49.37	15.17	15.46	51.20	64.83	1.99	0.0
70	54.66	58.13	10.00	7.07	64.66	65.83	0.64	0.0
80	63.84	63.84	1.98	1.98	65.83	65.83	0.0	0.0
90	65.83	65.83	0.00	0.00	65.83	65.83	0.0	0.0
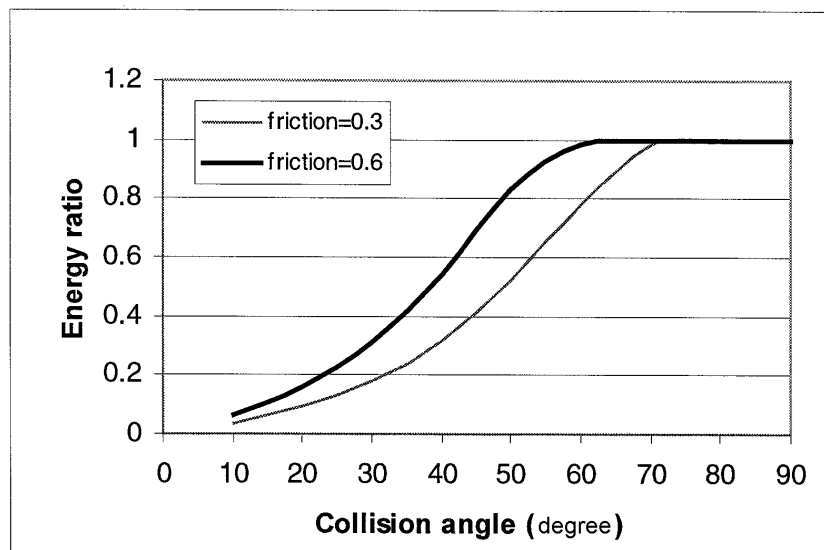
Fig.2.9. The energy ratio of a Ro-Ro vessel colliding with a rigid wall at different collision angles.

Example 2.   A Ship Drifting to a Bridge Pier

Bridges are exposed to the risk of collision with passing ships. Here we consider a ship drifting to a typical bridge pier which is treated as a rigid object. The ship is assumed to drift against the bridge pier at an initial velocity of v = 2 m/s in the direction normal to the impact surface. The principal particulars of the ship are presented in Table 2.6 and the sectional data of the ship is shown in Table 2.16. The calculated results for the energy loss vs. various impact locations are presented in Table 2.17. Fig. 2.10 shows the ratio between the energy loss and the initial kinetic energy of the ship.

The result shows that when the ship drifts against the bridge pier from its centre, the initial kinetic energy of the ship is totally lost. On the other hand, if the ship drifts to the bridge pier from the aft or fore parts of the ship, only about 20%~30% of the initial kinetic energy is lost. It should be noted that the higher value of the energy loss at the most forward point is caused due to head on collisions.

Table 2.16. Sectional data of the ship.

Section No.	X-coordinate (m)	Water-line breadth(m)
0.0 (stern)	-92.97	0.00
1.0	-83.67	2.02
2.0	-74.37	6.00
3.0	-65.08	9.94
4.0	-55.78	13.53
5.0	-46.48	17.34
6.0	-37.19	20.30
7.0	-27.89	22.54
8.0	-18.59	24.06
9.0	-9.30	24.81
10.0	0.00	24.97
11.0	9.29	24.56
12.0	18.59	23.22
13.0	27.89	20.49
14.0	37.19	16.97
15.0	46.48	13.28
16.0	55.78	8.99
17.0	65.08	6.32
18.0	74.37	3.98
19.0	83.67	2.38
20.0 (bow)	92.97	0.56

Table 2.17. Energy losses for a ship drifting against a bridge pier (V=2.0 m/s).

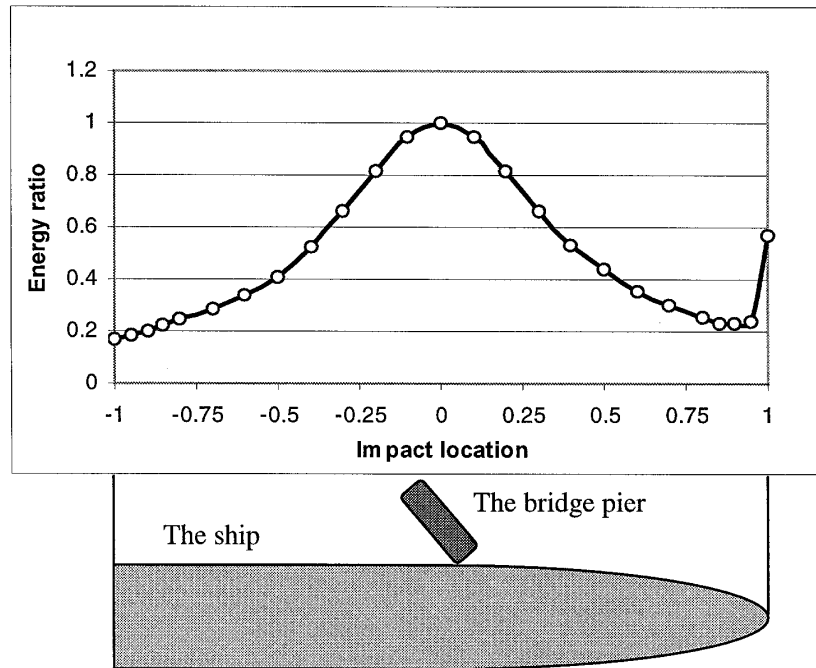| Collision point	2d/L	Energy loss (MJ)
1(bow)	1.00	52.93
2	0.95	22.57
3	0.90	21.37
4	0.80	23.51
5	0.70	27.84
6	0.60	33.04
7	0.50	40.56
8	0.40	49.46
9	0.30	61.53
10	0.20	75.87
11	0.10	88.21
12	0.00	93.26
13	-0.10	88.21
14	-0.20	75.87
15	-0.30	61.53
16	-0.40	48.65
17	-0.50	38.34
18	-0.60	31.91
19	-0.70	26.89
20	-0.80	22.88
21	-0.90	18.96
22	-0.95	17.25
23(stern)	-1.00	15.80

Fig. 2.10. A ship collision with a bridge pier. The energy ratio is defined as the ratio between the energy loss and the initial kinetic energy of the ship before the collision.

2.4 Ship Collision with Offshore Platforms

2.4.1 The Analysis Method

Petersen and Pedersen (1981) and Pedersen and Jensen (1991) showed that in minor collisions between supply vessels and offshore structures a considerable part of the kinetic energy can be stored as elastic energy of the ship and the platform. In such cases, the global dynamic load effects may be significant and a consistent simplified design procedure should be established. An efficient finite element method was employed by Bai and Pedersen (1993) to analyse the problem. In the simplified procedure presented by Pedersen and Jensen (1991), only a central collision was considered. Therefore, in the following we extend this simplified theory to analyse non-central collisions between supply vessels and offshore platforms.

Let us consider a collision situation shown in Fig. 2.11. A supply vessel drifts to a platform at a velocity of $\dot{\xi}(0)$ in a direction normal to the impact surface. To simplify the analysis, we assume that the impact force also acts in the direction normal to the impact surface, that is in the ξ - direction.
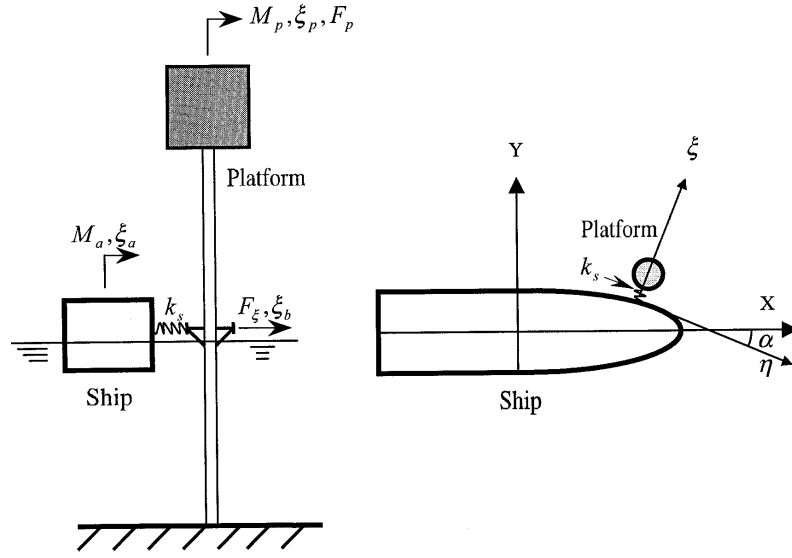
Fig. 2.11. Simplified model of a supply vessel impacting a platform.

The simplified theory of energy released for crushing of structures, Pedersen and Jensen (1991), is based on the assumption that the colliding system can be approximated as a two-mass system where one generalised mass represents the supply vessel and the other represents the platform. Thus, the following force-stiffness relations may represent the platform behaviour:

$$F_\xi = k_{11}\xi_b + k_{12}\xi_p \tag{2.44}$$

$$F_p = k_{21}\xi_b + k_{22}\xi_p = -M_p\ddot{\xi}_p \tag{2.45}$$

where F_ξ is the collision force between the supply vessel and the platform, F_p is the transmitted force acting on the generalised topside mass M_p of the platform, ξ_b is the displacement of the collision point, and ξ_p is the displacement of the topside.

The interaction between the ship and the platform is simplified as

$$F_\xi = \begin{cases} k_s(\xi_a - \xi_b), & for \;\; \dot{\xi}_a - \dot{\xi}_b \geq 0 \\ 0, & for \;\; \dot{\xi}_a - \dot{\xi}_b < 0 \end{cases} \tag{2.46}$$

Here $k_{11}, k_{22}, k_{12}, k_{21}, k_s$ are stiffness coefficients, and ξ_a is the displacement at the collision point of the supply vessel.

In Pedersen and Jensen (1991), it is shown that at the end of the collision where $\dot{\xi}_a = \dot{\xi}_b$, the displacement ($\xi_p$) of the platform topside can be assumed to be small. Therefore, from Eqs. (2.44) and (2.45) we get the generalised force F_p at this moment

$$F_p = \frac{k_{21}}{k_{11}} F_\xi \qquad (2.47)$$

From the previous analysis of ship collisions, the impact impulse of the collision between the supply vessel and the platform can be expressed as

$$I_\xi = \frac{M_a}{D_{a\xi}} [\dot{\xi}(0) - \dot{\xi}_a] \qquad (2.48)$$

where $D_{a\xi} = \dfrac{1}{1+m_{ax}} \sin^2 \alpha + \dfrac{1}{1+m_{ay}} \cos^2 \alpha + \dfrac{1}{1+j_a} \cdot \dfrac{[y_c \sin \alpha - (x_c - x_a) \cos \alpha]^2}{R_a^2}$, and M_a is the mass of the supply vessel.

From Eqs. (2.45) and (2.47), the impact impulse on the generalised platform mass can be expressed as

$$I_p = -M_p \dot{\xi}_p = \frac{k_{21}}{k_{11}} I_\xi \qquad (2.49)$$

At the end of the crushing, the velocity of the supply vessel and the velocity of the platform at the collision point are equal. From Eq. (2.46) we have $\partial F_\xi / \partial t = 0$ and by Eq. (2.44) we get

$$\dot{\xi}_a = -\frac{k_{12}}{k_{11}} \dot{\xi}_p \qquad (2.50)$$

From Eqs. (2.48) to (2.50), the velocity of the topside of the platform is obtained as

$$\dot{\xi}_p = -\frac{\dot{\xi}(0)}{\dfrac{k_{12}}{k_{11}} + \dfrac{k_{11}}{k_{21}} \dfrac{M_p D_{a\xi}}{M_a}}$$

The velocities of the ship at the end of the collision can be expressed as

$$v_{ax} = \dot{\xi}(0) \sin \alpha - \frac{\sin \alpha}{D_{a\xi}(1+m_{ax})} (\dot{\xi}(0) - \dot{\xi}_a)$$

$$v_{ax} = \dot{\xi}(0)\cos\alpha - \frac{\cos\alpha}{D_{a\xi}(1+m_{ay})}(\dot{\xi}(0) - \dot{\xi}_a)$$

$$\omega_a = \frac{y_c \sin\alpha - (x_c - x_a)\cos\alpha}{R_a{}^2(1+j_a)D_{a\xi}}(\dot{\xi}(0) - \dot{\xi}_a)$$

where

$$\dot{\xi}(0) - \dot{\xi}_a = \frac{\dot{\xi}(0)}{1 + \dfrac{k_{12}k_{21}}{k_{11}{}^2}\dfrac{M_a}{M_p D_{a\xi}}}$$

The energy to be absorbed by the crushing of the supply vessel and the deformation of the platform is

$$E_c = E_0 - (E_s + E_p) \tag{2.51}$$

where

$E_0 = \dfrac{1}{2}M_a[(1+m_{ax})\sin^2\alpha + (1+m_{ay})\cos^2\alpha]\dot{\xi}(0)^2$ is the initial kinetic energy of the supply vessel,

$E_p = \dfrac{1}{2}\dfrac{M_p\dot{\xi}(0)^2}{(\dfrac{k_{12}}{k_{11}} + \dfrac{k_{11}}{k_{21}}\dfrac{M_p D_{a\xi}}{M_a})^2}$ is the kinetic energy of the platform topside at the end of

the collision, and
$E_s = E_0 + \dfrac{1}{2}M_a\dot{\xi}(0)^2(\dfrac{1}{D_{a\xi}(1+\dfrac{k_{12}k_{21}}{k_{11}{}^2}\dfrac{M_a}{M_p D_{a\xi}})^2} - \dfrac{2}{D_{a\xi}(1+\dfrac{k_{12}k_{21}}{k_{11}{}^2}\dfrac{M_a}{M_p D_{a\xi}})})$ is the kinetic

energy of the supply vessel at the end of the collision.

The energy to be dissipated by the crushing of the ship structure is

$$E_{ship} = \frac{1}{2}k_s(\xi_a - \xi_b)^2 = \frac{F_\xi{}^2}{2k_s} = \frac{k_{11}}{k_{11}+k_s}(E_0 - E_s - E_p) \tag{2.52}$$

The energy stored in the deformation of the platform is

$$E_{platform} = \frac{k_s}{k_{11}+k_s}(E_0 - E_s - E_p) \tag{2.53}$$

Finally, the impact impulse between the ship and the platform can be expressed as

$$I_\xi = \frac{M_a}{D_{a\xi}} \cdot \frac{\dot{\xi}(0)}{1 + \dfrac{k_{12}k_{21}}{k_{11}^2}\dfrac{M_a}{M_p D_{a\xi}}} \tag{2.54}$$

2.4.2 Examples

Verification: Supply Vessel Impacting a Jack-up Rig

In order to check the accuracy of the present method, we first use the same example as in Pedersen and Jensen (1991), which is a supply vessel in a central collision with the leg of a jack-up rig. The stiffness coefficients are in this case

$k_{11} = 34.5$ MN/m, $k_{22} = 48.9$ MN/m

$k_{12} = k_{21} = -27.8$ MN/m, $k_s = 18.0$ MN/m.

The ship mass including the added mass is $M_a = 7.77 \cdot 10^6$ kg. The jack-up rig mass is $M_p = 19.7 \cdot 10^6$ kg. The ship sways into the jack-up rig at a speed of 2 m/s. The present result for the energy to be dissipated by the crushing of the supply vessel is $E = 8.13 MJ$. As expected, this result agrees with $E = 8.1 MJ$ determined by the similar procedure presented by Pedersen and Jensen (1991).

Application Example: Supply Vessel Drifting against a Flexible Jack-up Rig

As another example, let us consider a supply vessel colliding with the leg of the jack-up rig in different locations at a velocity of V = 2 m/s in a direction normal to the impacting ship surface. The length of the supply vessel is 82.5 m, the breadth is 18.8 m, the draught is 7.6 m and the displacement is 4000 t. The collision situation is presented in Fig. 2.12.

The energy absorption by the crushing of the supply vessel when the platform is rigid and flexible (the stiffness coefficients are the same as in the above example) are compared and shown in Table 2.18. Fig. 2.13 shows the ratio of the dissipated energy by the crushing of the supply vessel to the initial kinetic energy of the ship before the collision.

It is seen from the results that the energy absorbed by the crushing of the supply vessel decreases if the flexibility of the jack-up rig is taken into consideration. For the present example, the energy absorbed by the ship deformation in the central collision with the flexible platform is only about 50% of the absorbed energy in the case of the rigid platform.
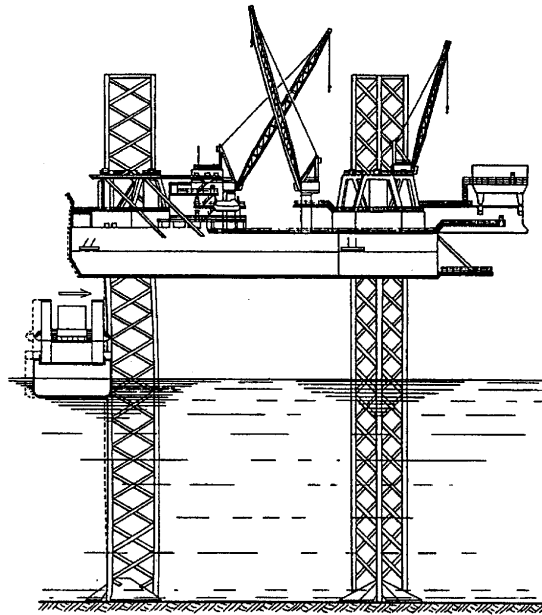
Fig. 2.12. Collision scenario between a supply vessel and a jack-up rig.

Table 2.18. Energy dissipated by the crushing of the supply vessel.

| Impact point	x_c (m)	y_c (m)	Angle $\alpha°$	Energy dissipated by ship (MJ)	
				Rigid case	Flexible case
1(bow)	40.0	0.0	90.0	8.40	4.85
2	38.5	2.6	45.0	4.00	2.47
3	36.6	4.1	37.5	3.88	2.40
4	34.6	5.6	32.5	4.02	2.48
5	30.8	7.5	21.7	4.22	2.59
6	27.0	9.0	14.4	4.77	2.91
7	23.1	9.4	7.3	5.46	3.29
8	19.3	9.4	0.0	6.32	3.76
9	15.4	9.4	0.0	7.98	4.63
10	11.6	9.4	0.0	9.97	5.63
11	7.7	9.4	0.0	12.19	6.67
12	3.9	9.4	0.0	14.03	7.49
13	0.0	9.4	0.0	14.80	7.82
14	-3.9	9.4	0.0	14.03	7.49
15	-7.7	9.4	0.0	12.19	6.67
16	-11.6	9.4	0.0	9.97	5.63
17	-15.4	9.4	0.0	7.98	4.63
18	-19.3	9.4	0.0	6.32	3.76
19	-23.1	9.4	0.0	5.06	3.07
20	-27.0	9.4	0.0	4.08	2.51
21	-30.8	9.4	0.0	3.35	2.09
22	-34.6	9.4	0.0	2.79	1.75
23	-38.5	9.4	0.0	2.33	1.48
24 (stern)	-40.0	9.4	0.0	2.19	1.39
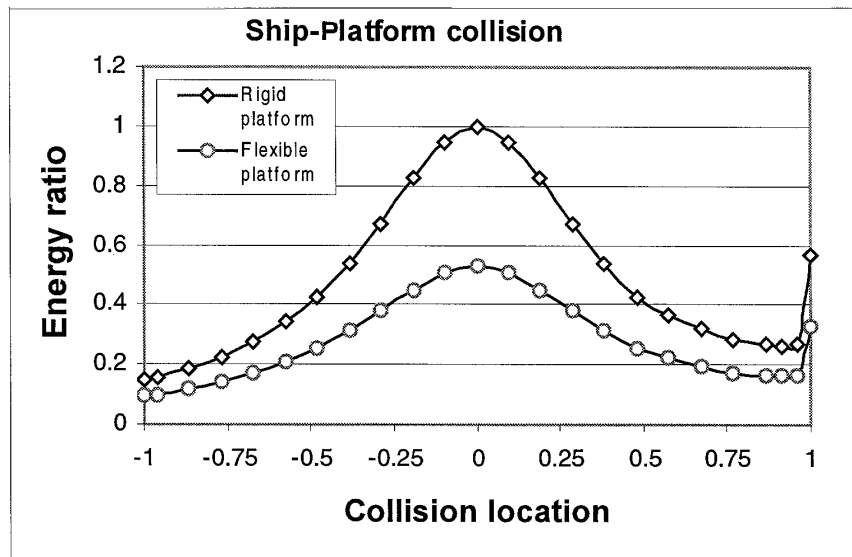
Fig.2.13. Collision between the supply vessel and the platform. The energy ratio is defined as theratio of the energy released for crushing the supply vessel to the total kinetic energy of the supply vessel before collision.

2.5 Concluding Remarks

In this chapter analytical methods have been derived for the energy released for the crushing and the impact impulse associated with ship-ship collisions, ship collisions with rigid walls, and ship collisions with flexible offshore platforms. The emphasis has been on the derivation of closed-form expressions for energy losses in any ship collisions. A comparison of the present method with some published comprehensive simulation results shows that good agreement has been achieved.

The analysis results show that the energy released for the crushing of the involved structures is mainly determined by the following parameters:

- Ship mass
- Ship velocity
- Collision location
- Collision angle

It is also indicates that the energy released for crushing is larger in the fore part of the struck ship than in the aft part of the struck ship.

Chapter 3

Internal Mechanics of Ship Collisions

3.1 Introduction and Literature Review

This chapter focuses on the structural response in collisions. The purpose is to establish simplified methods for calculating the force-penetration curve, the absorbed energy-penetration relationship and the resulting hole in the ship structures.

The side structure of ships is very complex. The deformed, destroyed and crushed modes of side structures are also very complex. However, a ship may be viewed as an assembling of plated structures. Such as shell plating, transverse frames, horizontal decks and bulkheads are built in various plates. Observations from full-scale ship accidents and model experiments reveal that the primary energy absorbing mechanisms of the side structure are

- Membrane deformation of shell plating and attached stiffeners
- Folding and crushing of transverse frames and longitudinal stringers
- Folding, cutting and crushing of horizontal decks
- Cutting or crushing of ship bottoms
- Crushing of bulkheads

The existing methods for analysis of structural damage in ship collisions may be divided into four categories:

- (1) Empirical methods
- (2) Finite element methods
- (3) Experimental methods and
- (4) Simplified methods

3.1.1   Empirical Methods

Minorsky (1959) analysed 26 collision cases of full-scale ship accidents and developed an empirical formula:

$$E = 47.2R_T + 32.7, \ (MJ)$$

$$R_T = \sum P_N L_N t_N + \sum P_n L_n t_n, \ (m^3)$$

where R_T is the destroyed material volume of both the striking ship and the struck ship, it is called the resistance factor, E is the absorbed energy, P_N, P_n are the depths of damage in the *Nth* and the *nth* members of the striking ship and the struck ship, respectively, L_N, L_n are the lengths of damage in the *Nth* and *nth* members of the striking ship and the struck ship, t_N, t_n are the thicknesses of damage in the *Nth* and *nth* members of the striking ship and the struck ship.

Fig. 3.1 presents the empirical curve of the energy-volume relationship derived by Minorsky. It shows that the results for the 18 low-energy cases of the 26 collisions are considerably scattered. But the correlation of the other 8 high-energy collisions is very good. Therefore, Minorsky's formula is generally considered valid for high-energy collisions.
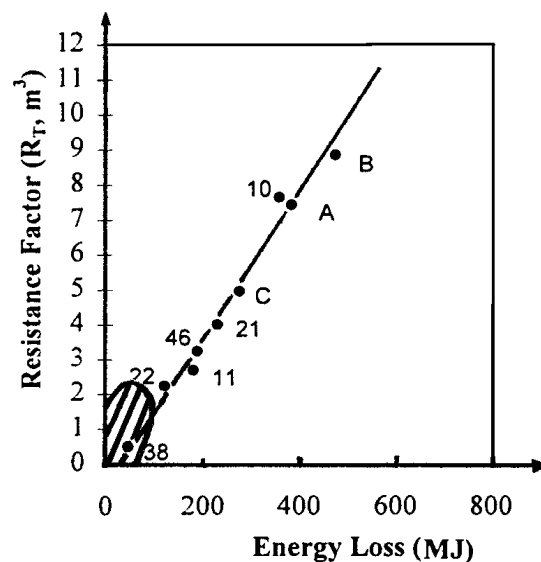

Fig. 3.1. Minorsky's original correlation.

Minorsky's formula is often used in analyses of ship collisions due to its simplicity. When Minorsky tried to establish a function of absorbed energy with some related parameters, he also noted that the resistance of some members would be proportional to t^2 or some

other function of the thickness t. Moreover, several other factors were tried out, but they did not provide a better correlation than the volume factor. Therefore, Minorsky's formula indicates that the absorbed energy of a ship is simply proportional to the volume of destroyed material in high-energy collisions. This may not always be true.

The simplicity of Minorsky's formula has aroused the interests of investigators to extend it to low-energy collisions. Based on the experiments, Woisin (1979) proposed a formula

$$E = 47.2 R_T + 0.5 \sum (h \cdot t_s^2), \ (MJ)$$

where $R_T \ (m^3)$ is the destroyed volume of materials, $h \ (m)$ is the height of broken or heavily deformed longitudinal members and $t_s \ (cm)$ is the thickness of the members.

Similarly, Vaughan (1978) established a formula which related the absorbed energy and the destroyed volume and area

$$E = 93 R_T + 33 A, \ (MJ)$$

where R_T is the destroyed volume of the materials (m^3) and A is area of tearing (m^2).

Jones' (1983) formula for low-energy collision is based on the plastic theory of a beam subject to a point load. The formula is

$$E = \frac{1}{2} R_T \sigma_0 (\frac{2w}{l})^2$$

where R_T is the volume of the side shell involved in membrane deformation, σ_0 is the flow stress of the material and $2w/l$ is the normalised final deflection over the span.

Deck cutting or crushing of a struck ship gives a large contribution to the collision resistance. Lu and Callidine (1990) performed a series of model tests of bare plates cut by rigid wedges and obtained an empirical relationship:

$$E = C \sigma_0 l^{1.4} t^{1.6}$$

where E is the absorbed energy, σ_0 is the flow stress of the material, l is the length of the cut, t is the thickness of the plate and C has a value in the range of $0.9 \sim 3.5$.

Paik (1994) also conducted a series of tests of stiffened plates cut by rigid wedges. The stiffeners were treated by the equivalent thickness method and by using dimensional analysis and a least-square approach the empirical formula was

$$E = C_{1.5} \sigma_0 l^{1.5} t_{eq}^{1.5}$$

where $C_{1.5} = 1.112 - 1.156\theta + 3.760\theta^2$, θ is the half angle of the wedge (rad), and t_{eq} is the equivalent plate thickness.

3.1.2   Finite Element Methods

The finite element method (FEM) is a powerful means of analysis of structural response in collisions. Many commercial codes are available, such as LS-DYNA3D, ABAQUS, MSC/DYTRAN. Many investigators have used FEM approaches to analyse the problems of collisions and grounding. For example, side collisions investigated by Kitamura (1997), Sano and Muragish (1996) and Kuroiwa (1996); grounding by Amdahl and Kavlie (1992) and Lemmen & Vredeveldt (1996); bow crushing by Lehmann and Yu (1998). A typical example of FEM analysis of a collision performed by Kitamura (1997) is presented in Fig. 3.2.
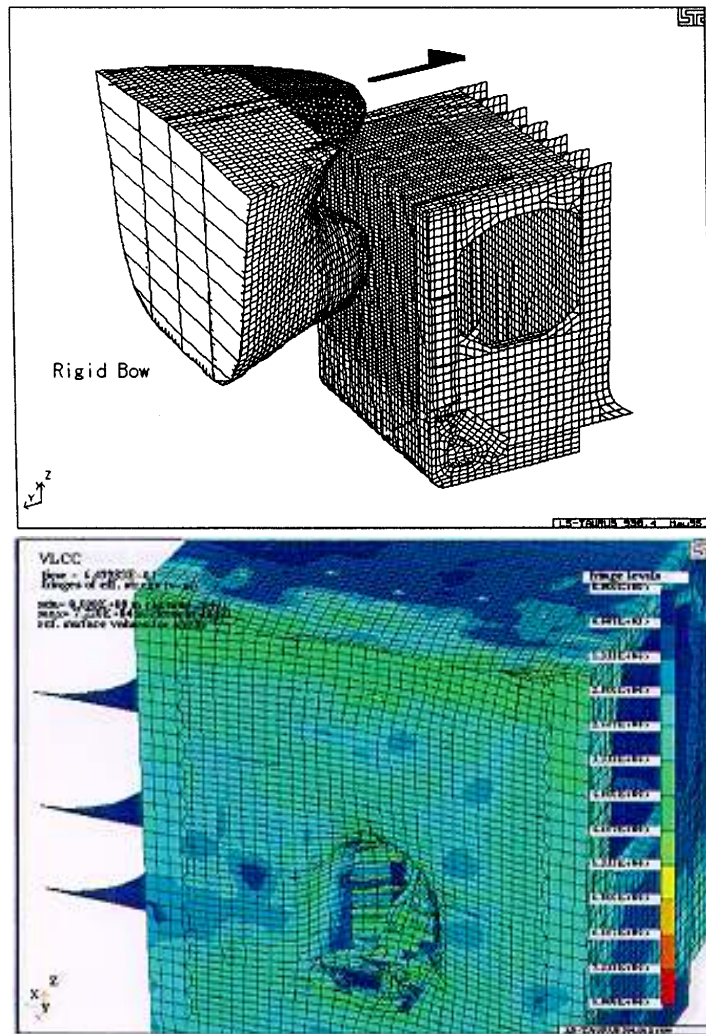

Fig. 3.2. Simulation of a ship-ship collision using FEM (Kitamura, 1997).

Usually, it is considered that FEM calculation may give accurate results and it may replace model experiments in some cases. But this is not always true. Fig. 3.3 presents an example with significant difference between simulation results and experimental results. Due to a large number of elements and the need to solve dynamic problems step by step, it is very time consuming to simulate collisions and grounding by use of FEM.
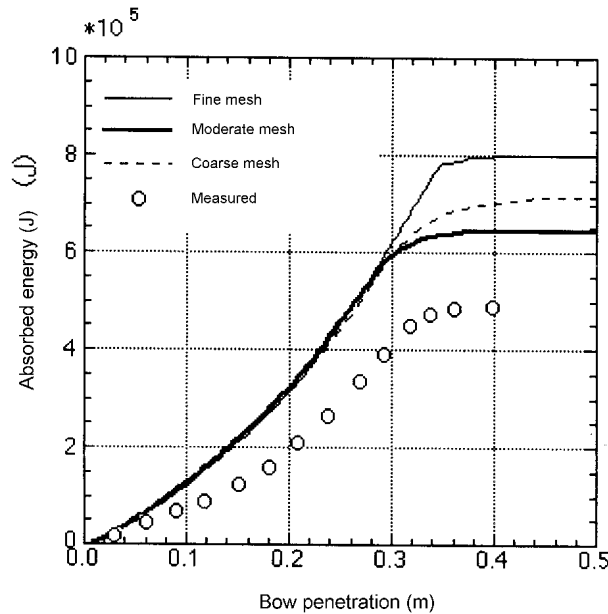

Fig. 3.3. Comparison of simulated results and experimental results for a corrugated panel impacted by a cylinder (Kitamura, 1997).

3.1.3 Experimental Methods

Many experiments on ship collisions have been carried out since the early 1960s. From 1962 to 1976, investigators in Italy, Germany and Japan conducted a series of model tests. Several authors have given detailed reviews on these experiments, for example, Amdahl (1983), Jones (1979), Ellina and Valsgard (1985), Samuelides (1989), and Pedersen et al. (1993). The main purpose of the experiments carried out in Italy, Germany and Japan was to design nuclear powered ships protecting the nuclear reactor from collision damage.

In Italy, 24 model experiments were conducted to examine the efficiency of different types of side structures towards various types of striking ships. The models represented the structures of existing ships on the scales 1/15 and 1/10. The striking bow ran down along an inclined path while the side structure model was mounted on a carriage which was free to move along the path. In order to account for the effect of the surrounding water, wings were attached to the carriage and immersed in water tanks on either side of it.

12 ship model tests were carried out in Germany (Woisin, 1979) during the period of 1967 to 1976. The model scales range from 1/12 to 1/7.5. The test set-up is shown in Fig. 3.4, which illustrates the striking bow running down from an inclined railway path. A typical damaged bow after collision test is presented in Fig. 3.5. The picture shows that the striking bow suffered heavy damage since the side structure was designed as a protection barrier of the resistance type. A protection side structure of the resistance type is shown in Fig. 3.6.
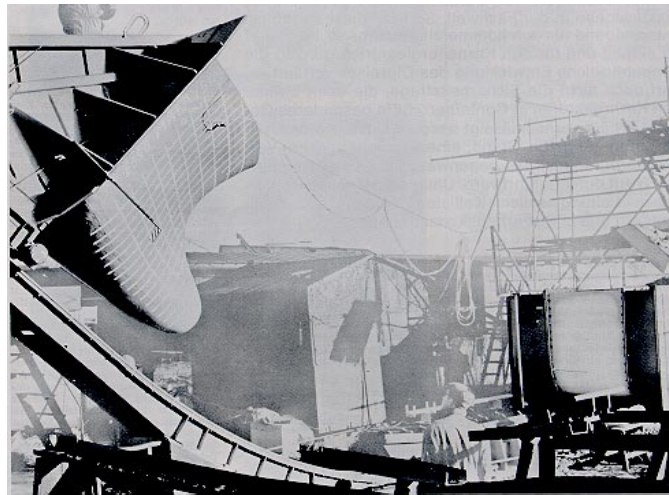
Fig. 3.4. The test set up for collision experiments in Germany (Woisin, 1979).

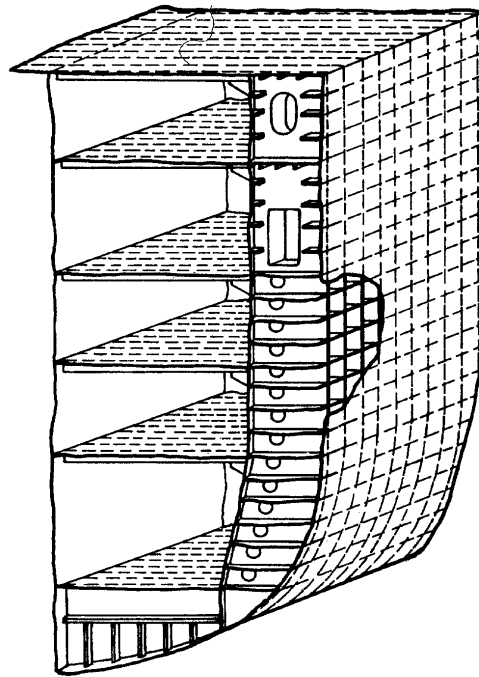*Fig. 3.5. A damaged bow after collision test in Germany.*

Fig. 3.6. Collision protection type of side structure (Woisin, 1979).

During the period of 1966 to 1970, a series of collision model tests was conducted in Japan. Both dynamic and static experiments were made which covered different aspects of the collision problem, such as the design of the side structure, the effect of the shape of the striking bow and the effect of the added mass. A detailed summary of the experiments was given by Akita et al. (1972). A typical load-penetration curve of one experiment is presented in Fig. 3.7, which shows a side structure struck by a rigid bow.
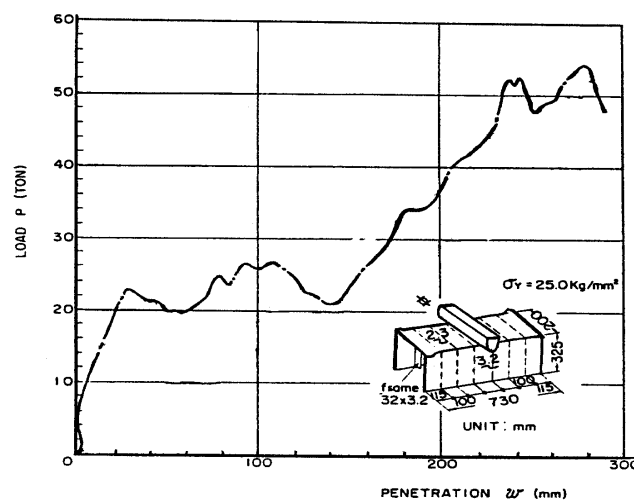

Fig. 3.7. Experimental result of a load-penetration relationship (Akita et al., 1972).

A 7-year (1991~1997) project on the prediction methodology of tanker structural failure and resulting oil spill was carried out in Japan. In the research project, two main aspects were focused on. One was the dynamic process of structural damage caused by collisions or grounding, and the other was the resulting process of oil spill and/or water ingress through the damaged hull. A series of full-scale ship collision experiments was carried out in the Netherlands jointly by Japan and the Netherlands (1991). Two inland waterway tankers 80 m in length were used. Following the 1991 collision experiment, new experiments of ship-ship collisions were carried out jointly by Japan-the Netherlands-Germany at the Netherlands in November 1997. A 1500 t tanker collided with another 1500 t tanker. The striking bow was a relatively hard bulb. The test section was installed in the middle of the struck ship and it was full-scale VLCC side of a conventional design and a newly developed design. A photo of the full-scale collision experiment in 1998 is shown in Fig. 3.8.

Fig. 3.8. Full-scale collision experiment in 1998 in the Netherlands.

In recent years, many static tests of side collisions were carried out since static tests are easier to control than dynamic ones. Ito et al. (1984) conducted a series of tests of double-sided hulls struck by a raked bow and a bulbous bow. The collision scenarios were grouped into five categories based on different locations of the impact. An example of the experiments by Ito et al. is given in Fig. 3.9, which is a double-sided hull colliding with a bulbous bow.
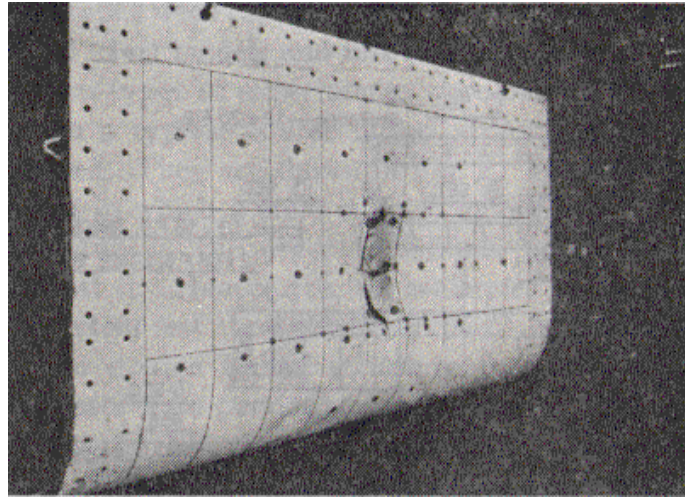
Fig. 3.9. A test of a double-sided hull struck by a bulbous bow (Ito et al., 1984).

Amdahl and Kavlie (1992) performed model tests simulating a double hull indented by a rigid hexagonal body. This test originally simulated grounding, but it is also very useful for side collision analysis. Amdahl and Kavlie's experimental set-up and an example of the load-deformation curve are shown in Fig. 3.10. It is seen that the relationship between the load and the deformation is very complex.
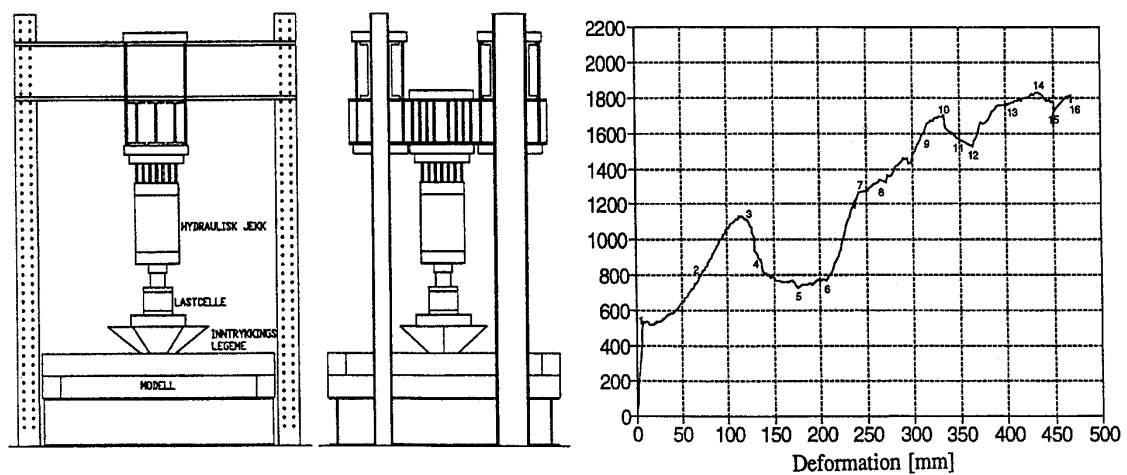

Fig. 3.10. Test set up and load-deformation relationship (Amdahl and Kavlie, 1992).

Full-scale dynamic collision tests were carried out by Qvist et al. (1995). The test model simulated the double side of a 40,000 dwt tanker. A 2.75 t rigid ball was used to simulate a striking bow, which was dropped from a height of 5 metres. The simulated collision velocity was approximately 20 knots. The kinetic energy of the dropped ball just before impact was $137.5kNm$. One of the tested models after the collision experiment is shown in Fig. 3.11.

Fig. 3.11. A full-scale side model after collision experiment in Denmark
(Qvist et al., 1995).

Similarly, a series of large-scale dynamic side collision experiments was conducted in Japan during the period of 1992 to 1996. The models were used to simulate the side collision of large oil tankers. One of the large experimental models after the collision test is shown in Fig. 3.12.

Fig. 3.12. Dynamic side collision experiment in Japan.

When a ship is engaged in a head-on collision with relatively hard objects, such as rigid walls, the bow of the ship will be crushed. Amdahl (1983) carried out several model tests of crushing of different bows. Valuable results were obtained. Fig. 3.13 shows one of the test models and an experimental result of the load-indentation curve. In Japan, several tests of bow crushing have also been performed, for example, Hagiwara et al. (1983) carried out a bow-crushing test, which was a 1/5 scale of a 17,000 dwt cargo ship with transverse framing. Fig. 3.14 shows the crushing test of a bow performed by Hagiwara et al. (1983).
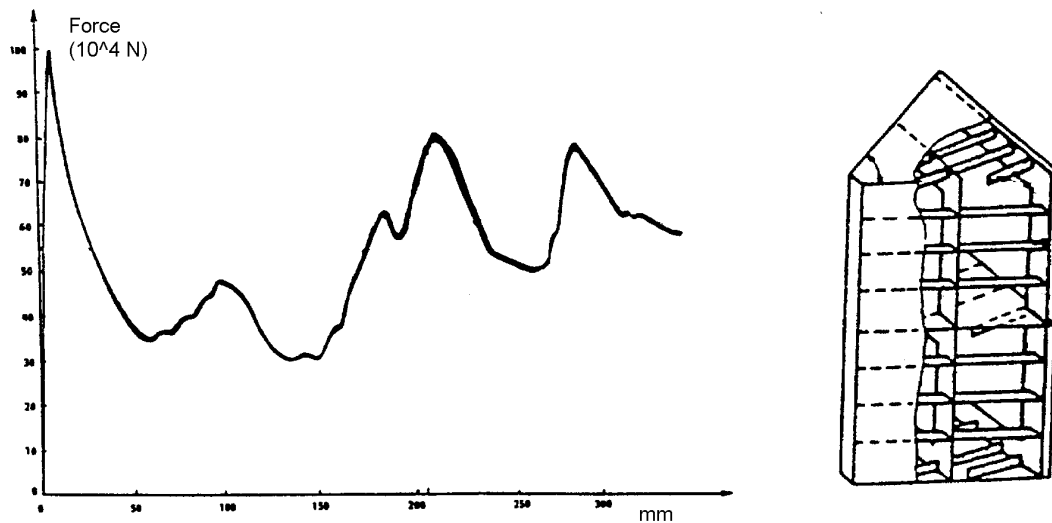

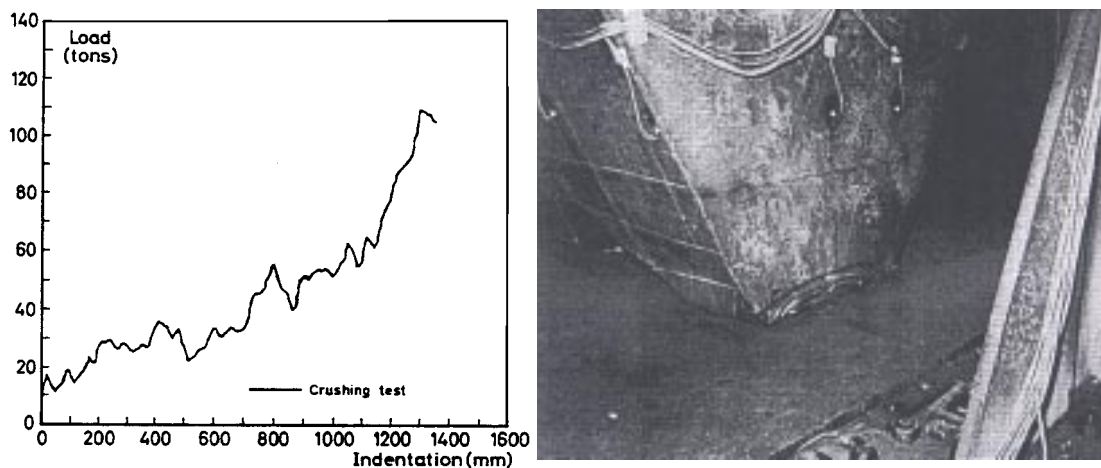*Fig. 3.13. A bow-crushing test and the load-indentation curve (Amdahl, 1983).*

Fig. 3.14. Model test of bow crushing (Hagiwara et al., 1983).

3.1.4   Simplified Analytical Methods

Simplified methods are based on the upper-bound theorem and some assumptions from observations of accidental damages and experimental studies. Usually, the methods can give good predictions through a fast simple analysis. Therefore, many authors have used simplified analytical methods for analysis of ship collisions.

A major assumption in the simplified analytical methods is that different structural members, such as side shell, decks and frames, do not interact but contribute independently to the total collision resistance.

McDermott et al. (1974) developed a method for analysis of tankers in minor collisions. The method is based on 14 basic assumptions. The mathematical model for the analysis procedure included bending and buckling of stiffened hull plating, membrane tension of hull plating and decks, and failure of frames. Analysis results indicated that most of the absorbed energy (about 70~85%) in a collision is that of membrane tension in the stiffened hull. Other absorbed energy is that of membrane tension in the stiffened deck and in-plane shearing of frames. Bending energy in the stiffened hull is very small and can often be neglected.

Reckling (1983) proposed a method which takes into account the deformation of both the striking ship and the struck ship. The energy absorbed in both ships, up to rupture of the struck ship hull, is computed by simple methods. A calculation example of two equal oil tankers of 141,000 dwt with bulbous bow was performed. The result showed that the absorbed energy under membrane tension of the side hull is only 18% of the total energy, while the energy absorbed in the web frames, decks and bottom of the struck ship is 40% of the total energy. A remarkable 42% of the total energy is absorbed by the striking bow structure.

Kinkead (1980) developed an analytical technique which was used as a basis for the calculation of critical velocities of five ships of a displacement in the range from 4,860 t to 121,400 t when they strike an LNG tanker of capacity of 27,400 m^3. The result obtained by the developed method was compared with a modified Minorsky formula.

Hysing (1995) and Scharrer (1996) conducted a series of calculations on collisions of Ro-Ro passenger vessels where the simplified method was used. The force-penetration curve and the energy-penetration curve are predicted and the hole size of the damaged side is also determined. Many valuable results are obtained.

Wang and Ohtsubo (1997) developed a series of formulas for the different failure modes of plates, which was used to analyse side collisions and ship grounding. The agreement between the calculation results and the experimental results is good.

Chang et al. (1980) presented a methodology for prediction of the structural response in collisions. The method is a synthesis of the FEM technique, the collapse theorem, and experimental data. The study showed that the collision force is a function of the thickness of the plate, the cross sectional area of the strongest section, and the yield and ultimate strength of the materials. Similarly, the energy absorbed by the destroyed metal is a function of both the metal volume and the thickness/area ratio and the yield and ultimate strength of the materials. This study is limited to perpendicular collisions.

Researches on bow crushing performed by Amdahl (1983), Yang and Caldwell (1988) and Kierkegaard (1993) are very valuable. These methods are based on the assumption that a complex structure can be divided into fundamental elements, such as L-, T- and X-sections. By adding the contributions from all the basic elements, the crushing behaviour of a bow can be determined. A typical calculation example performed by Kierkegaard is shown in Fig. 3.15.
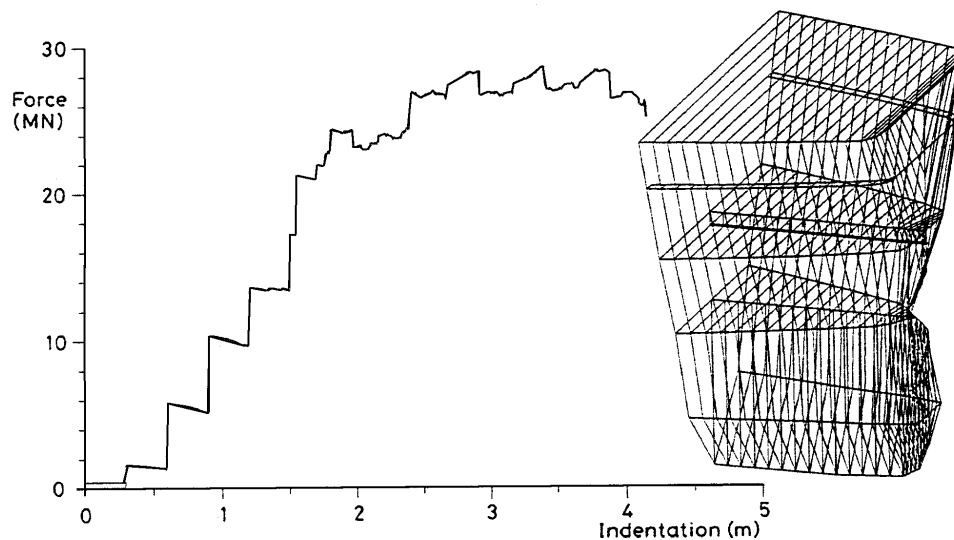

Fig. 3.15. Head-on crushing analysis of a 2,000 dwt tanker by use of a simplified method (Kierkegaard, 1993).

Wierzbicki (1983) and Abramowicz and Jones (1986) made valuable investigations of the axial crushing behaviour of basic structural elements. A typical example of the load-displacement curve and the corresponding crushing mode of a thin-walled box is presented in Fig. 3.16 (Ishiyama et al., 1983). Lehmann and Yu (1995) developed a formula for the analysis of progressive folding of a conical shell, which can be used to predict the crushing load of a bulbous bow.
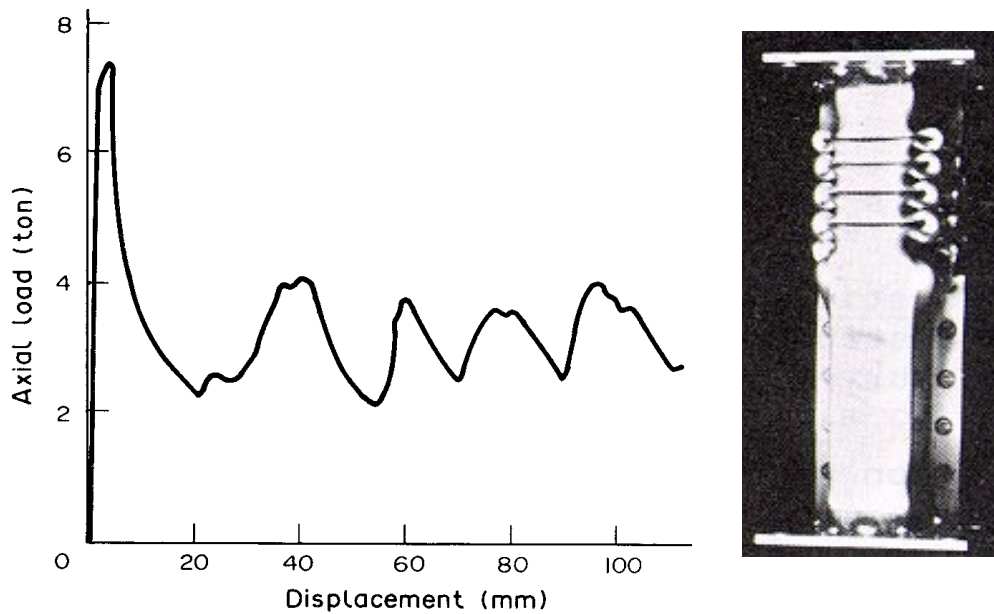
*Fig. 3.16. Load-displacement curve and corresponding crushing mode of a
thin-walled box (Ishiyama et al., 1983).*

Pedersen et al. (1993) studied the crushing load of ship bows. In the analysis, the
formulas proposed by Gerard (1958), Amdahl (1983) and Yang and Caldwell (1988) are
applied. Based on a series of calculations and analyses, an empirical expression is derived
for the estimation of the maximum bow collision loads. The proposed expression for a
merchant vessel between 500 dwt and 300,000 dwt has the following form:

$$P_{bow} = \begin{cases} P_0 \cdot \overline{L}[\overline{E}_{imp} + (5.0 - \overline{L})\overline{L}^{1.6}]^{0.5}, & for \quad \overline{E}_{imp} \geq \overline{L}^{2.6} \\ 2.24 \cdot P_0 [\overline{E}_{imp} \overline{L}]^{0.5}, & for \quad \overline{E}_{imp} < \overline{L}^{2.6} \end{cases}$$

where

$$\overline{L} = L_{pp} / 275 \quad m$$

$$\overline{E}_{imp} = E_{imp} / 1425 \quad MNm$$

$$E_{imp} = \frac{1}{2} m_x V_0^2$$

and

P_{bow} is the maximum bow collision load (MN)

P_0 is the reference collision load equal to 210 (MN)

E_{imp} is the energy to be absorbed by the crushing bow (MJ)

L_{pp} is the length of the ship (m)

m_x is ship mass plus added mass (5%) with respect to longitudinal motion ($10^6 kg$)

V is the initial speed of the ship (m/s).

An example of a 150,000 dwt bulk carrier in a fully loaded condition colliding head-on with a rigid wall at an initial impact speed of 18 knots is given in Fig. 3.17. Fig. 3.18 shows the maximum loads of bow crushing vs. various ship lengths.
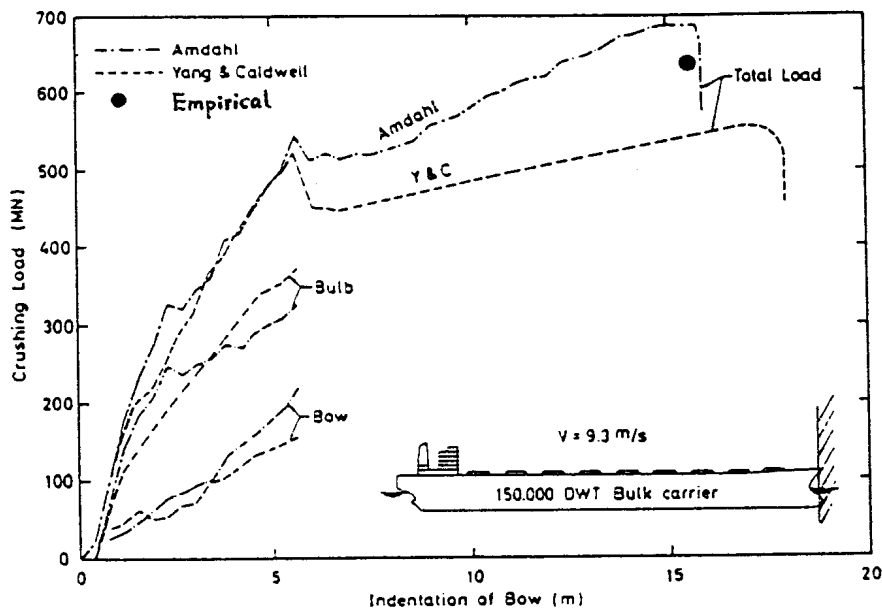

Fig. 3.17. Head-on load deflection curves for a 150,000 dwt bulk carrier at an initial speed of 9.3 m/s (Pedersen et al., 1993)

Similarly, Pedersen (1998) derived an empirical expression for a broadside ship impact load, which can be used for ship collisions with bridge piers. The empirical formula is

$$P_{side} = 263\beta[1.0 + 0.88(b/D)^{1.06}] \cdot [L/300]^{2.20} \quad (MN)$$

where

P_{side} is the broadside collision load (MN)

β is a factor accounting for the stiffening system of the ship

$\quad \beta = 1.00$ for a longitudinally stiffened vessel

$\quad \beta = 1.35$ for a transversely stiffened vessel

b is the width of the bridge pier in contact with the ship side

D is the moulded depth of the vessel

L is the ship length (m)

Fig. 3.19 shows the broadside collision loads vs. various ship lengths with the contact lengths b=5 m, b=10 m and b=15 m, respectively.
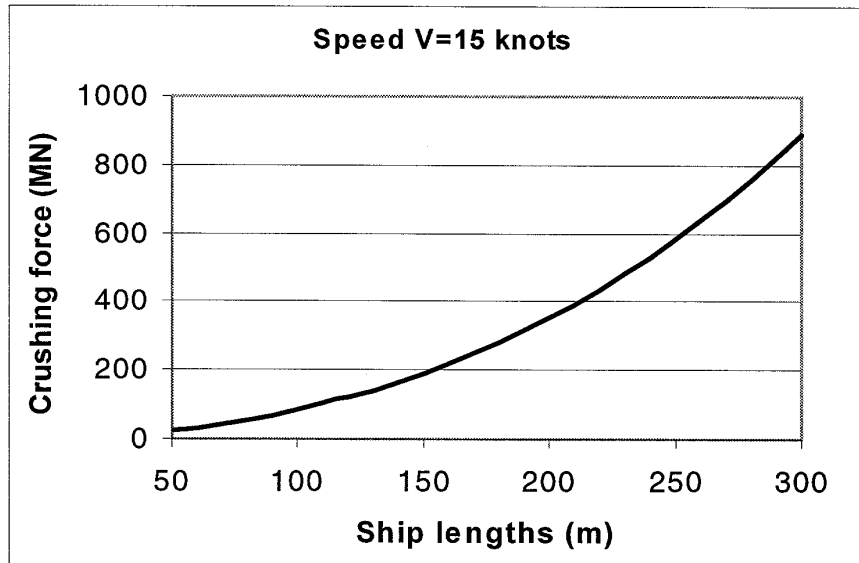

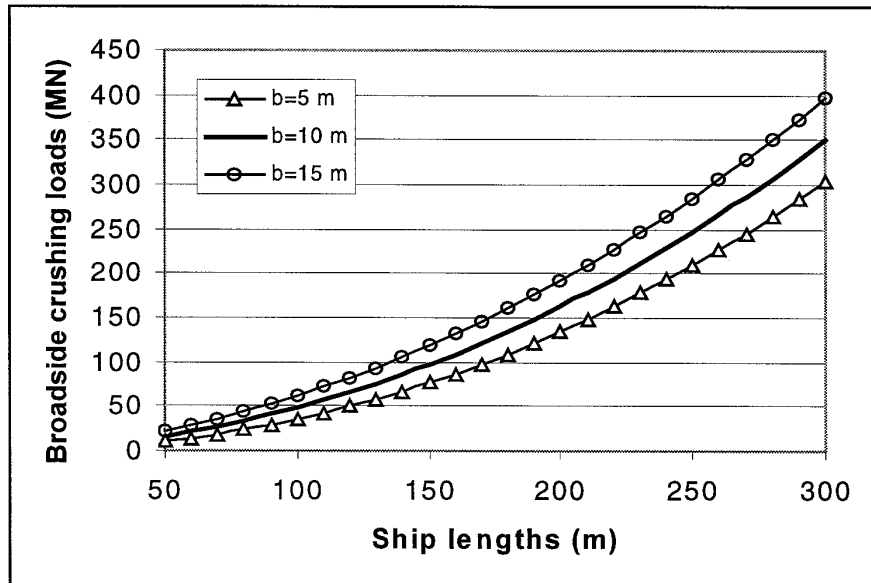*Fig. 3.18. Maximum head-on crushing loads of ship bow vs. various ship lengths.*

Fig. 3.19. Broadside crushing loads of ship side vs. various ship lengths.

In this thesis, we develop further the simplified method, which is also known as *limit analysis*, for ship collision analyses.

3.2   Foundation of the Simplified Method

3.2.1   Basic Theorems

The simplified method (or the limit analysis) is widely used in engineering analysis and design. It has been proved that the method is valuable for estimating the collapse load of a structure subject to extreme loads. The collapse load so obtained can be used as a realistic basis for design. It should be emphasised that the limit analysis is an approximate method. In order to describe the theory, we first give some related theorems. A basic assumption is that the material is perfectly plastic without strain hardening or softening.

The Virtual Work Principle

The virtual work principle can be expressed in the following formula:

$$\int_A F_i u_i \, dA + \int_V T_i u_i \, dV = \int_V \sigma_{ij} \varepsilon_{ij} \, dV$$

where A is the whole surface area, V is the volume of the structure, F_i and T_i are the external force and the body force respectively, σ_{ij} is any set of stresses, ε_{ij} is the strain field, u_i is the displacement. The rate form of the virtual work equation is

$$\int_A F_i \dot{u}_i \, dA + \int_V T_i \dot{u}_i \, dV = \int_V \sigma_{ij} \dot{\varepsilon}_{ij} \, dV$$

Lower-bound Theorem

If any system of generalised stresses can be found throughout a structure which is in equilibrium with the applied loads and which nowhere violates the yield condition, then the structure will not collapse or be at the point of collapse.

Upper-bound Theorem

If the work rate of a system of applied loads during any kinematically admissible collapse of the structure is equated to the corresponding internal energy dissipation rate, then the system of loads will cause collapse or be at the point of collapse.

Using the principle of virtual work we can prove the lower-bound and upper-bound theorems.

The two bound theorems can be used independently. If the calculated loads coincide in the two methods, the exact solution is found. But for large complex structures, it is very

difficult to find an exact solution. In this thesis we use the upper bound theorem to analyse the structural damage in ship collisions.

The upper-bound method was used by Wierzbicki (1983, 1993) for axial crushing of plate intersections and plate cutting, by Abramowicz (1994) and Amdahl (1983) for axial crushing of $L-$, $T-$ and $X-$ type elements, by Kierkegaard (1993) for ship bow crushing, by Paik and Pedersen (1995) for plate element crushing, and by Simonsen (1997) for ship grounding. In the MIT - Industry Joint Program on Tanker Safety was applied the method thoroughly to analysis of the damage of ship grounding. It was shown that the theoretical results are quite close to experimental results.

3.2.2 Formulation of the Upper-bound Method

The equilibrium for the external energy rate and the internal energy dissipation rate can be expressed as

$$F \cdot \dot{\delta} = \dot{E}_{\text{int}} \tag{3.1}$$

where F is the external force, $\dot{\delta}$ is the velocity at the force action point, $\dot{E}_{\text{int}}$ is the internal energy rate.

For a general solid body, the internal energy rate $\dot{E}_{\text{int}}$ can be expressed as

$$\dot{E}_{\text{int}} = \int_V \sigma_{ij} \dot{\varepsilon}_{ij} \, dV \tag{3.2}$$

where $\dot{\varepsilon}_{ij}$ is the rate of the strain tensor, V is the volume of the solid body. By use of von Mises' flow theory, the rate of plastic energy dissipation is given as

$$\dot{E}_{\text{int}} = \int_V \sigma_0 \dot{\varepsilon}_e \, dV \tag{3.3}$$

where $\dot{\varepsilon}_e = \sqrt{\frac{2}{3}(\dot{\varepsilon}_{ij} \dot{\varepsilon}_{ij})}$ and σ_0 is the flow stress.

For a plane stress condition, the von Mises yield condition gives

$$\sigma_{xx}^2 + \sigma_{yy}^2 - \sigma_{xx}\sigma_{yy} + 3\sigma_{xy}^2 = \sigma_0^2 \tag{3.4}$$

For a deforming plate, the rate of internal plastic energy dissipation can be written as the sum of the bending and the membrane energy dissipation rate:

$$\dot{E}_{\text{int}} = \dot{E}_b + \dot{E}_m \tag{3.5}$$

The bending energy rate can be expressed as

$$\dot{E}_b = \int_A M_{\alpha\beta}\, \dot{k}_{\alpha\beta}\, dA + \sum_{i=1}^{n} M_{0i}\, \dot{\theta}_i\, l_i,\ \ (\alpha,\beta=1,2) \tag{3.6}$$

where A is the plate area, $k_{\alpha\beta}$ is the curvature of the plating, and θ_i and l_i are the rotation and the length of the *ith* plastic hinge line, respectively. $M_{\alpha\beta}$ is the bending moment tensor, M_0 is the fully plastic bending moment $M_0 = (2/\sqrt{3})(\sigma_0^2 t/4)$, and t is the plate thickness. It is seen from the expression that the bending energy contains the continuous deformation field and the plastic hinge lines. In some practical applications, simplified velocity fields are assumed so that only the plastic hinge lines are considered and the continuous deformation of the curvature is neglected. In this case the bending energy is simplified as

$$\dot{E}_b = \sum_{i=1}^{n} M_{0i}\, \dot{\theta}_i\, l_i \tag{3.7}$$

The membrane energy rate of a deforming plate can be calculated from

$$\dot{E}_m = \int_A N_{\alpha\beta}\, \dot{\varepsilon}_{\alpha\beta}\, dA,\ \ (\alpha,\beta=1,2) \tag{3.8}$$

where $N_{\alpha\beta}$ is the membrane force tensor, $\dot{\varepsilon}_{\alpha\beta}$ is the strain rate tensor. By use of von Mises' yield criterion, the membrane energy rate can be expressed as

$$\dot{E}_m = \frac{2}{\sqrt{3}}\sigma_0 t \int_A \sqrt{\dot{\varepsilon}_{xx}^2 + \dot{\varepsilon}_{yy}^2 + \dot{\varepsilon}_{xx}\,\dot{\varepsilon}_{yy} + \dot{\varepsilon}_{xy}^2}\ \ dxdy \tag{3.9}$$

In the limit analysis method, a key point is the construction of a kinematically admissible velocity and displacement field. This is mainly based on observations from experimental tests, full-scale accidents and existing analysis work.

3.2.3 Material Strain-Rate Sensitivity

It is well known that the yield stress for mild steel is very sensitive to the strain rate. Fig. 3.20 shows an example of a stress-strain curve of hot rolled mild steel at various strain rates (Jones, 1989). This figure indicates that the yield stress of mild steel increases with

increasing strain rates. On the other hand, as Jones mentioned, aluminium is essentially insensitive to strain rate at the strain rates normally encountered in practice.
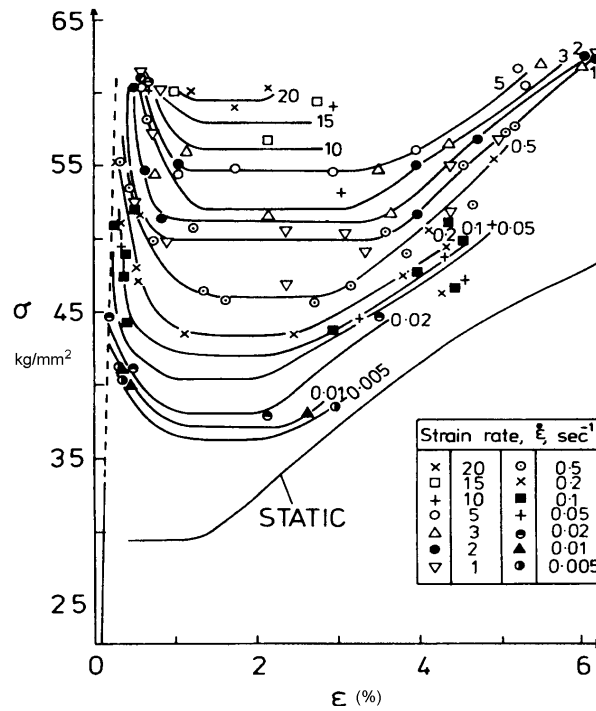

Fig. 3.20. Stress-strain curves for mild steel at various strain rates (Jones, 1989).

The strain rate effect is often described by Cowper-Symonds' empirical formula (Jones (1989):

$$\frac{\sigma_0^{\ d}}{\sigma_0} = 1 + (\frac{\dot\varepsilon}{C})^{\frac{1}{p}} \tag{3.10}$$

where $\sigma_0^{\ d}$ is the dynamic flow stress, σ_0 is the static flow stress, C and p are constants. For mild steel, $C = 40.4 s^{-1}$ and $p = 5$ may provide reasonable estimation of the dynamic flow stress. A comparison between the empirical formula with $C = 40.4 s^{-1}$, $p = 5$ and experimental results for mild steel is shown in Fig. 3.21 (Jones, 1989).

It is very complex to consider the effect of strain rate exactly in ship collisions. In this thesis, the strain rate effect is neglected. We simply use the mean value of the static yield stress σ_y and the static ultimate stress σ_u as the flow stress. That is

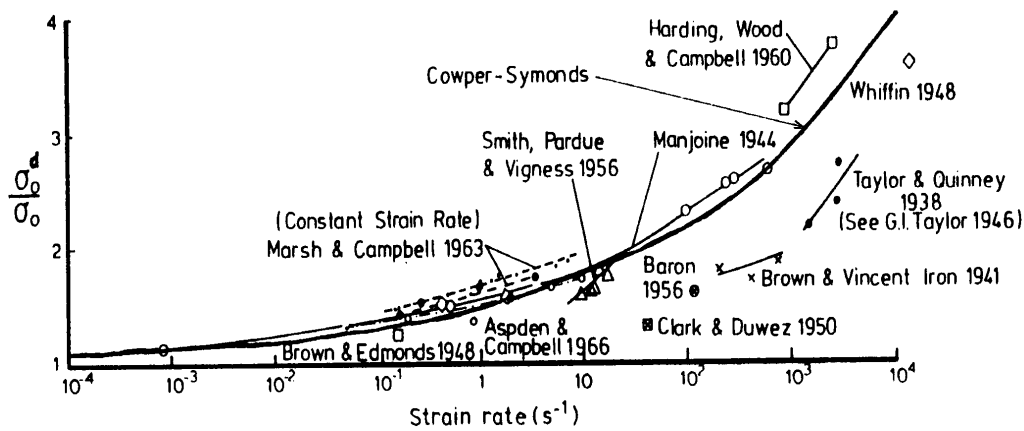$$\sigma_0 = \frac{1}{2}(\sigma_y + \sigma_u) \tag{3.11}$$

Fig. 3.21. Comparison between Cowper-Symonds' empirical relation (with $C = 40.4s^{-1}$, $p = 5$) and experimental results (Jones, 1989).

3.2.4 Rupture of Structures

When a structure has been deformed enough, it will rupture and be exposed to failure. It is an extremely complex problem to predict the rupture of structures accurately. Different loads may cause different failure modes. Jones et al. (1993) discussed the rupture criteria of ductile metal beams subjected to large dynamic loads. Three major failure criteria of the metal beams were discussed. The first is the **tensile tearing** failure mode, which is when the maximum strain equals the critical rupture strain of the material, and the beam ruptures. Thus

$$\varepsilon_{\max} = \varepsilon_c \tag{3.12}$$

The second failure model is the **transverse shear failure** mode which develops in a beam when large transverse shear deformations occur within a very short region of the plastic beam. When the total transverse shear displacement W_s in a particular location equals a critical value, the beam ruptures. The simple formula is

$$W_s = kH \tag{3.13}$$

where H is the beam thickness and k is a constant ($0 < k \leq 1.0$).

The third failure criterion is the **energy density failure** mode. It is assumed that rupture occurs in a rigid-plastic structure when the absorption of plastic work per unit volume reaches the critical value Θ_c:

$$\Theta = \Theta_c \qquad\qquad\qquad (3.14)$$

As Simonsen (1997) mentioned, the simplified methods are based on overall deformation mechanisms. It is not possible to trace the strain history of material elements at a very detailed level. Therefore, as many authors did, e.g. Wang (1996) and Paik and Pedersen (1995), we use the maximum strain failure criteria in this thesis. That is when the maximum strain in a structure reaches a critical strain, the structure ruptures.

In practical calculations, we need to know the critical strain of a material to predict the structural failure. Generally, this depends on axial tensile experiments. A typical stress-strain curve for mild steel is shown in Fig. 3.22.
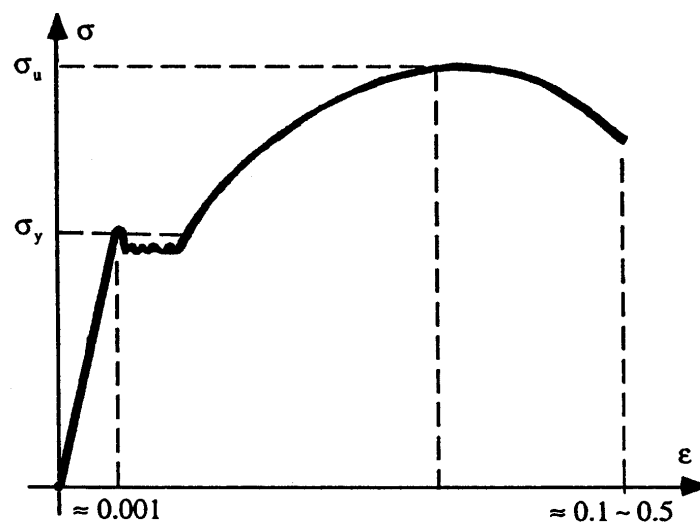

Fig. 3.22. A typical stress-strain curve of a mild steel.

Experiments conducted by Wen and Jones (1993) and Amdahl (1992) showed that the tensile ductility of mild steel is in the range of 0.20 to 0.35. Amdahl (1995) pointed out that due to scale effects and material imperfections, this value is far too large in the assessment of full-scale collisions. The critical strain value suggested (Amdahl, 1995) for side collisions is between 5% to 10%.

In the minor collision analyses performed by McDermott et al. (1974), the critical rupture strain for mild steel material in side collisions is evaluated from

$$\varepsilon_c = 0.10 \cdot \left(\frac{\varepsilon_f}{0.32}\right) \qquad\qquad\qquad (3.15)$$

where ε_f is the tensile ductility. It has been indicated by McDermott et al. that this formula may give reasonable agreement with experimental results in the deformation of

shell plating. So in this thesis, we either use McDermott's formula, if the tensile ductility of the material is known, or assume a value (say $\varepsilon_c = 5\% \sim 10\%$ for mild steel) for the critical rupture strain in side collisions.

When the critical rupture strain is known, the critical deflection or penetration of the shell plating can be determined. For example, a point load acting in the middle of a plate strip with a span of $2b$, as shown in Fig. 3.23. In this case, the strain in the plate strip due to transverse deflection can be calculated from

$$\varepsilon = \sqrt{1 + (\frac{\delta}{b})^2} - 1 \approx \frac{1}{2}(\frac{\delta}{b})^2 \qquad (3.16)$$

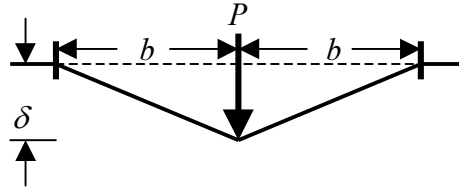where δ is the deflection at the middle point.

Fig. 3.23. Transverse deflection of a plate strip.

When the deflection is large enough, the strain in the plate strip reaches the critical rupture value. The critical rupture deflection or penetration is then determined from

$$\delta_c = b \cdot \sqrt{2\varepsilon_c} \qquad (3.17)$$

If the critical strain is $\varepsilon_c = 10\%$, then the critical penetration is $\delta_c = 0.447b$.

3.3   Collision Scenarios and Assumed Striking Bows

3.3.1   Collision Scenarios and Penetration Direction

A general scenario of a ship-ship collision is presented in Fig. 3.24. When a rigid striking ship with a forward speed of V_1 impacts against a struck ship with a forward speed of V_2 at an angle β, the penetration angle of the striking bow into the struck ship is not equal to the collision angle β if the forward speed of the struck ship is not zero. It will follow the direction of the relative velocity $\vec{V} = \vec{V}_1 - \vec{V}_2$ as shown in the following.

In Section 2.1, we derived the expressions (2.16) and (2.17) for the relative accelerations of the striking ship and the struck ship at a contact point, which are components of the relative accelerations in the perpendicular direction ξ and in the parallel direction η to the struck ship:

$$\ddot{\xi} = -(D_\xi + \mu D_\eta)F_\xi$$

$$\ddot{\eta} = -(\frac{1}{\mu}K_\xi + K_\eta)F_\eta$$

It is assumed that the acceleration or the collision force has a sinus function of time. This assumption is based on the experiment of the Dutch-Japanese full-scale ship collisions (Vredeveldt, 1992). The test results of the force-time relation and the assumed sinus curve are shown in Fig. 3.25.

Thus, the relative acceleration of the two ships at the impact point can be expressed as

$$\ddot{\xi} = A_1 \sin(\omega \cdot t)$$

$$\ddot{\eta} = A_2 \sin(\omega \cdot t)$$

where A_1 and A_2 are constants to be determined by the initial conditions, ω is the frequency and t is time. Thus, the relative velocity and the relative penetration are expressed by

$$\dot{\xi} = -\frac{A_1}{\omega}\cos(\omega \cdot t) + B_1$$

$$\dot{\eta} = -\frac{A_2}{\omega}\cos(\omega \cdot t) + B_2$$

and

$$\xi = -\frac{A_1}{\omega^2}\sin(\omega \cdot t) + B_1 t + C_1$$

$$\eta = -\frac{A_2}{\omega^2}\sin(\omega \cdot t) + B_2 t + C_2$$

At the beginning of a collision, $t = 0$, the initial penetration is zero and the relative velocity can be determined from the ship forward speeds V and V_2. At the end of the collision, $t = t_\Delta$, the relative velocity is equal to zero. The conditions are expressed as
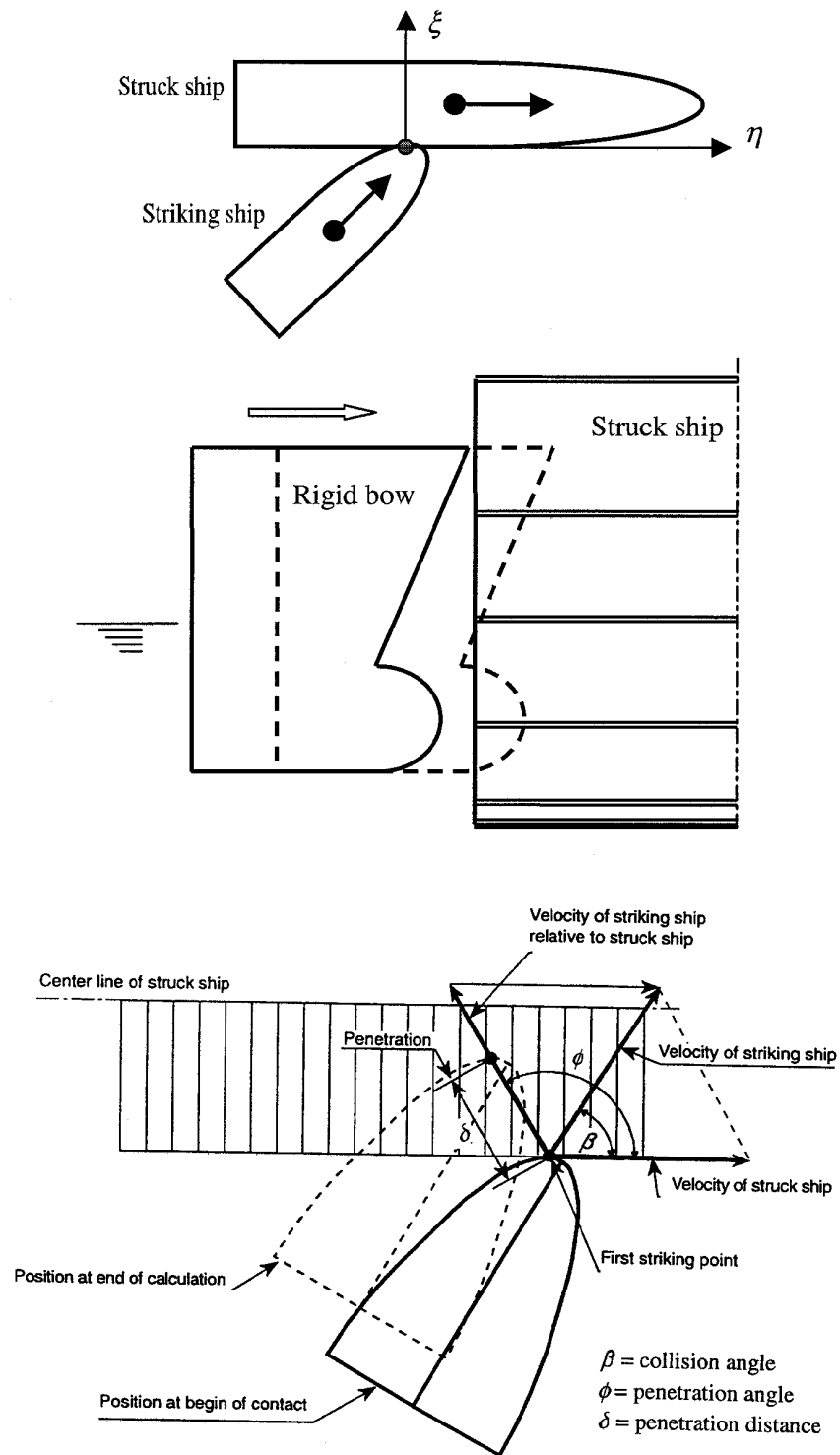
Fig. 3.24. General scenario of ship-ship collision and penetration direction.
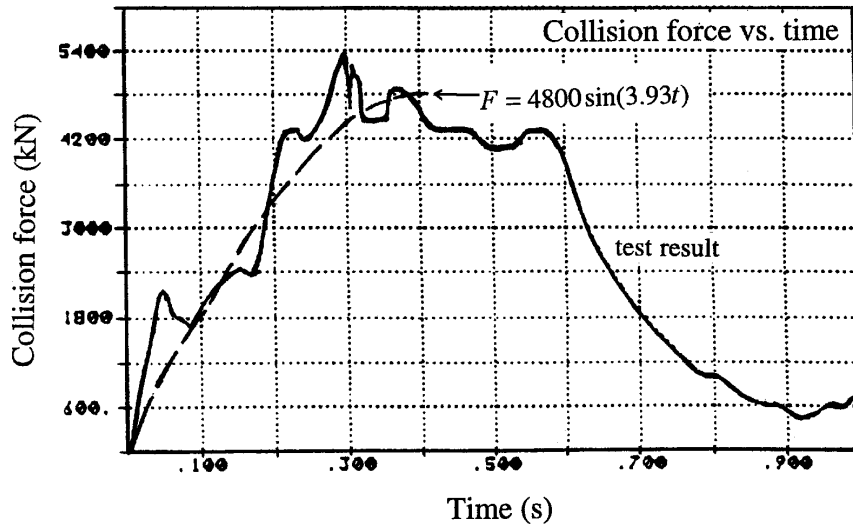
Fig. 3.25. Force-time relation from a full-scale ship collision experiment (Vredeveldt, 1992) and the assumed sinus curve for the force-time relation.

- when $t = 0$:

$$\dot{\xi}(0) = V_1 \sin \beta \,,$$

$$\dot{\eta}(0) = V_1 \cos \beta - V_2$$

$$\xi(0) = 0$$

$$\eta(0) = 0$$

- when $t = t_\Delta$:

$$\dot{\xi}(t_\Delta) = 0$$

$$\dot{\eta}(t_\Delta) = 0$$

where $t_\Delta = \dfrac{1}{4} \cdot \dfrac{2\pi}{\omega} = \dfrac{\pi}{2\omega}$ is the collision duration.

By use of the above-mentioned conditions, the relative acceleration, the relative velocity and the penetration are finally expressed as

$$\ddot{\xi} = -\frac{\pi}{2t_\Delta} \dot{\xi}(0) \sin(\frac{\pi}{2t_\Delta} \cdot t)$$

$$\ddot{\eta} = -\frac{\pi}{2t_\Delta} \dot{\eta}(0) \sin(\frac{\pi}{2t_\Delta} \cdot t)$$

(3.18)

$$\dot{\xi} = \dot{\xi}(0)\cos(\frac{\pi}{2t_\Delta} \cdot t)$$

$$\dot{\eta} = \dot{\eta}(0)\cos(\frac{\pi}{2t_\Delta} \cdot t)$$

(3.19)

and

$$\xi = \frac{2t_\Delta}{\pi}\dot{\xi}(0)\sin(\frac{\pi}{2t_\Delta} \cdot t)$$

$$\eta = \frac{2t_\Delta}{\pi}\dot{\eta}(0)\sin(\frac{\pi}{2t_\Delta} \cdot t)$$

(3.20)

The penetration angle ϕ, defined as an angle between the penetration direction and the forward direction of the struck ship, can be determined by

$$\tan\phi = \frac{\dot{\xi}}{\dot{\eta}} = \frac{\dot{\xi}(0)}{\dot{\eta}(0)} = \frac{V_1\sin\beta}{V_1\cos\beta - V_2}$$

(3.21)

Eq. (3.21) shows that the penetration direction follows the direction of the relative velocity $\vec{V} = \vec{V}_1 - \vec{V}_2$.

For special cases, the penetration angles are

- If the speed of struck ship is zero $V_2 = 0 \Rightarrow \phi = \beta$

  (3.22)

- If the speeds of two ships are equal $V_1 = V_2 \Rightarrow \phi = 90^0 + \beta/2$.

3.3.2 Assumed Striking Bows

Ship bows vary in size and shape. It seems very difficult to simulate striking bows by simple models. Therefore, some reasonable assumptions must be provided.

The category of different ships can be divided into nine groups based on Pedersen, Hansen and Nielsen (1996):

(1) Tankers
(2) Bulk carriers
(3) Chemical tankers
(4) Gas tankers
(5) Container vessels
(6) Passenger vessels

(7) Fishery vessels
(8) Navy vessels
(9) Others

Statistics showed (Nielsen, 1995) that about 40%~50% of all the above-mentioned ships have bulbous bows and the others have conventional bows. Therefore, in this thesis, two types of striking bows are assumed. One is the **conventional bow** and the other is the **bulbous bow**.

Conventional Striking Bows

A photo of a typical conventional bow and a simplified conventional bow are presented in Fig. 3.26. The basic data for describing the assumed conventional bow is

- θ = Half angle of the bow
- φ = Stem angle (raked angle)
- H_{deck} = Uppermost deck height
- B = Breadth of the ship

An analysis of the world fleet by Reardon and Sprung (1996) indicates that the half bow angle θ and the stem angle φ of four principal types of ships are

- $\theta = 28 \sim 38$ degrees and $\varphi = 74$ degrees for tankers and bulk carriers
- $\theta = 20$ degrees and $\varphi = 76$ degrees for general cargo ships
- $\theta = 17$ degrees and $\varphi = 63$ degrees for container vessels
- $\theta = 17$ degrees and $\varphi = 54$ degrees for passenger vessels

Fig. 3.27 shows the geometric sections of the assumed conventional bow. The formulas for describing the geometric relation can be expressed as

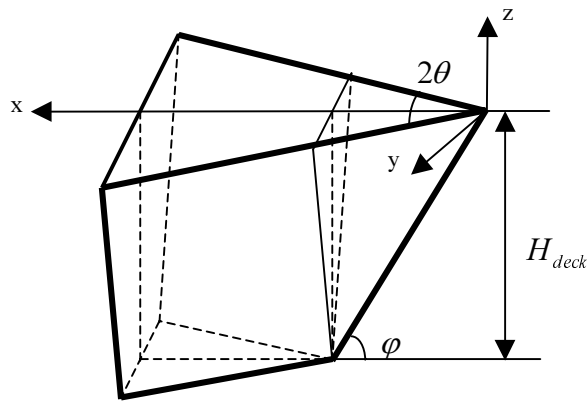- when the penetration $\delta \leq \delta_0 = \dfrac{H_{deck}}{\tan \varphi}$

$$\begin{aligned} Y_{d1} &= \delta \tan \theta \\ Z_d &= \delta \tan \varphi \end{aligned}$$

(3.23)

- when the penetration $\delta > \delta_0 = \dfrac{H_{deck}}{\tan \varphi}$

$$\begin{aligned} Y_{d1} &= \delta \tan \theta, \text{ if } Y_{d1} \geq B/2 \text{ then } Y_{d1} = B/2 \\ Y_{d2} &= (\delta - \delta \ ) \tan \theta, \text{ if } Y_{d2} \geq B/2 \text{ then } Y_{d2} = B/2 \\ Z_d &= H_{deck} \end{aligned}$$

(3.24)

Photo of a conventional bow

The assumed conventional bow

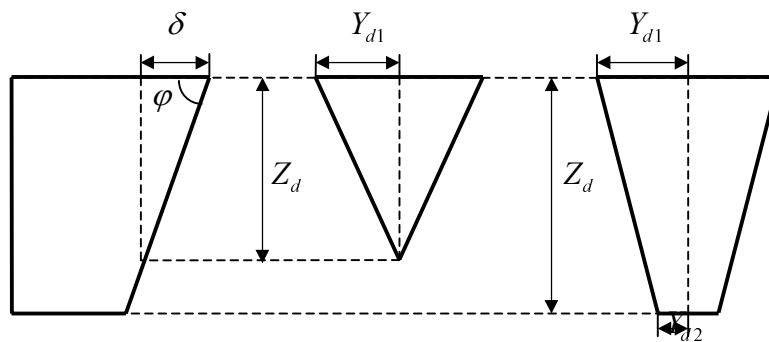*Fig. 3.26. A typical photo and assumed shape of a conventional bow.*

Fig. 3.27. Sectional geometry of the assumed conventional bow.

Bulbous Striking Bows

Today more and more bulbous bows are used in modern seagoing merchant vessels. As a model comparative experiments show that a ship with a bulbous bow requires far less propulsive power and has significantly better resistance characteristics than the same ship without bulbous bow (Schneekluth, 1987).

A picture of a bulbous bow and the present simplified model of a bulbous bow are presented in Fig. 3.28.
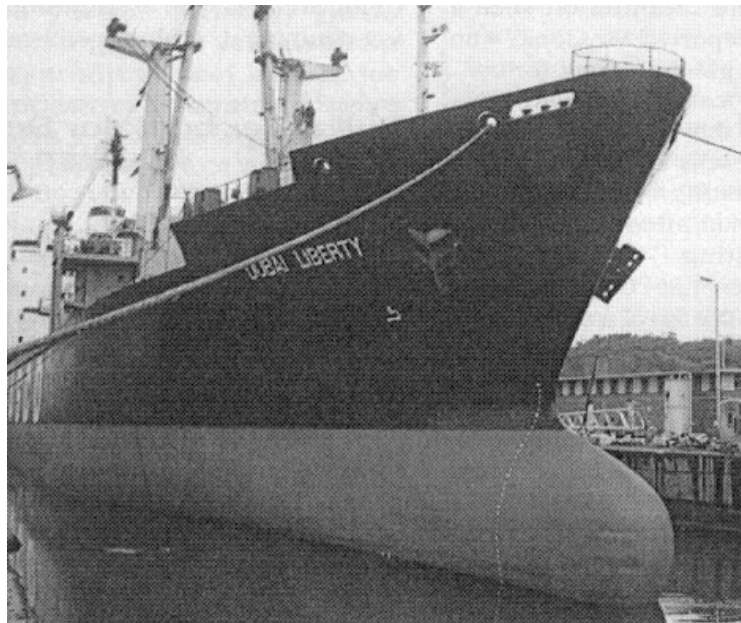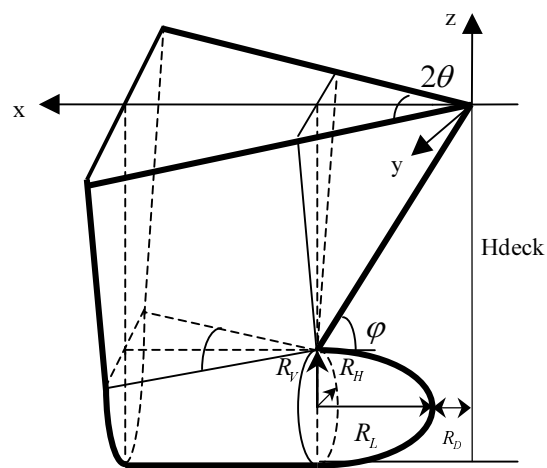

Photo of a bulbous bow

Assumed bulbous bow

Fig. 3.28. A typical photo and assumed shape of a bulbous bow.

The basic data for describing the assumed bulbous bow is as follows:

- θ = Half angle of bow
- φ = Stem angle
- H_{deck} = Uppermost deck height
- B = Breadth of the ship

and

- R_L = Bulb length
- R_V = Vertical radius of the bulb
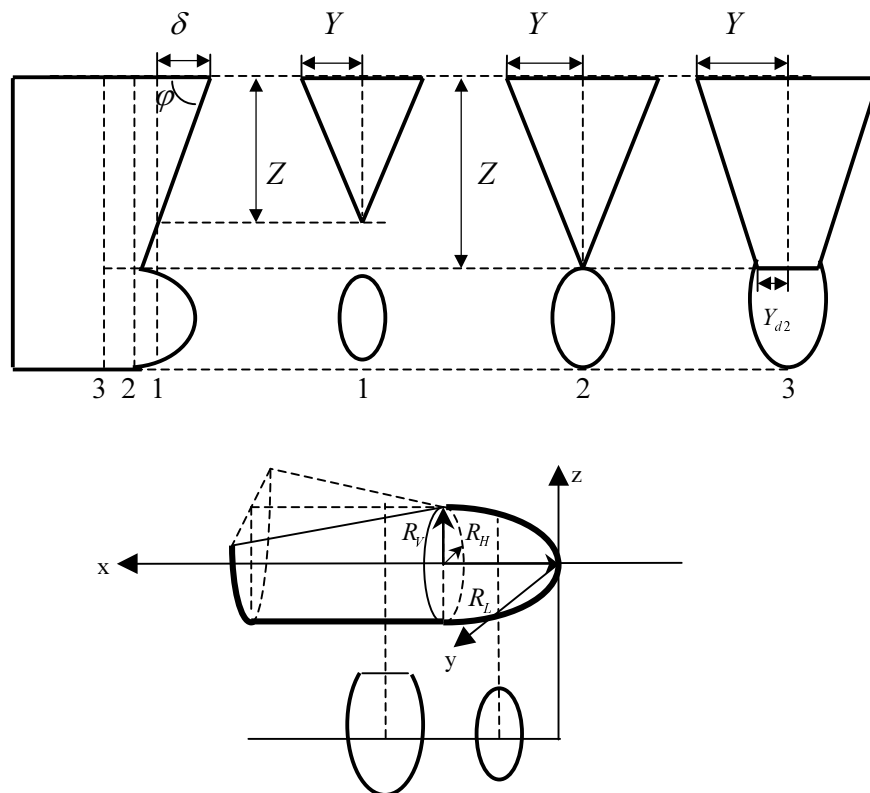- R_H = Horizontal radius of the bulb

Fig. 3.29. Sectional geometry of the assumed bulbous bow.

The detailed geometry of any section of the assumed bulbous bow is presented in Fig. 3.29. The bulbous bow can be divided into two parts, one is the upper part which is similar to the above-mentioned conventional bow, and the other is the lower-part bulb. We assume that the bulb has the form of an elliptic paraboloid. The three radii of the bulb are assumed to be proportioned to the height (H) of the uppermost deck. These can be expressed as

$$R_L = \lambda_L \cdot H_{deck}$$
$$R_V = \lambda_V \cdot H_{deck} \qquad (3.25)$$
$$R_H = \lambda_H \cdot H_{deck}$$

where λ_L, λ_V and λ_H are constant factors. Based on statistics of existing ships and the design guidelines for bulbs, reasonable values for the factors are

$$\lambda_L = 0.300$$
$$\lambda_V = 0.125 \qquad (3.26)$$
$$\lambda_H = 0.050$$

The distance R_D, between the bulb tip and the forward perpendicular, can be calculated from

$$R_D = \frac{H_{deck} - 2R_V}{\tan \varphi} - R_L \qquad (3.27)$$

For example, if the stem angle is $\varphi = 60°$ and by means of the data in Eq. (3.26), the distance R_D becomes

$$R_D = \frac{H_{deck} - 0.25H_{deck}}{\tan 60^0} - 0.3H_{deck} = 0.133H_{deck}$$

In order to describe the bulb, an xyz-coordinate is used as shown in Fig. 3.29. If a transformation $x = \delta - R_D$ is used, the formulas for describing the bulb can be written as follows:

- When $x \leq R_L$:

$$\frac{y^2}{R_H^{\ 2}} + \frac{z^2}{R_V^{\ 2}} = \frac{x}{R_L} \qquad (3.28)$$

In the xz-plane ($y = 0$), the equation becomes

$$\frac{z^2}{R_V^{\ 2}} = \frac{x}{R_L} \Rightarrow: z = \sqrt{\frac{x}{R_L}} \cdot R_V \qquad (3.29)$$

In the xy-plane ($z = 0$), the equation becomes

$$\frac{y^2}{R_H^{\ 2}} = \frac{x}{R_L} \Rightarrow: y = \sqrt{\frac{x}{R_L}} \cdot R_H \qquad (3.30)$$

- When $x > R_L$:

In the xz -plane ($y = 0$), the approximation is

$$z = R_V \tag{3.31}$$

In the xy -plane ($z = 0$), the equation becomes

$$\frac{y^2}{R^2} = \frac{x}{R} \Rightarrow : \; y = \sqrt{\frac{x}{R_L}} \cdot R_H \text{, and if } y \geq B/2 \text{ then } y = B/2 \tag{3.32}$$

Based on the present assumption, four parameters ($\theta, \varphi, H_{deck}$ and B) are important to the determination of the detailed geometric data of striking bows. For a given ship, these parameters may be known. But for statistical analyses, a large number of striking ships are involved in the calculations. In this case we do not have the exact scantlings of the striking ships. So we would like to use one parameter, such as the ship length, to determine the ship breadth and the forecastle deck height approximately. Unfortunately, there are not such formulas. But, based on a large number of existing ships (Nielsen, 1995; LR, 1996-97) we have found approximate data for the relations between the parameters, as shown in Table 3.1.

Table 3.1. Relationships for length, breadth, depth and height of the forecastle deck.

	Tankers	Bulk carriers	Chemical tankers	Gas tankers	Container ships	Passenger ships
L / B	5.5~7.5	5.0~8.0	5.5~7.5	5.5~7.0	5.5~9.0	5.5~8.0
L / D	10.0~14.0	10.0~14.0	10.0~14.0	10.5~12.5	10.0~13.5	10.0~25.0
H_{deck} / B	0.55~0.65	0.65~0.80	0.60~0.75	0.60~0.85	0.70~0.80	0.70~0.80

* L=length, B=breadth, D=depth and H$_{deck}$=forecastle deck height.

Based on the statistics of optimisation results according to economic criteria, Schneekluth (1987) gave the following formula for determining the ship length:

$$L = C \cdot \nabla^{0.3} V^{0.3} \tag{3.33}$$

where
$L =$ length between perpendiculars
$\nabla =$ displacement in tonnes
$V =$ speed in knots
$C = 3.2$, if the block coefficient has the approximate value of $C_B = 0.145 / F_n$ within the range of 0.48~0.85, where $F_n =$ Froude number.

3.4   Deformation of Side Shell Plating

When a rigid striking bow collides with a struck ship, the side structure of the struck ship will be deformed, destroyed or penetrated. The deformation and damage to the struck ship may include tension of the shell plating, crushing of the transverse frames and the longitudinal stringers, and crushing of the decks and the bottom. By calculating the resistance of each component and adding all the resistance, the total resistance and dissipated energy can be determined. Fig. 3.30 shows an initial deformation of a side shell plating. In the following, side shell deformation will be studied.
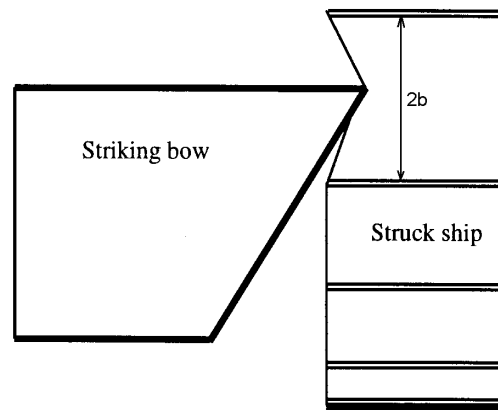

Fig. 3.30. A rigid bow strikes a side structure.

3.4.1   Shell Plate Subjected to a Lateral Point Load

First, we consider a case where a striking bow impacts the centre of a shell plate with boundaries at the adjacent decks and transverse frames. The distance between the two decks is $2b$, the spacing between the transverse frames is $2a$, and the thickness of the shell plate is t_p. The plate may suffer bending, shearing and tension deformations. With the increase of the transverse deformation, the relative contribution of the bending force becomes weaker and weaker and can be neglected. The membrane forces dominate the behaviour of the deformation. Therefore, the bending resistance is neglected and only the moderate large normal deflection of the shell plate is considered. The $xyz-$coordinate for shell plate is presented in Fig. 3.31. The following function is used as the deformation of the shell plate:

$$w(x, y, t) = \delta(t) \cdot f(x, y) \tag{3.34}$$

where $\delta(t)$ is the time-dependent deflection at the centre of the plate and $f(x, y)$ is the deformation function.
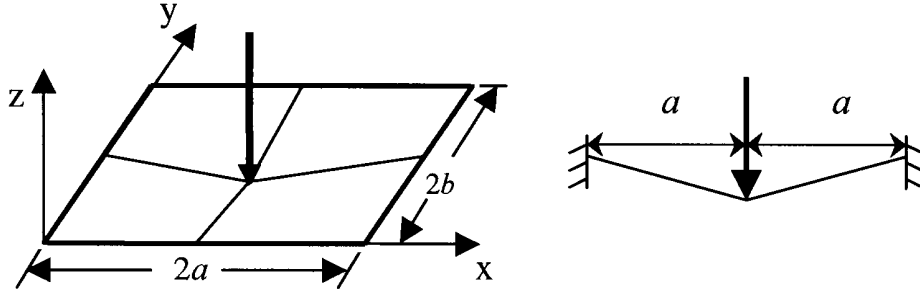
Fig. 3.31. Deformation of a rectangular plate subjected to a point load at its centre.

By Eq. (3.34), the non-linear strain and strain rate in the plate can be expressed as

$$\varepsilon_{xx} = \frac{1}{2}(\frac{\partial w}{\partial x})^2 = \frac{1}{2}\delta^2(\frac{\partial f}{\partial x})^2$$

$$\varepsilon_{yy} = \frac{1}{2}(\frac{\partial w}{\partial y})^2 = \frac{1}{2}\delta^2(\frac{\partial f}{\partial y})^2 \tag{3.35}$$

$$\varepsilon_{xy} = \frac{1}{2}\frac{\partial w}{\partial x}\frac{\partial w}{\partial y} = \frac{1}{2}\delta^2\frac{\partial f}{\partial x}\frac{\partial f}{\partial y}$$

and

$$\dot{\varepsilon}_{xx} = \delta\dot{\delta}(\frac{\partial f}{\partial x})^2$$

$$\dot{\varepsilon}_{yy} = \delta\dot{\delta}(\frac{\partial f}{\partial y})^2 \tag{3.36}$$

$$\dot{\varepsilon}_{xy} = \delta\dot{\delta}\frac{\partial f}{\partial x}\frac{\partial f}{\partial y}$$

The equilibrium equation of the rate of external work and the rate of internal energy dissipation can be expressed as

$$F_p \cdot \dot{\delta} = \frac{2}{\sqrt{3}}\sigma_0 t_p \iint_A (\dot{\varepsilon}_{xx}^2 + \dot{\varepsilon}_{yy}^2 + \dot{\varepsilon}_{xx}\dot{\varepsilon}_{yy} + \dot{\varepsilon}_{xy}^2)^{\frac{1}{2}} dxdy \tag{3.37}$$

where A is the plate area and F_p is the resistance force. From Eqs. (3.35) and (3.36) we have

$$\dot{\varepsilon}_{xx}^2 + \dot{\varepsilon}_{yy}^2 + \dot{\varepsilon}_{xx}\dot{\varepsilon}_{yy} + \dot{\varepsilon}_{xy}^2 = (\delta\dot{\delta})^2[(\frac{\partial f}{\partial x})^2 + (\frac{\partial f}{\partial y})^2]^2 = (\dot{\varepsilon}_{xx} + \dot{\varepsilon}_{yy})^2$$

Then Eq. (3.37) becomes

$$F_p \cdot \dot{\delta} = \frac{2}{\sqrt{3}} \sigma_0 t_p \delta \dot{\delta} \cdot U$$

where

$$U = \iint_A [(\frac{\partial f}{\partial x})^2 + (\frac{\partial f}{\partial y})^2] dx dy \qquad (3.38)$$

Therefore, the relationship between the resistance force and the deflection can be expressed in the general form

$$F_p = \frac{2}{\sqrt{3}} \sigma_0 t_p \delta \cdot U$$

In order to calculate the collision resistance, the deformation function should be known. It is assumed that the following deformation function is used for one quarter of the plate:

$$f(x,y) = (\frac{x}{a})^n (\frac{y}{b})^n \quad , \quad n \geq 1$$

That is

$$\frac{\partial f}{\partial x} = \frac{n}{a}(\frac{x}{a})^{n-1}(\frac{y}{b})^n$$

$$\frac{\partial f}{\partial y} = \frac{n}{b}(\frac{x}{a})^n(\frac{y}{b})^{n-1}$$

Integrating Eq. (3.38), we have

$$U = \frac{4n^2}{4n^2 - 1}(\frac{b}{a} + \frac{a}{b})$$

So the force-deflection relationship is

$$F_p = \frac{2}{\sqrt{3}} \frac{4n^2}{4n^2 - 1} \sigma_0 t \delta(\frac{b}{a} + \frac{a}{b}) = C \cdot \sigma_0 t \delta(\frac{b}{a} + \frac{a}{b}) \qquad (3.39)$$

where

$$C = \frac{2}{\sqrt{3}} \frac{4n^2}{4n^2 - 1}$$

$$
\begin{array}{ll}
n=1 & C = 1.540 \\
n=2 & C = 1.232 \\
n=3 & C = 1.188 \\
\quad \cdots\cdots & \\
n=\infty & C = 1.155
\end{array}
$$

The energy-deflection relationship is

$$E = \int_0^\delta FdW = \frac{1}{\sqrt{3}} \frac{4n^2}{4n^2 - 1} \sigma_0 t \delta^2 (\frac{b}{a} + \frac{a}{b}) \tag{3.40}$$

It is seen from Eq. (3.39) that the effect of the power n of the deformation function $f(x, y)$ on the resistance is not strong. Observations from experiments and full-scale tests show that a linear function is a good approximation if the collision speed is low. For a high-speed impact, the approximation $n = 2$ is reasonable.

For n = 1, the relationship between the resistance and the deflection is

$$F_p = \frac{4}{3} \frac{2}{\sqrt{3}} \sigma_0 t_p \delta (\frac{b}{a} + \frac{a}{b}) = \frac{1}{3} \frac{2}{\sqrt{3}} \sigma_0 t_p A \delta (\frac{1}{a^2} + \frac{1}{b^2}) \tag{3.41}$$

where $A = 2a \cdot 2b$ is the area of the plate. This equation is similar to the one given by Wierzbicki and Simonsen (1996).

The energy absorbed by the plate in this case can be calculated from

$$E_p = \int_0^\delta F_p d\delta = \frac{1}{3} \frac{1}{\sqrt{3}} \sigma_0 t_p A \delta^2 (\frac{1}{a^2} + \frac{1}{b^2}) \tag{3.42}$$

When the impact position is not located at the centre of the shell plate, as shown in Fig. 3.32, we may follow the same procedure for deriving the force-deflection relationship and the energy-deflection relationship. The derived expressions are

$$F_p = \frac{2}{\sqrt{3}} \frac{n^2}{4n^2 - 1} \sigma_0 t_p A \delta (\frac{1}{a_1 a_2} + \frac{1}{b_1 b_2}) \tag{3.43}$$

$$E_p = \frac{1}{\sqrt{3}} \frac{n^2}{4n^2 - 1} \sigma_0 t_p A \delta^2 (\frac{1}{a_1 a_2} + \frac{1}{b_1 b_2}) \tag{3.44}$$
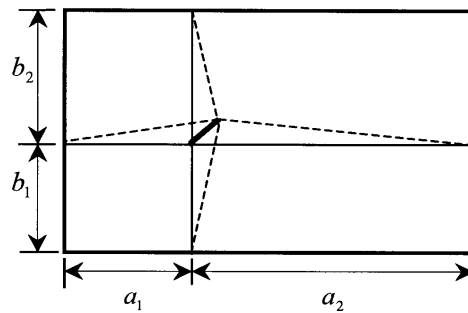

Fig. 3.32. Deformation of a rectangular plate subjected to an eccentric load.

The practical side shell is usually not a bare plate. It is often stiffened by longitudinals. In this case, the equivalent thickness method is employed to deal with the stiffeners. The idea of the equivalent method is to distribute the cross-sectional area of the stiffeners to the whole plate. That is

$$t_{eq} = t_p + A_s / d \tag{3.45}$$

where t_{eq} is the equivalent thickness of the stiffened plate, t_p is the thickness of the shell plate, A_s is the sectional area of the stiffener, and d is the stiffener spacing, as shown in Fig. 3.33.
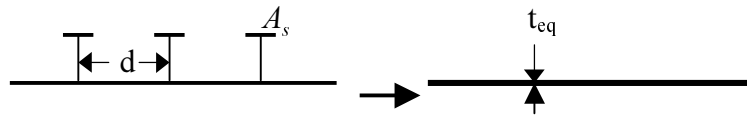

Fig. 3.33. Equivalent thickness of a stiffened plate.

For a stiffened panel, Eqs. (3.43) and (3.44) of the force-deflection relationship and the energy-deflection relationship become

$$F_p = \frac{2}{\sqrt{3}} \frac{n^2}{4n^2 - 1} \sigma_0 A \delta \left(\frac{t_{px}}{a_1 a_2} + \frac{t_{py}}{b_1 b_2} \right) \tag{3.46}$$

$$E_p = \frac{1}{\sqrt{3}} \frac{n^2}{4n^2 - 1} \sigma_0 t A \delta^2 \left(\frac{t_{px}}{a_1 a_2} + \frac{t_{py}}{b_1 b_2} \right) \tag{3.47}$$

where t_{px} and t_{py} are the equivalent thicknesses of the stiffened plate in the $x-$ and the $y-$ directions, respectively.

When the impact location is at the uppermost deck of the struck ship, as shown in Fig. 3.34, the force-deflection relationship and the energy-deflection relationship can be expressed as

$$F_p = \frac{2}{\sqrt{3}} \frac{n^2}{4n^2 - 1} \sigma_0 t_p A \delta \left(\frac{1}{a_1 a_2} + \frac{1}{(2b)(2b)} \right) \tag{3.48}$$

$$E_p = \frac{1}{\sqrt{3}} \frac{n^2}{4n^2 - 1} \sigma_0 t_p A \delta^2 \left(\frac{1}{a_1 a_2} + \frac{1}{(2b)(2b)} \right) \tag{3.49}$$
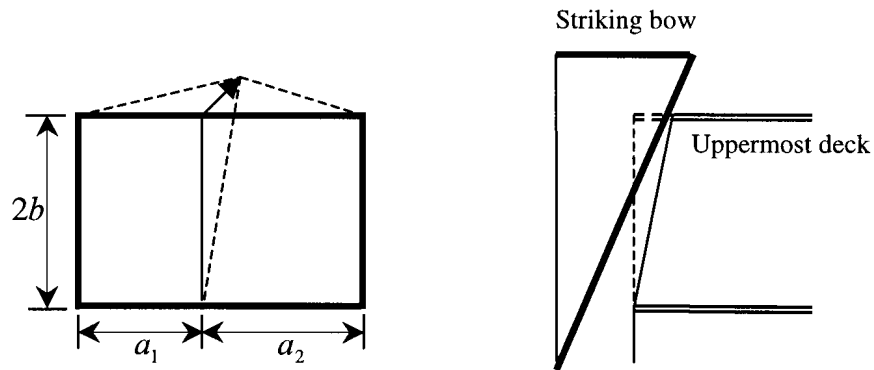
Fig. 3.34. Impact location at the uppermost deck of the struck ship.

3.4.2 Shell Plate Subjected to a Lateral Area Load

Central Impact

As shown in Fig. 3.35, a blunt object with a flat face (dimension $2a_0 * 2b_0$) hits perpendicularly the centre of a plate with the dimension $2a * 2b$. This situation may represent the case of dropped objects impacting decks.
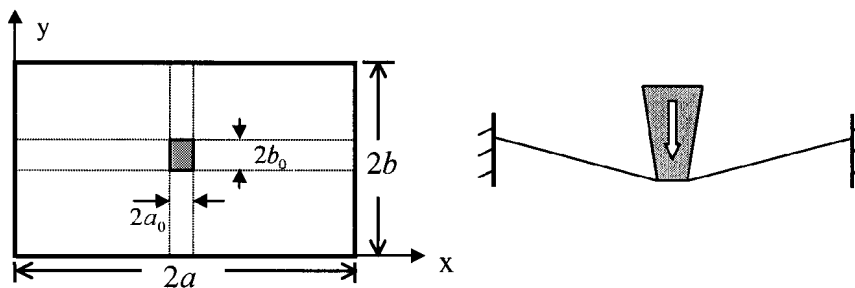

Fig. 3.35. Shell plate impacted by an object with rectangular impact section.

The derived formulas for the force-deflection relationship and the energy-deflection relationship of the blunt object impacting the centre of the plate are

$$F_p = \frac{2}{\sqrt{3}} \frac{4n^2}{4n^2 - 1} \sigma_0 t_p \delta \left(\frac{b - b_0}{a - a_0} + \frac{a - a_0}{b - b_0} \right)$$
$$+ \frac{2}{\sqrt{3}} \frac{4n^2}{2n - 1} \sigma_0 t_p \delta \left(\frac{b_0}{a - a_0} + \frac{a_0}{b - b_0} \right)$$

(3.50)

$$E_p = \frac{1}{\sqrt{3}}\frac{4n^2}{4n^2-1}\sigma_0 t_p \delta^2 (\frac{b-b_0}{a-a_0}+\frac{a-a_0}{b-b_0})$$

$$+\frac{1}{\sqrt{3}}\frac{4n^2}{2n-1}\sigma_0 t_p \delta^2 (\frac{b_0}{a-a_0}+\frac{a_0}{b-b_0})$$

(3.51)

If n =1, $2a = 2b$ and $2a_0 = 2b_0$, the force-deflection relationship and the energy-deflection relationship are simplified as

$$F_p = \frac{8}{3}\frac{2}{\sqrt{3}}\sigma_0 t_p \delta(1+\frac{3a_0}{a-a_0})$$

(3.52)

$$E_p = \frac{4}{3}\frac{2}{\sqrt{3}}\sigma_0 t_p \delta^2 (1+\frac{3a_0}{a-a_0})$$

(3.53)

Eccentric Impact

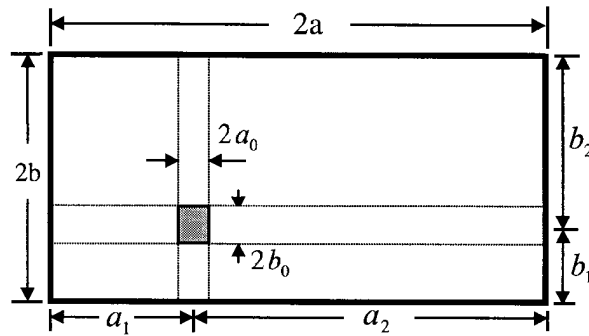Similarly, for the eccentric impact as shown in Fig. 3.36, the formulas are

Fig. 3.36. Shell plate impacted eccentrically by an object with rectangular section.

$$F_p = \frac{2}{\sqrt{3}}\frac{4n^2}{4n^2-1}\sigma_0 t_p \delta(\frac{(a-a_0)(b-b_0)}{(a-a_0)(a_2-a_0)}+\frac{(a-a_0)(b-b_0)}{(b-b_0)(b_2-b_0)})$$

$$+\frac{2}{\sqrt{3}}\frac{4n^2}{2n-1}\sigma_0 t_p \delta(\frac{(a-a_0)b_0}{(a-a_0)(a_2-a_0)}+\frac{a_0(b-b_0)}{(b-b_0)(b_2-b_0)})$$

(3.54)

$$E_p = \frac{1}{\sqrt{3}}\frac{4n^2}{4n^2-1}\sigma_0 t_p \delta^2 (\frac{(a-a_0)(b-b_0)}{(a_1-a_0)(a_2-a_0)}+\frac{(a-a_0)(b-b_0)}{(b_1-b_0)(b_2-b_0)})$$

$$+\frac{1}{\sqrt{3}}\frac{4n^2}{2n-1}\sigma_0 t_p \delta^2 (\frac{(a-a_0)b_0}{(a_1-a_0)(a_2-a_0)}+\frac{a_0(b-b_0)}{(b_1-b_0)(b_2-b_0)})$$

(3.55)

3.4.3 Plate Strip Subjected to a Lateral Line Load

As shown in Fig. 3.34, a plate strip impacted by an object deforms uniformly. The force-deflection relationship and the energy-deflection relationship can be easily determined by

$$F_p = \frac{2}{\sqrt{3}} \frac{n^2}{2n-1} \sigma_0 t_p \delta (\frac{2b}{a_1} + \frac{2b}{a_2}) \tag{3.56}$$

$$E_p = \frac{1}{\sqrt{3}} \frac{n^2}{2n-1} \sigma_0 t_p \delta^2 (\frac{2b}{a_1} + \frac{2b}{a_2}) \tag{3.57}$$
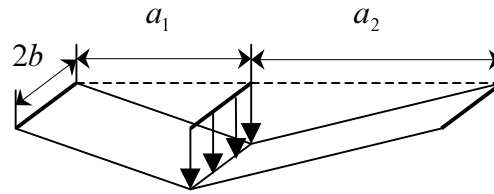

Fig. 3.37. Deformation of a plate strip subjected to a line load.

3.4.4 Circular Plate Subjected to Lateral Loads

An area load impacts the centre of a circular plate, such as a cylinder with a flat end hitting the centre of a circular plate, as shown in Fig. 3.38. The radius of the cylindrical impactor is a_0 and the radius of the circular plate is a. It is assumed that the deformation function is

$$f = (\frac{a-r}{a-a_0})^n$$

If n = 1, the force-deflection relationship and the energy-deflection relationship can be expressed as

$$F_p = \frac{2}{\sqrt{3}} \pi \sigma_0 t_p \delta (1 + \frac{2a_0}{a-a_0}) \tag{3.58}$$

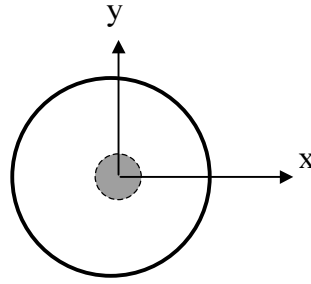$$E_p = \frac{2}{\sqrt{3}} \frac{\pi}{2} \sigma_0 t_p \delta^2 (1 + \frac{2a_0}{a-a_0}) \tag{3.59}$$

Fig. 3.38. Circular plate subjected to an area load at its centre.

If n = 2, the force-deflection relationship and the energy-deflection relationship are expressed as

$$F_p = \frac{2}{\sqrt{3}} \frac{2\pi}{3} \sigma_0 t_p \delta (1 + \frac{4a_0}{a - a_0}) \tag{3.60}$$

$$E_p = \frac{2}{\sqrt{3}} \frac{\pi}{3} \sigma_0 t_p \delta^2 (1 + \frac{4a_0}{a - a_0}) \tag{3.61}$$

3.4.5 Bulbous Bow Indenting into Shell Plating

Fig. 3.39 shows a bulb indenting into the side shell. In order to consider the effect of the radius of the bulb, a new formula will be developed. First, we analyse a bulb indenting into the centre of a circular plate, which is also shown in Fig. 3.39, then the formula is extended to the case of a rectangular plate.

In Section 3.3.2, the bulb was described as an elliptic paraboloid:

$$\frac{y^2}{R_H^2} + \frac{z^2}{R_V^2} = \frac{x}{R_L} \tag{3.62}$$

In order to simplify the analysis, we here further assume that the vertical radius R_V and the horizontal radius R_H of the bulb are equal, that is $R_V = R_H$. Thus, Eq. (3.62) becomes

$$\frac{x}{R_L} = \frac{y^2 + z^2}{R_V^2} = \frac{r^2}{R_V^2}$$

If the convenience, we take $w_b = x$, the expression for the bulb has a simple form:

$$w_b(r) = \frac{r^2}{R_b} \tag{3.63}$$
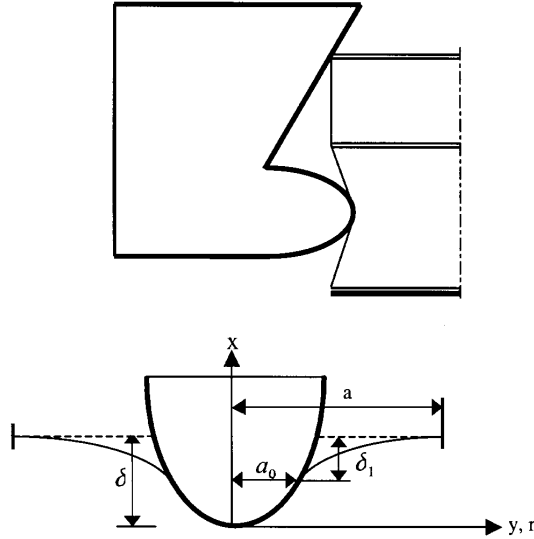
where $R_b = R_V{}^2 / R_L$.

Fig. 3.39. Bulbous bow striking a side structure and the assumed deformation.

Based on the observations from the experiments (see Fig. 3.40), the following appropriate function is used for the plate deformation:

$$w = \begin{cases} \delta_1 \cdot f_1(\delta_1, r, \theta) = \delta_1 \cdot (\dfrac{a-r}{a-a_0})^2, & a_0 \le r \le a \\[3mm] f_2(\delta, r, \theta) = \delta - \dfrac{r^2}{R_b}, & 0 \le r \le a_0 \end{cases} \tag{3.64}$$

where a is the radius of the plate, a_0 is the radius at the separating point between the bulb and the plate, δ is the deflection at the bulb tip and δ_1 is the deflection at the separating point.

The slopes at the separating point between the bulb and the plate are equal, which determines the separating radius a_0. That is

$$\frac{\partial w_b}{\partial r} = \frac{\partial w}{\partial r} \quad \Rightarrow \quad \frac{a_0}{R_b} = \frac{\delta_1}{a - a_0}$$
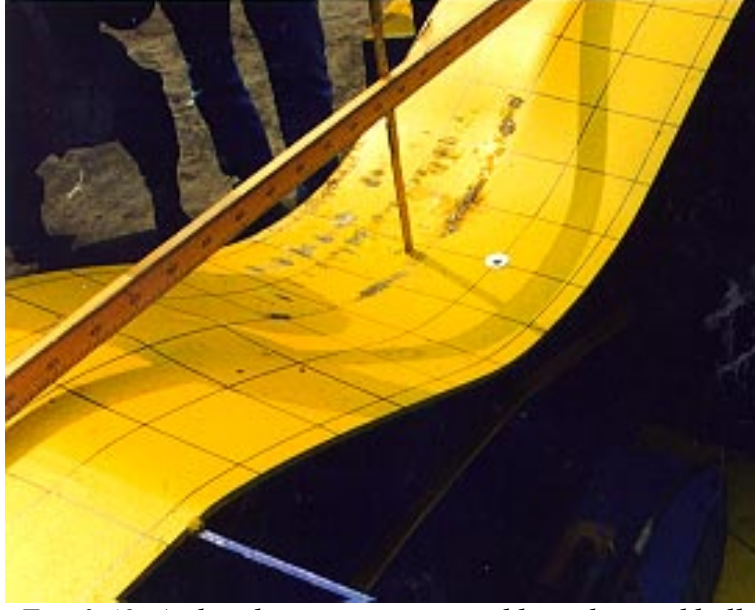
Fig. 3.40. A plated structure impacted by a dropped ball.

Then the separating radius is

$$a_0 = \frac{R_b}{a}\delta \qquad\qquad (3.65)$$

The deflection and the velocity at the separating point are expressed as

$$\delta_1 = \delta(1 - \frac{R_b\delta}{a^2})$$
$$\dot{\delta}_1 = \dot{\delta}(1 - \frac{2R_b\delta}{a^2}) \qquad\qquad (3.66)$$

The equilibrium of the external work rate and the internal energy dissipation rate is

$$F_p \cdot \dot{\delta} = \frac{2}{\sqrt{3}}\sigma_0 t[\iint\limits_{a_0 < r \le a}(\dot{\varepsilon}_{r1})r dr d\theta + \frac{\partial}{\partial T} \iint\limits_{0 \le r \le a_0}(\varepsilon_{r2})r dr d\theta]$$

where T is time. The strain and the strain rate are calculated from

$$\varepsilon_{r1} = \frac{1}{2}(\frac{\partial w}{\partial r})^2 = 2\delta_1^2\frac{(a-r)^2}{(a-a_0)^4}$$

$$\dot{\varepsilon}_{r1} = (\frac{4\delta_1\dot{\delta}_1}{(a-a_0)^4} + \frac{8\delta_1^2\dot{a}_0}{(a-a_0)^5})(a-r)^2$$

$$\varepsilon_{r2} = \frac{1}{2}(\frac{\partial f_2}{\partial r})^2 = 2(\frac{r}{R_b})^2$$

Through some derivations, the force-deflection relationship is written as

$$F_p = \frac{2\pi}{3}\frac{2}{\sqrt{3}}\sigma_0 t\delta(1 + 3\frac{R_b\delta}{a^2} + 6(\frac{R_b\delta}{a^2})^2) = 2.42\sigma_0 t\delta(1 + 3\frac{R_b\delta}{a^2} + 6(\frac{R_b\delta}{a^2})^2) \qquad (3.67)$$

The energy-deflection relationship is

$$E_p = 1.21\sigma_0 t\delta^2(1 + 2\frac{R_b\delta}{a^2} + 3(\frac{R_b\delta}{a^2})^2) \qquad (3.68)$$

The above method can be extended to get an approximate solution for the bulbous bow impacting the centre of a square plate (with a dimension of $2a \cdot 2a$). Combining the analysis of the point load acting at the center of a square plate and Eq (3.67), the force-deflection relationship is expressed as

$$F_p = \frac{32}{15}\frac{2}{\sqrt{3}}\sigma_0 t\delta(1 + 3\frac{R_b\delta}{a^2} + 6(\frac{R_b\delta}{a^2})^2) \qquad (3.69)$$

Similarly, the force-deflection relationship for a bulbous bow impacting the centre of a rectangular plate with a dimension of $2a \cdot 2b$ is expressed as

$$F_p = \frac{16}{15}\frac{2}{\sqrt{3}}\sigma_0 t\delta[(\frac{b}{a} + \frac{a}{b}) + 3(\frac{R_b\delta}{a^2} + \frac{R_b\delta}{b^2}) + 6((\frac{R_b\delta}{a^2})^2 + (\frac{R_b\delta}{b^2})^2)] \qquad (3.70)$$

As shown in Fig. 3.41, for a bulbous bow impacting a rectangular plate eccentrically, the force-deflection relationship is expressed as

$$F_p = 1.23\sigma_0 t\delta[ab(\frac{1}{a_1 a_2} + \frac{1}{b_1 b_2}) + \frac{3}{2}(R_b\delta)(\frac{1}{a_1^2} + \frac{1}{a_2^2} + \frac{1}{b_1^2} + \frac{1}{b_2^2})$$
$$+ 3(R_b\delta)^2(\frac{1}{a_1^4} + \frac{1}{a_2^4} + \frac{1}{b_1^4} + \frac{1}{b_2^4})] \qquad (3.71)$$
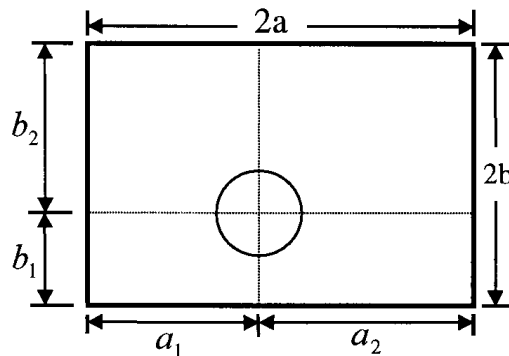

Fig. 3.41. A bulbous bow impacting shell plate eccentrically.

Comparison Example

The examples are taken from Simonsen (1997). The basic data is presented in Table 3.2. The comparison of the resistance forces obtained by the present method and Simonsen's method is shown in Figs. 3.42 and 3.43. The comparison shows that good agreement has been found.

Table 3.2. Basic data of the examples of bulbs indenting into circular plates.

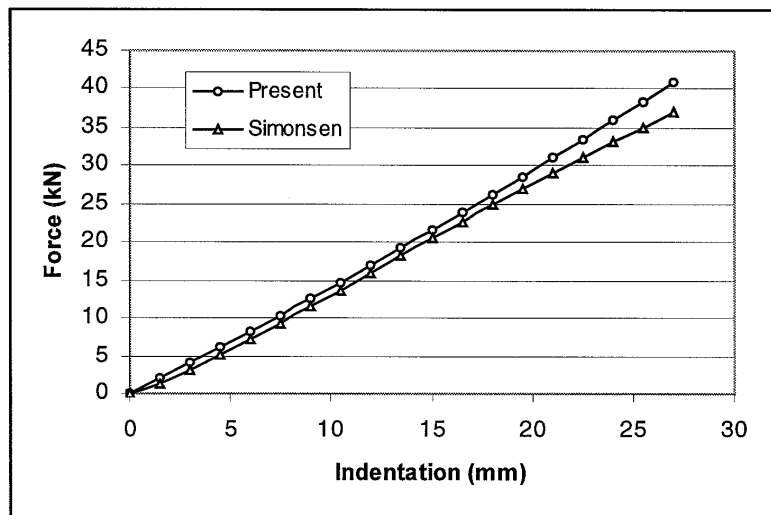| No.	t (mm)	a (mm)	R_b (mm)	$\sigma_y (MPa)$	$\sigma_u (MPa)$	$\sigma_0 = 0.5(\sigma_y + \sigma_u)$
1	2.1	100	15.0	208	319	264
2	2.1	100	30.0	208	319	264

Fig. 3.42. Comparison of the present calculation and Simonsen's result (Case #1).
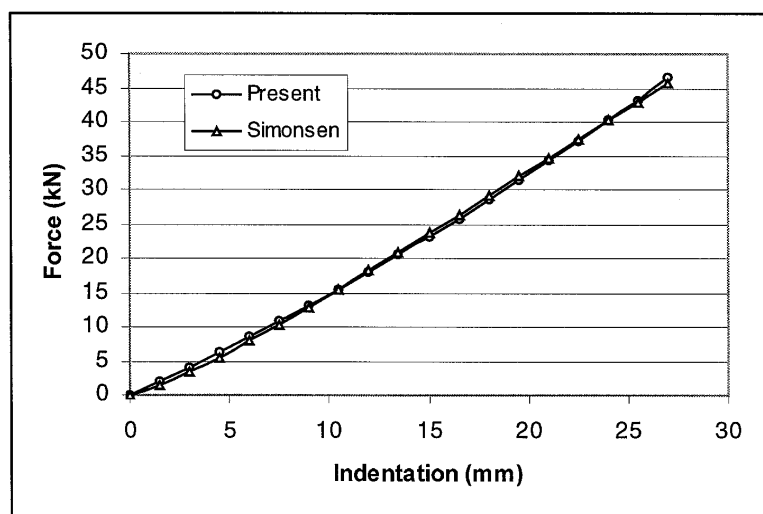

Fig. 3.43. Comparison of the present calculation and Simonsen's result (Case #2).

Calculation Example

In order to investigate the influence of the bulb radius on the collision resistance, an example of a bulb indenting into the side shell of a Ro-Ro vessel is calculated. For a Ro-Ro vessel with a length of 180 m, the spacing of the transverse frames is 2.4 m, and the thickness of the shell plating is 8~10 mm. Therefore, the chosen data for the present calculation is a=1.2 m (simplified as a circular plate), t_p =8 mm, and the flow stress of the material is $\sigma_0 = 300 MPa$. According to statistics, the radius of a bulb can be approximated as $R_b = 0.01L$, where L is the length of the striking ship. In this example, three cases are selected: R_b =0.6 m, R_b =1.2 m and R_b =2.4 m which correspond to striking ships with lengths of 60 m, 120 m and 240 m, respectively. The present calculation results are shown in Fig. 3.44. The results indicate that the bulb radius has significant influence on the resistance, especially at the relatively large penetrations.
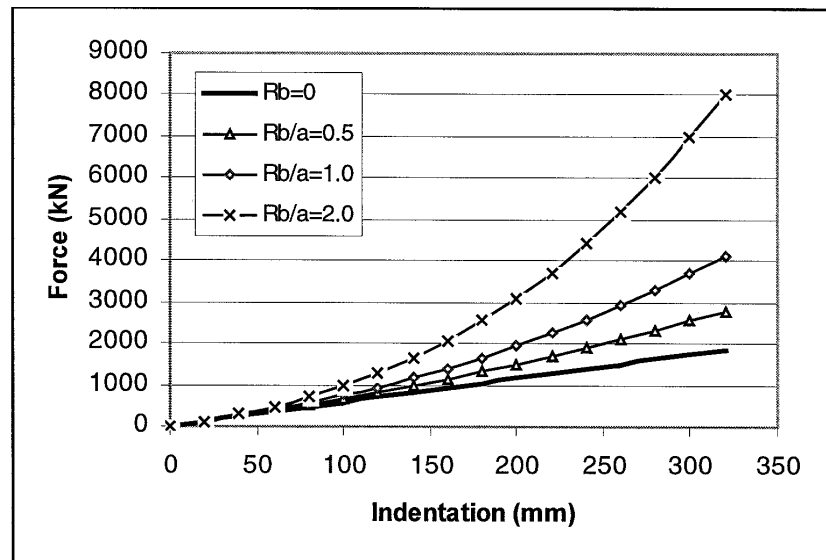

Fig. 3.44. The influence of the radius of the bulb on the resistance force.

3.4.6 Shell Plate Subjected to an Oblique Load

Fig. 3.45 shows a model of an oblique collision. The normal deflection of the one-quarter $(a_1 \cdot b_1)$ of the plate can be expressed as

$$w(x,y,t) = W(t) \cdot f(x,y,t)$$

where $W(t) = \delta(t)\sin\phi$ is the perpendicular deflection, ϕ is the penetration angle, δ is the penetration along the direction angle ϕ and $f(x,y,t) = (\dfrac{x}{a_1 + \delta\cos\phi}) \cdot (\dfrac{y}{b_1})$ is the deformation function.

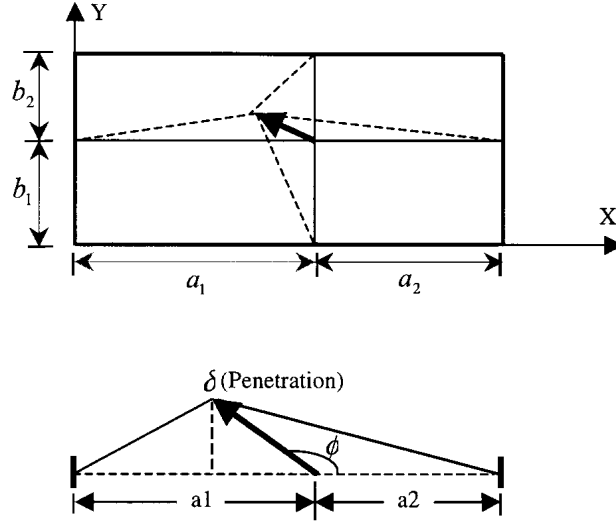*Fig. 3.45. Model of an oblique collision.*

Then the strain and the strain rate in the plate can be calculated from

$$\varepsilon_{xx} = \frac{1}{2}(\frac{\partial w}{\partial x})^2 = \frac{1}{2}W^2(\frac{\partial f}{\partial x})^2$$

$$\varepsilon_{yy} = \frac{1}{2}(\frac{\partial w}{\partial y})^2 = \frac{1}{2}W^2(\frac{\partial f}{\partial y})^2 \qquad (3.72)$$

$$\varepsilon_{xy} = \frac{1}{2}\frac{\partial w}{\partial x}\frac{\partial w}{\partial y} = \frac{1}{2}W^2\frac{\partial f}{\partial x}\frac{\partial f}{\partial y}$$

and

$$\dot{\varepsilon}_{xx} = W\dot{W}(\frac{\partial f}{\partial x})^2 + W^2\frac{\partial f}{\partial x}\frac{\partial \dot{f}}{\partial x} = W\dot{W}(\frac{\partial f}{\partial x})^2(\frac{a_1}{a_1 + \delta\cos\phi})$$

$$\dot{\varepsilon}_{yy} = W\dot{W}(\frac{\partial f}{\partial y})^2 + W^2\frac{\partial f}{\partial y}\frac{\partial \dot{f}}{\partial y} = W\dot{W}(\frac{\partial f}{\partial y})^2(\frac{a_1}{a_1 + \delta\cos\phi}) \qquad (3.73)$$

$$\dot{\varepsilon}_{xy} = W\dot{W}\frac{\partial f}{\partial x}\frac{\partial f}{\partial y} + \frac{1}{2}W^2(\frac{\partial \dot{f}}{\partial x}\frac{\partial f}{\partial y} + \frac{\partial f}{\partial x}\frac{\partial \dot{f}}{\partial y}) = W\dot{W}\frac{\partial f}{\partial x}\frac{\partial f}{\partial y}(\frac{a_1}{a_1 + \delta\cos\phi})$$

By use of the equilibrium for the energy rate, the perpendicular component of the collision resistance is found to be

$$F_{\xi} = \frac{1}{3}\frac{2}{\sqrt{3}}\sigma_0 t_p A\delta \sin\phi(\frac{a_1 a_2 + (\delta\cos\phi)^2}{(a_1 + \delta\cos\phi)^2(a_2 - \delta\cos\phi)^2} + \frac{1}{b_1 b_2}) \qquad (3.74)$$

where $A = (a_1 + a_2)(b_1 + b_2)$ is the area of the plate. When $\phi = 90^0$ the formula reduces to $F_{\xi} = \frac{1}{3}\frac{2}{\sqrt{3}}\sigma_0 t_p A\delta(\frac{1}{a_1 a_2} + \frac{1}{b_1 b_2})$, that is the same form as the previously derived formula for the perpendicular collision (Eq. (3.43)) when n=1). The parallel component of the resistance (in the shell plating plane) comes mainly from the friction of the relative movement. It is determined by

$$F_{\eta} = \mu \cdot F_{\xi} \qquad (3.75)$$

where μ is the coefficient of friction. The total resistance force is

$$F_p = F_{\xi}\sqrt{1 + \mu^2} \qquad (3.76)$$

The collision resistance in the penetration direction is expressed as

$$F_{pene.} = F_{\xi}\sin\phi + F_{\eta}\cos\phi$$
$$= \frac{1}{3}\frac{2}{\sqrt{3}}\sigma_0 t_p A\delta \sin\phi(\frac{a_1 a_2 + (\delta\cos\phi)^2}{(a_1 + \delta\cos\phi)^2(a_2 - \delta\cos\phi)^2} + \frac{1}{b_1 b_2})(\sin\phi + \mu\cos\phi) \qquad (3.77)$$

By integration of Eq. (3.76) with respect to the penetration δ, the work by the external force is determined by

$$E = \int_0^{\delta} F_{pene.} d\delta \qquad (3.78)$$

Example

Fig. 3.46 shows an example of the influence of the penetration angle ϕ on the total resistance at various deflections in the perpendicular direction to the plate. The absorbed energy is shown in Fig. 3.47. The parameters of the present example are: $\sigma_0 = 300 MPa$, t_p =10 mm, $a_1 = a_2$ =1.2 m, $b_1 = b_2$ =1.4 m and $\mu = 0.3$. The obvious observation from the figures is that the collision resistance is non-linear to deflections for the oblique collision, but that it is a linear function for the perpendicular collision.
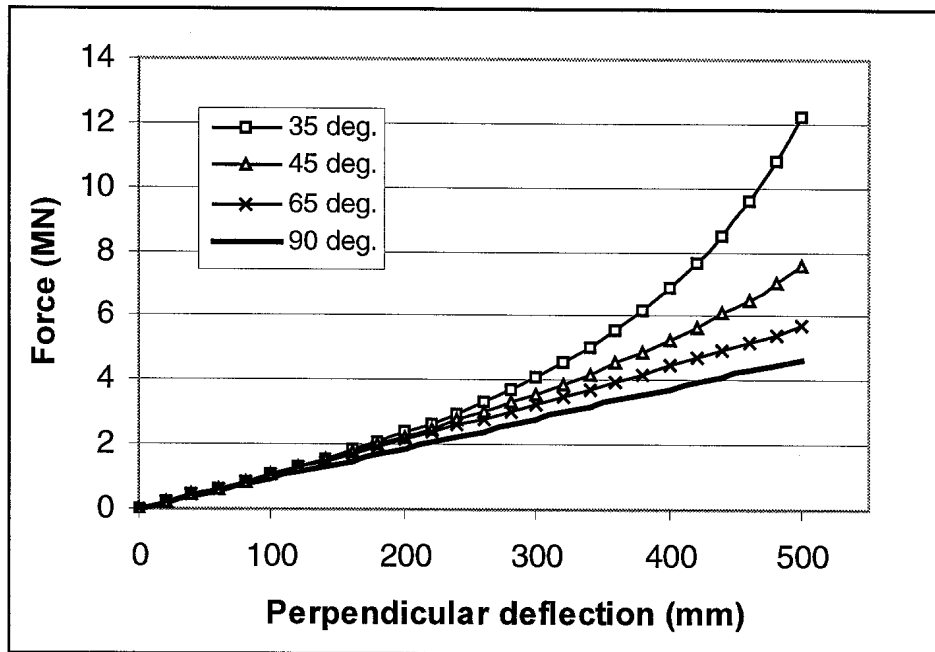
Fig. 3.46. The influence of the penetration angle on the total resistance.
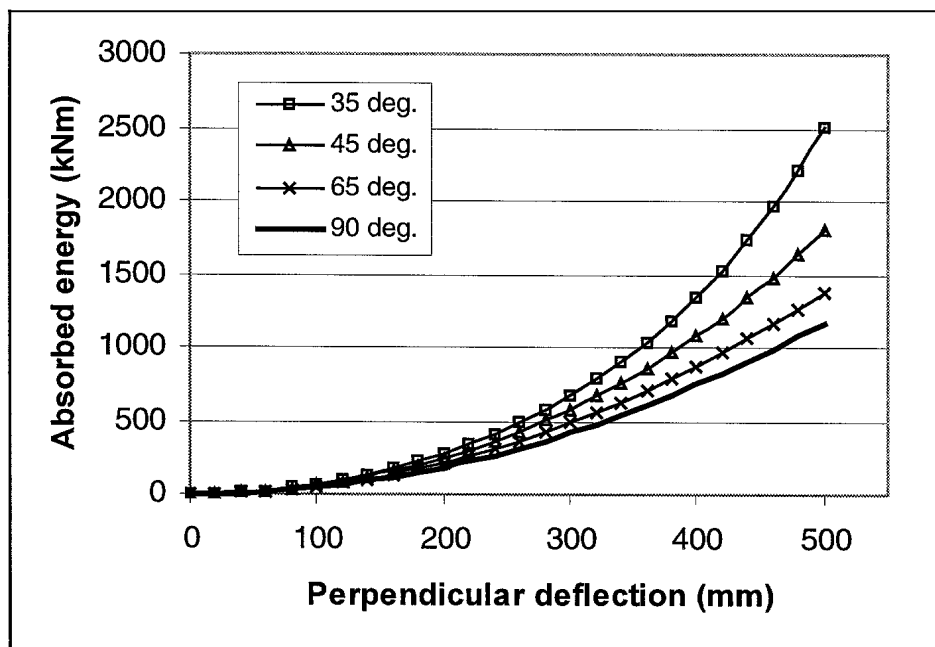
Fig. 3.47. The influence of the penetration angle on the absorbed energy.

3.5 Crushing of Frames and Stringers

3.5.1 Crushing of Frames and Stringers

The Analysis Method

Frames may suffer in-plane distortions if the webs are well reinforced with horizontal stiffeners, or suffer folding when the webs are not reinforced with stiffeners. McDermott et al. (1974) studied in-plane distortion. The resistance of frames can be approximated by the shear forces leading to yielding:

$$F_w = (1/\sqrt{3})\sigma_0 t\delta \text{ , when } \delta < H_{web}$$
$$F_w = (1/\sqrt{3})\sigma_0 A_w \text{ , when } \delta \geq H_{web} \tag{3.79}$$

where H_{web} is the web height and A_w is the section area of the web frame.

For a very deep web, the most often observed deformation mode in ship accidents and experiments is folding or crushing when an external load is in the web plane. A typical picture of a model test of web crushing and the assumed deformation mode for the present analysis are shown in Fig. 3.48.

Fig. 3.48. Web crushing test and the assumed deformation mode for web crushing.

Wang (1995) and Wierzbicki and Simonsen (1996) studied the case of a web crushing. The folding deformation mode of the frame includes bending and membrane tension. The equilibrium of the principle of virtual work is used to determine the crushing force:

$$F \dot{\delta} = \dot{E}_b + \dot{E}_m$$

where F is the crushing force, δ is the indentation, $\dot{E}_b$ is the bending energy rate, $\dot{E}_m$ is the membrane energy rate.
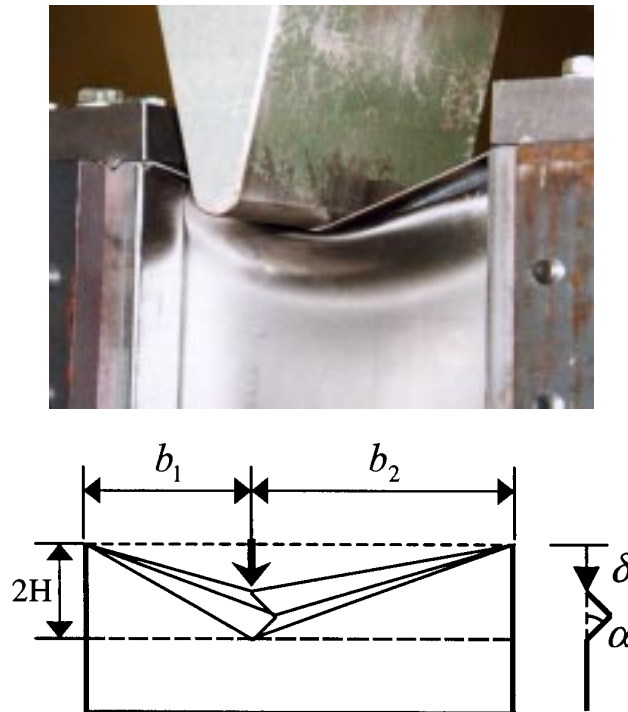
Bending Energy Rate

Three bending hinge lines are formed in the folding or crushing process. The upper plastic hinge line is created between the web and its attached shell plating. The middle hinge moves out of its original plane and the lower hinge remains in the web plane. The lengths of the hinge lines are assumed to be equal, which is the length of the web ($= b_1 + b_2$). Therefore, the rate of the bending energy can be determined from

$$\dot{E}_b = 4M_0 \dot{\alpha} \cdot (b_1 + b_2)$$

where $M_0 = \dfrac{2}{\sqrt{3}} \dfrac{\sigma_0 t^2}{4}$, α is the bending angle (see Fig. 3.48).

The relationship between the bending angle α and the indentation δ can be found from a geometric analysis. That is

$$\delta = 2H(1 - \cos\alpha) \approx H\alpha^2$$

$$\dot{\alpha} = \frac{\dot{\delta}}{2\sqrt{H\delta}}$$

where $2H$ is the folding length. Thus, the rate of the bending energy is

$$\dot{E}_b = \frac{1}{\sqrt{3}} \sigma_0 t^2 \frac{(b_1 + b_2)}{\sqrt{H\delta}} \cdot \dot{\delta} \tag{3.80}$$

When the first fold has been completed, the total bending energy is expressed as

$$E_b = 2\pi M_0 (b_1 + b_2) = \frac{\pi}{\sqrt{3}} \sigma_0 t^2 (b_1 + b_2) \tag{3.81}$$

Membrane Energy Rate

The main contribution to the membrane energy is the in-plane stretching. It can be written as

$$\dot{E}_m = \iint_{S1} \frac{2}{\sqrt{3}} \sigma_0 t \dot{\varepsilon}_1 \, dS + \iint_{S2} \frac{2}{\sqrt{3}} \sigma_0 t \dot{\varepsilon}_2 \, dS$$

where $S_1 = 2H \cdot b_1$ and $S_2 = 2H \cdot b_2$ are the deformed area of the web.

For the upper fibre in the web (such as a part b_1), the strain and the strain rate can be calculated from

$$\varepsilon_0 = \frac{1}{2} \left(\frac{\delta}{b_1} \right)^2 \text{ and } \dot{\varepsilon}_0 = \frac{\delta \dot{\delta}}{b_1^2}$$

For the lower fibre in the deformed part of the web, the indentation is assumed to be linear with the level of the fibre. That is

$$\delta_z(z) = \left(\frac{z}{2H} \right)\delta, \quad z = [0, \ 2H]$$

So the strain rate at each level becomes

$$\dot{\varepsilon}_1 = \left(\frac{z}{2H} \right)^2 \frac{\delta \dot{\delta}}{b_1^2}$$

The average strain rate in the whole area $S_1 = 2H \cdot b_1$ can be obtained by integrating the strain rate over the area:

$$\dot{\varepsilon}_{av} = \frac{1}{S_1} \iint_{S_1} \dot{\varepsilon}_1 \, ds = \frac{1}{2H \cdot b_1} \iint_{S1} \left(\frac{z}{2H} \right)^2 \frac{\delta \dot{\delta}}{b_1^2} \, ds = \frac{1}{3} \frac{\delta \dot{\delta}}{b_1^2} = \frac{1}{3} \dot{\varepsilon}_0 \tag{3.82}$$

It is seen that the average strain rate is only 1/3 of the strain rate in the upper fibre. By multiplication of the area and the average strain, the rate of the total membrane energy is

$$\dot{E}_m = \frac{2}{3} \frac{2}{\sqrt{3}} \sigma_0 t H \left(\frac{\delta}{b_1} + \frac{\delta}{b_2} \right) \dot{\delta} \tag{3.83}$$

When the first fold is finished, $\delta = 2H$, the total membrane energy is

$$E_m = \frac{1}{3} \frac{2}{\sqrt{3}} \sigma_0 t H \delta^2 \left(\frac{1}{b_1} + \frac{1}{b_2} \right) \overset{\delta=2H}{=} \frac{4}{3} \frac{2}{\sqrt{3}} \sigma_0 t H^3 \left(\frac{1}{b_1} + \frac{1}{b_2} \right) \tag{3.84}$$

The Total Energy and Crushing Force

By adding the contributions of bending and membrane, the total energy rate can be expressed as

$$\dot{E} = \dot{E}_b + \dot{E}_m = \frac{1}{\sqrt{3}}\sigma_0 t^2 \frac{(b_1+b_2)}{\sqrt{H\delta}} \cdot \dot{\delta} + \frac{2}{3}\frac{2}{\sqrt{3}}\sigma_0 tH(\frac{\delta}{b_1}+\frac{\delta}{b_2})\dot{\delta}$$

$$E = E_b + E_m = \frac{\pi}{\sqrt{3}}\sigma_0 t^2 (b_1+b_2) + \frac{4}{3}\frac{2}{\sqrt{3}}\sigma_0 tH^3(\frac{1}{b_1}+\frac{1}{b_2})$$

The instantaneous crushing force and the mean crushing force can be expressed as

$$F = \frac{\dot{E}}{\dot{\delta}} = \frac{1}{\sqrt{3}}\sigma_0 t^2 \frac{(b_1+b_2)}{\sqrt{H\delta}} + \frac{2}{3}\frac{2}{\sqrt{3}}\sigma_0 tH\delta(\frac{1}{b_1}+\frac{1}{b_2}) \tag{3.85}$$

$$F_m = \frac{E}{2H} = \frac{\pi}{2\sqrt{3}}\sigma_0 t^2 (b_1+b_2)\frac{1}{H} + \frac{2}{3}\frac{2}{\sqrt{3}}\sigma_0 tH^2(\frac{1}{b_1}+\frac{1}{b_2}) \tag{3.86}$$

By minimising the mean crushing force, we get the optimum folding length:

$$\frac{\partial F_m}{\partial H} = 0 \quad \Rightarrow:$$

$$H = (\frac{3\pi}{16}b_1 b_2 t)^{\frac{1}{3}} = 0.8383(b_1 b_2 t)^{\frac{1}{3}} \tag{3.87}$$

Then the instantaneous crushing force and the mean crushing force can be simplified as

$$F = 0.631\sigma_0 t^{1.83}\frac{(b_1+b_2)}{(b_1 b_2)^{0.17}\delta^{0.5}} + 0.645\sigma_0 t^{1.33}\delta\frac{(b_1+b_2)}{(b_1 b_2)^{0.67}} \tag{3.88}$$

$$F_m = (1.082+0.541)\sigma_0 t^{\frac{5}{3}}\frac{(b_1+b_2)}{(b_1 b_2)^{\frac{1}{3}}} = 1.623\sigma_0 t^{\frac{5}{3}}\frac{(b_1+b_2)}{(b_1 b_2)^{\frac{1}{3}}} \tag{3.89}$$

When $b_1 = b_2 = b$, that is the impact point is located in the middle of the web, the formulas reduce to

$$F = 1.262\sigma_0 t^{1.83}b^{0.67}\frac{1}{\delta^{0.5}} + 1.290\sigma_0 t^{1.33}\delta\frac{1}{b^{0.33}}$$

$$F_m = 3.25\sigma_0 t^{1.67}b^{0.33} \qquad\qquad (\delta \le 2H) \tag{3.90}$$

$$H = 0.838t^{0.33}b^{0.67}$$

In the above derivation, the crushing distance is $2H$ when the first fold is completed. But actually the web plate can not be totally compressed, the shorted distance is smaller than $2H$. Normally, the effective crushing length is 75% of the folding length $2H$ for bare plate (Abramowicz, 1983). Therefore, the mean crushing force after considering the effective folding length is expressed as

$$F_m = 4.33\sigma_0 t^{1.67} b^{0.33} \tag{3.91}$$

When the first fold is completed, that is $\delta = 2H$, the tension strain in the upper fibre of the web is

$$\varepsilon_0 = \frac{1}{2}(\frac{\delta}{b})^2 = 1.404(\frac{t}{b})^{\frac{2}{3}} \tag{3.92}$$

If the strain reaches the critical strain ε_c, the web ruptures. The critical indentation is determined from $\delta_c = (\sqrt{2\varepsilon_c}) \cdot b$.

If a typical example of a Ro-Ro vessel is considered, the geometric data of the web is b=1.2 m, t=10 mm. Then we get the tension strain $\varepsilon_0 = 5.8\%$. This means that possible subsequent folding may form before the web rupturing (if the critical strain is greater than 5.8%).

Subsequent Folding

After the first fold has been finished, the second fold forms at a further indentation. The crushing mode is illustrated in Fig. 3.49. It is assumed that the second folding pattern is similar to the first fold (Simonsen, 1997). In the subsequent folding, the first folded web is compressed. The behaviour is like that of a beam indented centrally by a transverse load. The resistance force of the first folded web can be determined from

$$F_1 = 4.62\sigma_0 tH \frac{\delta - 2H}{b} \tag{3.93}$$

Eq. (3.90) is still valid for calculating the resistance of the second fold. By taking into account the resistance of the first folded web, the crushing force for the second folding process can be expressed as

$$F = 4.33\sigma_0 t^{1.67} b^{0.33} + 4.62\sigma_0 tH \frac{\delta - 2H}{b} \tag{3.94}$$

In a similar way, the crushing force in the third fold, the fourth fold etc. can be determined. In summary, the resistance force of web crushing can be determined as follows:

$$F = \begin{cases} 4.33\sigma_0 t^{1.67} b^{0.33}, \dots\dots\dots\dots\dots\dots\dots\dots\dots\dots\dots\dots\dots\dots\delta \leq 2H \\ 4.33\sigma_0 t^{1.67} b^{0.33} + 4.62\sigma_0 tH \dfrac{\delta - 2H}{b}, \dots\dots\dots\dots\dots 2H < \delta \leq 4H \\ \dots\dots\dots\dots\dots \\ 4.33\sigma_0 t^{1.67} b^{0.33} + 4.62\sigma_0 tH(n-1)(\dfrac{\delta - n \cdot H)}{b}), \dots\dots(n-1)(2H) < \delta \leq n(2H) \end{cases}$$ (3.95)
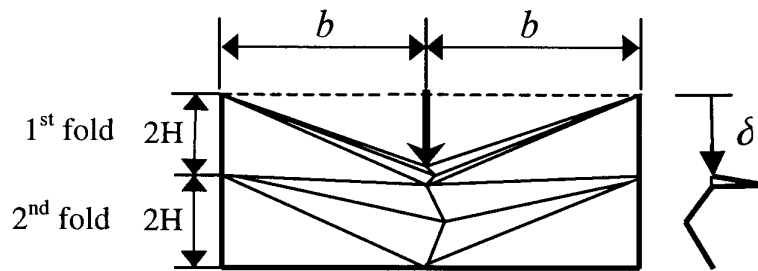
Fig. 3.49. Subsequent folding of web crushing.

Through several folds, when the penetration is greater than the critical penetration, the web ruptures in the $n_0 th$ fold:

$$n_0 = Int[\frac{\delta_c}{2H}] + 1 = Int[0.6(\frac{b}{t})^{0.33}\sqrt{2\varepsilon_c}] + 1$$ (3.96)

Concertina Tearing

After the web has ruptured, the folding mode changes to concertina tearing (if the web is deep enough). Wierzbicki (1994) studied concertina tearing. He found that the concertina tearing force can be expressed as

$$F_{con.} = 5.04\sigma_0 t^{1.67} b^{0.33} + \frac{8}{3}R_c \cdot t$$ (3.97)

where R_c is the specific work of fracture. Wierzbicki gave the range of the specific work of fracture for mild steel: $R_c = 300 \sim 1000(N/mm)$.

In fact, when Wierzbicki derived the formula for the concertina tearing force, he only considered the deformation within one fold. The deformation may extend to more than one fold as discussed above. There is also some uncertainty in Wierzbicki's formula due

to the introduction of the specific parameter of fracture R_c. Therefore, we shall investigate further the concertina tearing force.

Observations from many experiments show that the rupture of the webs occurs during the second fold. Using Eq. (3.92) and setting indentation $\delta = 3H$, we obtain the maximum strain in the web with various ratios of b/t, as shown in Fig. 3.50.
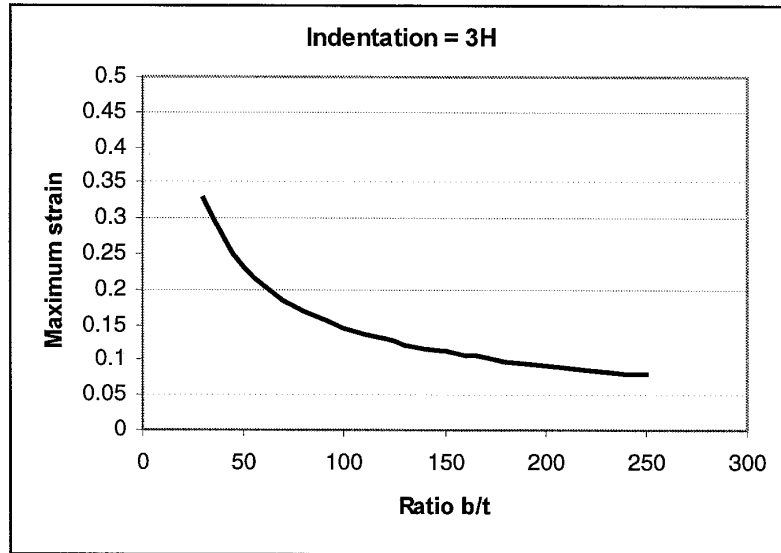
Fig. 3.50. Maximum strain in the web with various ratios of b/t
When the indentation is $\delta = 3H$.

It is seen from Fig. 3.50 that the maximum strain in the web is in the range of 11%~25% when the ratio of b/t ranges from 150 to 45. This range of strain is typical critical rupture value for steel materials. Therefore, it is reasonable to assume that when the indentation is equal to $\delta = 3H$, the upper fiber of the web starts to rupture. With further indentation, the concertina folding forms. Thus, the mean crushing force in the second lobe may represent the concertina tearing force.

The dissipated energy in the first folded lobe before rupture can be calculated from

$$E_{m1} = \int_{2H}^{3H} (4.62\sigma_0 tH(\delta - 2H)/b)d\delta = 2.31\sigma_0 tH^3/b$$

After rupture has started, the resistance from the first folded lobe does not vanish completely. The lower-level fibre in the first folded lobe still offers resistance and it is assumed that the resistance keeps constant. Thus, the dissipated energy during this indentation can be estimated from

$$E_{m2} = [4.62\sigma_0 tH(3H - 2H)/b] \cdot H = 4.62\sigma_0 tH^3/b$$

The mean crushing resistance from the first folded lobe during the second folding process is calculated from

$$F_{m1} = (E_{m1} + E_{m2})/(2H) = 3.465\sigma_0 t H^2 / b = 2.435\sigma_0 t^{1.67} b^{0.33}$$

By adding the contributions from the first folded lobe and the second newly crushed lobe, the mean crushing force for concertina tearing is expressed as

$$F_c = (2.435 + 4.33)\sigma_0 t^{1.67} b^{0.33} = 6.77\sigma_0 t^{1.67} b^{0.33} \tag{3.98}$$

Comparison with Experiments

Comparison with DTU Crushing Test

Simonsen and Ocakli (1999) at the Danish Technical University made a series of model tests of web crushing. Here we use one of them for comparison. The model after crushing test is shown in Fig. 3.51. The experiment is quasi-static. A wedge indents into the web in the middle position. The length of the web is $2b = 150$ mm, the thickness is $t = 1.0$ mm. The width of the attached flange is 50 mm, the thickness of the flange is 1.0 mm. The properties of the material are $\sigma_0 = 223.2 N/mm^2$ and $\varepsilon_c = 9.0\%$. The comparison of the present calculation with the experimental result is presented in Fig. 3.52. From the figure it is seen that the agreement is good. When the penetration is equal to the critical rupture value $\delta_c = b \cdot \sqrt{2\varepsilon_c} = 31.8$ mm, the web and the attached flange rupture and the crushing resistance drops immediately. After that the crushing of the web is concertina tearing with a constant force.

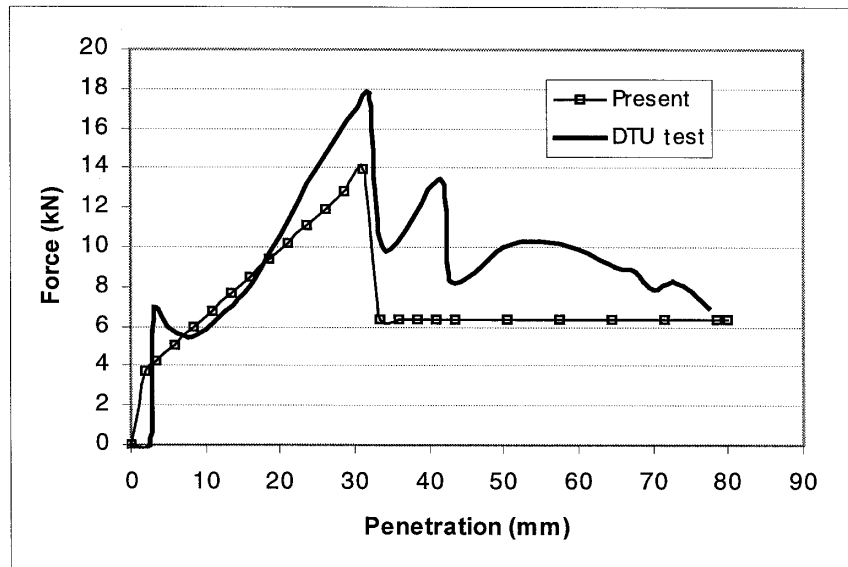*Fig. 3.51. A web model after crushing test (Simonsen et al. 1999).*

Fig. 3.52. Comparison of the present result and a model test of web crushing.

Comparison with MIT Crushing Experiment

To check further the accuracy of the present formulas, here we make another comparison with MIT model test (Simonsen, 1997). The test model is a web with a flange. Two sides of the web are clamped. A rigid object indented the model at the middle of the web (similar to Fig. 3.48).

The basic data of the model is presented in Table 3.3. The comparison of the crushing force obtained by the present method and the experimental result is shown in Fig. 3.53. Very good agreement is found. In this comparison, rupture did not happen. The comparison of the folding length by the present method and the test result is shown in Table 3.4. The comparison shows that the agreement is very good.

Table 3.3. The basic data of MIT test model.

Length of web $2b$	166.8 mm
Width of flange	41.7 mm
Thickness of all plates	0.737 mm
Flow stress σ_0	236 MPa

Table 3.4. Comparison of the half-folding length.

MIT test	13.9 mm
Present	14.5 mm
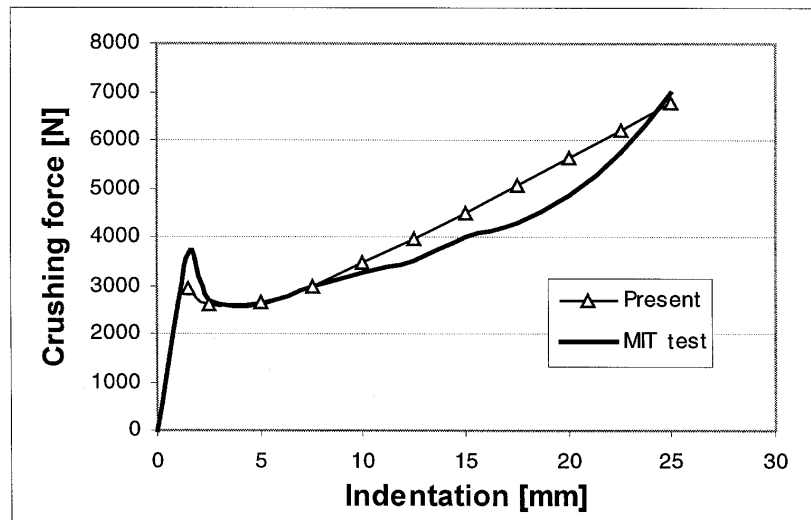
Fig. 3.53. Crushing force comparison between the present result and MIT test result.

Comparison with Concertina Folding Tests

The first comparison example of concertina folding is the model test performed by Yahiaoui et al. (1994). The picture of the model after testing is shown in Fig. 3.54, which is very regular concertina folding. The main parameters of the model are: $\sigma_0 = 330 MPa$, $b = 25$ mm, $t = 1.14$ mm. The comparison of the mean crushing forces obtained by the present method, experimental result and Wierzbicki's formula are: 8073N, 8500N and 6760N, respectively. The comparison of force-indentation curves is presented in Fig. 3.55. Reasonable agreement is found between the present method and the experimental result. Wierzbicki's result is a little lower than the test result.
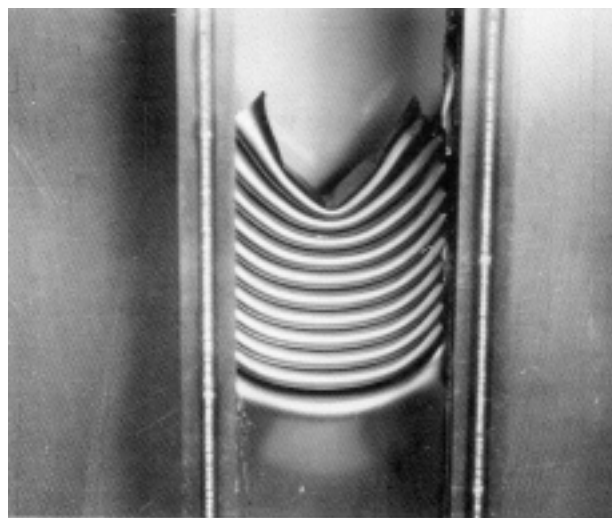
Fig. 3.54. A picture of concertina folding of a plate with a thickness of 1.14 mm (Yahiaoui, 1994).
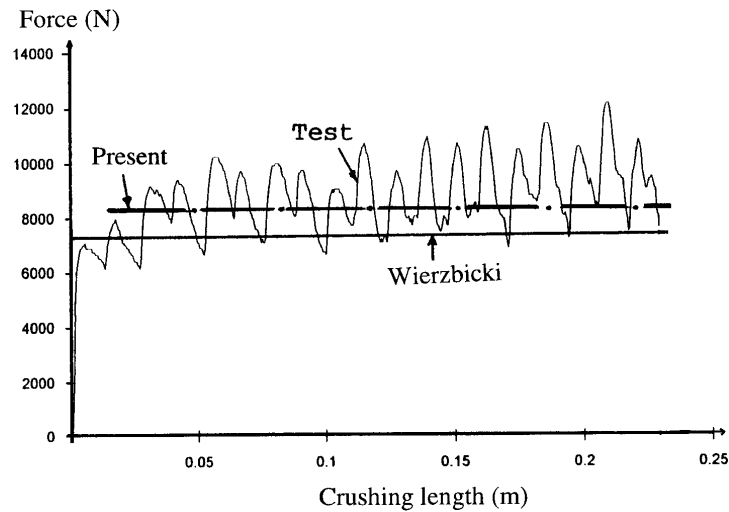
Fig. 3.55. Comparison of the concertina tearing forces of a plate.

The second comparison example is a series of model tests performed by Maxwell (1993). The numbers of the five specimens which failed in concertina tearing are Test #1, #6, #9, #10 and #15 in Maxwell's test. The related parameters of the five models are: $\sigma_0 = 300MPa$, $b = 152.4$ mm, $t = 0.74$ mm.

The results of concertina tearing forces obtained by the present method, Wierzbicki's method and the tests are compared and shown in Fig. 3.56. Acceptable agreement is found from this comparison. However, the present result is somewhat higher than Wierzbicki's result and the test result.
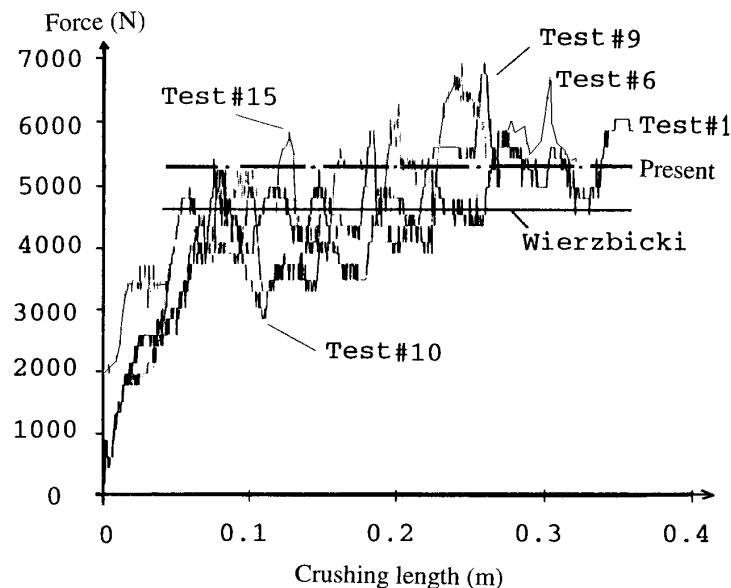
Fig. 3.56. Comparison of five tests which failed in the concertina tearing mode
(plate thickness is 0.74).

3.5.2 Bulbous Bow Impact on a Stringer

In Section 3.5.1, a conventional bow crushing a web or stringer was analysed. In this section, we analyse a bulbous bow collision with a web or stringer. The collision scenario of a bulbous bow impacting the side of a ship in a stringer position is shown in Fig. 3.57. When the bulbous bow indents into the side of a ship, the shell plate will stretch and the stringer web will fold and crush. The simplified analysis model is presented in Fig. 3.58. The length of the stringer is $2b$, which is the transverse web frame spacing. It is assumed that the transverse web frames do not deform unless the ship bow pushes the web frame directly. The width of the shell plate is d. The thickness of the shell plate is t and the thickness of the stringer web is t_w.

Formulas

The dissipated energy of a bulbous bow impacting the side stringer is composed of the tension of the side plate and the crushing of the stringer web:

$$E = E_{plate} + E_{deck}$$

As shown in Fig. 3.58, the deformation of the side plate can be assumed to be

$$w_1(x,y,t) = \delta_1(t) \cdot f_1(x,y) = \delta_1 (\frac{b-x}{b-b_0})^2, \quad b_0 \leq x \leq b \tag{3.99}$$

where δ_1 is the deflection at the separating point between the bulb and the plate, b_0 is the radius at the separating point. Following the similar procedures as section 3.4.5, the collision resistance due to the side shell stretching is expressed as

$$F_{plate} = \frac{8}{3} \frac{2}{\sqrt{3}} \sigma_0 t \delta (1 + \frac{3}{2} \frac{R_b \delta}{b^2}) \frac{d}{b} \tag{3.100}$$

By integrating Eq. (3.100) with respect to the indentation δ, the dissipated energy of the shell plate is obtained as

$$E_{plate} = \frac{4}{3} \frac{2}{\sqrt{3}} \sigma_0 t \delta^2 (1 + \frac{R_b \delta}{b^2}) \frac{d}{b} \tag{3.101}$$

Eq. (3.90) for the web crushing force is used here for stringer web crushing, we rewrite the formula

$$F_{web} = 1.262 \sigma_0 t_w^{1.83} b^{0.67} \frac{1}{\delta^{0.5}} + 1.290 \sigma_0 t_w^{1.33} \delta \frac{1}{b^{0.33}} \tag{3.102}$$

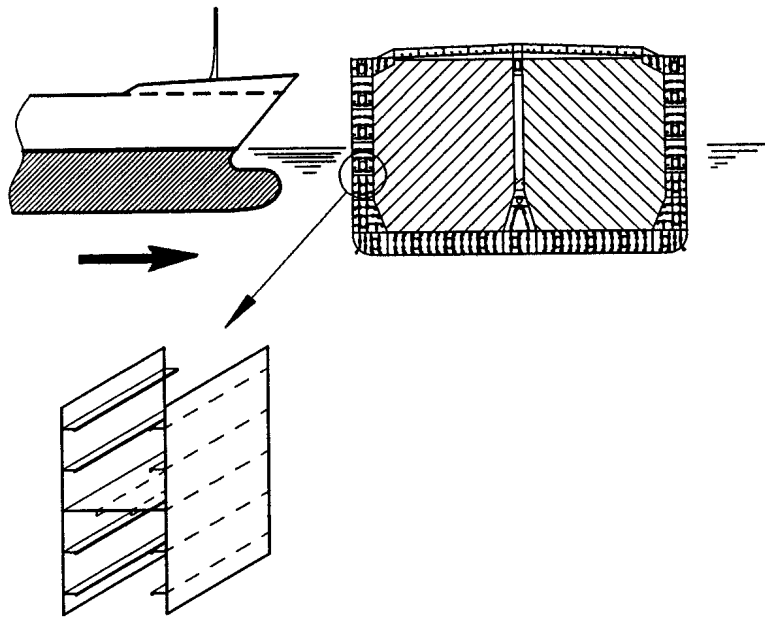$$H = 0.838 t_w^{0.33} b^{0.67} \text{ (Half-fold length)}$$

Fig. 3.57. A bulbous bow impacts a side stringer.
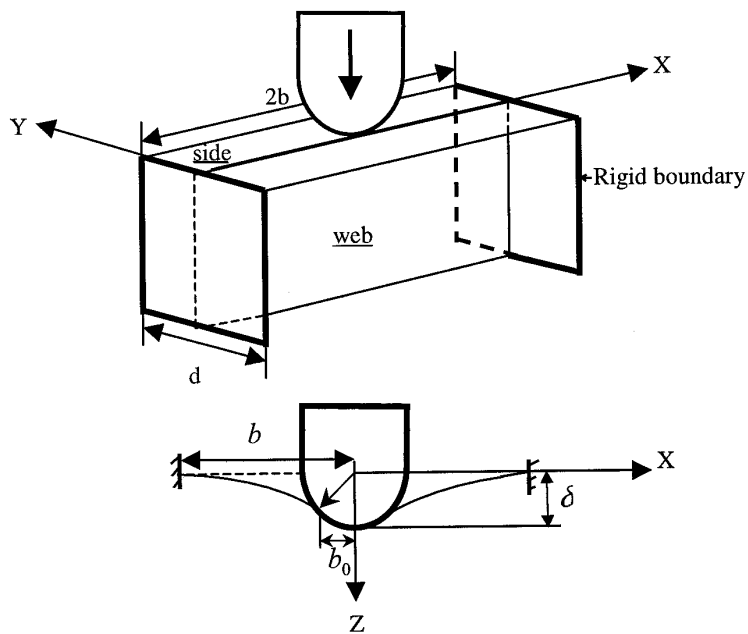

Fig. 3.58. A analysis model for a bulbous bow impacting a stringer.

By integration of Eq. (3.102), the relationship of the dissipated energy and the indentation in the stringer web crushing can be expressed as

$$E_{web} = 2.524\sigma_0 t_w^{1.83} b^{0.67} \delta^{0.5} + 0.645\sigma_0 t_w^{1.33} \delta^2 \frac{1}{b^{0.33}}$$ (3.103)

By adding the contributions from shell plate and stringer web, the total collision resistance and absorbed energy can be written as

$$F = F_{plate} + F_{web}$$
$$= 3.08\sigma_0 t\delta(1 + 1.5\frac{R_b\delta}{b^2})\frac{d}{b} + 1.262\sigma_0 t_w^{1.83} b^{0.67} \frac{1}{\delta^{0.5}} + 1.290\sigma_0 t_w^{1.33} \delta \frac{1}{b^{0.33}}$$ (3.104)

$$E = E_{plate} + E_{web}$$
$$= 1.54\sigma_0 t\delta^2(1 + \frac{R_b\delta}{b^2})\frac{d}{b} + 2.522\sigma_0 t_w^{1.83} b^{0.67} \delta^{0.5} + 0.645\sigma_0 t_w^{1.33} \delta^2 \frac{1}{b^{0.33}}$$ (3.105)

Comparison with the Qvist (1995) Experiment

Qvist et al. (1995) carried out a large-scale impact test at the B&W Shipyard in Denmark. The model is used to simulate part of the side structure of a 40,000 dwt tanker on a full scale and a large tanker (>100,000 dwt) on the scale 1/2. The pictures of the test model before and after testing are shown in Fig. 3.59 and the detailed parameters of the model are presented in Table 3.5 and in Fig. 3.60.

Table 3.5. Parameters of the test model.

$2b$	1350 mm
d	450 mm
R_b	500 mm
$t = t_w$	8 mm
σ_0	$317.5 MPa$

A steel ball (M=2750 kg) dropped from a height of 5 m collided with the stringer model in the middle point. This means that the impact velocity is V=10 m/s. Thus the energy to be dissipated by destroying the stringer model is $E = \frac{1}{2}MV^2 = 137.5(kNm)$.

The calculated results for the indentation at the end of the impact and the test results are shown in Table 3.6. Table 3.7 shows the calculated results of the energy distribution in the shell plating and the stringer web at the end of the collision. From the comparison it is seen that good agreement was achieved, and it should also be noted that the shell plating absorbed much more energy than the stringer web. The present calculation curves for the absorbed energy vs. various indentations are shown in Fig. 3.61. In this calculation, no rupture occurs.

Table 3.6. Comparison of the calculation results and the test results.

Methods	Indentation at the end of impact
Experiment, 1st model	190 mm
Experiment, 2nd model	175 mm
Dyna3D simulation	180 mm
Present calculation	171 mm

Table 3.7. Distribution of dissipated energy in shell plating and stringer web.

	$(E_{plate})/(E_{total})$	$(E_{web})/(E_{total})$
Present calculation	66%	34%

Fig. 3.59. Experiment of a steel ball impacting a side-stringer model
(Qvist et al., 1995).
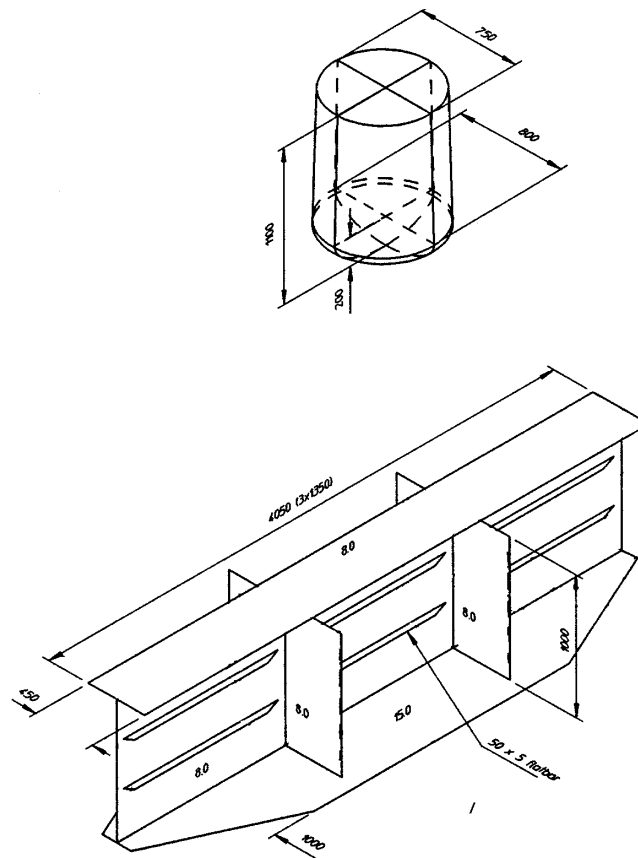
Fig. 3.60. The detailed parameters of the impact test model (Qvist et al., 1995).
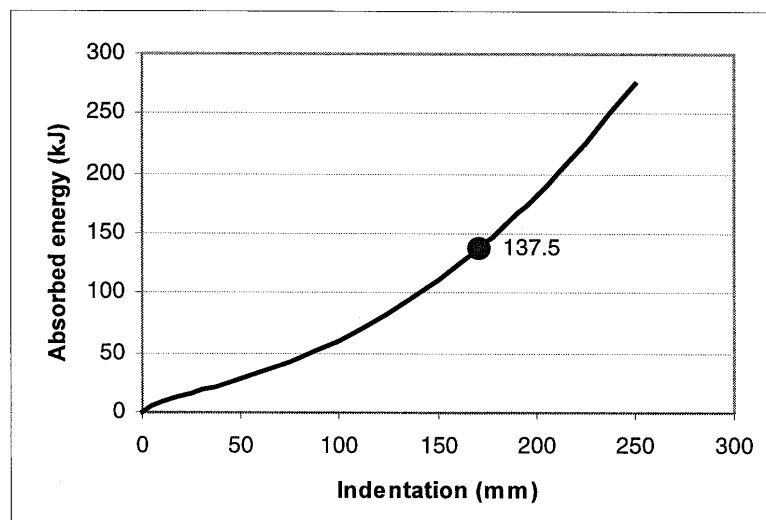
Fig. 3.61. Calculated result for the dissipated energy vs. various indentations.

3.6 Crushing of Web and Stringer Intersections

As shown in Fig. 3.62, a striking bow impacts the side structure of a ship at an intersection of a transverse web frame and a longitudinal stringer. The intersection is dented and crushed by the direct pushing of the striking bow. The analysis model for the damage mode of the intersection is depicted in Fig. 3.63.
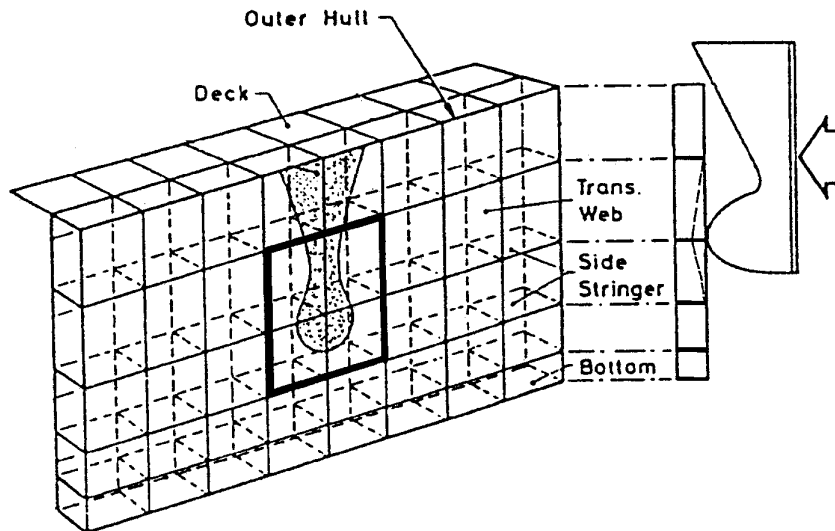
Fig. 3.62. A bow indents into the side of a ship at the intersection of a transverse web and a longitudinal stringer.
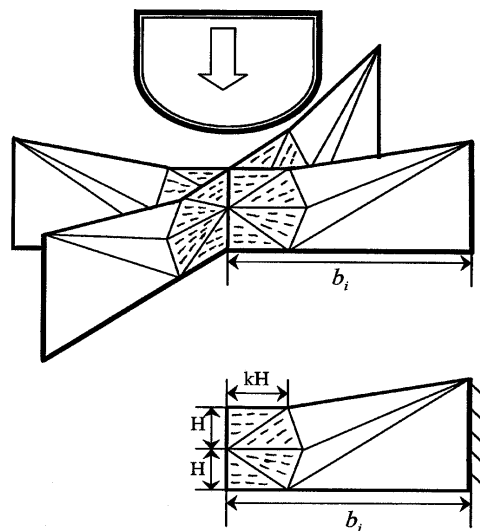
Fig. 3.63. Damage mode of the intersection of a transverse web and a stringer.

3.6.1   Formulas for the Mean Crushing Force

First, we derive the formula for the crushing of an individual plate unit as shown in the lower part of Fig. 3.63. When the first fold has been completed, the total dissipated energy can be obtained by adding the bending energy and the in-plane deformation energy:

$$E = E_b + E_{m1} + E_{m2}$$

where E_b is the bending energy along the plastic hinge lines, E_{m1} is the in-plane deformation energy in the area ($kH \cdot 2H$), and E_{m2} is the in-plane deformation energy in the area ($(b - kH) \cdot 2H$).

For the bending energy, three horizontal hinge lines are considered and the inclined hinge lines are neglected, because the dissipated energy in the inclined hinge lines is small (Paik and Pedersen, 1995). Therefore, the bending energy can be expressed as

$$E_b = 4M_0 b \frac{\pi}{2} = 1.8138\sigma_0 t^2 b \tag{3.106}$$

Amdahl (1983) and Paik & Pedersen (1995) studied the dissipated energy in the area of ($kH \cdot 2H$). Here we use it directly:

$$E_{m1} = 2\frac{1}{\sqrt{3}} N_0 H^2 (\sqrt{k^2 + \frac{1}{4}} \cdot \arcsin \frac{1}{\sqrt{4k^2 + 1}} + k) = 1.4896\sigma_0 t H^2 \tag{3.107}$$

where $k = 0.5733$ (Amdahl, 1983) and $N_0 = (2/\sqrt{3})\sigma_0 t$.

The membrane energy in the area of ($(b - kH) \cdot 2H$) is determined from

$$E_{m2} = \frac{4}{3}\frac{2}{\sqrt{3}}\sigma_0 t H^3 \frac{1}{b - kH} = 1.5396\sigma_0 t H^3 \frac{1}{b - kH} \tag{3.108}$$

Thus, the total dissipated energy can be expressed as

$$E = 1.8138\sigma_0 t^2 b + 1.4896\sigma_0 t H^2 + 1.5396\sigma_0 t H^3 \frac{1}{b - kH} \tag{3.109}$$

When the total dissipated energy is known, the mean crushing force can be calculated from

$$F_m = \frac{E}{2H} = \sigma_0 t (0.9069 t b \frac{1}{H} + 0.7448H + \frac{0.7698H^2}{b - kH}) \tag{3.110}$$

where $2H$ is the folding length. For simplicity, we use the first two terms to minimise the mean crushing force:

$$\frac{\partial F_m}{\partial H} = 0 \Rightarrow: H = 1.103(tb)^{\frac{1}{2}} \tag{3.111}$$

Now we need to verify the accuracy of the folding length. Several examples have been studied. One of the examples is shown in Fig. 3.64, which gives the mean crushing force with various folding lengths H. The data of the example is b=1.2 m, t=8 mm, and $\sigma = 300 MPa$. By simulation we get the optimum half-folding length $H = 99$ mm, and the minimum mean crushing force is $F_m = 403.9(kN)$. By application of Eq. (3.111), we obtain the half-folding length $H_1 = 108$ mm, and the related mean crushing force is $F_1 = 405.5(kN)$. The relative error of the mean crushing force is only 0.4%. Therefore, using Eq. (3.111) to calculate the optimum folding length and thus obtained mean crushing force has good accuracy.
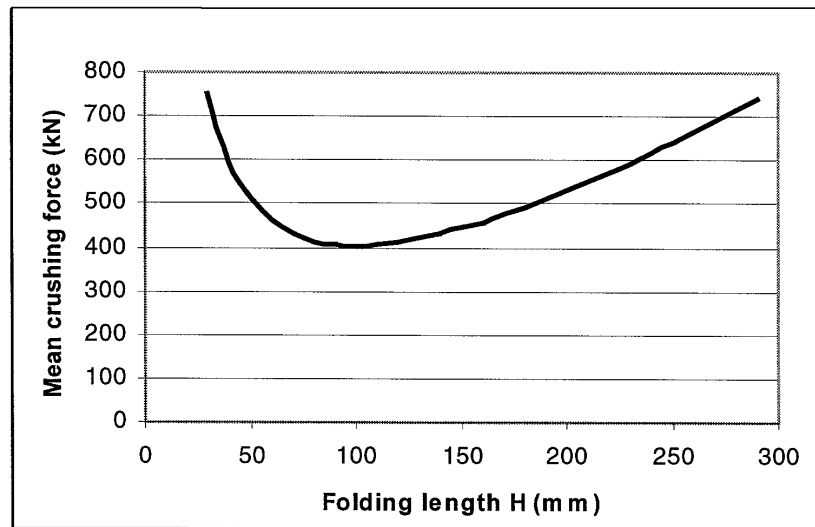
Fig. 3.64. Mean crushing force with various folding lengths.

By substitution of Eq. (3.111) into Eq. (3.110), the mean crushing force is expressed as

$$F_m = 1.6437\sigma_0 t^{1.5} b^{0.5} + 0.9365\sigma_0 t^2 (\frac{b}{b - kH}) \tag{3.112}$$

To simplify further Eq. (3.112), we calculate the ratio of kH/b. The result of kH/b with various b/t is shown in Fig. 3.65.
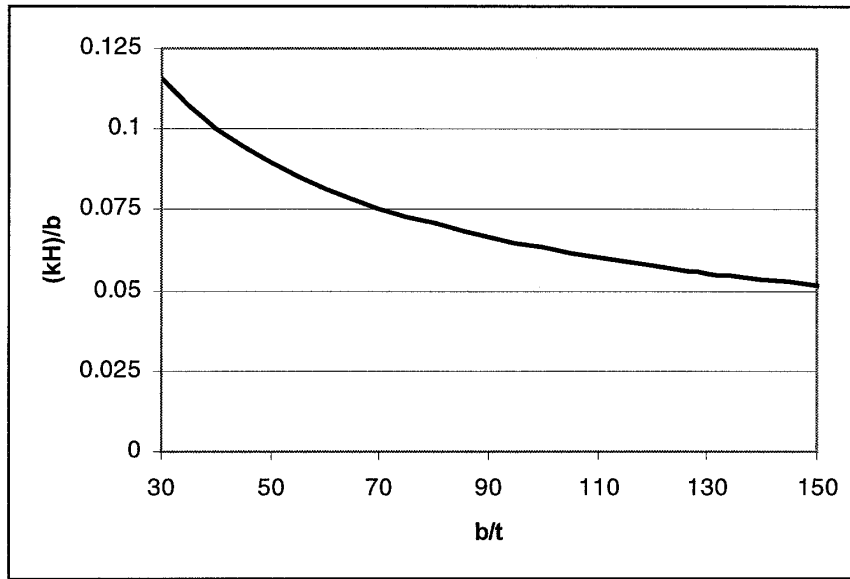
Fig. 3.65. The value of (kH / b) with various (b / t).

From Fig. 3.65 it is seen that, for a wide range of the ratio b/t =30~150, the value of kH/b = 11%~5%. If we assume that $kH/b = 7.5\%$, Eq. (3.112) becomes

$$F_m = 1.6437\sigma_0 t^{1.5} b^{0.5} + 1.012\sigma_0 t^2 \tag{3.113}$$

The indenting and crushing mechanism of the L-, T-, and X-sections can be generated by the individual plate unit. Thus the mean crushing force of the L-, T-, and X-sections can be expressed as

(1) L—section: $\quad F_L = 2.3245\sigma_0 t^{1.5} c^{0.5} + 2.025\sigma_0 t^2$ $\hspace{2cm}$ (3.114)

$\qquad\qquad\qquad\quad c = b + b$
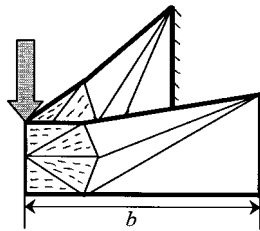
(2) T—section: $\quad F_T = 2.8470\sigma_0 t^{1.5} c^{0.5} + 3.036\sigma_0 t^2$ (3.115)
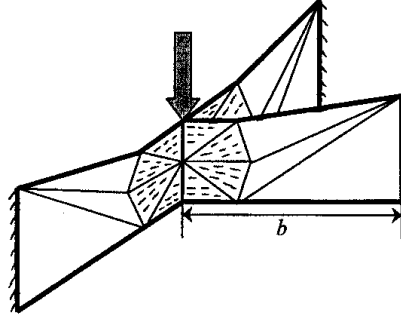
$$c = b + b + b$$

(3) X—section: $\quad F_X = 3.2874\sigma_0 t^{1.5} c^{0.5} + 4.048\sigma_0 t^2$ (3.116)

$$c = b + b + b + b$$
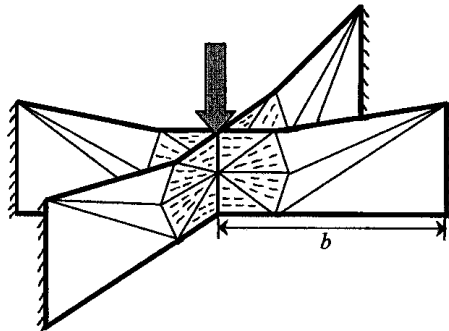
3.6.2 Subsequent Crushing

When the first fold has been completed, the maximum strain in the web plate can be calculated from

$$\varepsilon_{max} = \frac{1}{2}(\frac{\delta}{b - kH})^2 = 2.43(\frac{t}{b - 0.63(bt)^{0.5}})$$

For example, b=1.2 m, t=8 mm, the maximum strain is $\varepsilon_{max} = 1.7\%$. It is smaller than the critical rupture strain of normal steel materials. So subsequent folds will form before the web plate ruptures. It is assumed that the following folds have the same geometry as the first, as shown in Fig. 3.66.
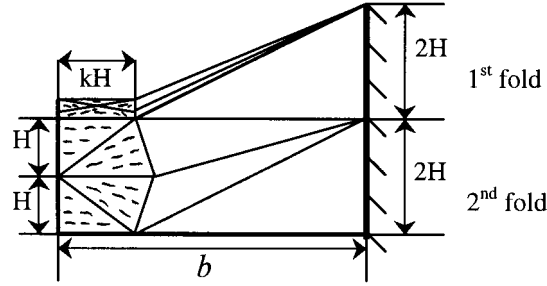
Fig. 3.66. The subsequent denting and crushing mode.

For the second folding process, the crushing resistance is composed of two parts. One is the newly crushed second fold and the other is the completely compressed first fold. That is

$$F = F_{fold1} + F_{fold2}$$

Eq. (3.113) is still valid for the mean crushing resistance of the newly crushed second fold, which is

$$F_{fold2} = 1.6437\sigma_0 t^{1.5} b^{0.5} + 1.012\sigma_0 t^2$$

The fully compressed first fold can be approximated as a plate strip. The resistance can be determined from

$$F_1 = 2.31\sigma_0 tH(\delta - 2H)/b_1$$

where $b_1 = b - kH \approx 0.925b$. Then the mean crushing resistance of the first folded lobe is

$$F_{fold1} = (\int_{2H}^{4H} F_1 d\delta)/(2H) = (6.704\sigma_0 t^{2.5} b^{0.5})/(2H) = 3.04\sigma_0 t^2$$

Therefore, during the second folding the mean crushing force is

$$F = 3.04\sigma_0 t^2 + 1.6437\sigma_0 t^{1.5} b^{0.5} + 1.012\sigma_0 t^2$$
$$= 1.6437\sigma_0 t^{1.5} b^{0.5} + (1+3)1.012\sigma_0 t^2 \qquad (3.117)$$

Similarly, the mean crushing force of the *Nth* fold can be expressed as

$$F_N = 1.6437\sigma_0 t^{1.5} b^{0.5} + [1 + 3(N-1)]1.012\sigma_0 t^2$$
$$= 1.6437\sigma_0 t^{1.5} b^{0.5} + (3N-2)1.012\sigma_0 t^2 \qquad (3.118)$$

After several folds, when the penetration reaches the critical penetration, the web plate ruptures. The rupture occurs in the $N_0 th$ fold:

$$N_0 = Int[\frac{\delta_c}{2H}] + 1 = Int[0.408(\frac{b}{t})^{0.5}\sqrt{2\varepsilon_c}] + 1 \tag{3.119}$$

After rupture, the mean crushing force is assumed to be constant, and it is calculated from

$$F_{N0} = 1.6437\sigma_0 t^{1.5}b^{0.5} + (3N_0 - 2)1.012\sigma_0 t^2 \tag{3.120}$$

By combining the individual plate units, the mean crushing force of the subsequent *Nth* fold for the L-, T-, and X-sections can be expressed as

- L—section:

$$F_L = 2.3245\sigma_0 t^{1.5}c^{0.5} + (3N - 2)2.025\sigma_0 t^2$$
$$c = b + b \tag{3.121}$$

- T—section:

$$F_T = 2.8470\sigma_0 t^{1.5}c^{0.5} + (3N - 2)3.036\sigma_0 t^2$$
$$c = b + b + b \tag{3.122}$$

- X—section:

$$F_X = 3.2874\sigma_0 t^{1.5}c^{0.5} + (3N - 2)4.048\sigma_0 t^2$$
$$c = b + b + b + b \tag{3.123}$$

3.6.3   Comparison to Amdahl's DYNA3D Simulation

Amdahl and Kavlie (1992) studied crushing of a cruciform by DYNA3D FEM calculation. Different mesh sizes are used. All edges of the model are restrained to displacement in the axial direction only. All vertical side edges are fully clamped. The calculation model and the related data are shown in Fig. 3.67.

The data of the example is

$c = 4*540 = 2160 \ mm$

$t = 3 \ mm, \ h = 500 \ mm$

$\sigma_0 = (335 + 480)/2 = 407.5 MPa$

Rupture strain $\varepsilon_c = 7\%$
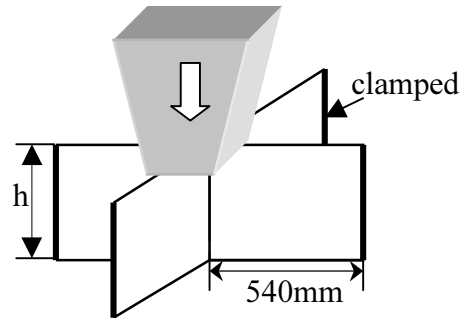
Fig. 3.67. Crushing of X-section and the related data (Amdahl and Kavlie, 1992).

Using Eq. (3.111), we get the folding length $2H = 88.8$ mm, and by application of Eq. (3.123) we get the mean crushing force $F_X(N = 1) = 323.31 + 14.85 = 338.2(kN)$. For the following *Nth* fold, the mean crushing force is $F_X(N) = 323.31 + (3N - 2)14.85(kN)$. By Eq. (3.119), the rupture occurs in the fold $N_0 = 3$.

The comparison of the present result with Amdahl and Kavlie's simulation result is shown in Fig. 3.68. Good agreement is found. From the results it is observed that the in-plane deformation in the area of $(b - kH) \cdot N(2H)$ becomes more important up to rupture.
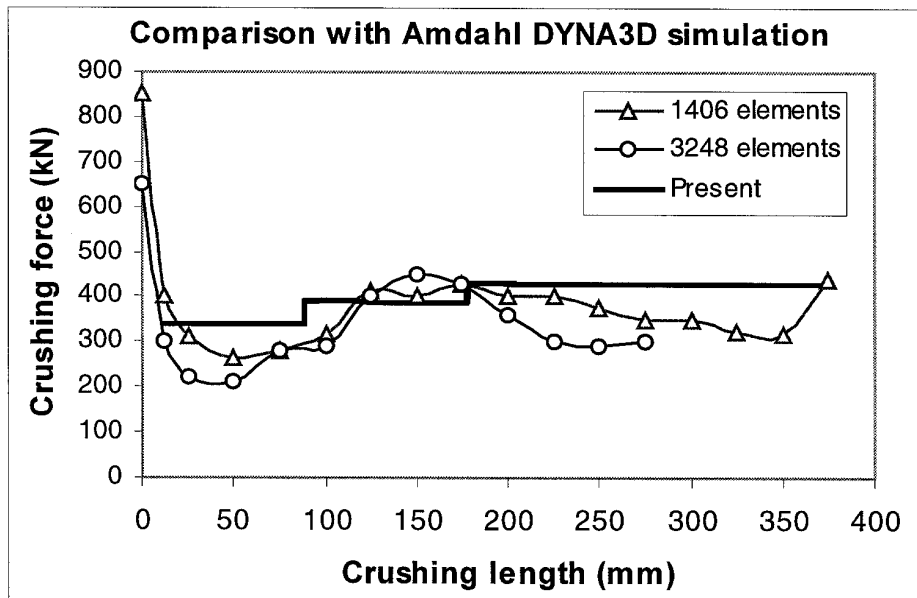
Fig. 3.68. Comparison of the crushing force of the X-section obtained by the present method and Amdahl and Kavlie's FEM simulation.

3.7 Cutting of Bare Plates

3.7.1 Introduction

In the following, we study plate cutting by a rigid wedge. The idealised model may represent a deck cutting where a ship is impacted by a striking bow or a bottom plate is torn when a ship grounds on a rock. The simplified model is illustrated in Fig. 3.69.
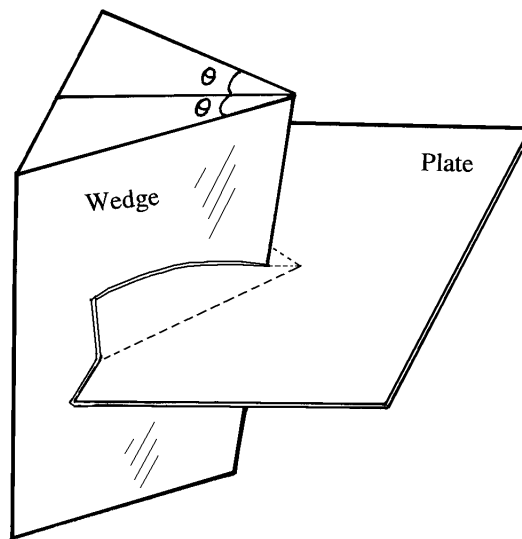
Fig. 3.69. Simplified model of bare plate cutting by a rigid wedge.

Due to the importance of the problem, many authors have made investigations of plate cutting by experimental studies and theoretical analyses. Most of the studies have been experimental and through a series of model tests empirical formulas have been obtained. Representative work was presented by e.g. Lu and Calladine (1990), Paik (1994), Lee and Hong (1997), Vaughan (1980) and Jones and Jouri (1987). These comprehensive experimental studies made the problem of plate cutting easier to understand and several useful empirical formulas were established. However, theoretical methods for understanding the mechanism are also important. Due to the complexity of the phenomenon, theoretical approaches are so far mostly based on experimental observations.

A very detailed theoretical method for the plate-cutting problem was presented by Wierzbicki and Thomas (1993). They carefully built a damage model and by some reasonable assumptions a closed-form solution was developed. A crack opening in the front of the wedge tip exists in their model. Ohtsubo and Wang (1995) argued that many experimental observations show that there is no evidence of crack opening ahead of the wedge tip, and using a model similar to that of Wierzbicki and Thomas for the curved

surfaces and assuming a velocity field for the near-wedge tip area, Ohtsubo and Wang derived an alternative formula for analysing plate cutting. Moreover, Simonsen and Wierzbicki (1997) and Zheng and Wierzbicki (1996) derived formulas for a plate steady-state cutting.

In the present approach, an assumption similar to that of Wierzbicki and Thomas for the separated curved surface is employed in which the material rolls up into two cylindrical surfaces behind the wedge tip. It is assumed that there is no crack opening in the front of the wedge tip. The material in the front of the wedge tip is stretched and ruptured due to direct indentation by the wedge tip. By assuming a plastic deformation area in the front of the wedge tip, new analytical formulas for a plate cutting force and absorbed energy are obtained in which the material critical rupture strain is included in the solution. This is the present method differing from the existing methods. Comparisons between the present results, experimental results and some existing formulas show that reasonable agreement has been achieved.

3.7.2   The Mechanics of Plate Cutting

Description of the Analysis Model

When a rigid wedge advances into a plate at a velocity of V, the plate will be separated and damaged in different modes. However, many experiments have shown that the most frequent damage mode is the plate rolling up into curved surfaces behind the tip of the wedge. Fig. 3.70 shows a picture of a plate cutting experiment performed by Thomas (1992). Based on observations from experiments, Wierzbicki and Thomas (1993) carefully constructed a damage model and established an analytical theory. They assumed that a crack opening appears in the front of the tip of the wedge. Therefore, a dimensionless parameter $\overline{\delta}_t$, termed the crack opening displacement (COD), was introduced. But many experiments revealed that there is no crack opening in the front of the wedge tip.

In the present model, we assume that the plate rupture in the front of the wedge tip is due to tension by the wedge tip pushing. The analysis model is shown in Fig. 3.71. The present idea is that plastic deformation takes place inside the line ***ABCDEF***, outside this line no plastic deformation occurs. The deformed area can be divided into two parts by the line ***BE*** located in the wedge tip. The first part in the front of the wedge tip (inside the line ***BCDE***) suffers membrane stretching due to the wedge tip pushing. With the wedge advancing, the material on the line ***BE*** ruptures, separates and forms two cylindrical surfaces behind the wedge tip. These two cylindrical surfaces are the second part of the deformed plate which undergoes bending deformation. Due to the rupture failure caused by the tension of the deformed plate in the front of the wedge tip, the critical rupture strain will be introduced in the present analysis. This is the present method differing from other existing models. This is that the cutting force should depend on the properties of the plate material: the flow stress and also the critical rupture strain.
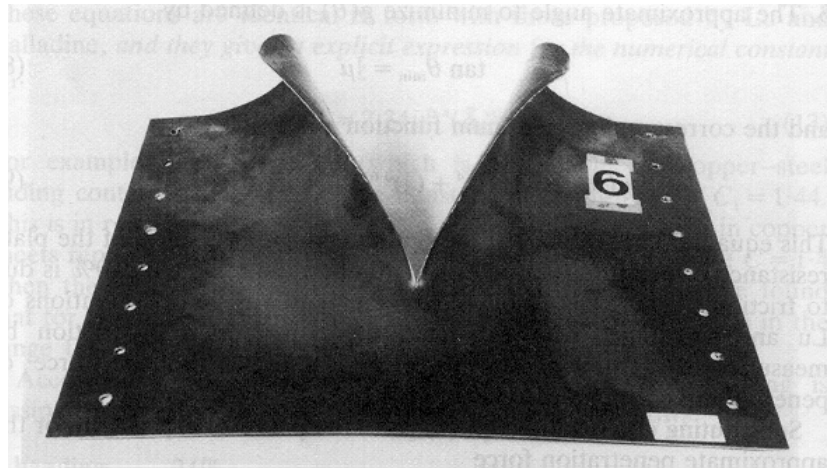
Fig. 3.70. A typical picture of a plate cutting experiment (Thomas, 1992).
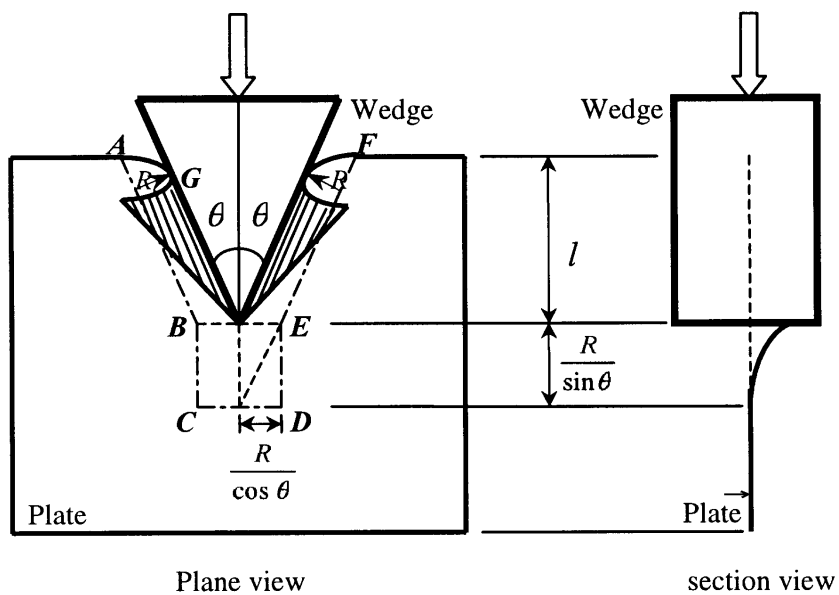
Fig. 3.71. The present analysis model of plate cutting by a rigid wedge.

Bending Energy Rate

It is assumed that all plastic bending is concentrated in two moving hinge lines, *AB* and *EF*. The length of the hinge line is

$$l_{AB} = \frac{l}{\cos\theta}$$

where *l* is the cutting length.

The rate of bending energy can be determined from

$$
\begin{aligned}
\dot{E}_b &= 2M_0 \frac{V\sin\theta}{R} l_{AB} \\
&= 2\left(\frac{2}{\sqrt{3}}\frac{1}{4}\sigma_0 t^2\right)\left(\frac{V\sin\theta}{R}\right)\left(\frac{l}{\cos\theta}\right) \\
&= \frac{1}{\sqrt{3}}\sigma_0 t^2 \frac{l}{R} V\tan\theta
\end{aligned}
\tag{3.124}
$$

where σ_0 is the flow stress of the material, t is the plate thickness, and R is the radius of the curved cylindrical surface to be determined.

Membrane Energy Rate

It is assumed that membrane energy is absorbed in the area **BCDE**, which is located in the front of the wedge tip. The mechanism of the deformation is that, with the direct pushing of the wedge tip, the plate stretches in the direction parallel to the line **BE**. The material on the upper level (line **BE**) is in the critical rupture status, and the tension decreases to zero on the line **CD**. Therefore, the rate of membrane energy can be expressed as

$$
\dot{E}_m = \iint_S \frac{2}{\sqrt{3}}\sigma_0 t \dot{\varepsilon}_{11} \, dS
\tag{3.125}
$$

where S is the area of the tension field (inside **BCDE**). $\dot{\varepsilon}_{11}$ is the tension strain rate in the direction parallel the line **BE**. Now we determine the boundary of the area. The point **B** is the intersection of the moving hinge the line **AB** and line **BE,** which crosses the point of the wedge tip and is perpendicular to the wedge moving direction. The boundary **BC** is the line which crosses the point **B** and is parallel to the wedge moving direction. The boundary **CD** is the crossed intersection point of the line **AB** and the wedge central axis and perpendicular to the wedge moving direction.

From geometric analysis, the length (H) of the line **BC** can be determined from

$$
H = \frac{R}{\sin\theta}
$$

The half length (b) of the line **CD** is

$$
b = \frac{R}{\cos\theta}
$$

For the upper fibre on the line **BE**, the strain can be calculated from

$$\varepsilon_0 = \frac{1}{2}(\frac{\delta}{b})^2$$

where δ is the indentation in the middle of the line **BE**. Thus, the strain rate is

$$\dot{\varepsilon_0} = \frac{\delta \dot{\delta}}{b^2}$$

For the lower level of the plate, the indentation is assumed to decrease linearly to zero on the line **CD**. That is

$$\delta_x = \frac{x}{H}\delta, \quad x = [0, H]$$

where x is a distance measured from the line **CD**. Thus the strain rate in each fibre can be expressed as

$$\dot{\varepsilon}_{11} = (\frac{x}{H})^2 \frac{\delta \dot{\delta}}{b^2} = (\frac{x}{H})^2 \frac{\delta}{b^2} V \tag{3.126}$$

Substituting Eq. (3.126) into Eq. (3.125) and integrating Eq. (3.125), we get the rate of the membrane energy:

$$\dot{E}_m = \frac{2}{3}\frac{2}{\sqrt{3}}\sigma_0 t \delta \frac{H}{b} V \tag{3.127}$$

As mentioned above, the upper fibre on the line **BE** is in the critical rupture status, so its strain reaches the material critical rupture strain. Thus, the critical rupture indentation is

$$\delta = b\sqrt{2\varepsilon_f} \tag{3.128}$$

where ε_f can be taken to be the material ductility determined by a tensile test.

Finally, the rate of membrane energy can be written as

$$\dot{E}_m = \frac{2}{3}\frac{2}{\sqrt{3}}\sqrt{2\varepsilon_f} \cdot \sigma_0 tR\frac{1}{\sin\theta} V \tag{3.129}$$

Plastic Resistance Force

The equilibrium of the wedge-plate system can be expressed by the principle of virtual work:

$$F_p V = \dot{E}_b + \dot{E}_m \qquad\qquad (3.130)$$

where F_p is the plastic resistance force. Substituting Eqs. (3.124) and (3.129) into Eq.(3.130), we get

$$F_p = \frac{1}{\sqrt{3}} \sigma_0 t^2 \frac{l}{R} \tan\theta + \frac{2}{3} \frac{2}{\sqrt{3}} \sqrt{2\varepsilon_f} \cdot \sigma_0 tR \frac{1}{\sin\theta} \qquad\qquad (3.131)$$

Minimising the plastic force with respect to the rolling radius R, we have

$$\frac{\partial F_p}{\partial R} = 0 \Rightarrow$$
$$R = 0.7282 t^{0.5} l^{0.5} \varepsilon_f^{-0.25} \sin\theta (\cos\theta)^{-0.5} \qquad\qquad (3.132)$$

Substituting Eq. (3.132) into Eq. (3.131), the expression for the plastic force is

$$F_p = \sigma_0 t^{1.5} l^{0.5} \varepsilon_f^{0.25} (\cos\theta)^{-0.5} (0.7928 + 0.7928)$$

$$= 1.586 \sigma_0 t^{1.5} l^{0.5} \varepsilon_f^{0.25} (\cos\theta)^{-0.5} \qquad\qquad (3.133)$$

It is seen that in the present method, the contributions of the bending and the membrane to the plastic force are equal. In the formula of Wierzbicki and Thomas, the bending is 40% and the membrane is 60% of the total dissipated plastic energy.

Eq. (3.133) shows that the cutting force depends on the material properties (σ_0 and ε_f) and the geometric parameters (t, l and θ). The critical rupture strain enters the solution of the cutting force with a power of 0.25. This means that the influence of the critical strain on the cutting force is relatively weak, which is somewhat similar to the solution of Wierzbicki and Thomas who observed that the dimensionless crack opening displacement ($\bar{\delta}_t$) enters the solution of the cutting force with a power of 0.2.

Contribution of Friction

Plate cutting experiments showed that the contribution of friction is very important in the cutting process. For a mild steel plate, Lu and Calladine estimated the contribution of friction by measuring the ratio of the withdrawal force to the penetration force and found that the mean value is $\eta = 0.4$. A thick plate cutting experiment performed by Astrup (1994) showed that there were heavy scores on the wedge surface due to friction. Therefore, the friction force should be included in the plate cutting analysis.

The fiction resistance is due to the relative motion on the contact surface between the wedge and the curled plate. The normal force on the curled surface of the plate is

$$F_n = \frac{1}{4}\frac{F_p}{\sin\theta}$$

Using Coulomb's friction law and projecting the force in the advancing direction of the wedge, we obtain the friction contribution:

$$F_f = 2\mu F_n \cos\theta = F_p \frac{1}{2}\frac{\mu}{\tan\theta} \tag{3.134}$$

Total Cutting Force

By adding the plastic resistance force F_p and the friction force F_f, the final expression for the total cutting force is

$$F = F_p + F_f = 1.586\sigma_0 t^{1.5}l^{0.5}\varepsilon_f^{0.25}(\cos\theta)^{-0.5}(1+\frac{1}{2}\frac{\mu}{\tan\theta}) \tag{3.135}$$

The total energy dissipated by plastic deformation and friction can be calculated from

$$E = \int_0^l Fdl = 1.057\sigma_0 t^{1.5}l^{1.5}\varepsilon_f^{0.25}(\cos\theta)^{-0.5}(1+\frac{1}{2}\frac{\mu}{\tan\theta}) \tag{3.136}$$

Dimensionless expressions for the cutting force and the dissipated energy can be written as

$$\frac{F}{\sigma_0 t^2} = [1.586\varepsilon_f^{0.25}(\cos\theta)^{-0.5}(1+\frac{1}{2}\frac{\mu}{\tan\theta})](\frac{l}{t})^{0.5} \tag{3.137}$$

$$\frac{E}{\sigma_0 t^3} = [1.057\varepsilon_f^{0.25}(\cos\theta)^{-0.5}(1+\frac{1}{2}\frac{\mu}{\tan\theta})](\frac{l}{t})^{1.5} \tag{3.138}$$

3.7.3   Comparisons and Discussions

Previously Presented Formulas for the Cutting Force

For convenience, some of the previously presented formulas for the cutting force are listed below:

(1) Ohtsubo and Wang (analytical, 1995)

$$F = 1.51\sigma_0 t^{1.5} l^{0.5} (\sin\theta)^{0.5} (1 + \frac{\mu}{\tan\theta}) \qquad (3.139)$$

(2) Wierzbicki and Thomas (analytical, 1993)

$$F = 1.67\sigma_0 t^{1.6} l^{0.4} (\bar{\delta}_t)^{0.2} \frac{1}{(\cos\theta)^{0.8}} [(\tan\theta)^{0.4} + \frac{\mu}{(\tan\theta)^{0.6}}] \qquad (3.140)$$

$\bar{\delta}_t$ is the COD parameter, $\bar{\delta}_t = 1.0$ is normally used suggested by Wierzbicki and Thomas.

(3) Paik (empirical, 1994)

$$F = 1.5 C_{1.5}\sigma_0 t^{1.5} l^{0.5} \qquad (3.141)$$
$$C_{1.5} = 3.760\theta^2 - 1.156\theta + 1.112$$

(4) Lu and Calladine (empirical, 1990)

$$F = 1.3 C_{1.3}\sigma\ t^{1.7} l^{.3} \qquad (3.142)$$
$C_{1.3}$ is an empirical constant, for a mild steel material the constant is $C_{1.3} = 2.3$.

In the following calculation examples, the coefficient of friction μ takes the value which was suggested by the related papers.

Comparison with MIT Thin Plate Cutting Experiments

In the Joint Industry Program on Tanker Safety at Massachusetts Institute of Technology (MIT), Thomas (1992) made a series of model tests of plate cutting. Here we use two of them as comparison examples. The first is a plate with thickness of 0.794 mm (Test #1 in Thomas, 1992) which was cut by a rigid wedge with a semi-angle of $\theta = 20°$. The flow stress of the material is $\sigma_0 = 114.5 MPa$, the critical rupture strain of the material is $\varepsilon_f = 10\%$, the coefficient of friction is assumed to be $\mu = 0.2$. A comparison between the present calculation and experimental results is shown in Fig. 3.72. Good agreement is found.

Fig. 3.72. Comparison between the present calculation and MIT experimental results (wedge semi-angle $\theta = 20°$).

The second comparison example is a plate with thickness of 1.47 mm (Test #5 in Thomas, 1992). The semi-angle of the wedge is of $\theta = 30°$. The flow stress of the material is $\sigma_0 = 228 MPa$, the critical rupture strain of the material is $\varepsilon_f = 25\%$, and the coefficient of friction is assumed to be $\mu = 0.2$. A comparison between the present calculation and MIT experimental results is presented in Fig. 3.73. Again good agreement is found.
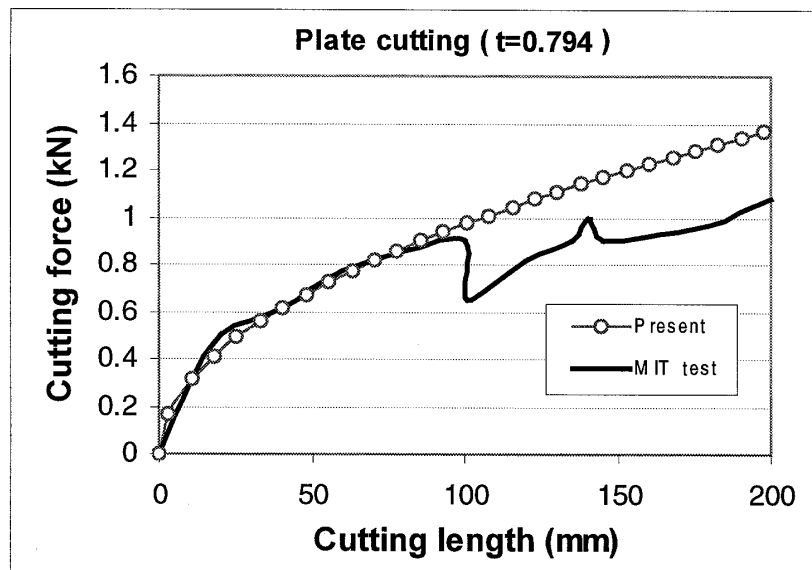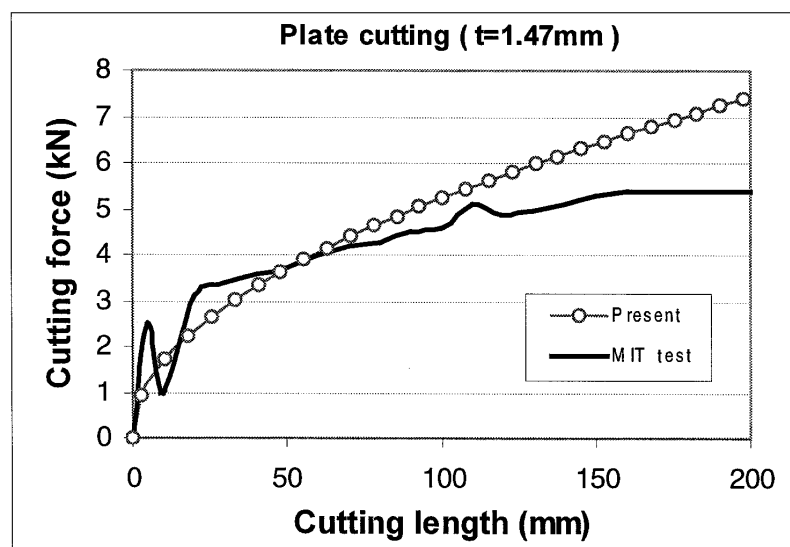

Fig. 3.73. Comparison between the present calculation and MIT experimental results (wedge semi-angle $\theta = 30°$).

Comparison with Astrup's Thick Plate Cutting Experiments

Astrup (1994) carried out cutting tests of very thick plates. The thickness of the tested plates is in the range of 15 mm to 25 mm, which is a typical bottom thickness of oil carriers. First we compare the experimental result for the 15 mm plate (Test #P1-15 in Astrup) with the results obtained by the different formulas. The semi-angle of the rigid wedge is $\theta = 30°$. The flow stress of the material is $\sigma_0 = 480.5\,\text{MPa}$, and the critical rupture strain is $\varepsilon_f = 30\%$. As Astrup pointed out, there was large friction between the wedge and the plate. Astrup believed that the friction in his experiments is larger than in Lu and Calladine's experiments, and a coefficient of friction of 0.5 to 0.55 is not unreasonable. Therefore, here we assumed that the coefficient of friction is $\mu = 0.5$. In the present calculation, the contribution of friction is 30% of the total cutting force. A comparison of results obtained by the different methods is shown in Fig. 3.74. Reasonable agreement is achieved between the present result and the test result. But all other formulas also give good agreement.
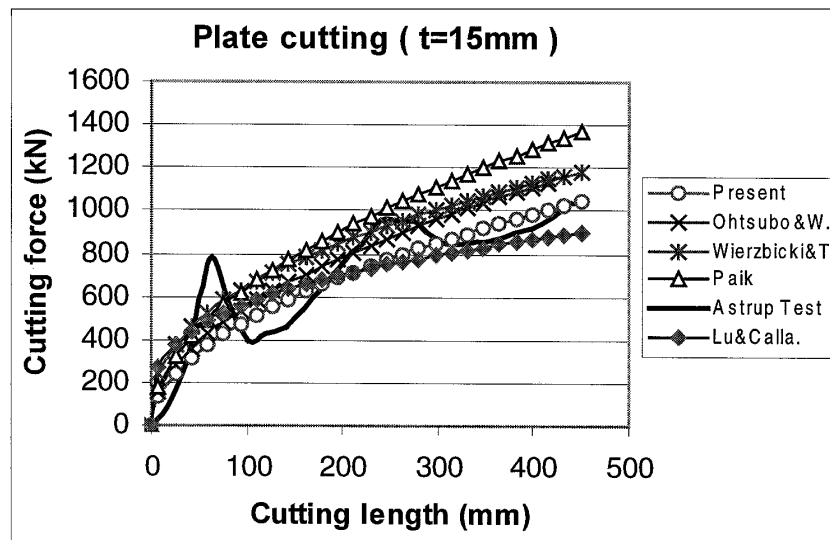
Fig. 3.74. Comparison of the cutting forces for a thick plate (t=15 mm, $\theta = 30°$).

The second comparison example is the 20 mm plate (Test #S2-20 in Astrup). The flow stress of the plate is $\sigma_0 = 459.5\,\text{MPa}$, the critical rupture strain is 31%, the coefficient of friction is again taken to be $\mu = 0.5$. Results obtained by the different methods are presented in Fig. 3.75. The figure shows that the present method, Ohtsubo and Wang's method and Wierzbicki and Thomas' method agree well with Astrup's test result. Paik's result is somewhat higher than the test result and Lu and Calladine's result is lower than the test result.
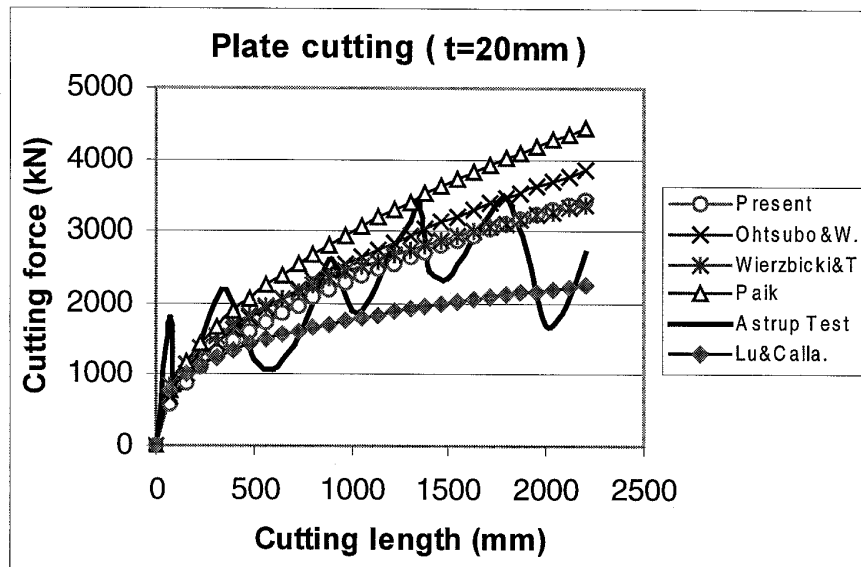
Fig. 3.75. Comparison of the cutting forces for a very thick plate (t=20 mm, $\theta = 30°$).

Comparison with Paik's Stiffened Plate Experiments

Paik (1994) has made many plate-cutting tests of longitudinally stiffened plates (stiffened in the cutting direction) and derived empirical formulas using test results. He used the equivalent thickness concept to deal with stiffeners. The idea is to distribute the cross sectional area of the stiffeners to the whole plate.

Fig. 3.76 shows a comparison of dissipated energies obtained by the different methods. The equivalent thickness is $t_{eq} = 4.669$ mm (Test #T3-11 in Paik), the flow stress of the material is $\sigma_0 = 439.5$ MPa, the critical rupture strain is 26%, and the coefficient of friction is assumed to be $\mu = 0.4$.

Fig. 3.77 gives another example of comparison of the absorbed energies with various cutting lengths. The equivalent thickness is $t_{eq} = 10.5$ mm (Test #T7-4 in Paik), the flow stress of the material is $\sigma_0 = 364.5$ MPa, the critical rupture strain is 40%, and the coefficient of friction is also $\mu = 0.4$.

It is seen from the figures that the present calculation results and Ohtsubo and Wang's results are somewhat lower than the experimental results, especially at relatively large cutting lengths. But all the differences may be acceptable. As it is concluded by Paik, the equivalent plate thickness approach to stiffened plates is useful.
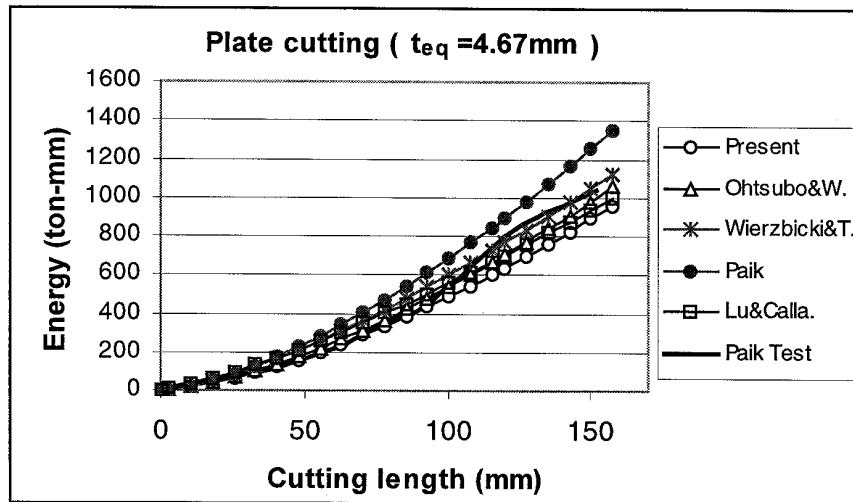
Fig. 3.76. Dissipated energy in a stiffened plate (t_{eq} =4.67 mm, θ = 30°).
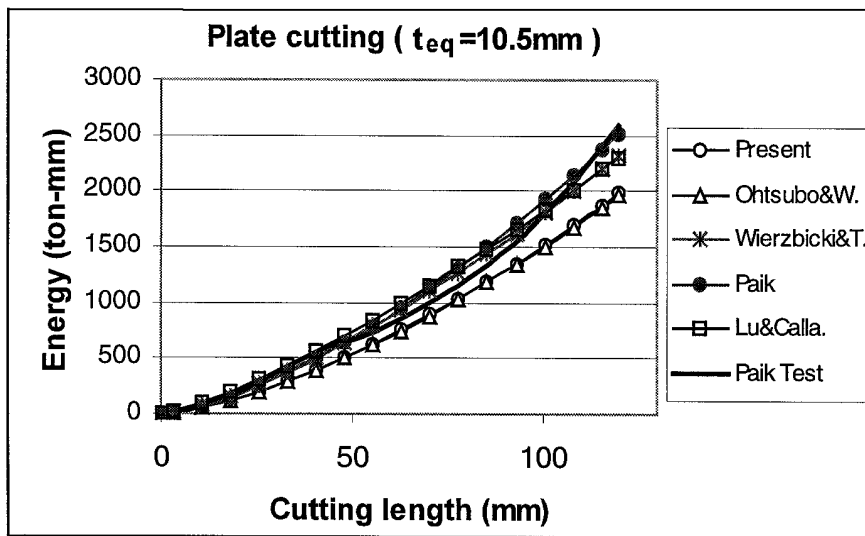
Fig. 3.77. Dissipated energy in a stiffened plate (t_{eq} =10.5 mm, θ = 30°).

Dimensionless Cutting Force

As discussed in the above comparisons, good agreement is achieved between the different methods and experiments. In order to demonstrate further the correlation among the different methods, we shall carry out calculations on the dimensionless cutting force ($F/(\sigma_0 t^2)$) as a function of the dimensionless cutting length (l/t). Figs. 3.78 and 3.79

show the calculation results obtained. In these calculations, the coefficient of friction is $\mu = 0.2$, the critical rupture strain is 25%. It is seen that the agreement is good between the results obtained by the present method, Wierzbicki and Thomas, Ohtsubo and Wang and Lu and Calladine's. It seems that Paik's result is always high, especially in the case of a larger semi-angle of the wedge.
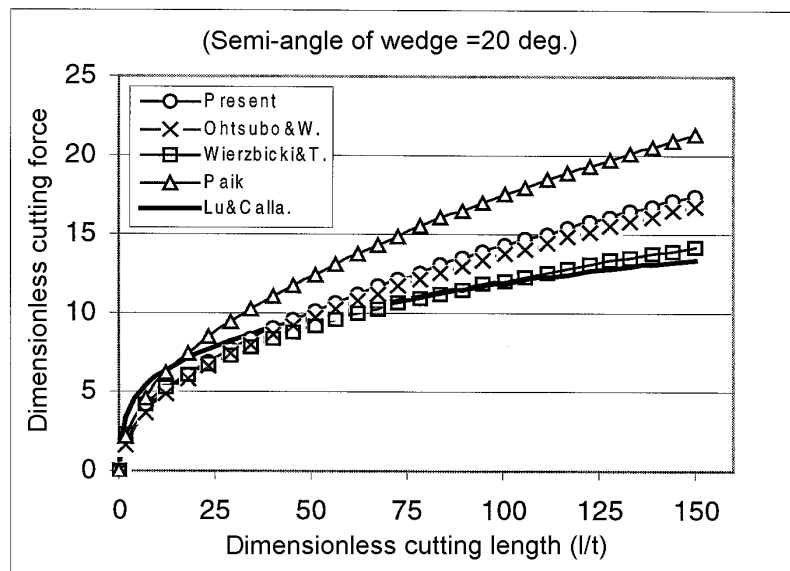
Fig. 3.78. Comparison of the dimensionless cutting forces (semi-angle $\theta = 20^0$).
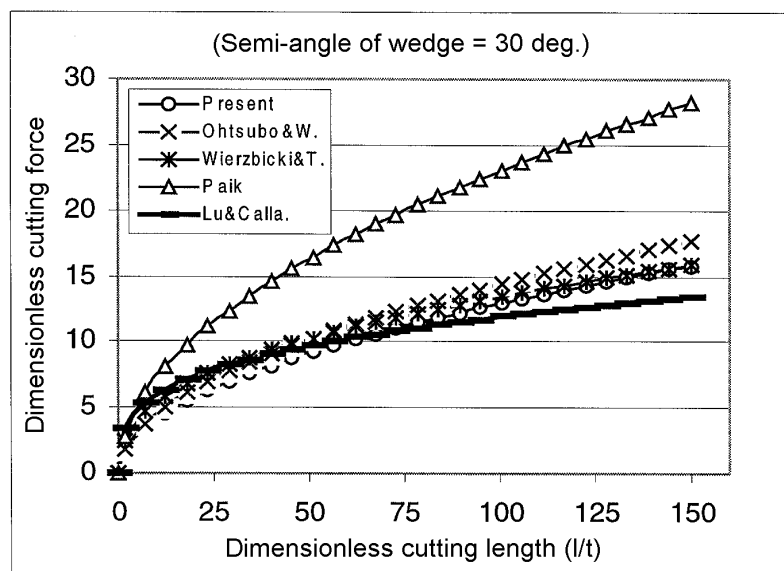
Fig. 3.79. Comparison of the dimensionless cutting forces (semi-angle $\theta = 30^0$).

Effect of Wedge Angle and Friction

In Lu and Calladine's empirical formula, the wedge angle is not included in the solution. They concluded that the wedge angle is not very important to a certain range of angles (in their tests, the wedge semi-angle is $\theta = 10° \sim 20°$). But all other formulas have included the wedge angle effect. For most of the existing experiments, the semi-angle of the wedge is between $10°$ and $30°$. Here we choose the range of semi-angle of the wedge between $5°$ and $85°$ to see the effect of the wedge angle on the cutting force.

It is also believed that the friction between the wedge and the plate is important. And it is very difficult to determine exactly the coefficient of friction. This means that there is some uncertainty of calculating the cutting force due to friction. However, we can estimate the range of the value of the friction coefficient from some experiments, such as that of Lu and Calladine (1990). A wide range of the coefficient of friction for steel material may be $\mu = 0.1 \sim 0.5$. Here we take the coefficient of friction to be 0.1 to 0.5 and investigate the influence of the friction on the cutting force. To do this, the formula for the cutting force is rewritten as

$$F = 1.586 \sigma_0 t^{1.5} l^{0.5} \varepsilon_f^{0.25} \cdot g(\theta, \mu) \tag{3.143}$$

where the function $g(\theta, \mu) = \dfrac{1}{\sqrt{\cos\theta}} (1 + \dfrac{1}{2} \dfrac{\mu}{\tan\theta})$ reflects the effects of the wedge angle and the friction on the cutting force.

Fig. 3.80 shows calculation results for the function $g(\theta, \mu)$ with various friction coefficients from 0.1 to 0.5 and semi-angles from 5 to 85 degrees. It is seen from the figure that the effects of both the wedge angle and the friction on the cutting force are relatively weak. For example, the values of the function $g(\theta, \mu)$ are between 1.34 and 1.46 when the semi-angles of the wedge are between 20 degrees and 60 degrees and the coefficient of friction is 0.3. On the other hand, the values of the function $g(\theta, \mu)$ are between 1.30 and 1.42 when the friction coefficients are between 0.2 and 0.4 and the semi-angle of the wedge is 45 degrees.

3.7.4   Concluding Remark

An analytical formula for plate cutting by a rigid wedge is developed. The characteristic of the present method is that the critical rupture strain enters the solutions of the cutting force and the absorbed energy. Thus, the cutting force depends on material properties (σ_0 and ε), geometric parameters (t, l and θ) and friction coefficient (μ).

Comparisons of the present method, experimental results and some existing formulas for both thin plates and thick plates show that the general agreement is acceptable. The influence of both the wedge angle and the friction on the cutting force is very weak.
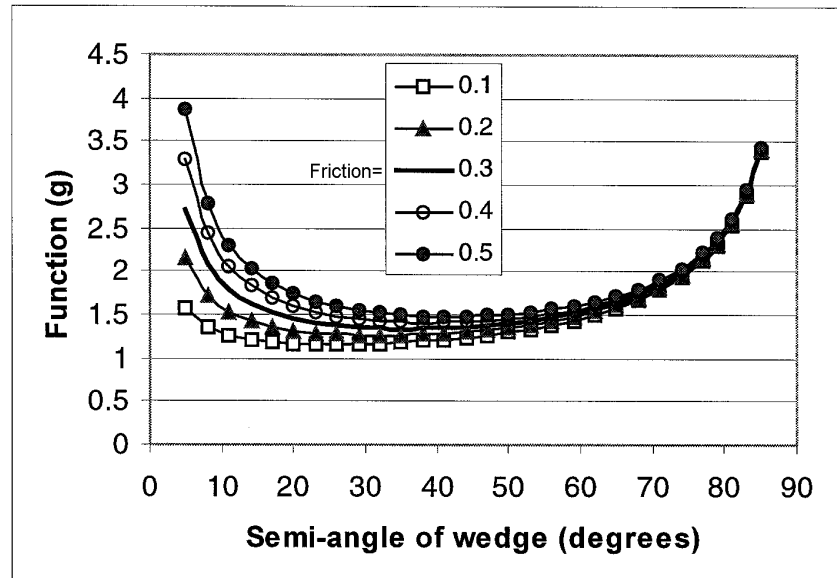
Fig. 3.80. Influence of the wedge angle and the friction on the cutting force.

3.8 Crushing of Stiffened Deck and Bottom

3.8.1 Introduction

In Section 3.7, cutting of a bare plate by a rigid wedge was studied. Actually, ship decks are not bare plates, but stiffened by transverses and longitudinals. If the stiffeners are not heavy, the deck may be simplified as a bare plate by using the equivalent thickness method. But if a deck is heavily stiffened, an alternative analysis method for damage to a stiffened deck (or bottom) must be developed.

Observations from collision accidents show that the damage modes of ship decks are folding, crushing and tension rupture. Some illustrations of damaged decks from collision accidents are shown in Fig. 3.81.

Fig. 3.82 shows the analysis model of a bow crushing into the side of a struck ship. The stiffened decks or bulkheads are divided into different elements (L-, T-, and X-elements), which are crushed by the striking bow. With further penetration, more and more elements are crushed and destroyed. Typical axial crushing modes of L-, T- and X- elements are shown in Fig. 3.83 (Amdahl, 1983 and Kierkegaard, 1993).
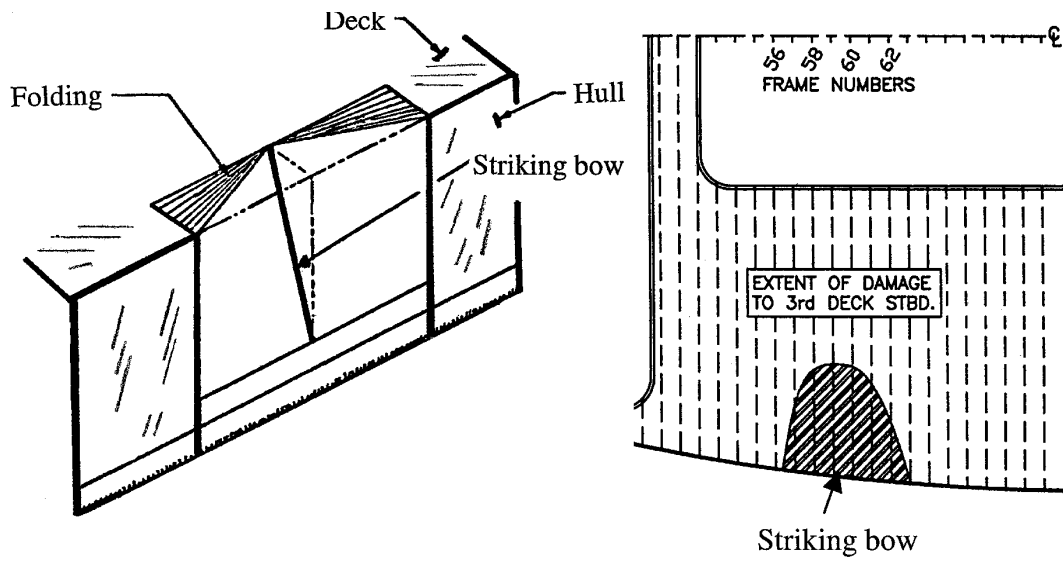
Fig. 3.81. Illustrations of deck damages observed in collision accidents.
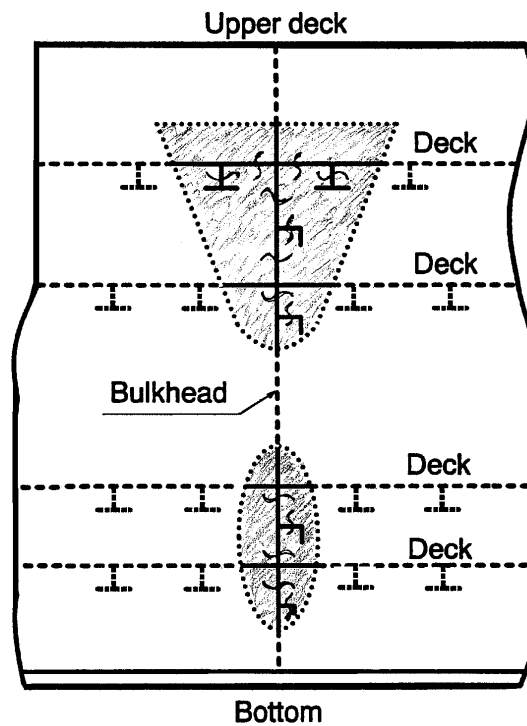
Fig. 3.82. A striking bow crushes the deck structures and the side of a struck ship.
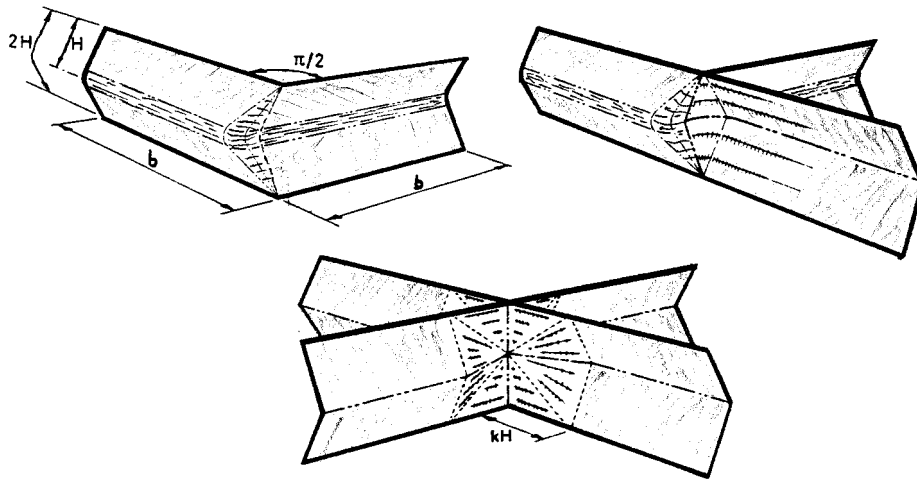
Fig. 3.83. Axial crushing modes of L-, T- and X- elements (Kierkegaard, 1993).

Many authors have investigated axial crushing of the basic elements, using theoretical methods and experimental methods. Amdahl (1983), Wierzbicki and Abramowicz (1983), Jones and Birch (1990), Kierkegaard (1993), Abramowicz (1994), Paik and Pedersen (1995) and Lee and Choung (1996) did comprehensive work on the element axial crushing. Paik and Wierzbicki (1997) carried out a benchmark study on the crushing strength by comparing the existing theoretical formulas and experimental results. Here we choose some of the existing formulas and compare them, and then select one for the purpose of the present use.

3.8.2   Some Existing Formulas for Mean Crushing Force

The mean axial crushing force of a combined structure with L-, T- and X-elements can be analysed by the following existing formulas:

(1) Amdahl J. (1983)

$$F_{Amd.} = 2.42\sigma_0 A \cdot (\frac{n_{AT}t^2}{A})^{0.67}\{0.87 + 1.27\frac{n_X + 0.31n_T}{n_{AT}}[\frac{A}{(n_X + 0.31n_T)t^2}]^{0.25}\}^{0.67}$$

(2) Yang and Caldwell (1988)

$$F_{Y\&C} = \sigma_0(1.178t^2 L\frac{1}{H} + 0.215n_{AT}tH + 6.935n_{AT}t^2 + 0.265n_T tH + 0.589n_T t^2 + 0.75n_X tH + 0.375n_X t^2)$$

$$H = \frac{1.178 \cdot tL}{0.215n_L + 0.48n_T + 0.75n_X}$$

(3) Abramowicz W. (1994)

$$F_{Abr.} = (n_L + 1.2n_T + 2.1n_X)(3.263\sigma_0 c^{0.33} t^{1.67})$$
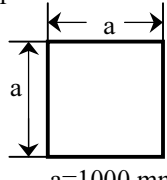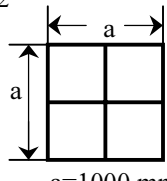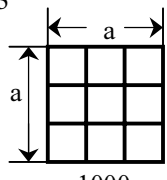
(4) Paik and Pedersen (1995)

$$F_{P\&P} = \sigma_0 A\{2.9273(\frac{t}{b})^{0.5} + 0.3661\frac{t}{b}\}$$

where n_L is the number of L-elements, n_T is the number of T-elements, n_X is the number of X-elements or the cruciform, t is the average thickness of the section, $c = L/n$, L is the total cross-sectional length, $n = n_L + n_T + n_X$ is the total number of all the elements, $n_{AT} = n_L + n_T$, $A = t \cdot L$ is the section area of the materials, b is the cross-sectional length of an individual plate.

In order to compare the existing formulas, we consider a square tube with different frames inside the tube as shown in Table 3.8. The sectional length of the tube is $a = 1000$ mm, all plate thickness is $t = 10$ mm. The comparison of the mean crushing strengths ($F_m /(\sigma_0 A)$) for the three cases is presented in Table 3.8.

Table 3.8. Comparison of the mean crushing strengths obtained by the different formulas.

Case No.	Amdahl (1983)	Yang and Caldwell (1988)	Abramowicz (1994)	Paik and Pedersen (1995)	Average $(\sum_{i}^{N} F_i)/N$
#1 a=1000 mm	**0.101** -34.8%	**0.170** +9.7%	**0.151** -2.6%	**0.199** +28.4%	**0.155** 0%
#2 a=1000 mm	**0.235** -8.2%	**0.264** +3.1%	**0.240** -6.3%	**0.283** +10.6%	**0.256** 0%
#3 a=1000 mm	**0.314** -4.8%	**0.325** -1.5%	**0.330** 0%	**0.349** +5.8%	**0.330** 0%

From the comparison in Table 3.8 it is seen that Paik and Pedersen's results are high and Amdahl's results are low. Yang and Caldwell's and Abramowicz's results are between the high and low values. But all the formulas have an acceptable agreement, especially for the case where the number of n_T or n_X is large. Due to the simplicity of the expression of Abramowicz's formula, we prefer to use this formula to calculate the deck crushing resistance. The expression is

$$F = (n_L + 1.2n_T + 2.1n_X)(3.263\sigma_0 t^{1.67}c^{0.33}) \tag{3.144}$$

3.8.3 Analysis Procedure for Deck Crushing

The Initial Collision Phase

For the initial collision phase, it is reasonable to assume that the deck fails in the folding deformation. The collision location is assumed to be in the middle between two web frames. The collision situation is shown in Fig. 3.84.
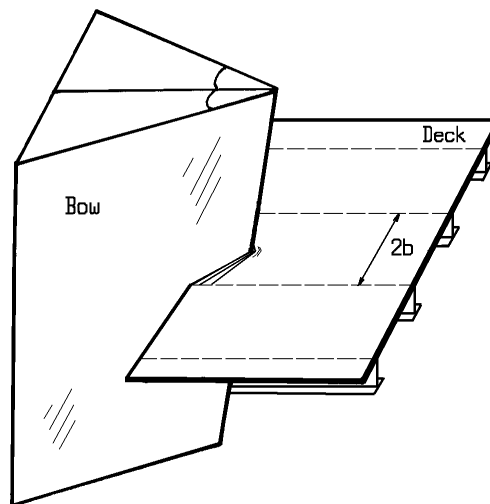
Fig. 3.84. Initial deformation of the deck folding.

The previously derived formula for web crushing (see Section 3.5.1) applies to analysis of the initial crushing of the deck. Here we write the formulas for the mean crushing force again:

$$F = \begin{cases} 4.33\sigma_0 t_d^{1.67} b^{0.33} \dots\dots\dots\dots\dots\dots\dots\dots\delta \le 2H \\ \\ 6.77\sigma_0 t_d^{1.67} b^{0.33} \dots\dots\dots\dots\dots\dots\dots\dots\delta > 2H \end{cases} \tag{3.145}$$

where

δ is the penetration, $H = 0.8383(b^2 t_d)^{\frac{1}{3}}$, t_d is the thickness of the deck plate and $2b$ is the spacing between heavy transverse stiffeners.

Further Crushing

When the striking bow touches the heavy stiffeners of the deck, as shown in Fig. 3.85, crushing of the deck structure (such as the basic elements L-, T- and X-) will happen. Then Abramowicz's formula Eq. (3.144) is employed for analysing the crushing force.

In this figure:

$$n_L = 0$$
$$n_T = 4 + 4$$
$$n_X = 0$$
$$N_{deck} = 3$$
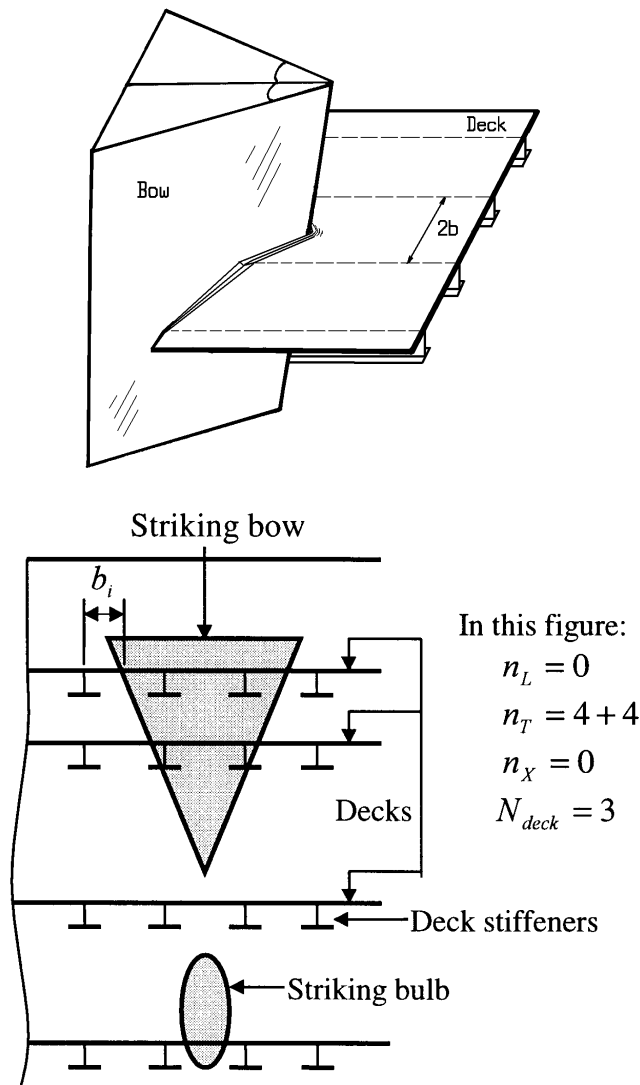
Fig. 3.85. Further crushing of ship decks.

It is assumed that the basic elements are not deformed and crushed until the striking bow pushes them directly. The deck plate between the touching point and the non-deformed stiffener (b_i in Fig. 3.85) suffers tension and bending deformation. Its behaviour is similar to web folding. Therefore, the collision force for the further deck crushing can be expressed as

$$F = \sum_{i=1}^{N_{deck}} \{(n_L + 1.2n_T + 2.1n_X)(3.263\sigma_0 t_i^{1.67} c_i^{0.33}) + 4.33\sigma_0 t_d^{1.67} b_i^{0.33}\} \qquad (3.146)$$

where n_L, n_T, n_X are the numbers of the L-, T- and X-elements crushed in each deck, t_i is the average thickness of the basic elements in deck i, c_i is the average cross-sectional length of an element in the deck i, t_d is the thickness of the deck plate, b_i is the distance between the touching point and the non-deformed stiffeners and N_{deck} is the number of crushed decks.

3.9 Estimation of Rupture Hole in Shell Plating

3.9.1 Introduction

When the penetration of a striking bow into the side of a struck ship is large enough, the strain in the side shell plating reaches its critical value and the shell plating cracks and ruptures. With increasing penetration, the crack extends and finally a hole is formed. Observations from accidents of full-scale ship collisions show that the exact shape of the damaged hole in the shell plating is very complicated. Fig. 3.86 shows the hole in the side of a 53,900 t container ship struck by a 22,700 dwt bulk carrier.

It is very difficult to predict the shape of the hole precisely. In this thesis, we try to use a simple geometric analysis to calculate the size of the damaged hole. The purpose is to get the main dimensions of the hole. Based on observations from experiments and collision accidents, we assume that the side shell plating conforms to the striking bow after the shell plating has ruptured.

Fig. 3.87 shows a hole of a side damaged by a raked bow, which was a model test carried out by Ito et al. (1984). Fig. 3.88 shows a damaged hole of a side struck by a bulb in a collision accident. Fig. 3.89 shows the side damage of full-scale collision experiments sponsored by Japanese ASIS (1998). These photos indicate that the present assumption is reasonable.
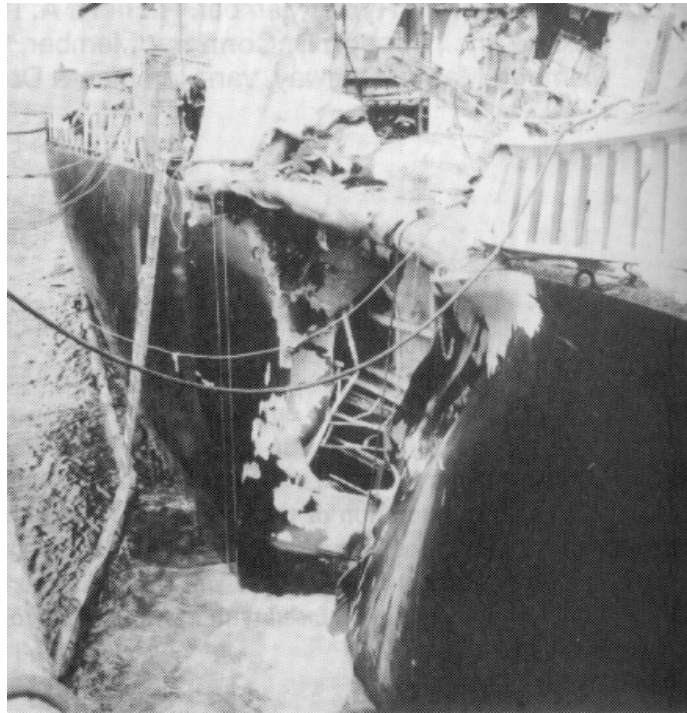
Fig. 3.86. Side damage to a 53,900 t container ship struck by a 22,700 dwt bulk carrier in 1996.
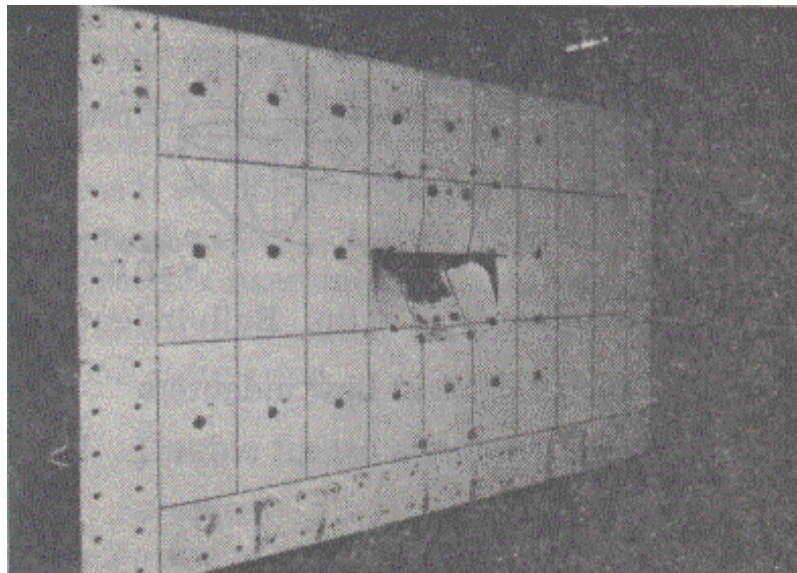
Fig. 3.87. Damaged hole of a side struck by a raked bow (model tests, Ito et al., 1984).

Fig. 3.88. Damage to a ship side struck by a bulb in a collision accident.

Fig. 3.89. Side damage of full-scale collision experiments sponsored by Japanese ASIS (1998).

3.9.2 Hole Created by a Conventional Bow

Perpendicular Penetration

The assumption is that the shell plating conforms to the striking bow after the shell plating has ruptured as discussed above. Therefore, for a given penetration δ and knowing the shape of the striking bow, we may by geometric analysis, obtain the size of the hole. Fig. 3.90 shows an illustration of a hole created by a conventional bow during perpendicular penetration.
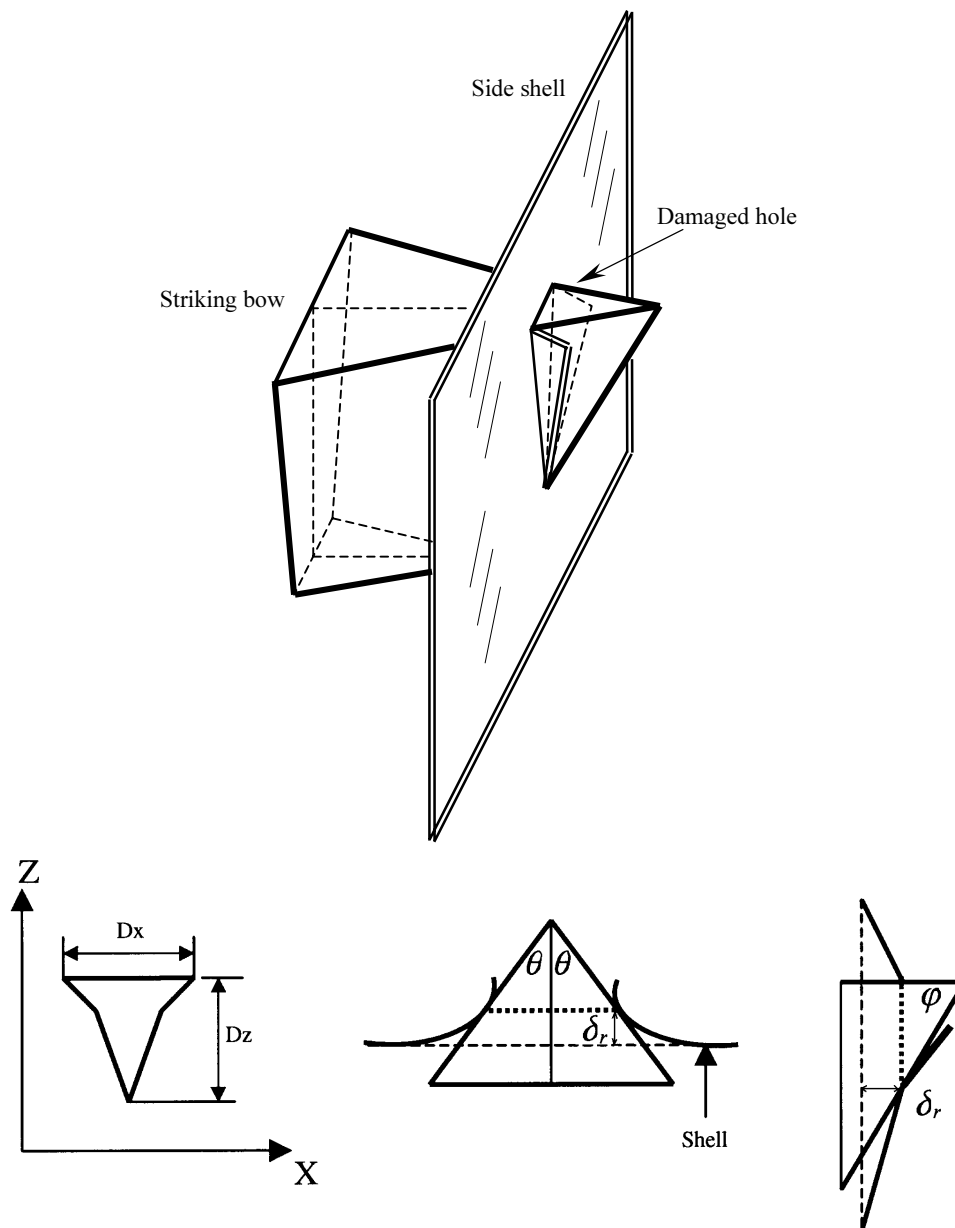
Fig. 3.90. A hole created by a conventional striking bow.

The length of the hole (along the ship length) can be easily determined from

$$D_X = 2(\delta - \delta_r)\tan\theta \tag{3.146}$$

where δ is the penetration, δ_r is the critical penetration at which the shell plating starts to rupture, θ is the half entrance angle of the striking bow. If $D_X \geq B$, set $D_X = B$, where B is the breadth of the striking ship.

The height of the hole (in the vertical direction) can be calculated from

$$D_Z = (\delta - \delta_r)\tan\varphi \tag{3.147}$$

where φ is the stem angle of the striking bow. If $D_Z \geq H_{deck}$, set $D_Z = H_{deck}$. Here H_{deck} is the height of the forecastle of the striking ship.

Comparison with Scharrer's Calculation Results

Examples are calculated and compared with Scharrer's (1996, from GL) results. The considered case is a 160 m ship striking a 150 m Ro-Ro vessel. The half entrance angle of the striking bow is assumed to be $\theta = 40$ degrees, the stem angle of the striking bow is $\varphi = 70$ degrees. The calculation results and the comparisons are presented in Fig. 3.91. Good agreement is found for the vertical height of the damaged hole. But there is a difference in the calculated length of the hole. The reason is that we use a simplified shape of the striking bow. The upper deck width of the striking bow has some difference between the present and Scharrer.
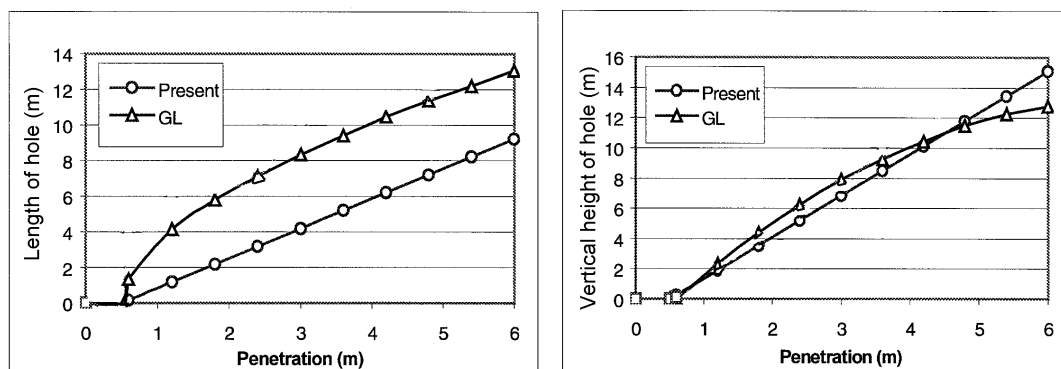
Fig. 3.91. Comparison of damaged hole sizes between the present and GL calculations.

Oblique Collision

For an oblique collision, we have shown that the penetration direction follows the direction of the relative velocity $\vec{V} = \vec{V}_1 - \vec{V}_2$. Here $\vec{V}_1$ is the velocity of the striking ship and $\vec{V}_2$ is the velocity of the struck ship. Fig. 3.92 shows an illustration of the hole in an

oblique collision. α is the collision angle defined between $\vec{V}$ and $\vec{V}_2$, β is the penetration angle defined between $\vec{V}$ and $\vec{V}_2$.
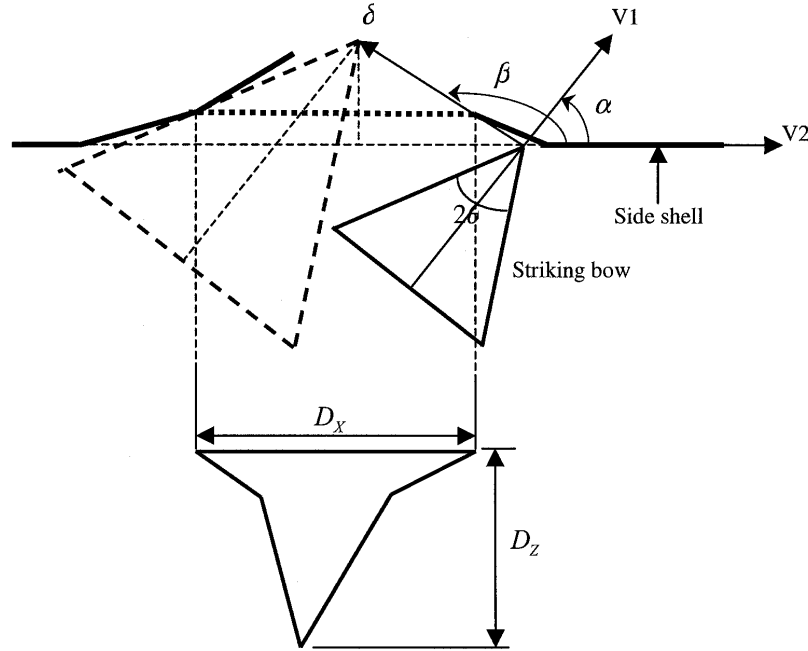
Fig. 3.92. Illustration of the hole created by a raked bow in an oblique collision.

By means of geometric analyses, the size of the hole is expressed as follows:

- When $\alpha \geq 90°$ and $\theta \geq (\beta - \alpha)$

   Length of the hole: $D_X = (\delta \sin \beta - \delta_r)(\dfrac{1}{\tan(\alpha - \theta)} - \dfrac{1}{\tan(\alpha + \theta)})$ (3.148)

   Height of the hole: $D_Z = (\delta \sin \beta - \delta_r)\dfrac{\tan \varphi}{\sin \alpha}$ (3.149)

- Other cases

   Length of the hole: $D_X = (\delta \sin \beta - \delta_r)(\dfrac{1}{\tan(\alpha - \theta)} - \dfrac{1}{\tan \beta})$ (3.150)

   Height of the hole: $D_Z = (\delta \sin \beta - \delta_r)\dfrac{\tan \varphi}{\sin \alpha}$ (3.151)

where δ_r is the critical rupture penetration in the direction normal to the struck ship. If $D_Z \geq H_{deck}$, set $D_Z = H_{deck}$. This means that the maximum height of the damaged hole is the deck height H_{deck} of the striking ship. But the length of the damaged hole may be larger than the breadth of the striking ship in an oblique penetration.

Comparison with Scharrer's Calculations

Scharrer (1996, from GL) made a series of calculations of raked bows striking Ro-Ro vessels in oblique collisions. Here we take an example from his calculations and make a comparison with the present calculations. The striking ship is 160 m in length, the breadth is 24.6 m, the deck height is 16.3 m, the half entrance angle of the striking bow is 40 degrees and the stem angle is 70 degrees. The struck ship is a Ro-Ro vessel with length of 150 m. The speed of the striking ship is equal to the speed of the struck ship. Therefore, the relation of the collision angle α and the penetration angle β is $\beta = 90^0 + \alpha / 2$. The considered collision cases are shown in Table 3.9.

Table 3.9. Collision cases of the 160m striking ship and the Ro-Ro vessel.

	Collision angle α (degrees)	Penetration angle β (degrees)
Case #1	60	120
Case #2	90	135
Case #3	120	150

The comparisons of the present calculation results and Scharrer's calculations are presented in Figs. 3.93, 3.94 and 3.95, respectively, for the three collision cases. These figures show that the agreement for the vertical height of the hole is very good. But there are some differences in the length of the hole between the present results and Scharrer's results. As discussed above, the reason for this is that the striking bow used in the present calculation is a simplified bow.
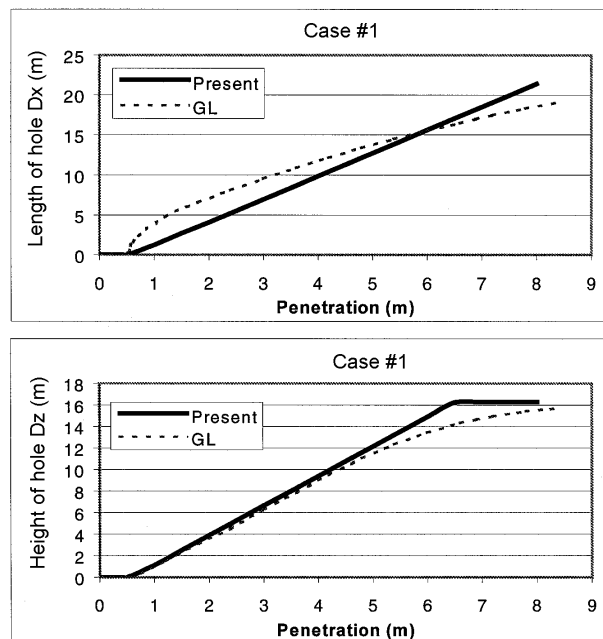
Fig. 3.93. Comparison of the hole sizes for collision case#1.
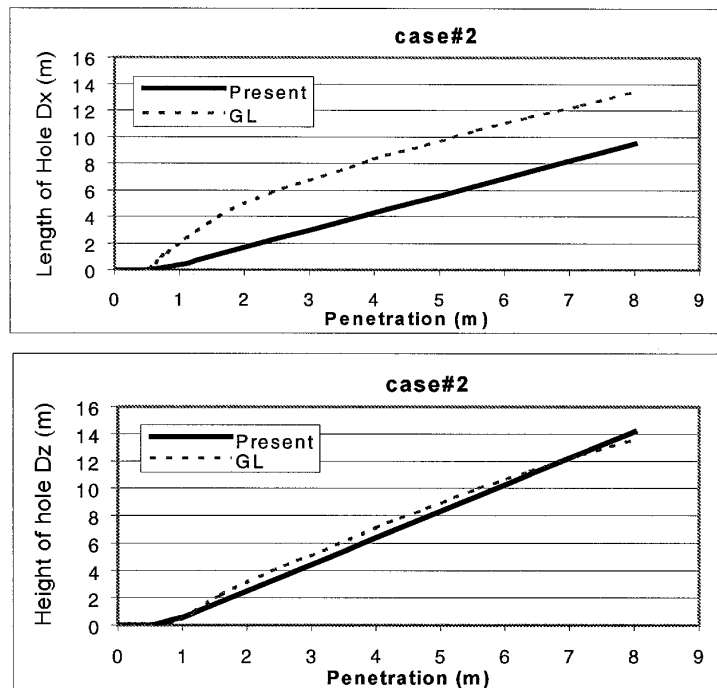
Fig. 3.94. Comparison of the hole sizes for collision case#2.
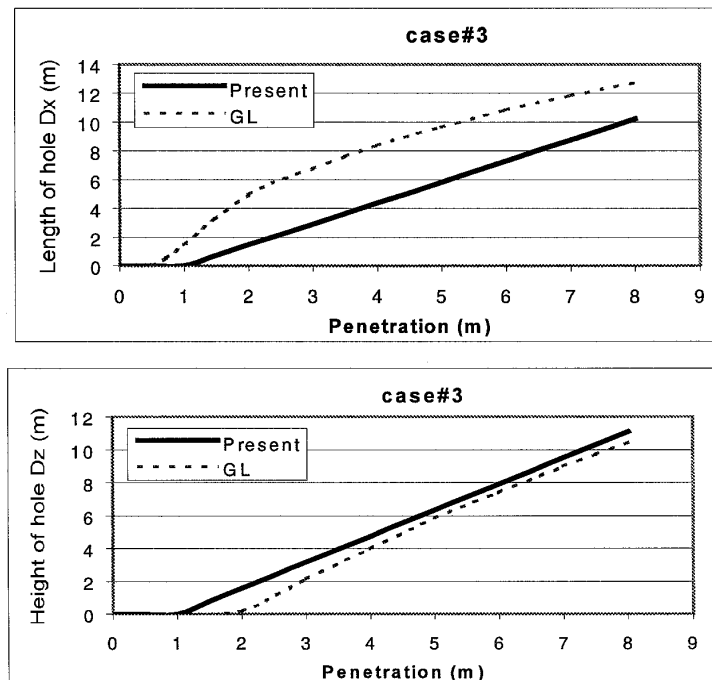
Fig. 3.95. Comparison of the hole sizes for collision case#3.

3.9.3 Holes Created by a Bulbous Bow

In Section 3.3, the bulb of the striking bow is described by three radii: $R_L = \lambda_L H_{deck}$, $R_V = \lambda_V H_{deck}$, $R_H = \lambda_H H_{deck}$, where λ_L, λ_V and λ_H are coefficients, and H_{deck} is the deck height of the striking bow. Fig. 3.96 illustrates the holes created by a bulbous bow. As described in Fig. 3.96, the penetration of the upper part of the striking bow is δ. When the penetration reaches $\delta_1 = R_D \sin\alpha / \sin\beta$, the bulb starts to come into contact with the shell plating of the struck ship. Thus, the actual penetration of the bulb into the struck ship is

$$\delta_b = \delta - R_D \sin\alpha / \sin\beta$$

where R_D is the distance between the bulb tip and the forward perpendicular of the striking ship.

For a bulbous bow, besides the upper hole created by the upper part of the striking bow, the bulb will create a lower hole. The calculation procedure for the upper hole is similar to that for the case of the conventional bow. Here we only discuss the damaged hole created by the bulb itself.

From geometric analysis, the following formulas are derived:

- When $\alpha \geq 90^0$ and $\delta_b \sin\beta \left(\dfrac{1}{\tan\alpha} - \dfrac{1}{\tan\beta} \right) \leq \sqrt{\dfrac{\delta_b \sin\beta}{R_L \sin\alpha} \cdot \dfrac{R_H}{\sin\alpha}}$

  Length of the hole: $D_X = \sqrt{\dfrac{\delta_b \sin\beta - \delta_r}{R_L \sin\alpha} \cdot \dfrac{2R_H}{\sin\alpha}}$ \hfill (3.152)

  Height of the hole: $D_Z = \sqrt{\dfrac{\delta_b \sin\beta - \delta_r}{R_L \sin\alpha}} \cdot 2R_V$ \hfill (3.153)

- Other cases

  Length of the hole: $D_X = (\delta_b \sin\beta - \delta_r)\left(\dfrac{1}{\tan\alpha} - \dfrac{1}{\tan\beta} \right) + \sqrt{\dfrac{\delta_b \sin\beta - \delta_r}{R_L \sin\alpha} \cdot \dfrac{R_H}{\sin\alpha}}$ \hfill (3.154)

  Height of the hole: $D_Z = \sqrt{\dfrac{\delta_b \sin\beta - \delta_r}{R_L \sin\alpha}} \cdot 2R_V$ \hfill (3.155)

where δ_r is the critical rupture penetration in the direction normal to the struck ship. If $D_Z \geq 2R$, then set $D_Z = 2R$.
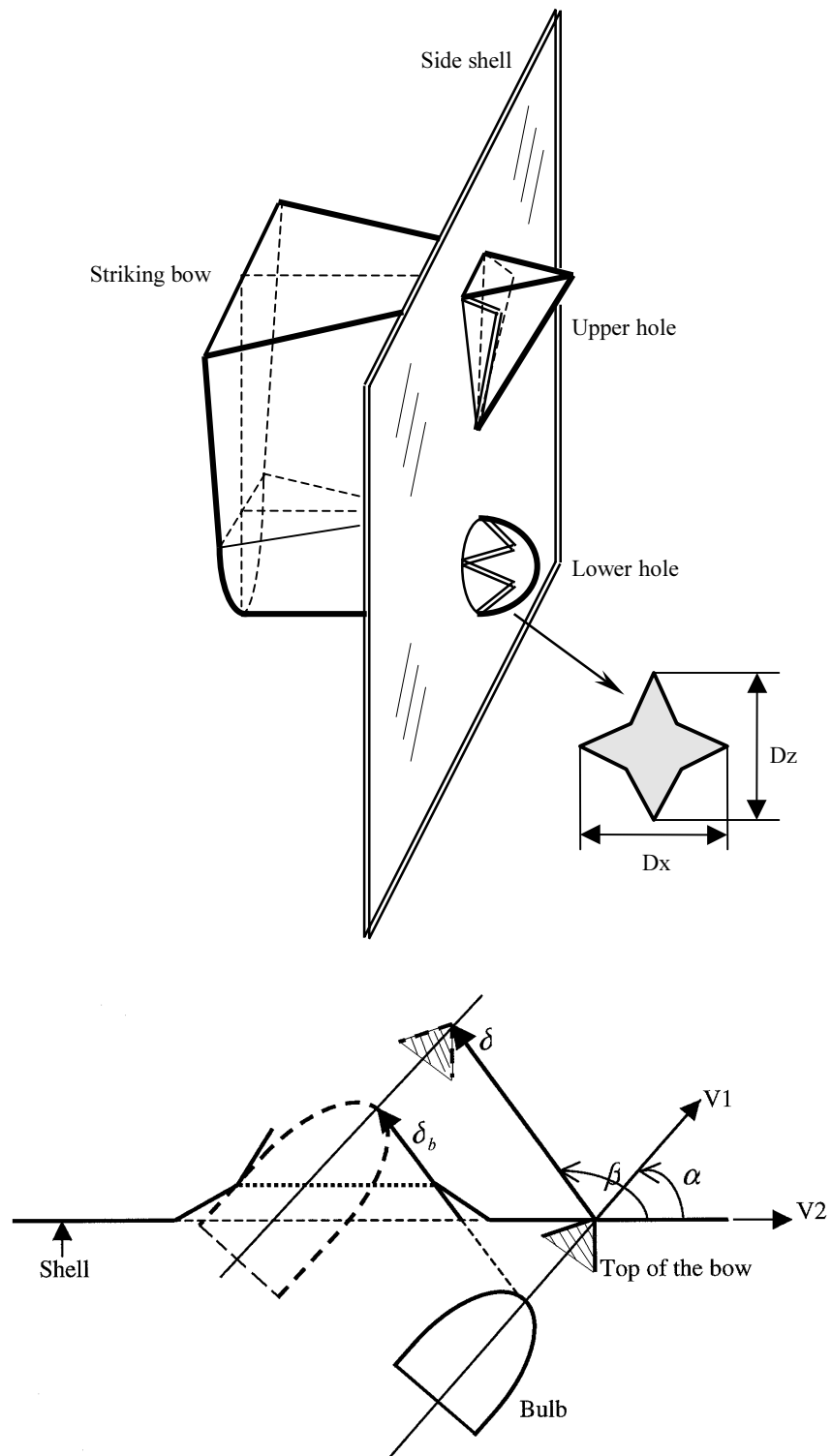
Fig. 3.96. Illustration of the holes created by a bulbous bow.

Calculation Examples

The striking ship is 160 m in length, the breadth is 24.6 m, and the deck height is 16.3 m. The dimensions of the bulb are assumed to be: $R_L = 0.25 H_{deck} = 4.08(m)$, $R_V = 0.15 H_{deck} = 2.45(m)$, $R_H = 0.12 H_{deck} = 1.96(m)$, $R_D = 0.1 H_{deck} = 1.63(m)$.

The struck ship is a Ro-Ro vessel with a length of 150 m. The considered collision cases are shown in Table 3.10. The calculation results are presented in Figs. 3.97, 3.98 and 3.99, respectively, for the collision cases.

Table 3.10. Collision cases of the bulbous bow striking the Ro-Ro vessel.

	Collision angle α (degrees)	Penetration angle β (degrees)
Case #0	90	90
Case #1	60	120
Case #2	90	135
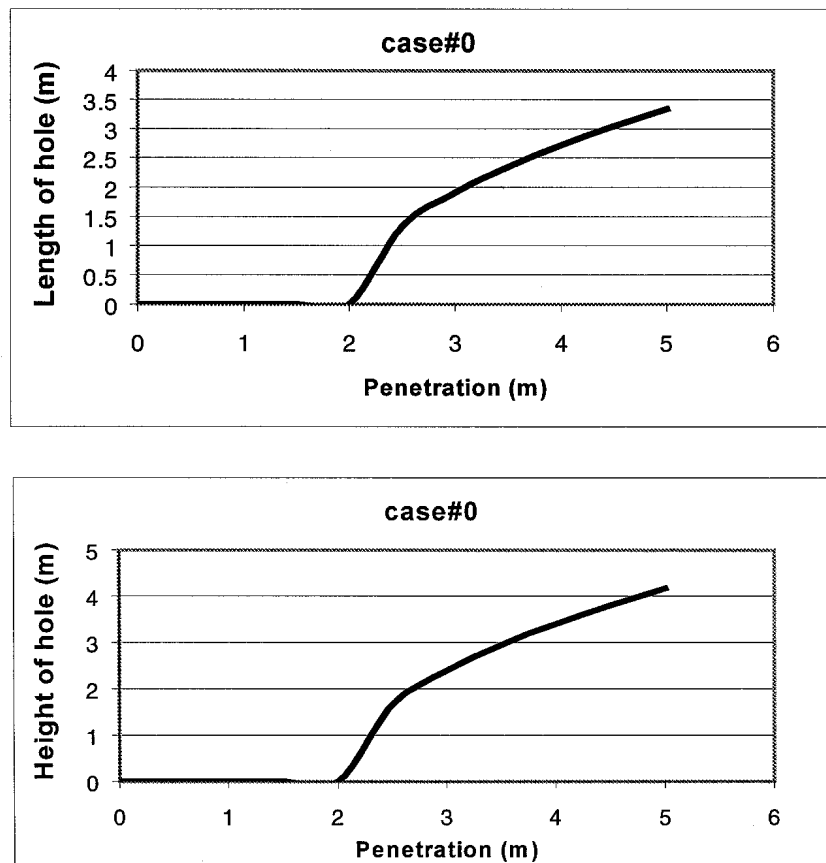
Fig. 3.97. The size of the hole created by the bulb (case#0).
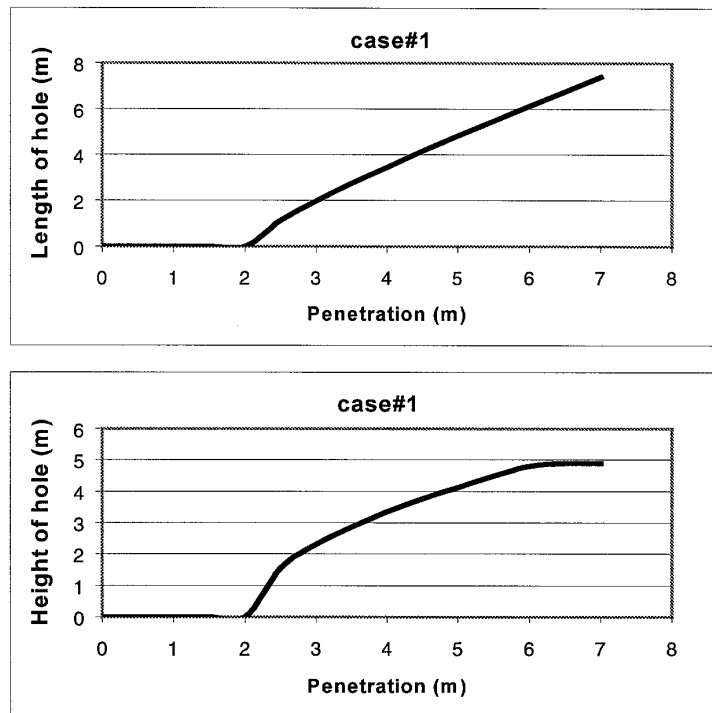
Fig. 3.98. The size of the hole created by the bulb (case#1).
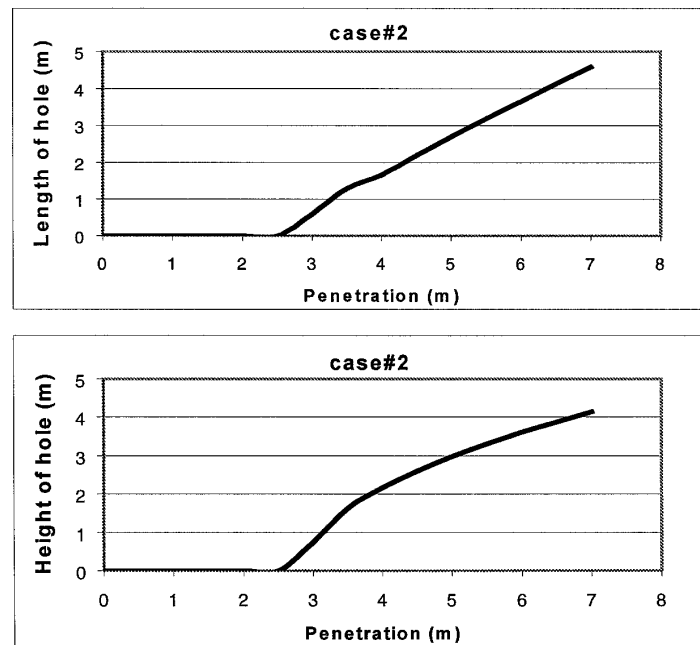
Fig. 3.99. The size of the hole created by the bulb (case#2).

Chapter 4

Analysis Examples for Full Scale Ship Collisions

In the previous chapters, external dynamics and internal mechanics of ship collisions have been treated. In this chapter, we use these methods for analyses of full-scale collisions. Calculations for several cases, such as high-speed craft, Ro-Ro vessels, and tankers, are carried out.

4.1 Impact of High-Speed Craft with Floating Objects

4.1.1 Introduction

High-speed craft are highly weight-sensitive structures. Therefore, novel building materials with high strength-to-weight ratios such as aluminium, fibre-reinforced plastic (FRP) single-skin plates or sandwich panels are widely used. In order to provide sufficient strength to withstand local impact loads, all the major classification societies have recently established empirical rule requirements for the minimum panel thickness for these new hull materials. As usual, deviations from these minimum requirements may be accepted, provided equivalent load resistance can be documented. But due to lack of analysis procedures, such documentation can at present only be obtained by physical experiments.

Aamlid (1995, 1997), Hildebrand (1994) and Wen and Jones (1993) carried out a series of model tests by dropping objects which impacted panels to examine impact strength of the panels. Valuable results were obtained for understanding the local impact phenomena.

It is the purpose of the present section to use analytical methods for describing the impact phenomena. Comparisons show that an acceptable agreement is found between the present results and test results. By the present method, the minimum thickness

requirements of the DNV rules (1993) can be converted into the critical impact energy and the minimum object mass which just ruptures the panels at a given ship speed.

4.1.2 Analysis Procedures

Energy to Be Dissipated by the Ship Structure

As shown in Fig. 4.1, a ship sailing at a forward speed of V, impacts against a motionless floating object. It is reasonably assumed that the mass M of the object is small compared to the mass of the ship.
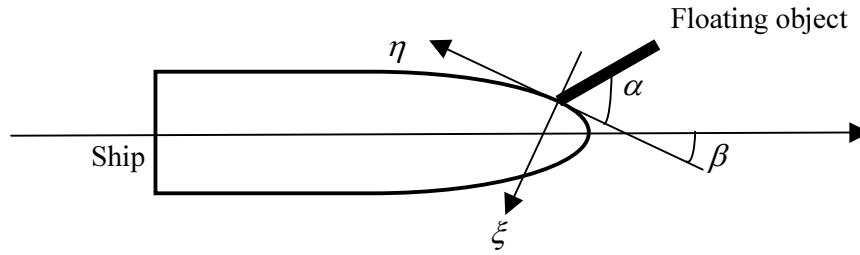
Fig. 4.1. Scenario of ship collision with a floating object.

The floating object may slide away after impacting the ship panel if the collision is light, but in the case of rupture, no sliding will occur in the contact area. In the latter case, the derived formulas for the energy to be dissipated by the shell plating in the perpendicular and the parallel directions of the shell plating (further simplify Eqs. 2.21 and 2.22) are:

$$E_\xi = \frac{1}{2} MV^2 \cdot \frac{\sin^2 \beta}{D_{a\xi} + \mu \cdot D_{a\eta}}$$

$$\text{(4.1)}$$

$$E_\eta = \frac{1}{2} MV^2 \cdot \frac{\cos^2 \beta}{\dfrac{1}{\mu} K_{a\xi} + K_{a\eta}}$$

where

$$D_{a\xi} = \frac{1}{1 + m_{ax}} \sin^2 \alpha + \frac{1}{1 + m_{ay}} \cos^2 \alpha + \frac{3}{1 + j_a} \cos^2 \alpha$$

$$D_{a\eta} = (\frac{1}{1 + m_{ax}} - \frac{1}{1 + m_{ay}} - \frac{3}{1 + j_a}) \sin \alpha \cos \alpha$$

$$K_{a\xi} = (\frac{1}{1 + m_{ax}} - \frac{1}{1 + m_{ay}} - \frac{3}{1 + j_a}) \sin \alpha \cos \alpha$$

$$K_{a\eta} = \frac{1}{1 + m_{ax}} \cos^2 \alpha + \frac{1}{1 + m_{ay}} \sin^2 \alpha + \frac{3}{1 + j_a} \sin^2 \alpha$$

$$\mu = \frac{D_{a\xi} \cos \beta - K_{a\xi} \sin \beta}{K_{a\eta} \sin \beta - D_{a\eta} \cos \beta}$$

and m_{ax} is the added mass coefficient for the surge motion of the object, m_{ay} is the added mass coefficient for the sway motion of the object, j_a is the added mass coefficient of moment for the rotation around the centre of gravity, α is the impact angle between the object and the shell plating, β is the shell face angle between the shell plating and the ship sailing direction.

Rupture Energy

Let us consider a sharp object impacting the centre of a shell plate bounded by longitudinal stiffeners and transverse frames. The stiffener spacing is $2b$, the frame spacing is $2a$, t is the thickness of the plate, A is the area of the plate, σ_0 is the flow stress of the material. As the impact speed is relatively high, the deformation function is taken to be $f(x,y) = (x/a)^2 (y/b)^2$. Thus, the work by the perpendicular impact force (normal to the plate) is (see Section 3.4):

$$E_\xi = \frac{1}{15}[1 + (\frac{a}{b})^2]\frac{2}{\sqrt{3}}\sigma_0 tA\varepsilon_1$$

where ε_1 is the strain in the plate caused by the perpendicular impact force. The work by the parallel impact force is expressed approximately:

$$E_\eta = (\frac{1}{8} + \frac{2}{21}\frac{a}{b})\frac{2}{\sqrt{3}}\sigma_0 tA\varepsilon_2$$

where ε_2 is the strain in the plate caused by the parallel impact force. When the maximum strain is equal to the critical strain ε_c, the plate is assumed to rupture, that is

$$\frac{E_\xi}{\frac{1}{15}(1 + (\frac{a}{b})^2)} + \frac{E_\eta}{\frac{1}{8}(1 + \frac{2}{21}\frac{a}{b})} = \frac{2}{\sqrt{3}}\sigma_0 t\varepsilon_c A \tag{4.2}$$

Substituting Eq. (4.1) into Eq. (4.2), we get

$$\frac{1}{2}MV^2 = \frac{\frac{2}{\sqrt{3}}\varepsilon_c\sigma_0 tA}{\dfrac{\sin^2\beta}{\frac{1}{15}(1 + (\frac{a}{b})^2)(D_{a\xi} + \mu D_{a\eta})} + \dfrac{\cos^2\beta}{(\frac{1}{8} + \frac{2}{21}\frac{a}{b})(\frac{1}{\mu}K_{a\xi} + K_{a\eta})}} \tag{4.3}$$

When the ship velocity V is known, the mass M of the floating object, which just ruptures the shell plating, can be determined from Eq. (4.3). The critical rupture energy is expressed as

$$E_c = \frac{1}{2}MV^2\{\frac{\sin^2\beta}{D_{a\xi}+\mu D_{a\eta}} + \frac{\cos^2\beta}{\frac{1}{\mu}K_{a\xi}+K_{a\eta}}\} \tag{4.4}$$

For a dropped sharp object impacting the centre of a clamped panel in air, as shown in Fig. 4.2, the critical rupture energy is

$$E_c = \frac{\frac{2}{\sqrt{3}}\varepsilon_c\sigma_0 tA}{\frac{\sin^2\alpha}{\frac{1}{15}(1+(\frac{a}{b})^2)}+\frac{\cos^2\alpha}{(\frac{1}{8}+\frac{2}{21}\frac{a}{b})}} \tag{4.5}$$
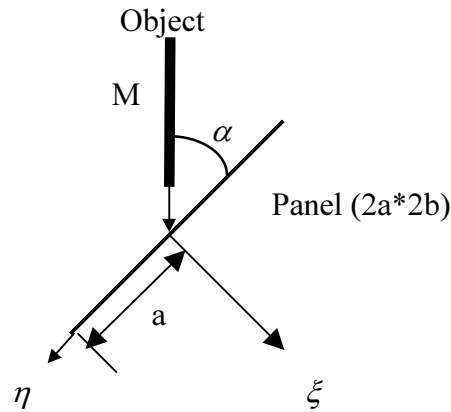
Fig. 4.2. A dropped object impacts a panel.

Similarly, for a dropped cylinder impacting perpendicularly to the centre of a clamped circular plate in air, as shown in Fig. 4.3, the critical energy is (see Section 3.4):

$$E_c = \frac{\pi}{\sqrt{3}}\sigma_0 t(\frac{1}{3}\varepsilon_c(a-a_0)(a+3a_0)+t\cdot a_0\sqrt{2\varepsilon_c}) \tag{4.6}$$

Here a is the radius of the circular plate and a_0 is the radius of the cylinder.
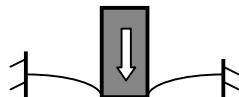
Fig. 4.3. A cylinder impacts the centre of a clamped circular plate.

4.1.3 Comparison with Experiments

Comparison with Aamlid's Model Test

Aamlid (1995) carried out a series of model tests where a dropped cylinder impacts plates. The radius of the cylinder is 40 mm, the dimensions of the clamped plate are $500*500 \ mm^2$. The cylinder impacts the centre of the plate at an angle $\alpha = 35°$. Since the impact is oblique, it can be assumed that the impactor is a sharp object for the initial impact. The flow stress of the material is $\sigma_0 = 260 MPa$ and the critical strain is $\varepsilon_c = 10\%$. A comparison of the present results with the experimental results is shown in Table 4.1. It is seen that the agreement is reasonable.

Table 4.1. Comparison of the critical energies for just rupturing panels.

Thickness of plates (mm)	Critical energy (kJ)	
	Test results	Present results
2	1.86	2.72
3	4.33	4.08
4	>5.87	5.44

Comparison with Experiment by Wen and Jones

An experimental investigation is reported by Wen and Jones (1993), where fully clamped circular plates are struck perpendicularly by blunt projectiles. The related parameters of the tests and a comparison of the present calculations and the test results are shown in Table 4.2. A damaged model after the test is shown in Fig. 4.4. The agreement is good. It is seen from the comparisons that the present method can give good predictions of the critical rupture energy of panels.

Table 4.2. Comparison between the test results and the present calculations for the critical rupture energy.

Related parameters					Critical energy (Nm)	
$t \ (mm)$	$a \ (mm)$	$a_0 \ (mm)$	$\sigma_0 \ (N/mm^2)$	$\varepsilon_c \ (\%)$	Present	Test
2	25.4	2.975	303.9	11.28	35.0	39.2
4	50.8	5.95	372.2	10.47	319.6	310.0
6	76.2	8.925	331.6	9.97	917.1	1004.7
8	101.6	11.9	327.4	12.72	2708.9	2437.6
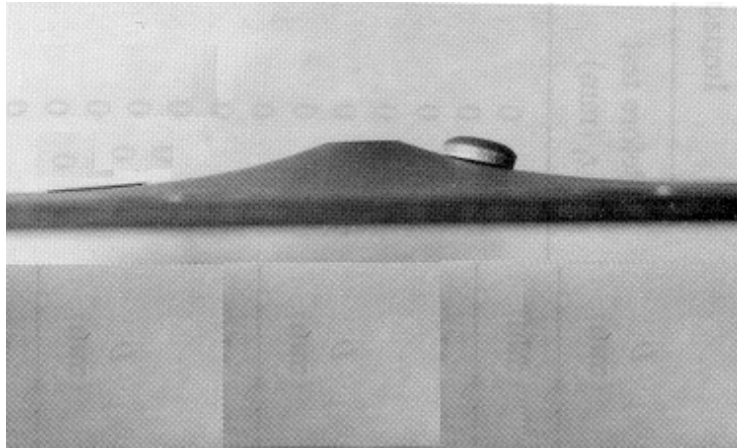
Fig. 4.4. A damaged plate after impact test (Wen and Jones, 1993).

4.1.4   The Influence of the Impact Angle

A Dropped Object Impacting a Plate at Various Angles α in Air

Here we consider a dropped object impacting the centre of a plate, such as the deck, at various angles α, to examine the influence of the impact angle α on the critical energy. The parameters of the plate are 500*500 *mm* , $t = 3$ mm, $\sigma_0 = 260\,MPa$ and $\varepsilon_c = 10\%$.

Fig. 4.5 shows the critical energy with various impact angles. It is seen that the perpendicular impact requires the least energy to rupture the plate.
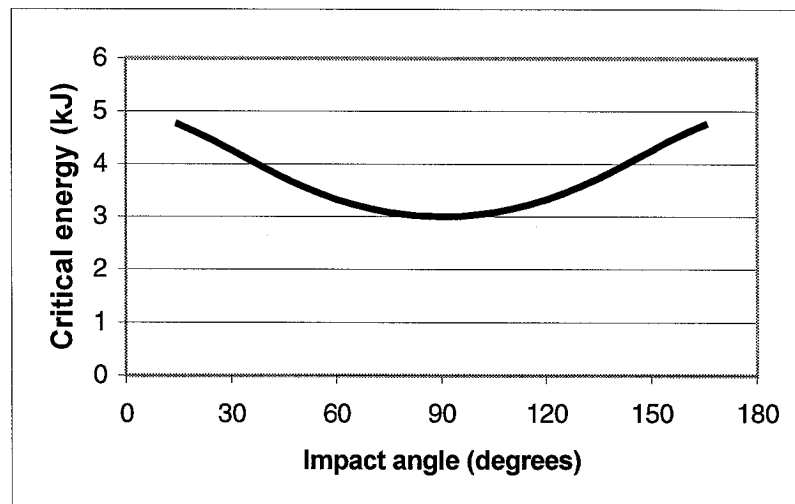
Fig. 4.5. Critical energy vs. different impact angles α (dropped object).

Ship Collision with a Floating Object in Water

Let us consider a high-speed ship sailing at a velocity of V=20 m/s colliding with a floating slender object, as shown in Fig. 4.1. The purpose is to examine which impact angle is the most dangerous as regards of the rupture shell plating. For the chosen example, the dimensions of the shell plating are 500*500 *mm* , $t = 3$ mm, $\sigma_0 = 260 MPa$, $\varepsilon_c = 10\%$. The calculation results of the critical object mass vs. different impact angles, for the panel face angle $\beta = 35°$, $50°$ and $70°$ respectively, are presented in Fig. 4.6. The results show that when the impact angle α equals the shell face angle β, the object mass which just ruptures the shell plating is the minimal. This means that when the slender object is orientated to the ship sailing direction, it most easily ruptures the shell plating.
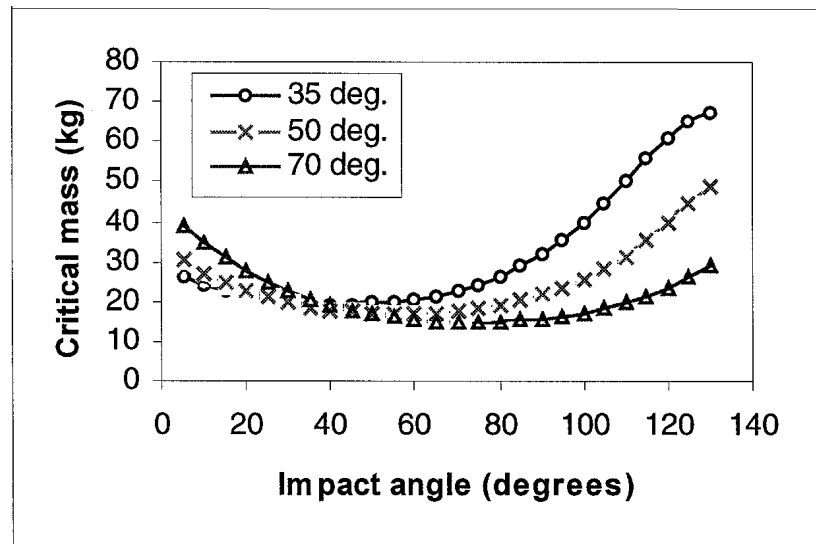
Fig. 4.6. Critical mass of the floating object which just ruptures the shell plate vs. various impact angles (shell face angles: $\beta = 35°$, $50°$ and $70°$, respectively).

Simplified Formulas

It is seen from the above analyses, the easiest way to rupture the shell plating is when the floating object is orientated to the craft sailing direction. In this case, the expression for the critical object mass which just ruptures the shell plating for a moving craft at a speed of V can be simplified as

$$M_c = \frac{\frac{4}{\sqrt{3}}\varepsilon_c\sigma_0 tA}{[\frac{\sin^2\beta}{\frac{1}{15}(1+\lambda^2)} + \frac{\cos^2\beta}{(\frac{1}{8}+\frac{2}{21}\lambda)}](1+m_{ax})V^2} \tag{4.7}$$

where s is the stiffener spacing, λ is the aspect ratio of the plate and $A = s^2\lambda$ is the plate area. The critical rupture energy is

$$E_1 = \frac{\frac{2}{\sqrt{3}}\varepsilon_c\sigma_0 tA}{[\frac{\sin^2\beta}{\frac{1}{15}(1+\lambda^2)} + \frac{\cos^2\beta}{(\frac{1}{8}+\frac{2}{21}\lambda)}]} \qquad (4.8)$$

As shown in Fig. 4.7, a ship collides with a floating object with the line contact s_0. The floating object lies in the ship sailing direction. The critical energy which just ruptures the shell plating can be expressed as

$$E_2 = \frac{\frac{2}{\sqrt{3}}\varepsilon_c\sigma_0 t[s\lambda(s-s_0)]}{\{\frac{\sin^2\beta}{[\frac{1}{15}+\frac{1}{15}\frac{(s\lambda)^2}{(s-s_0)^2}+\frac{1}{3}\frac{s_0}{(s-s_0)}]} + \frac{\cos^2\beta}{[\frac{1}{8}+\frac{2}{21}\frac{s\lambda}{s-s_0}+\frac{1}{2}\frac{s_0}{s-s_0}]}\}(1+m_{ax})} \qquad (4.9)$$
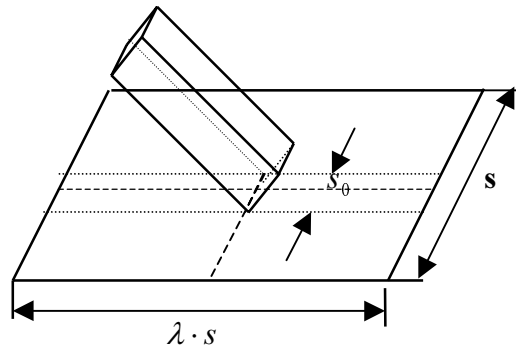
Fig. 4.7. An object impacts a panel with line contact.

4.1.5 Applications to High-Speed Craft

Aluminium Craft

The minimum thickness requirement of the DNV rules (1993) for aluminium high-speed craft is

$$t = \frac{t_0 + kL}{\sqrt{\sigma_y \big/ 240}} \frac{s}{S_R}, \quad (mm) \tag{4.10}$$

where

σ_y is the yield stress (MPa)

s is the actual stiffener spacing (m)

$S_R = \frac{2(100 + L)}{1000}$ (m), $0.5 \le \dfrac{s}{S_R} \le 1.0$

L is the ship length (m)

$k = 0.03$ for the shell plating

Here we use the present method for converting the minimum thickness requirement into the critical object mass which just ruptures the shell plating for a given craft speed where the object is in the sailing direction of ships.

Fig. 4.8 presents the results of the critical object mass vs. craft length, when the ship velocity is V=20 m/s and the shell face angles are $\beta = 35°$ and $70°$, respectively. The related parameters are $\sigma_y = 220 MPa$, $\varepsilon_c = 10\%$, $t_0 = 4$ mm, $k = 0.03$, $s = 0.3$ m and $\lambda = 1.5$.
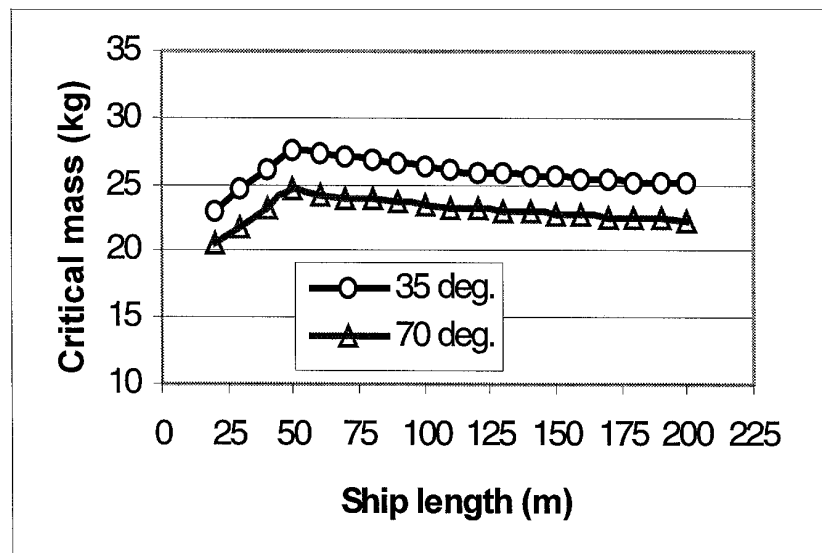
Fig. 4.8. Critical object mass vs. various craft lengths (speed V=20 m/s, $\beta = 35°, 70°$).

It is seen from the figure that when the shell face angle increases, the shell plating ruptures more easily. According to the present results, a 25 kg mass object may rupture the hull of a high-speed craft moving at a speed of 20m/s. The corresponding critical energy is about 5 kJ.

FRP Single -Skin Craft

Here we use the method for predicting the critical energy of FRP single-skin craft. However, before we first make a comparison with FRP single-skin plate tests, which were carried out by Aamlid (1997). The tests were clamped square plates with the dimensions 500*500 mm^2, struck by a dropped cylinder with a diameter $s_0 = 80$ mm. The impact angle was $\alpha = 35°$. The test rig and a damaged model after an impact test are shown in Fig. 4.9. The ultimate stress of the material is $\sigma_u = 180 MPa$, the critical strain is $\varepsilon_c = 3.5\%$ (Hildebrand, 1994). The comparison of the critical energy obtained by the present method and the test results is shown in Table 4.3. Good agreement is found.

Table 4.3. Comparison of the critical energies for FRP single-skin plates.

Thickness of the FRP (mm)	Critical energy (kJ)	
	Test results	Present results
2.9	0.99	1.28
8.1	3.40	3.57
11.2	5.87	4.92
13.1	>5.87	5.76
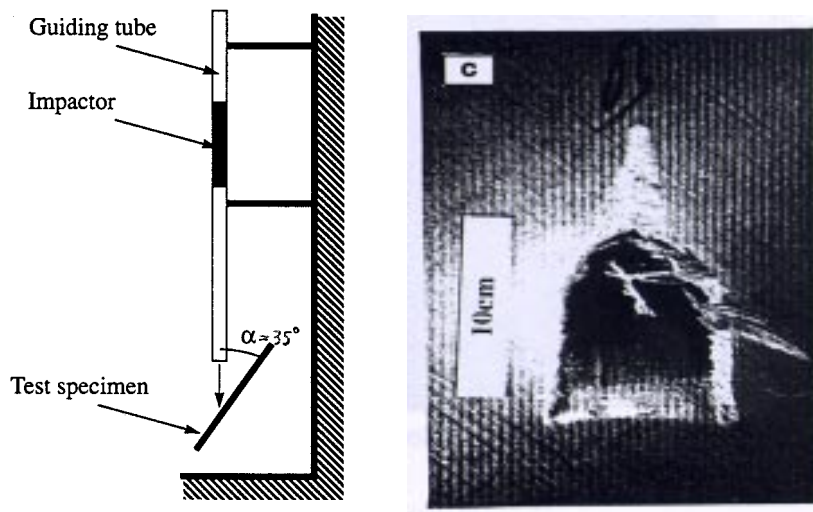
Fig. 4.9. Test rig and a picture of a damaged FRP single-skin plate (Aamlid, 1997).

Now we convert the thickness requirement into the critical energy. The thickness requirement of the DNV rules for FRP single-skin craft is

$$t = \frac{t_0 + kL}{\sqrt{\dfrac{\sigma_u}{160}}}, \ (mm) \qquad (4.11)$$

where σ_u is the ultimate tensile stress (MPa), L is the ship length (m) and k is the constant. The present calculation results for the critical energy with various ship lengths are shown in Fig. 4.10 where the shell face angles are $\beta = 35°$ and $70°$, respectively. The related data is the stiffener spacing $s = 0.3$ m, $\lambda = 1.5$, $\sigma_u = 180\,MPa$, $\varepsilon_c = 3.5\%$, $t_0 = 5$ mm, $k = 0.09$.

From the results it is observed that the critical energy increases with increasing ship length.
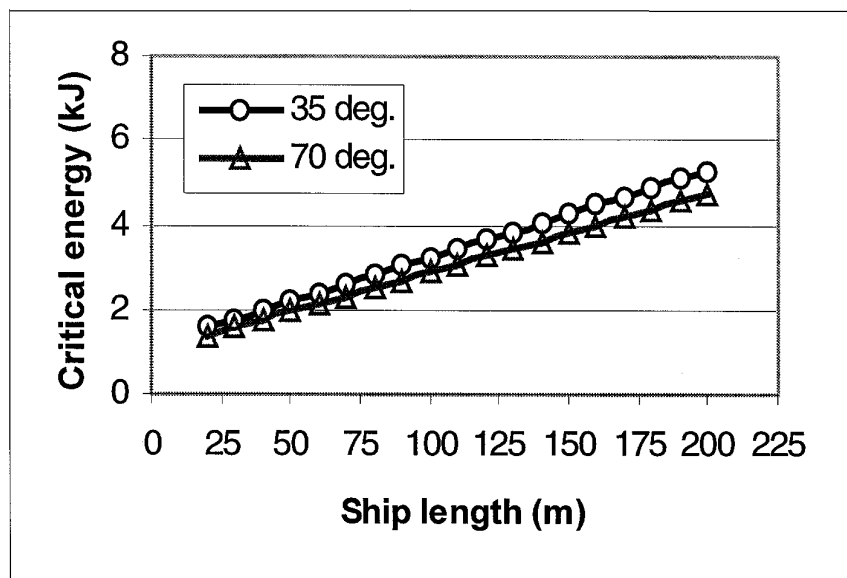
Fig. 4.10. Critical energy of FRP single-skin craft vs. ship length.

Comparison of Aluminium Craft and FRP Single -Skin Craft

Let us compare the impact strength of an aluminium craft and an FRP single-skin craft designed according to DNV thickness requirements.

The calculation results for the critical energy are presented in Fig. 4.11, where the shell face angle is $35°$. The results show that the aluminium craft is safer than the FRP single skin craft when the craft length is less than 130 m.
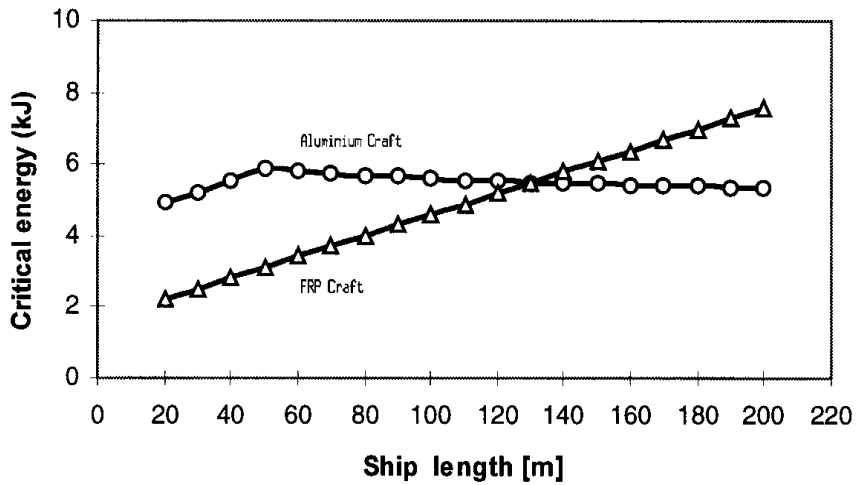
Fig. 4.11. Comparison of impact strengths of an aluminium craft and an FRP craft.

Example Case: The Craft 'BERLIN EXPRESS'

The ferry 'BERLIN EXPRESS' transports cars and passengers between Denmark and Germany. It is shown in Fig. 4.12. The length of the craft is 86.5 m, the breadth is 17.4 m, the depth is 3.6 m, the displacement is 500 t, and the service speed is 32 knots.

Here we use the present method for predicting the critical energy and the minimum mass of a floating object which just ruptures the shell plating. The properties of the aluminium shell plating are: the yield stress 220 MPa, the ultimate stress 300 MPa and the critical strain 10%. In the bow area, the typical spacing of longitudinal stiffeners is 275 mm, the aspect ratio is $\lambda = 1.033$, the plate thickness is 10 mm and the shell face angle is 20 degrees.

The calculated result for the critical energy is 4.88 kJ, the minimum mass of a floating object which can rupture the plating is 34.2 kg. Thus, a 35 kg floating object may rupture the shell plating when the ferry sails at full service speed.

Fig. 4.12. The ferry 'BERLIN EXPRESS'.

4.1.6 Concluding Remarks

A study on the impact strength of high-speed craft colliding with floating objects and dropped objects impacting the plating has been presented. The comparisons show that acceptable agreement between the present results and experimental results is achieved. The existing minimum thickness requirements of aluminium craft and FRP single-skin craft are converted into critical impact energies or critical object masses. The major conclusions are summarised as follows:

(1) The impact strength is determined by the following parameters:
   - Thickness, size and aspect ratio of the shell plating
   - Impact location and angle
   - Materials properties

(2) For a dropped object impacting a panel in air (such as the deck plate), the perpendicular impact requires the least energy to rupture the panel.

(3) For a high-speed craft colliding with a floating slender object, the shell plating ruptures most easily when the slender object is orientated to the sailing direction of the craft.

(4) Simple formulas have been presented from which the critical energy and the critical object mass can be determined.

4.2 Collisions of Ro-Ro Vessels

4.2.1 Introduction

Ro-Ro vessels are key transport systems for many countries today. They provide a cost-effective alternative to other means of transportation. The tragic accident of the Estonia created a major concern for the safety of Ro-Ro ships. Therefore, several countries started to reassess the safety of Ro-Ro vessels.

In this section, investigations of collisions of Ro-Ro vessels are performed. Firstly, the case of Ro-Ro vessels struck by other ships is dealt with. Two Ro-Ro vessels are selected. One is a Ro-Ro vessel with a length of 150 m and the other is a RoRo vessel with a length of 180 m. Conventional and bulbous bows striking the Ro-Ro vessels are investigated. Force-penetration curves and energy-penetration curves are calculated and compared with Hysing's (1995, from DNV) and Scharrer's (1996, from GL) calculations.

Secondly, the collision analysis for a newly designed ferry is carried out. The length of the new Ro-Ro vessel is 173 m. This vessel is assumed to be struck by a 160 m ship with a forward speed of 4.0 m/s. The collision energy and the structural damage are calculated.

4.2.2   Ro-Ro Vessel Collision Analysis

(1)   The Striking Ship

Conventional bow (V-bow)

The main particulars of the conventional striking ship are presented in Table 4.4.

Table 4.4. Main particulars of the conventional striking ship.

Length (m)	Breadth (m)	Depth (m)	Deck height (m)	Minimum draught (m)	Maximum draught (m)	Angle 2θ (degrees)	Angle φ (degrees)
160	24.6	13.3	16.3	5.5	10.0	80	70

Bulbous bow (bulb-bow)

The main particulars of the striking ship with bulbous bow are presented in Table 4.5. The radii of the bulb are determined by

$$R_L = 0.250 H_{deck}, \ R_V = 0.125 H_{deck}, \ R_H = 0.050 H_{deck}$$

where H_{deck} is the deck height of the striking bow.

Table 4.5. Main particulars of the bulbous striking ship.

Length (m)	Breadth (m)	Depth (m)	Deck height (m)	Minimum draught (m)	Maximum draught (m)	Angle 2θ (degrees)	Angle φ (degrees)
160	24.6	13.3	16.3	5.5	10.0	80	60

(2)   The Struck Ship (Ro-Ro Vessels)

The main particulars of the two selected Ro-Ro vessels are shown in Table 4.6. The critical rupture strain is assumed to be 5%. The detailed structures of the midship section are presented in Figs. 4.13 and 4.14, respectively.

Table 4.6. Main particulars of the Ro-Ro vessels.

	150 m Ro-Ro vessel	180 m Ro-Ro vessel
Length between perpendiculars	150.0 m	180.0 m
Breadth	27.0 m	31.5 m
Depth	8.5 m	9.3 m
Height to uppermost deck	19.4 m	21.1 m
Design draught	6.0 m	7.0 m
Design displacement	15 800 t	27 000 t
Yield strength of steel	235 N/mm^2	N/mm^2

(3)   The Collision Situations

The striking ship impacts the struck ship perpendicularly at midship. The collision position is in the middle between two transverse web frames. Two different draughts of the striking ship are selected, a ballast condition and a fully loaded condition. The data is shown in Table 4.7.

Table 4.7. Draughts of the striking ship used for the calculations.

	150 m Ro-Ro vessel		180 m Ro-Ro vessel	
	Lower position	Upper position	Lower position	Upper position
160 m striking	9.11 m	6.41 m	9.17 m	6.38 m

(4)   Calculation Results

Five cases were calculated and compared with Hysing's and Scharrer's results. Figs. 4.15 and 4.16 show the comparison of the collision force and the dissipated energy of the 160 m conventional ship striking the 150 m Ro-Ro vessel at the upper position and the lower position, respectively. Fig. 4.17 shows the comparison of the collision force and the dissipated energy of the 160 m conventional ship striking the 180 m Ro-Ro vessel at the upper position. Fig. 4.18 shows the dissipated energy of the 160 m conventional ship striking the 180 m Ro-Ro vessel at the lower position. Fig. 4.19 shows the collision force and the dissipated energy of the 160 m bulbous ship striking the 150 m Ro-Ro vessel at the upper position.

The comparisons indicate that good agreement has been achieved between the present calculation results and both Hysing's and Scharrer's results. Regarding the complexity of the ship-ship collision problem, such agreement may be acceptable.

The results also show that the collision resistance increases with the increase of the penetration since more and more decks and transverse frames etc. are crushed.

150 m RoRo Vessel

PL 5.0

540 x 7

150 x 10

PL 5.0

540 x 7

150 x 10

PL 5.0

600 x 7

150 x 10

PL 10.0

480 x 7

150 x 12

PL 9.5

750 x 12

150 x 75 x 8

PL 9.5

750 x 12

PL 10.5

PL 12.0

PL 7.5

130 x 65 x 8

PL 10.0

130 x 65 x 8

STR3

PL 11.5

450 x 7

STR2

PL 16.2

STR1

PL 12.0

Z = 19.4 m

Z = 16.7 m

Z = 14.0 m

Z = 11.3 m

Z = 8.5 m

Z = 7.1 m

T = 6.0 m   Z = 5.7 m

Z = 3.5 m

Z = 1.2 m

Z = 0

Web frame spacing = 2.4 m   STR1: 700 x 12/100 x 20
                                   STR2: 600 x 12/100 x 20
                                   STR3: 200 x 9/90 x 13
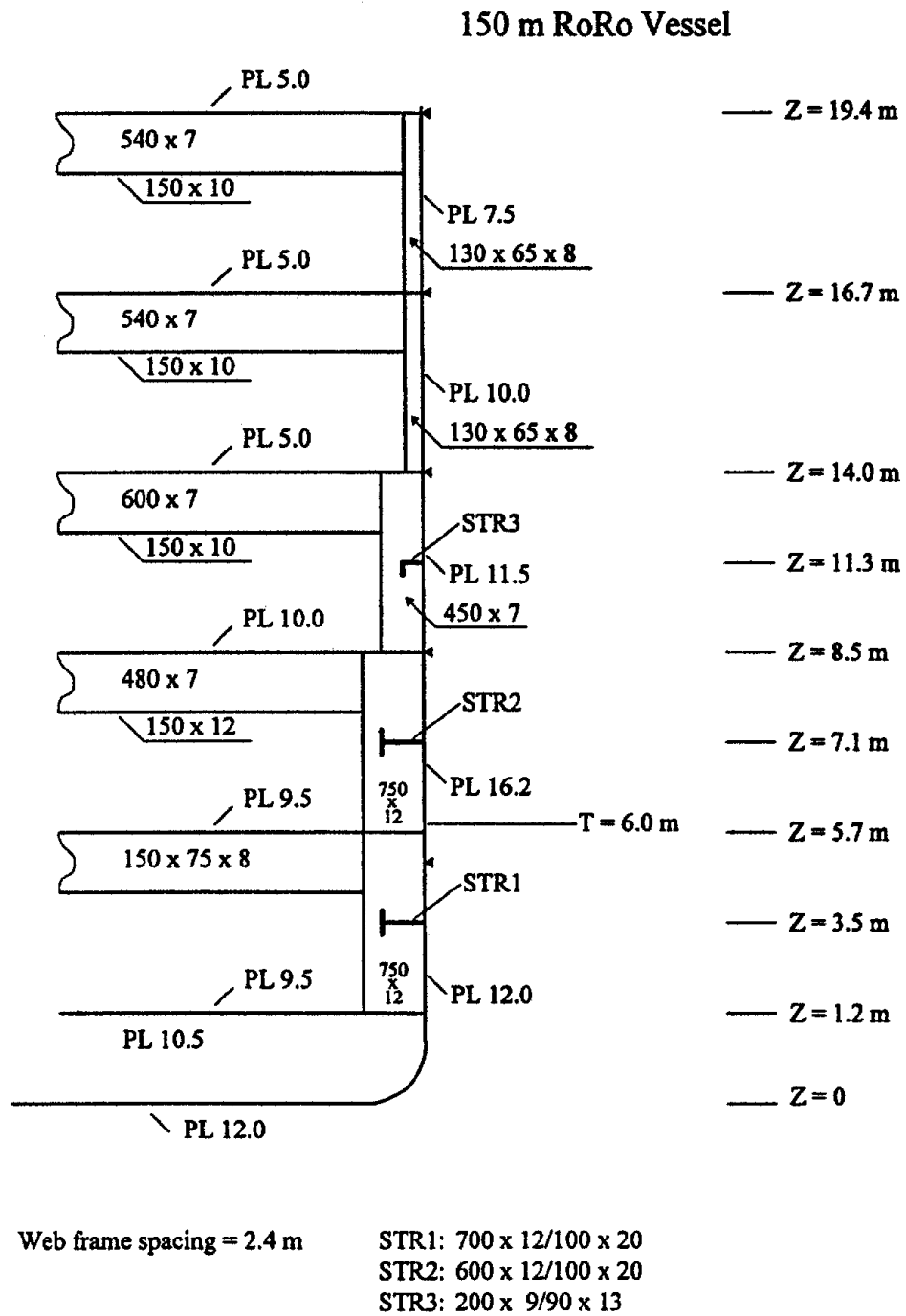
Fig. 4.13. Midship section of the 150 m Ro-Ro vessel (Hysing, 1995).
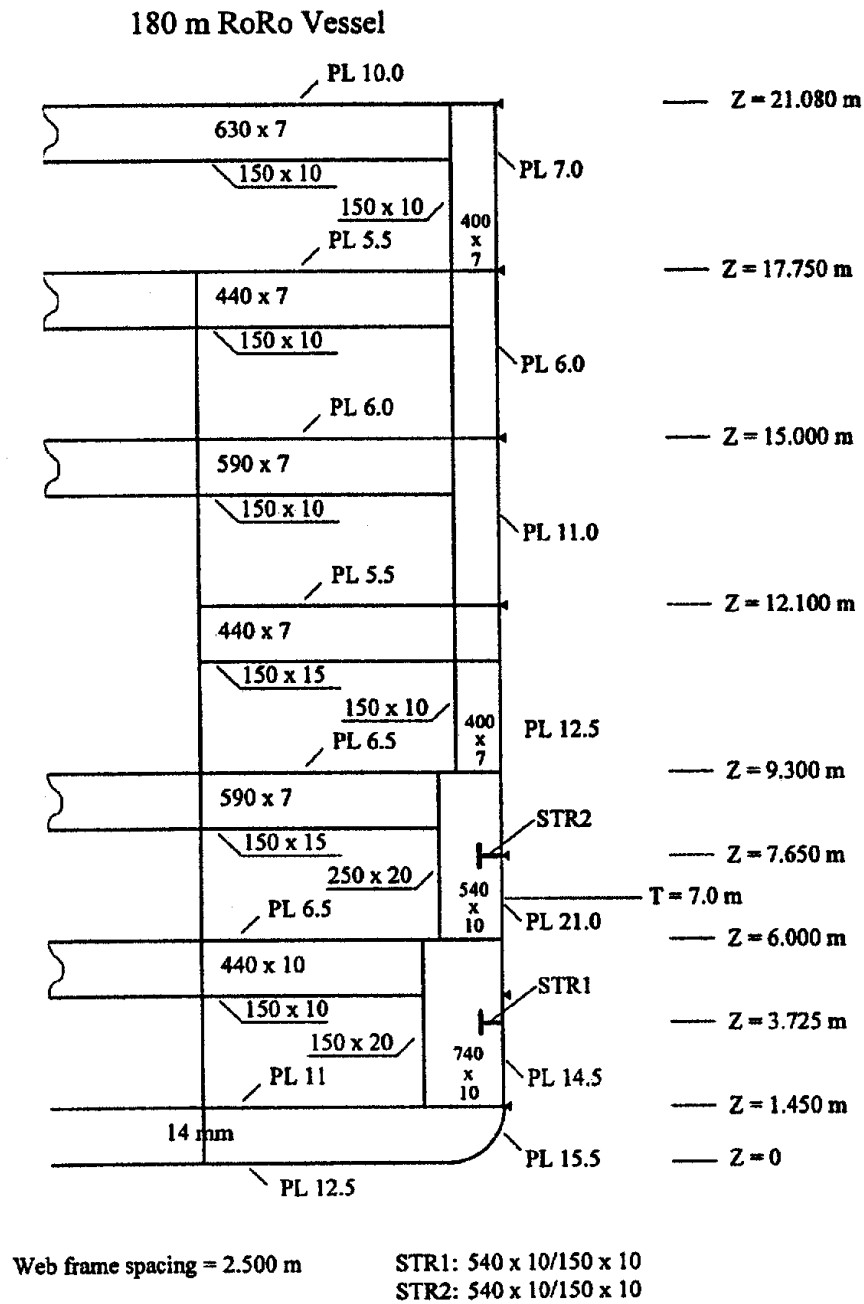
180 m RoRo Vessel

Fig. 4.14. Midship section of the 180 m Ro-Ro vessel (Hysing, 1995).
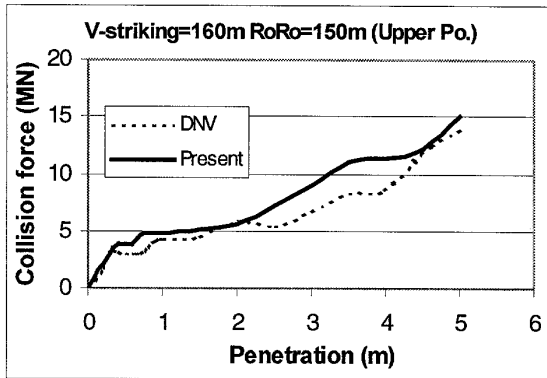
Force-penetration curve
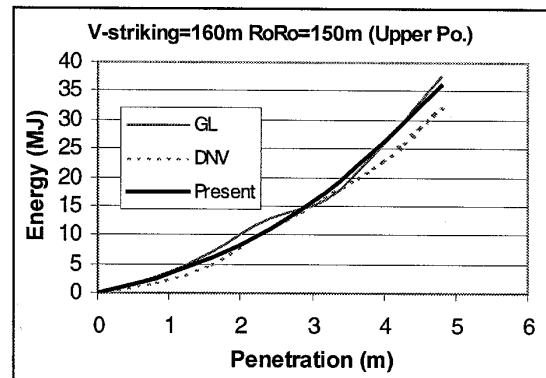
Energy-penetration curve

Fig. 4.15. Collision between 150 m Ro-Ro vessel and 160 m striking ship (upper position).
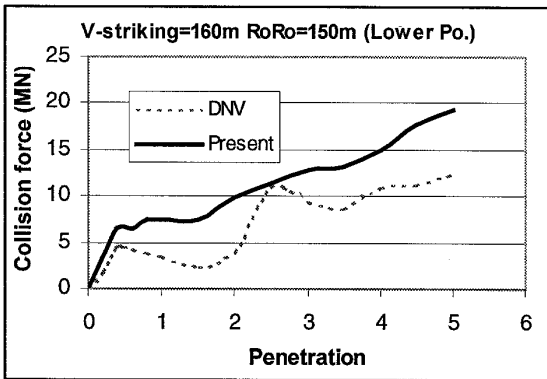
Force-penetration curve
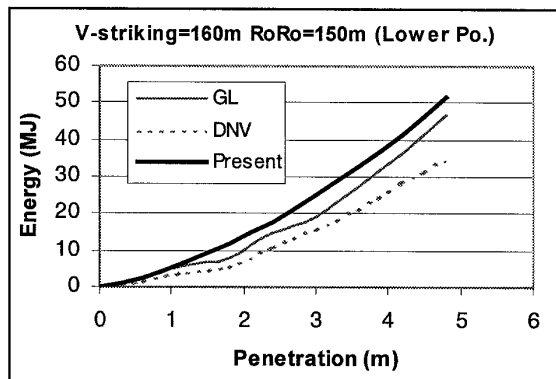
Energy-penetration curve

Fig. 4.16. Collision between 150 m Ro-Ro vessel and 160 m striking ship (lower position).
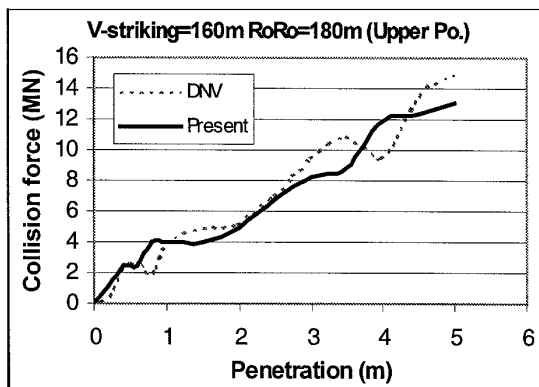
Force-penetration curve
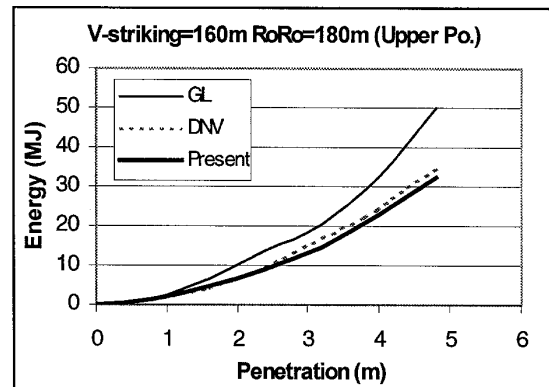
Energy-penetration curve

Fig. 4.17. Collision between 180 m Ro-Ro vessel and 160 m striking ship (upper position).
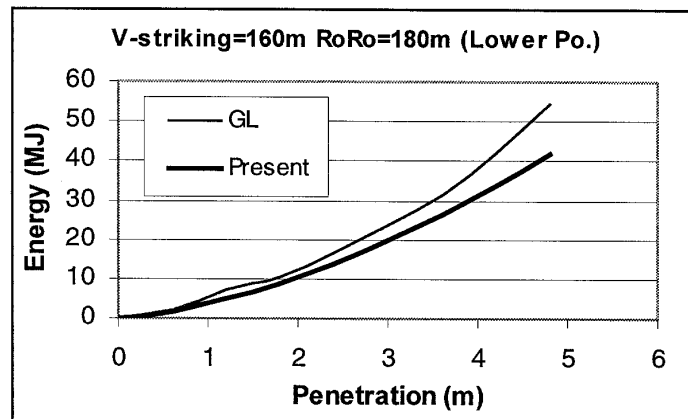
Energy-penetration curve

Fig. 4.18. Collision between 180 m Ro-Ro vessel and 160 m striking ship (lower position).
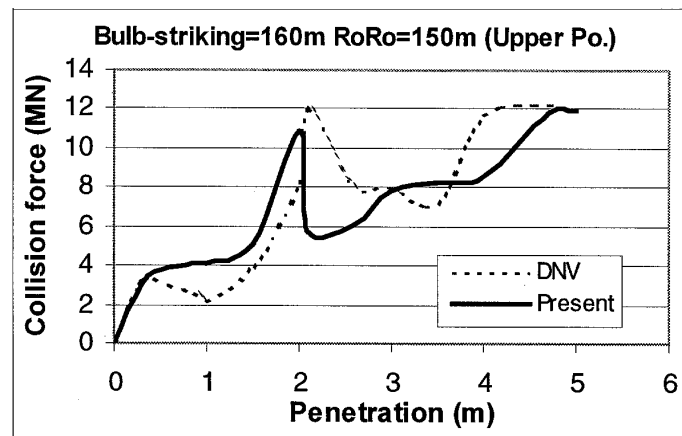
Force-penetration curve
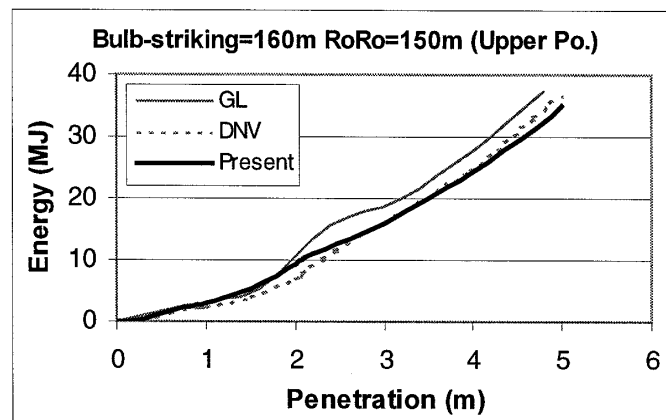
Energy-penetration curve

Fig. 4.19. Collision between 150 m Ro-Ro vessel and 160 m striking ship with a bulbous bow (upper position).

4.2.3 Collision Analyses for a Newly Designed Ferry

The midship cross-section of the newly designed fast ferry is shown in Fig. 4.20. The main particulars of the new ferry are as follows:

Length(Lpp)   = 173 m
Breadth   = 26.0 m
Depth   = 15.7 m
Draught   = 6.5 m
Displacement   = 16,073 t
Max speed   = 27 knots
Frame spacing   = 2.4 m

Fig. 4.20. Midship cross-section of the newly designed fast ferry.

The main dimensions of the striking ship are presented in Table 4.4. The displacement of the striking ship is 6,000 t, the draught is 5.5 m. It is assumed that the striking ship collides with the ferry at a forward speed of 4.0 m/s. Two cases are calculated here. One is when the ferry (the struck ship) sails with a forward speed of 4.0 m/s, the other is when the speed of the ferry is zero (V=0).

The collision energy to be dissipated by destroying the ferry is calculated. Fig. 4.21 shows the energy loss with various collision angles where the collision position is located at the centre of the struck ship. Fig. 4.22 presents the collision energy loss with different collision locations where the collision is perpendicular to the struck ship. The results show that both collision angle and collision location influence the energy loss significantly. For the central perpendicular collision, the energy loss is 39.38 MJ when the speed of the struck ship is zero, and the energy loss is 50.22 MJ when the speed of the struck ship is 4.0 m/s.
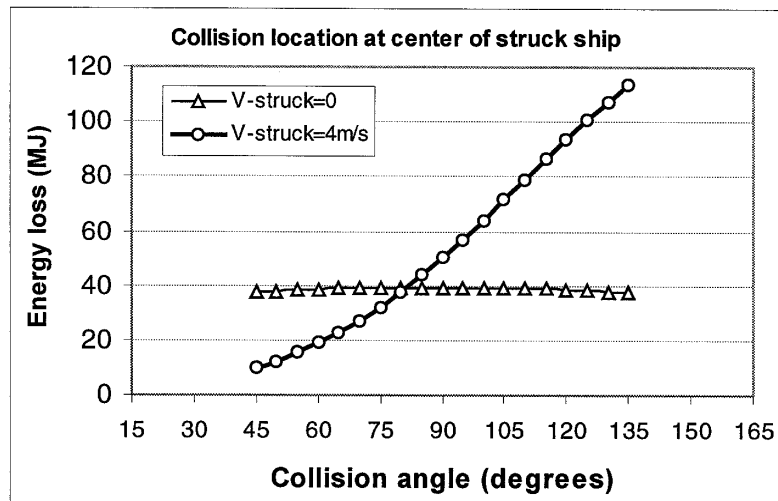
Fig. 4.21. Energy loss with various collision angles when the impact is at the centre of the struck ship.
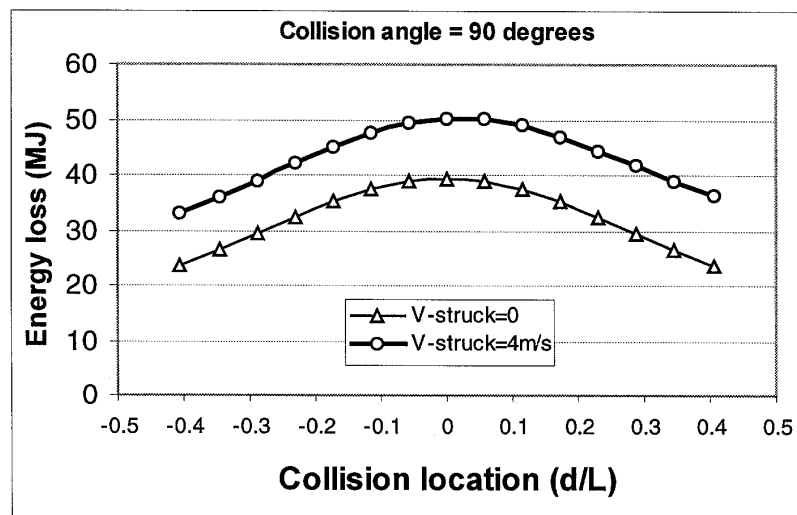
Fig. 4.22. Energy loss with various collision locations when the collision is perpendicular.

When the energy loss to be dissipated by destroying the side structures is known, the subsequent damages to the struck ship are calculated. The analysis procedure is as follows:

It is assumed that the collision position is located in the middle between two transverse frames. In an initial collision, the shell plating of the struck ship is subjected to tension. With increasing penetration, the striking bow comes into contact with frames, stringers and horizontal decks. The frames, the stringers and the decks are then crushed. It is assumed that frames, stringers and decks are not deformed and crushed until the striking bow touches them directly. By calculation of the resistance of deformed shell plating, frames and decks etc, the collision resistance and the absorbed energy are obtained. When the calculated absorbed energy is equal to the energy loss, which is determined from the outer analysis, the calculation stops. After the maximum penetration has been determined, the size of a hole in the shell plating created by the striking bow is calculated.

The required parameters in this calculation are

(1). The striking ship
Entry angle of the bow (degrees); stem angle of the bow (degrees); height of the uppermost deck (m); draught (m).

(2). The struck ship (RoRo ferry): depth (m); draught (m).

Deck information: number of decks, deck level (m) measured from the bottom, deck thickness, size of the transverse stiffeners on decks.

Stringer information: number of stringers, stringer level (m) measured from the bottom, the size of the stringers.

Transverse frame information: frame spacing (m), fame size.

Shell plating information: thickness of shell plating.

Material properties: flow stress ($305.5 \ N/mm^2$), critical strain (5%).

(3). Collision situation
Collision angle (degrees).

Fig. 4.23 shows the calculated results of the collision resistance with various penetrations when the speed of the struck ship is zero and the collision angle is 90 degrees. Fig. 4.24 shows the results of the energy absorbed by the struck ship with different penetrations. It is seen from the results that when the penetration of the striking bow into the side of the struck ship is 5.0 m, the energy dissipated by the struck ship is 39.3 MJ. All the energy loss is dissipated by the struck ship at this penetration (the striking bow is assumed to be

rigid). This means that the indentation stops at this penetration. The damage length is 8.38 m. The ratio between the damage length and the vessel length is 4.8%.
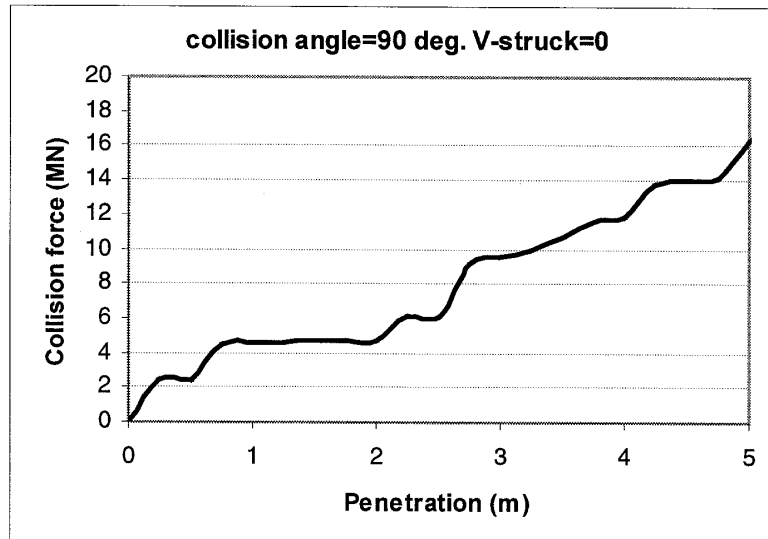
Fig. 4.23. Collision resistance of the struck ship with various penetrations when the speed of the struck ship is zero.
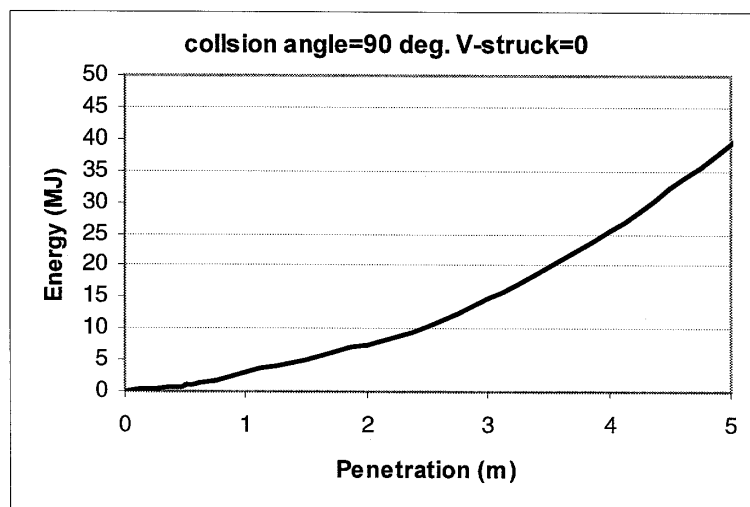
Fig. 4.24. Dissipated energy of the struck ship with various penetrations when the speed of the struck ship is zero.

Fig. 4.25 shows the collision resistance with various penetrations when the speed of the struck ship is 4.0 m/s and the collision angle is 90 degrees. The penetration is measured along the penetration angle $\beta = 90 + \alpha / 2 = 135$ degrees. Fig. 4.26 shows the absorbed energy of the struck ship with various penetrations. When the penetration reaches 7.85 m,

the energy dissipated by the struck ship is 50.3 MJ. All the energy loss is dissipated by the struck ship at this penetration. Therefore, the penetration stops and the max penetration is 7.85 m in this collision case. The perpendicular indentation is $7.85 \cdot \sin(135°) = 5.55$ m. The damage length is 10.5 m. The ratio between the damage length and the ship length is 6.1%. This example indicates that when a struck ship has forward speed, the collision energy loss and the resulting damage are larger than when the speed of the struck ship is zero.
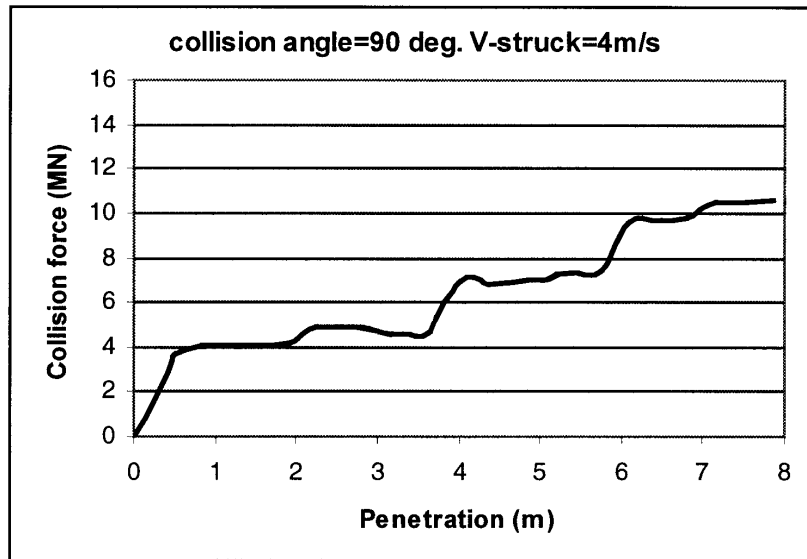
Fig. 4.25. Collision resistance with various penetrations when the struck ship has a forward speed of 4.0 m/s and the collision angle is 90 degrees.
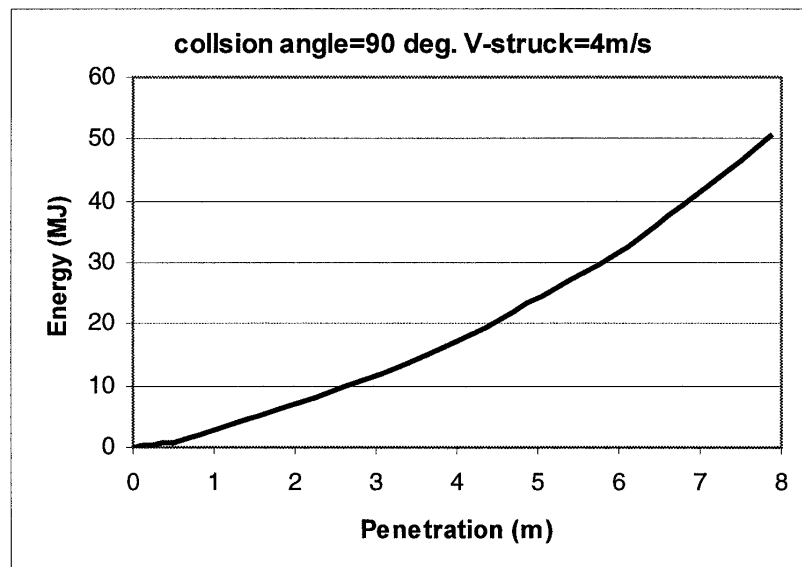
Fig. 4.26. Dissipated energy of the struck ship with various penetrations when the struck ship has a forward speed of 4.0 m/s and the collision angle is 90 degrees.

4.3 Collision Damage in Unidirectional Stiffened Double Hull Tanker

4.3.1 Introduction

The unidirectional stiffened double hull concept is an advanced double hull design in which the entire hull is stiffened by longitudinal girders and double-skinned transverse bulkheads. The structural simplification is significant in comparison with the traditional double hull stiffened by longitudinal stiffeners and transverse frames.

Fig. 4.27 shows sketches of an advanced design hull (ADH) and a conventional double hull. It is seen from the figure that the longitudinal girders run from bulkhead to bulkhead and connect the outer hull and inner hull in the ADH. The advantage of this design is its simplicity of manufacture, maintenance and repairs. The purpose of the present section is to investigate the collision strength of the ADH design.

Conventional Double Hull   **Advanced Double Hull (Unidirectional)**
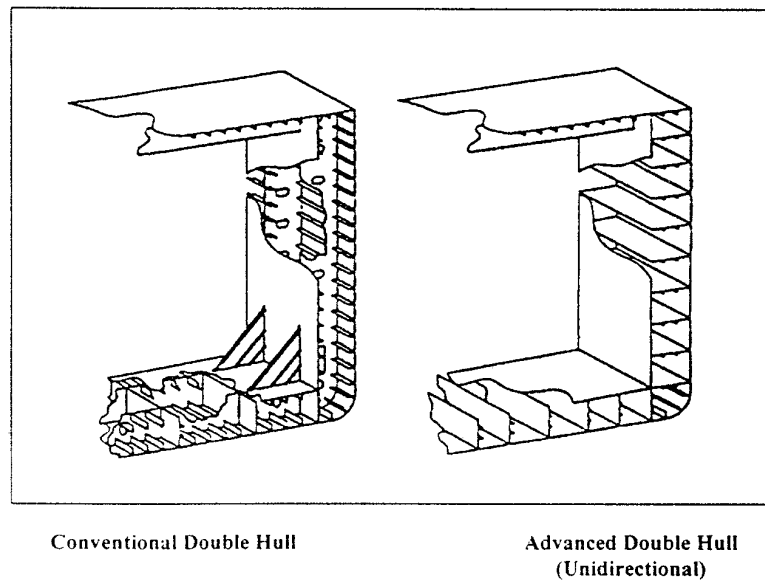
Fig. 4.27. Sketches of a conventional double hull and a unidirectional double hull.

4.3.2 Vertical Striking Bow

The Analysis Procedure

First, we consider a vertical bow striking an ADH side structure. The collision situation and the related parameters are presented in Fig. 4.28. To get a solution for the collision resistance, the deformation zone must be determined. The vertical height (2b) of the deformation zone can be assumed to be the distance between the non-deformed

longitudinal girders (see Fig. 4.28). The longitudinal length (2a) of the deformation zone will be determined by minimising the collision force. This will be discussed in detail in the following.
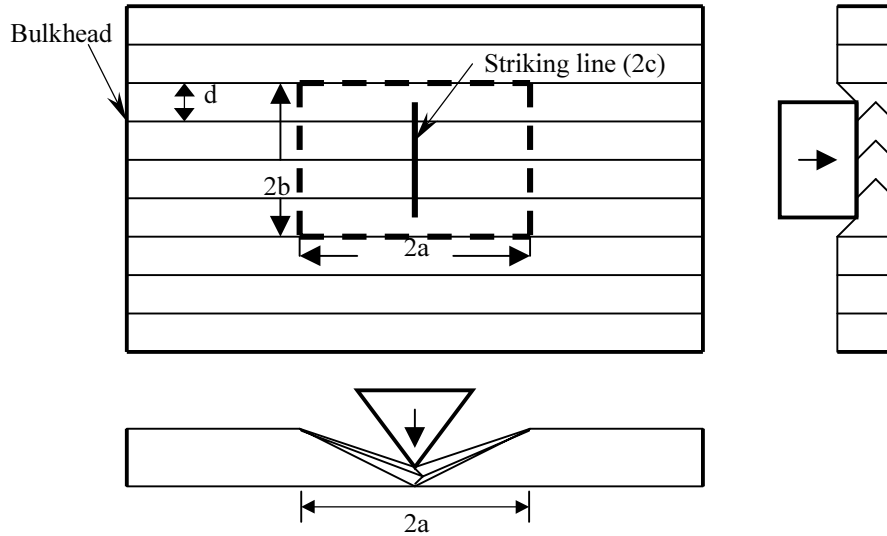
d = Spacing of the longitudinal girders
w = Distance between the double hull
2a = Horizontal length of the deformation zone
2b = Vertical height of the deformation zone
2c = Length of the striking line
2L = Distance between bulkheads

Fig. 4.28. Collision situation and deformation mode of an advanced design hull struck by a vertical bow.

The collision resistance is composed of the shell plating tension and the girder crushing. For the shell plating tension, we have the following formula (further simplify Eq. 3.56 when n=1) to calculate the resistance force:

$$F_p = \frac{4}{\sqrt{3}} \sigma_0 t_p \delta(\frac{2c}{a}) \tag{4.12}$$

In the present case of the unidirectional stiffened double hull, the spacing between the longitudinal girders is relatively small, and the shell plating will rupture at a very early stage of deflection. Therefore, only the tension in the longitudinal direction is included in Eq. (4.12).

For the girder crushing, we separate one girder with shell plating from the whole double hull to analyse the crushing force and to determine the longitudinal length (2a) of the deformation zone. The girder unit is shown in Fig. 4.29.
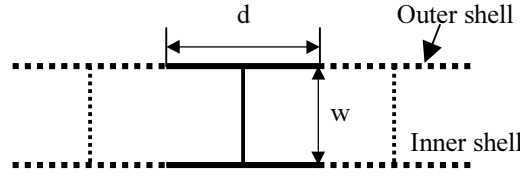
Fig. 4.29. A longitudinal girder unit in double side.

When the striking bow pushes the girder directly, the gird suffers folding deformation. The derived formula for the mean crushing force of a girder is expressed as (further simplify Eq. (3.86) in section 3.5)

$$F_m = \frac{\pi}{\sqrt{3}} \sigma_0 t_w^{\ 2} \frac{a}{H} + \frac{8}{3\sqrt{3}} \sigma_0 t_w \frac{H^2}{a} \tag{4.13}$$

where $2H$ is the folding length and t_w is the thickness of the girder.

The mean resistance of the girder flange (plate strip) can be calculated from

$$F_{pm} = (\int_0^{2H} F_{flange} d\delta)/(2H) = \frac{4}{\sqrt{3}} \sigma_0 t_p H(\frac{d}{a}) $$

where d is the girder spacing and t_p is the thickness of the shell plate.

Adding the resistance of the girder and the girder flange, we obtain the mean resistance of the girder unit:

$$F_{gird} = \frac{\pi}{\sqrt{3}} \sigma_0 t^{\ 2} \frac{a}{H} + \frac{8}{3\sqrt{3}} \sigma_0 t \ \frac{H^2}{a} + \frac{4}{\sqrt{3}} \sigma_0 t_p H(\frac{d}{a}) \tag{4.14}$$

It is assumed that the folding length of the girder is equal to the distance between the double hull. That is $2H = w$. The reason is that the width w of the double hull is small compared to the length of the girder. By minimising the mean force F_{gird}, we get the optimum length ($2a$) of the deformation zone in the longitudinal direction, that is

$$\frac{\partial F_{gird}}{\partial a} = 0 \quad \Rightarrow \quad a = \sqrt{\frac{8}{3\pi} \frac{H^3}{t_w} + \frac{4}{\pi} \frac{t_p H^2 d}{t_w^{\ 2}}} \tag{4.15}$$

If $a \geq L$, that is the deformation length beyond the length of the bulkhead, then set $a = L$. By adding the resistance of shell plate tension and girder crushing, the total collision resistance and dissipated energy can be obtained from $F = \sum (F_p + F_m)$.

Comparison with Ueda's Model Experiment

A collision experiment of a unidirectional double hull was carried out by Ueda et al. (1995). The double hull model and the rigid bow model are shown in Fig. 4.30. The double hull model was used to simulate a 40,000 t oil tanker on a scale of $\lambda = 1/10$. The damaged model after the static collision test is presented in Fig. 4.31.
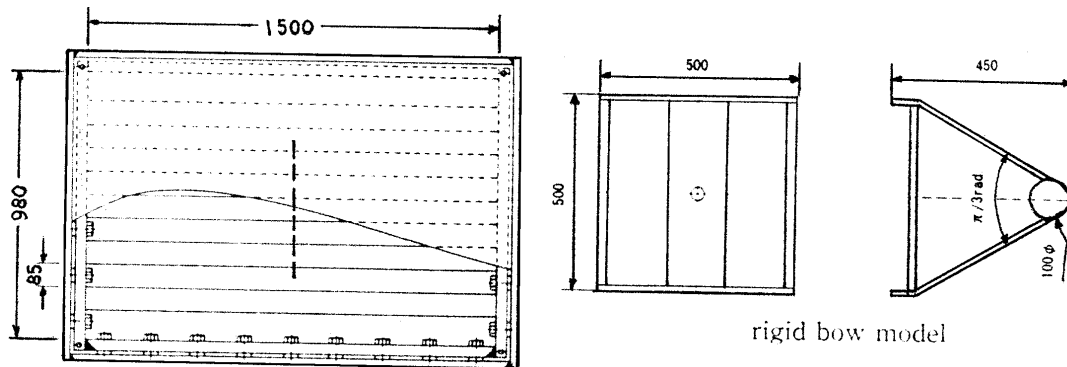
Fig. 4.30. The double hull model and the rigid bow model (Ueda, 1995).
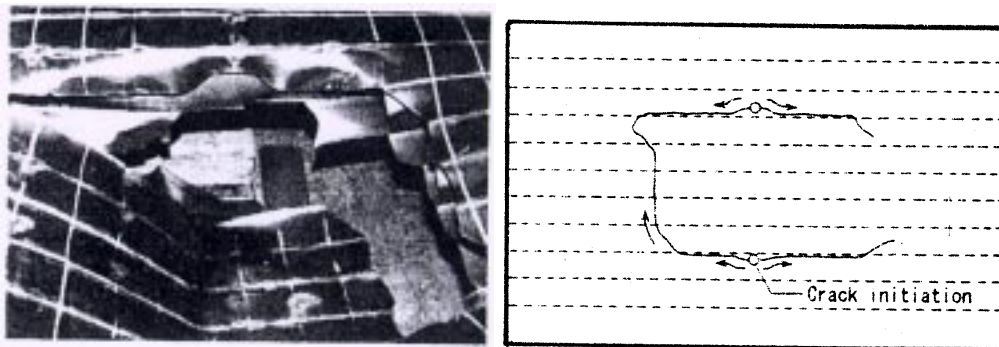
Fig. 4.31. Damaged double hull model after the static crushing test (Ueda, 1995).

The related parameters of the model are

2c = 500 mm,	Height of the striking bow
$t_p = t_w = 1.6$ mm,	Thickness of all plates and girders
w = 123.6 mm,	Distance between the double hull
d = 85 mm,	Girder spacing
N = 6,	Number of crushed girders
$\sigma_0 = 375.5 MPa$,	Flow stress of the material

The present calculation results for the collision force and the absorbed energy are compared with Ueda's test results in Figs. 4.32 and 4.33, respectively. In the present calculation, the critical rupture strain ε_c is assumed to be 7% and 10%, respectively. It is seen from the comparison that good agreement is found between the present results and Ueda's experimental results. The peak values in the force-penetration curve are the points where the outer shell and the inner shell just rupture.
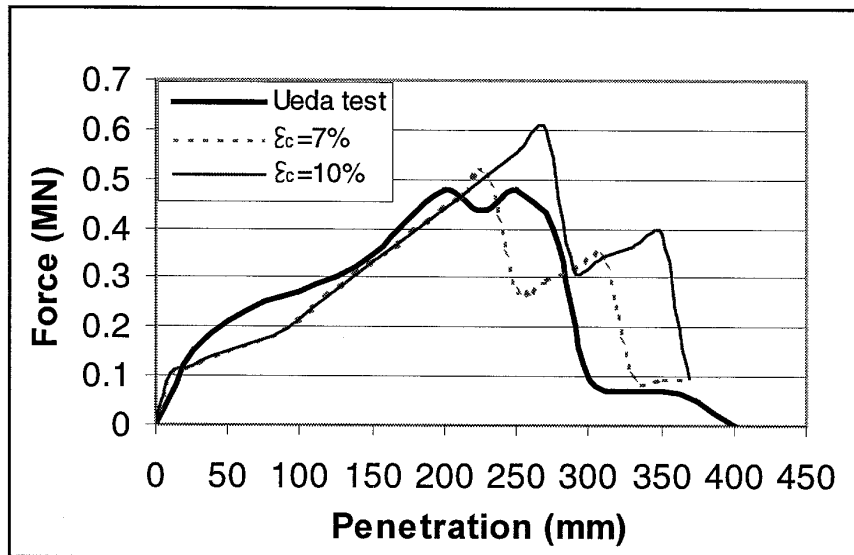
Fig. 4.32. Comparison of the force-penetration relationship obtained by the present calculation and Ueda's (1995) test results.
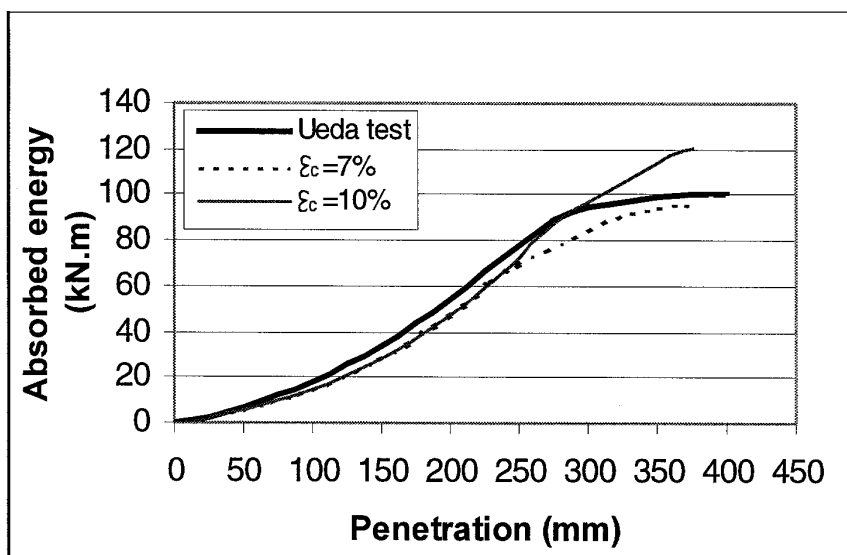
Fig. 4.33. Comparison of the energy-penetration relationship obtained by the present calculation and Ueda's (1995) test results.

Application to a Full-Scale Tanker

In Ueda's (1995) double hull model test, the model scale is 1/10 of a 40,000 t oil tanker. The present application example is the full-scale 40,000 t tanker, which is struck by a vertical rigid bow in the middle between the bulkheads. The collision situation is similar to the case of the above-mentioned model test. The related parameters are

$2c = (500 \ast 10)$ mm $= 5$ m,	Height of the vertical striking bow
$t_p = t_w = 1.6 \ast 10$ mm $= 16$ mm,	Thickness of all plates and web girders
w $= 123.6 \ast 10$ mm $= 1236$ mm,	Distance between the double hull
d $= 85 \ast 10$ mm $= 850$ mm,	Girder spacing
N=6,	Number of crushed girders
$\sigma_0 = 375.5 MPa$, $\varepsilon_c = 7\%$.	

The calculation results of the force-penetration relationship and the energy-penetration relationship are shown in Figs. 4.34 and 4.35, respectively.

If Figs. 4.33 and 4.35 are compared, it is found that the energy dissipated by the full-scale tanker is just equal to 10^3 times the energy absorbed by the tested model. That means the relationship of the absorbed energy between the full-scale ship and the model test is $E_{full-scale} = \lambda^3 \cdot E_{model}$, where λ is the geometric scale between the full-scale ship and the model. It is noted that the penetration is also scaled at the factor λ and the materials properties are the same. This result may also be obtained from the analytical formulation.
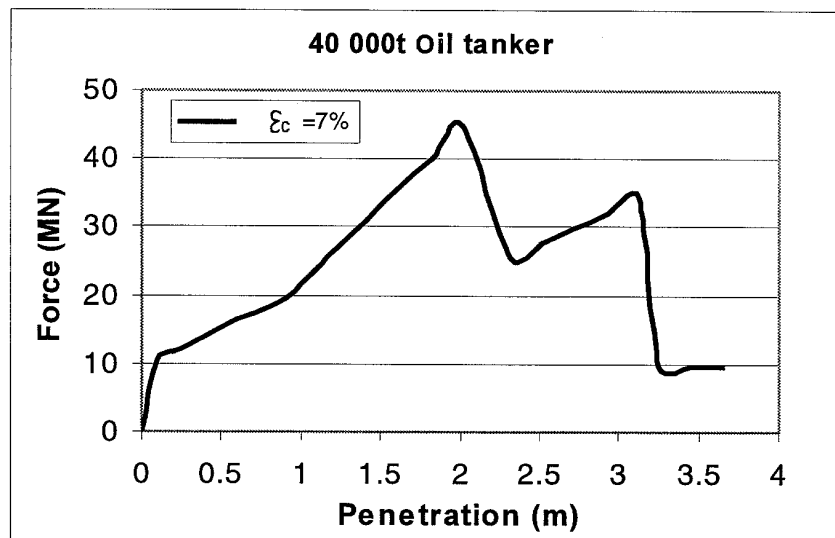
Fig. 4.34. Calculation result of the force-penetration curve of the 40,000 t tanker struck by a vertical rigid bow.
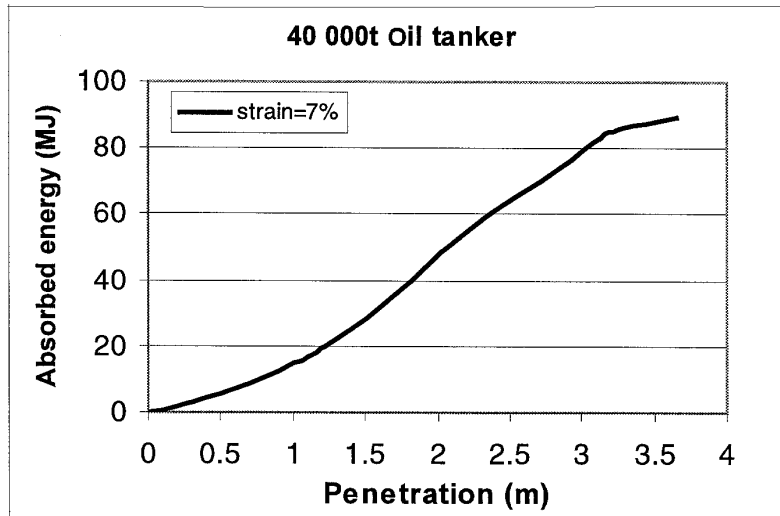
Fig. 4.35. Calculation result of the energy-penetration curve of the 40,000 t tanker struck by a vertical rigid bow.

4.3.3 Raked Striking Bow

Analysis Procedure

Here we analyse a raked bow striking the ADH hull. The collision case and the assumed deformation mode are shown in Fig. 4.36.

φ = Stem angle of the raked bow
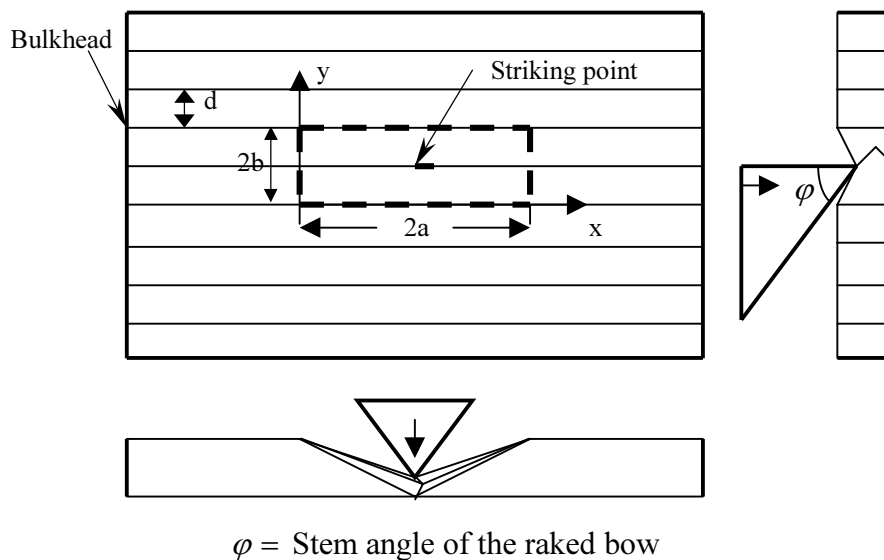
Fig. 4.36. Collision situation and deformation mode of an ADH struck by a raked rigid bow.

To analyse the collision resistance, several steps must be analysed separately.

(1) Initial collision

As shown in Fig. 4.36, a raked bow strikes the double hull at a longitudinal girder at the beginning. Before the striking bow touches other longitudinal girders, it is assumed that the deformation zone is confined between the two longitudinal girders. The tension resistance of the shell plate ($2a \cdot 2b$) can be expressed as (see Eq. 3.41 in Section 3.4.1):

$$F_p = \frac{4}{3}\frac{2}{\sqrt{3}}\sigma_0 t_p \delta(\frac{d}{a} + \frac{a}{d})$$

The mean resistance of the plate can be calculated from

$$F_{pm} = (\int_0^{2H} F_p d\delta)/(2H) = \frac{4}{3}\frac{2}{\sqrt{3}}\sigma_0 t_p H(\frac{d}{a} + \frac{a}{d})$$

By adding the mean tension force of the plate and the mean crushing force of the girder, the total mean force becomes

$$F_{m1} = \frac{\pi}{\sqrt{3}}\sigma_0 t_w^2 \frac{a}{H} + \frac{8}{3\sqrt{3}}\sigma_0 t_w \frac{H^2}{a} + \frac{4}{3}\frac{2}{\sqrt{3}}\sigma_0 t_p H(\frac{d}{a} + \frac{a}{d})$$

By minimising the mean force F_{m1}, we get the length (2a) of the deformation zone in the longitudinal direction, that is

$$\frac{\partial F_{m1}}{\partial a} = 0 \quad \Rightarrow \quad a_1 = \sqrt{\frac{8(t_w H^3 d + t_p H^2 d^2)}{3\pi t_w^2 d + 8t_p H^2}} \tag{4.16}$$

Thus, the total force-penetration relationship can be written as

$$F_1 = \frac{\pi}{\sqrt{3}}\sigma_0 t_w^2 \frac{a_1}{H} + \frac{8}{3\sqrt{3}}\sigma_0 t_w \frac{H^2}{a_1} + \frac{4}{3}\frac{2}{\sqrt{3}}\sigma_0 t_p \delta(\frac{d}{a_1} + \frac{a_1}{d}) \tag{4.17}$$

(2) Striking bow touching other girders

Usually, the stem angles φ of the raked bow are between 60^0 and 70^0. The critical deflection angle of the shell plate before deformation and after deformation can be determined from $\theta = \tan^{-1}(\sqrt{2\varepsilon_c})$. Assuming that the critical rupture strain is between $\varepsilon_c = 5\%$ and $\varepsilon_c = 10\%$, we get the range of the critical deflection angle: $\theta = 17.5^0 \sim 24^0$

and $90° - \theta = 66^0 \sim 72.5^0$. Therefore, it may be assumed that the shell plate ($2a_1 \cdot 2d$) ruptures in the transverse direction when the striking bow just touches the second longitudinal girder. But the shell plate may preserve the resistance in the longitudinal direction (if $a_1 > d$). The resistance of the plate ($2a_1 \cdot 2d$) becomes

$$F_{p1} = \frac{4}{3}\frac{2}{\sqrt{3}}\sigma_0 t_p \delta(\frac{d}{a_1})$$
(4.18)

Apart from the tension of the first plate ($2a_1 \cdot 2d$), the second plate ($2a \cdot d$) will be stretched due to the direct pushing.
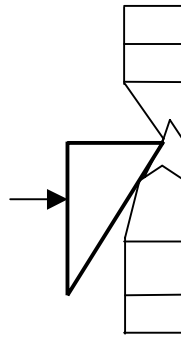
Fig. 4.37. Striking bow crushing other longitudinal girders.

By minimising the mean force, we get the length of the second deformation zone in the longitudinal direction:

$$a_2 = \sqrt{\frac{8t_w H^3 d + 4t_p H^2 d^2}{3\pi t_w^2 d + 4t_p H^2}}$$
(4.19)

Thus, the total resistance of the second deformation phase can be expressed as

$$
\begin{aligned}
F_2 &= \frac{\pi}{\sqrt{3}}\sigma_0 t_w^2 \frac{a_1}{H} + \frac{8}{3\sqrt{3}}\sigma_0 t_w \frac{H^2}{a_1} + \frac{4}{3}\frac{2}{\sqrt{3}}\sigma_0 t_p \delta(\frac{d}{a_1}) \\
&+ \frac{\pi}{\sqrt{3}}\sigma_0 t_w^2 \frac{a_2}{H} + \frac{8}{3\sqrt{3}}\sigma_0 t_w \frac{H^2}{a_2} + \frac{2}{3}\frac{2}{\sqrt{3}}\sigma_0 t_p \delta(\frac{d}{a_2}+\frac{a_2}{d})
\end{aligned}
$$
(4.20)

For the following deformation, the analysis procedure is similar to the above. When the striking bow reaches the inner shell plate, the inner shell plate starts to deform.

Calculation Example

The application example is similar to the previous one, that is the full-scale 40,000 t oil tanker. The main parameters of the tanker are rewritten here:

$t_p = t_w = 16$ mm,   Thickness of all plates and web girders

w = 1236 mm,   Distance between the double hull

d = 850 mm,   Girder spacing

$\varphi = 65^0$,   Stem angle of the raked bow

$\sigma_0 = 375.5 MPa$, $\varepsilon_c = 7\%$.

The calculation results of the collision force and the absorbed energy are presented in Fig. 4.38. The critical energy just causing inner hull rupture is $E_c = 12.5 MNm$ at the penetration of $\delta_1 = 0.73w + d\sqrt{2\varepsilon_c} = 1.22$ m.
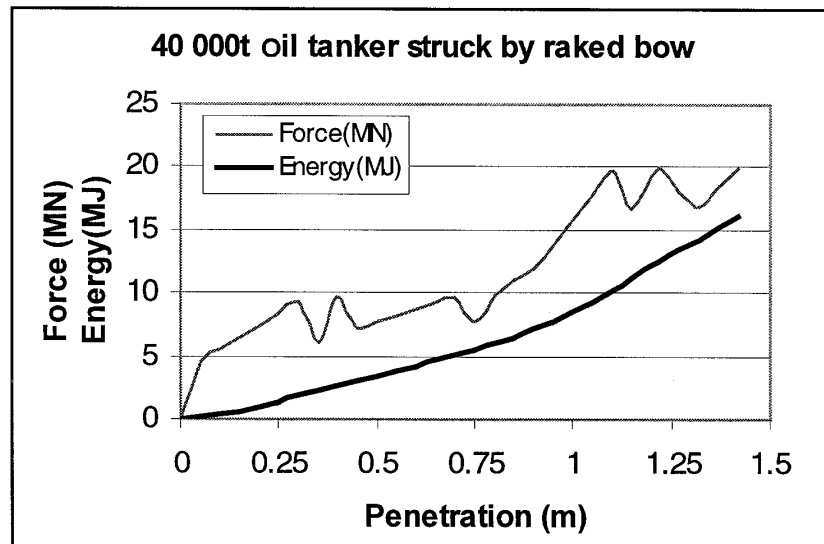
Fig. 4.38. Force-penetration and the energy-penetration relations for a 40,000 t oil tanker struck by a raked bow.

4.3.4   Concluding Remarks

- In this section, collision analysis of unidirectional double hull tankers struck by other ships has been performed. The comparison of the present results with Ueda's test results shows that good agreement has been achieved.

- The ADH design has a high capability to resist grounding with its relatively tight spacing of longitudinal girders (Rodd, 1997). But due to the relatively small spacing between girders, earlier rupture of the shell plates may occur in side collisions.

4.4   Collision of a Product Tanker

4.4.1   Analysis Example

In the late 1980s, Burmeister & Wain Shipyard (in Denmark) developed a new design of a 84,000 dwt product tanker. This vessel is based on the outstanding performance of the low-operating-cost 64,000 dwt Panamax bulk carrier. The tanker has high cargo flexibility. It is able to transport crude oil as well as all different types of oil products coming from the refineries. The principal dimensions of the tanker are

Length overall	228.60 m
Length (Lpp)	224.10 m
Breadth	32.24 m
Depth	21.60 m
Design draught	11.58 m
Deadweight	84,000 t
Service speed	14.6 knots

The product tanker has a double skin: a double bottom, double sides and a double deck, as shown in Fig. 4.39. It was a transverse web frame stiffened double sides. The double skin contributes to safety and insulation of the cargo against thermal loss and against strong sunlight superheating of the cargo.

The purpose of the present section is to analyse the collision strength of the product tanker and to examine its capability to resist collisions.
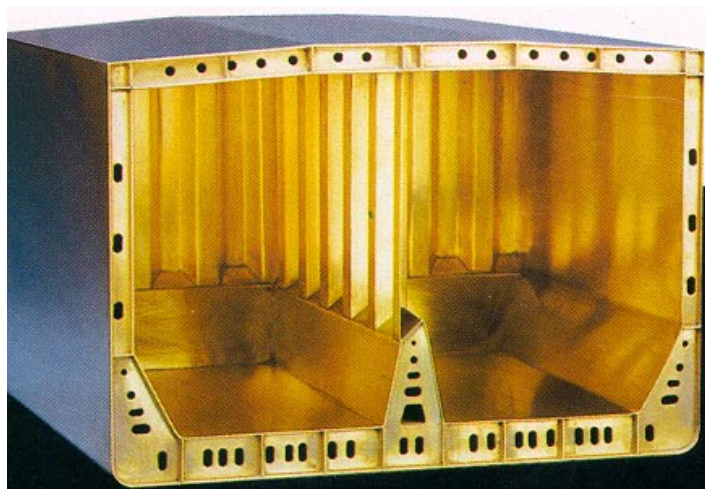
Fig. 4.39. Midship of the 84,000 dwt product tanker.

It is assumed that a raked bow strikes the side of the product tanker. The collision situation and the analysis model are shown in Fig. 4.40.

φ = Stem angle of the striking bow

2θ = Entry angle of the striking bow
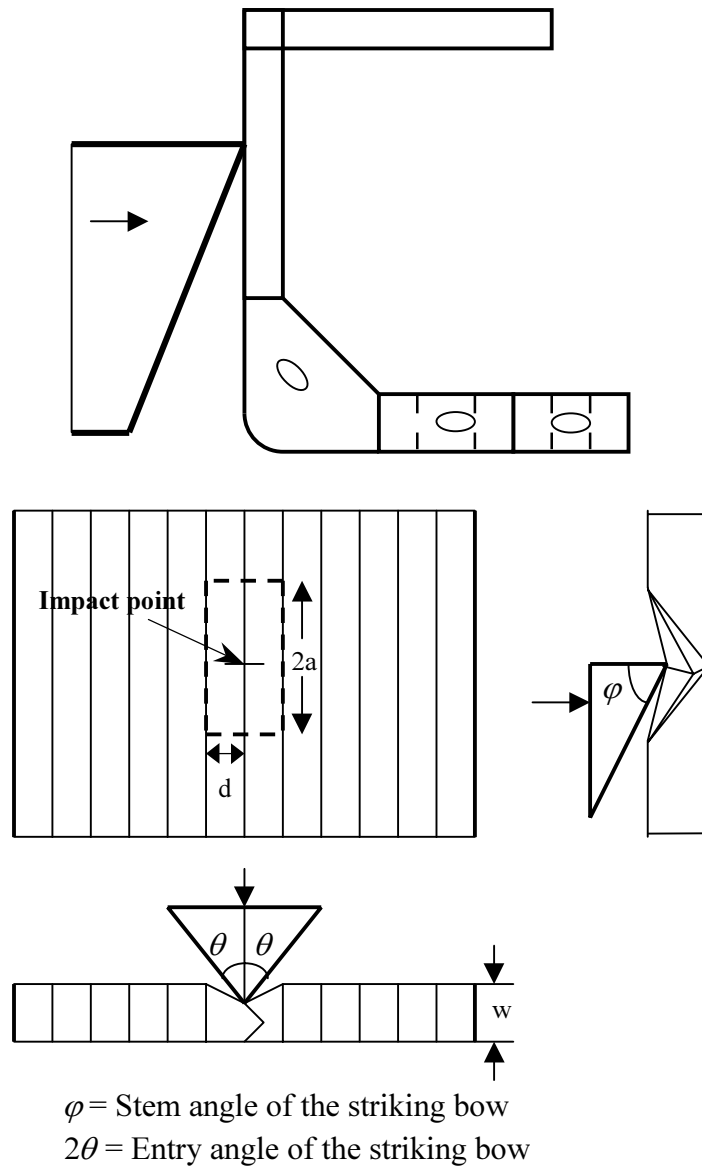
Fig. 4.40. A raked bow strikes the side of the product tanker.

The analysis procedure is similar to the method of the collision analysis of the unidirectional double hull. The related parameters of this example are

The thickness of the outer shell is $t_{p1} = 17$ mm

The thickness of the inner shell is $t_{p2} = 15$ mm

The web thickness is $t_w = 10$ mm

The transverse web spacing is $d = 900$ mm

The width of the double hull is $w = 900$ mm

The bulkhead spacing is 28.8 m

The stem angle of the striking bow is $\varphi = 65^0$

The entry angle of the striking bow is $2\theta = 80^0$

The flow stress of the material is $\sigma_0 = 375 MPa$

The critical rupture strain is $\varepsilon_c = 7\%$

The calculation results for the force-penetration relationship and the energy-penetration relationship are presented in Fig. 4.41. The results show that the force-penetration curve changes quickly due to the rupture of the shell plates.
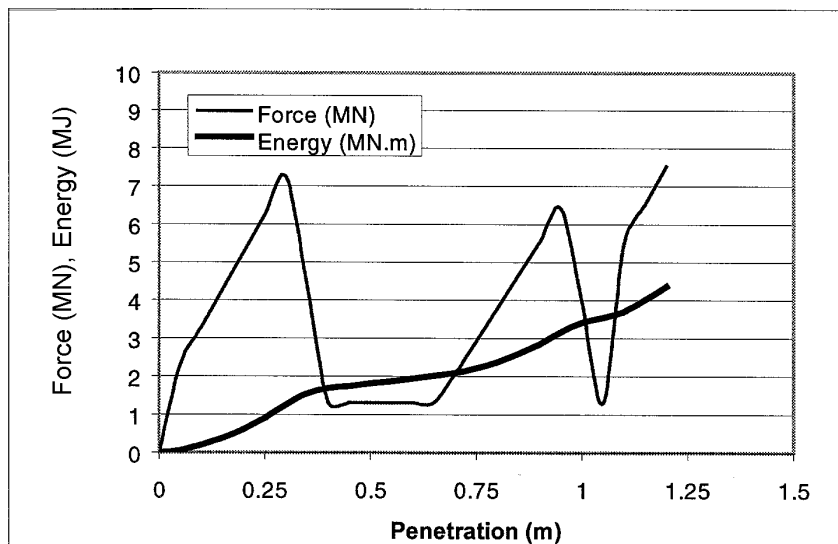
Fig. 4.41. Force-penetration and energy-penetration relationships for a 84,000 dwt product tanker struck by a raked bow.

The calculation results for absorbed energy distributions in the shell plating and the transverse frames are presented in Fig. 4.42. It is seen from the results that the shell plating dissipated more energy than the frames. Due to the relatively narrow width of the double sides, not much energy could be absorbed by the side structure before the inner shell plating ruptured.

4.4.2 Concluding Remark

An example of a side collision of an 84,000 dwt product tanker struck by a raked bow is presented. In comparison with the longitudinal unidirectional stiffened double hull tanker, the transverse web frame stiffened vessel seems weak in regard to resisting side

collisions. The side shell ruptures at relatively small penetration. Thus, not much energy can be absorbed before the shell ruptures.
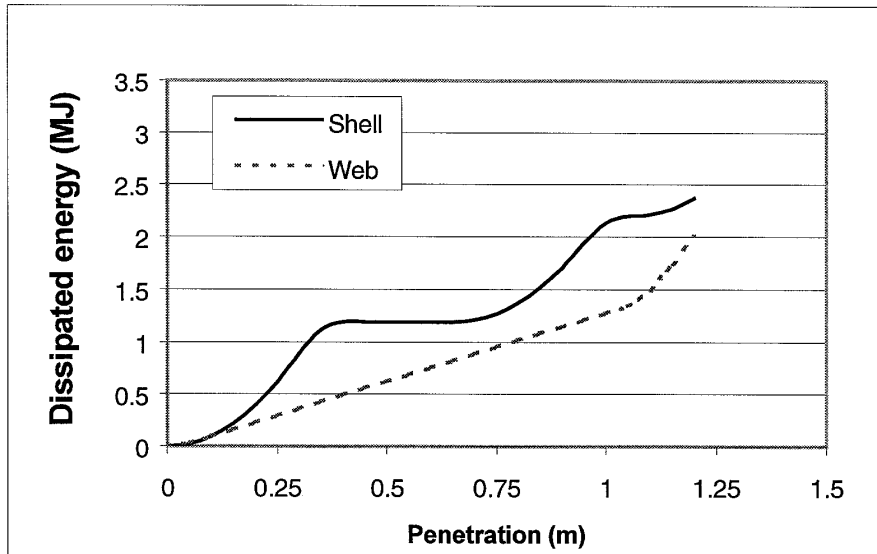
Fig. 4.42. Energy distributions in the shell plating and the transverse webs.

4.5   Collision of Double Hull Oil Tankers

4.5.1   Introduction

In the past 30 years, ship collisions and grounding have caused heavy oil spills on the sea and polluted the environment seriously. The notable oil spills from single-hull tankers in the world caused by collisions and grounding since 1970 are shown in Table 4.8.

Table 4.8. Notable oil spills in the world caused by collisions and grounding.

No.	Date	Location and Description		Tons spilt
1	March 20, 1970	Traelhavet Bay, Sweden,	**Collision**	100,000
2	Dec.19, 1972	Gulf of Oman,	**Collision**	115,000
3	May 12, 1976	La Coruna, Spain,	Grounding	100,000
4	Dec.15, 1976	Nantucket, Mass,	Grounding	26,000
5	March 16, 1978	Portsall, France,	Grounding	223,000
6	July 19, 1979	Trinidad ,	**Collision**	300,000
7	Nov.1, 1979	Galveston Bay, Tex,	**Collision**	36,000
8	March 24, 1989	Alaska,	Grounding	34,000
9	Dec.3, 1992	Spain,	Grounding	84,000
10	Jan.5, 1993	Shetland Islands,	Grounding	87,000
11	Feb.15, 1996	Wales, UK,	Grounding	65,000

In this section, calculation examples of double hull oil tankers struck by a raked bow or a bulbous bow are given.

4.5.2 Example 1 --- 100,000 dwt Tanker

It is assumed that a raked bow strikes the side of a 100,000 dwt tanker at an intersection of a transverse frame and a longitudinal stringer. The basic data of the striking bow are: entry angle of the bow $2\theta = 80^0$ and the stem angle of the bow $\varphi = 65^0$. The detailed structural parameters of the tanker are presented in Fig. 4.43. The flow stress of the materiel is $\sigma_0 = 300 MPa$ and the critical rupture strain is assumed to be $\varepsilon_c = 7\%$.

Dimensions:
Outer shell thickness: 20.6mm
Inner shell thickness: 15.0mm
Web frame thickness: 14.3mm
All stiffeners: 450x15/150x20
Long. stiffener spacing: 912mm
Trans. web spacing: 3215mm
Double side width: 2057mm
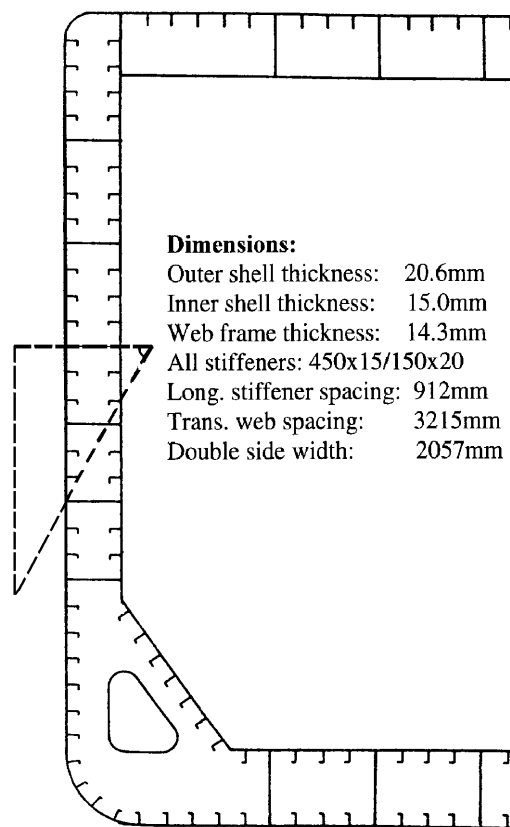
Fig. 4.43. Mid-ship section of the 100,000 dwt double hull tanker.

The calculation results for the collision force and the absorbed energy of the 100,000 dwt oil tanker are shown in Fig. 4.44 and Fig. 4.45, respectively. The energy dissipated in the equivalent shell (including the stiffeners) and the frames (including the transverse frames and the longitudinal stringers) are shown in Fig. 4.46.

Fig. 4.44 indicates that there are two peaks on the force curve, one is related to rupture of the outer shell plating and the other is connected with rupture of the inner shell plating. It is seen from Fig. 4.46 that the equivalent shell plating absorbs more energy than the frames. For example, at the penetration of 2.5 m, the equivalent shell plating absorbs 62.5% of the total dissipated energy, and the frames (including the transverse frames and the longitudinal stringers) absorb 37.5% of the total dissipated energy.
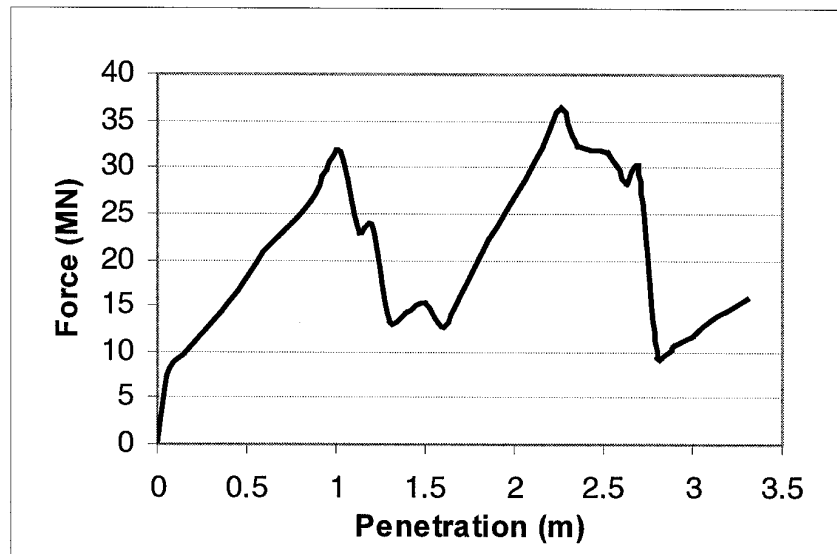
Fig. 4.44. Collision force curve of the 100,000 dwt tanker struck by a raked bow.
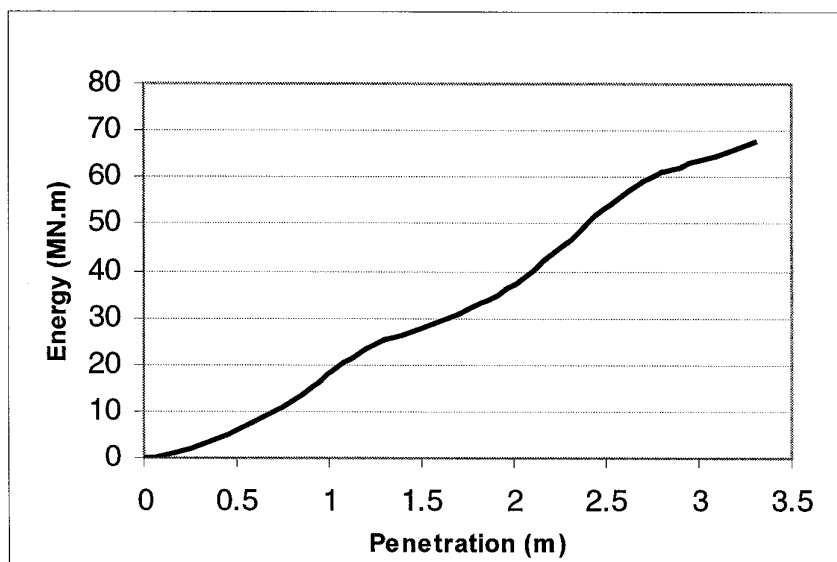
Fig. 4.45. Dissipated energy curve of the 100,000 dwt tanker struck by a raked bow.
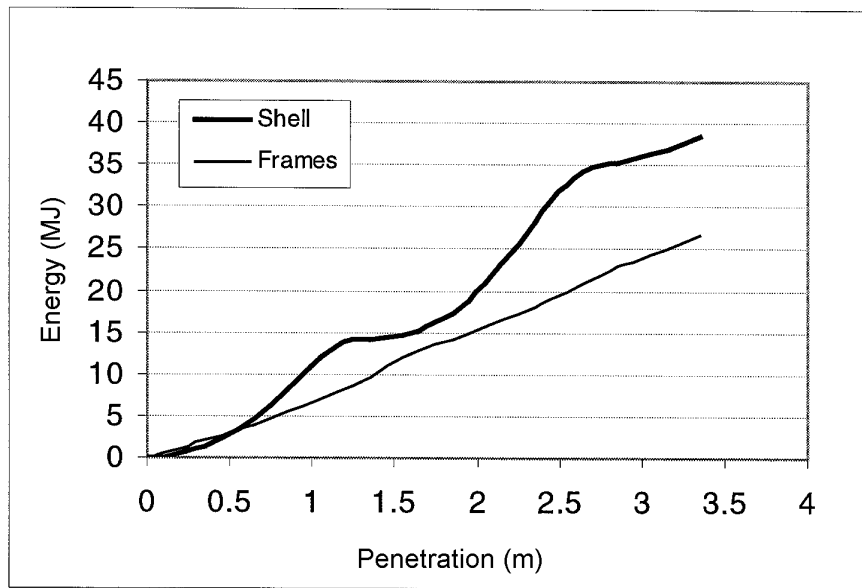
Fig. 4.46. Dissipated energies in equivalent shell plating and frames of the 100,000 dwt tanker struck by a raked bow.

4.5.3 Example 2 --- 293,000 dwt Tanker

This example analyses collision between the bow of a container ship and the side of a 293,000 dwt double hull VLCC. The principal dimensions of the striking ship and the struck ship are

Parameter	The striking ship	The struck ship
Length Lpp.	210.0 m	327.0 m
Breadth	32.2 m	56.4 m
Depth	21.0 m	30.6 m
Draught	11.9 m	19.8 m
Forecastle deck	24.0 m	*
Displacement	50,000 t	264,500 t
Service speed	25.0 knots	14.5 knots

The striking ship has a bulbous bow. The entry angle of the bow is $2\theta = 80$ degrees and the stem angle is $\varphi = 65$ degrees. The radii of the bulb are $R_L = 0.25 H_{deck} = 6$ m, $R_V = 0.125 H_{deck} = 3$ m and $R_H = 0.05 H_{deck} = 1.2$ m.

The detailed scantlings of the midship section of the struck ship are presented in Fig. 4.47. The flow stress of the material is $\sigma_0 = 305.5 MPa$ and the critical rupture strain is assumed to be $\varepsilon_c = 10\%$.
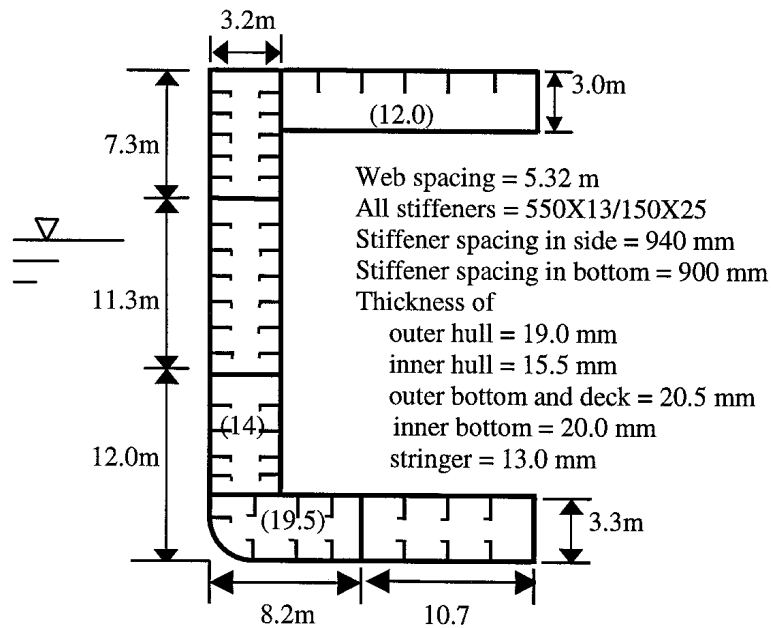
Fig. 4.47. Midship cross-section of the 293,000 dwt double hull tanker.

It is assumed that the striking ship sailing at a forward speed of 4.0 m/s, collides with the midship of the 293,000 dwt tanker at a right angle while the struck ship is at a standstill before the collision. The collision position is at a transverse frame. The damage to the struck ship is created by both the bulb and the flare. From the external mechanics, the collision energy to be dissipated by the ship structure is found to be 367.9MJ. The results for the collision resistance of the struck ship with various penetrations are given in Fig. 4.48.
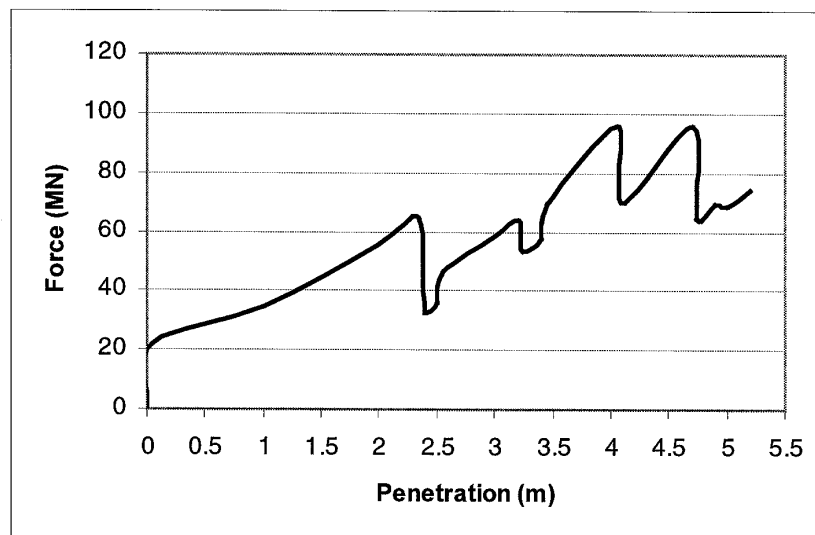
Fig. 4.48. The collision resistance of a 293,000 dwt tanker struck by a 50,000 t ship.

From Fig. 4.48, it is seen that the collision resistance of the struck ship is very high. The bow of the striking ship may deform. To give a very rough estimation of the energy absorbed by the striking bow, the following empirical formula is used (Pedersen et al., 1993 and Hysing, 1995):

$$E_{bow} = \frac{P_{bow}^{2}}{155} \cdot (\frac{275}{L_s})$$

where E_{bow} (MJ) is the energy dissipated by the striking bow, P_{bow} (MN) is the plastic resistance of the striking bow, which is equal to the maximum collision resistance of the struck ship, and L_s (m) is the length of the striking ship.

The energy absorbed by the struck ship with various penetrations is presented in Fig. 4.49. By use of the above empirical formula, the energy absorbed by the striking bow is 77.1 MJ. When the penetration reaches 5.20 m, the total energy absorbed by the striking bow and the side of the struck ship is 367.9 (MJ). This means that all the kinetic energy loss is dissipated completely. Therefore, the penetration stops. The struck ship absorbs 79% and the striking bow absorbs 21% of the total energy.
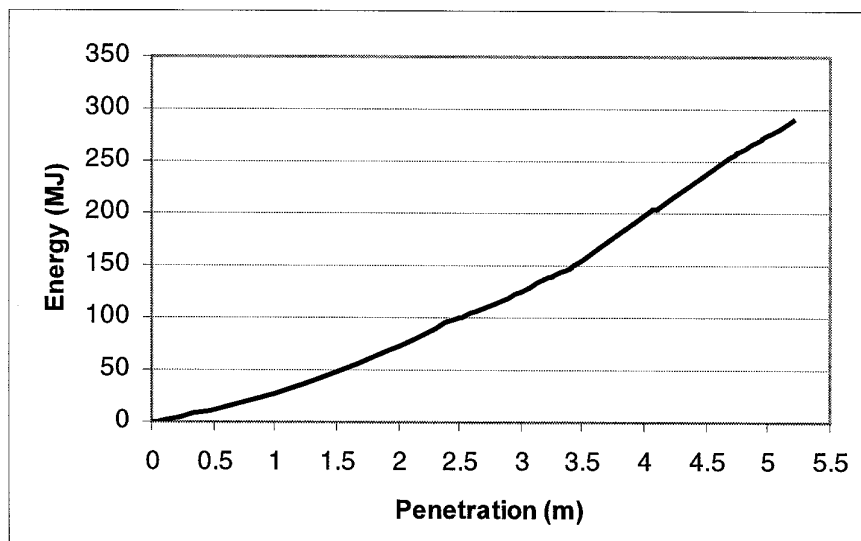
Fig. 4.49. Dissipated energy of the struck ship with various penetrations (a 293,000 dwt tanker struck by a 40,000 t container ship).

The critical situation for an oil tanker is defined as starting oil leak. That is the inner hull of the double side ruptures. The critical collision energy of the 293,000 dwt tanker struck by the 50,000 t container ship is then calculated as 330.1MJ. Thus, the critical collision speed of the 50,000 t container ship striking the tanker is 7.4 knots. The critical collision speed of the oil tanker struck by different sizes of striking ships is calculated and shown in Fig. 4.50. It is assumed that all striking ships have the same shape of striking bow in this calculation.
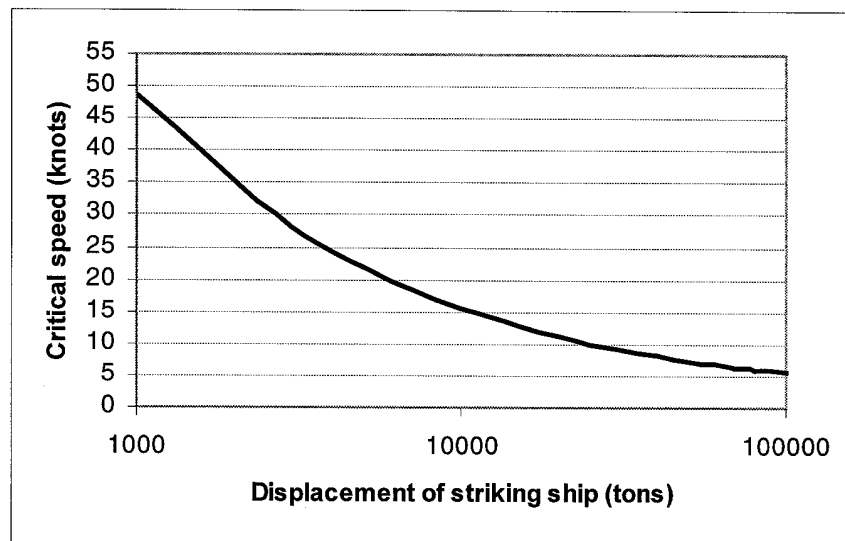
Fig. 4.50. Critical collision speed of a 293,000 dwt tanker struck by various ships.

The probability distribution of collision accidents for five years from 1987 to 1991 on the sea around Japan is presented in Fig. 4.51, which was given by Ito et al. (1994).
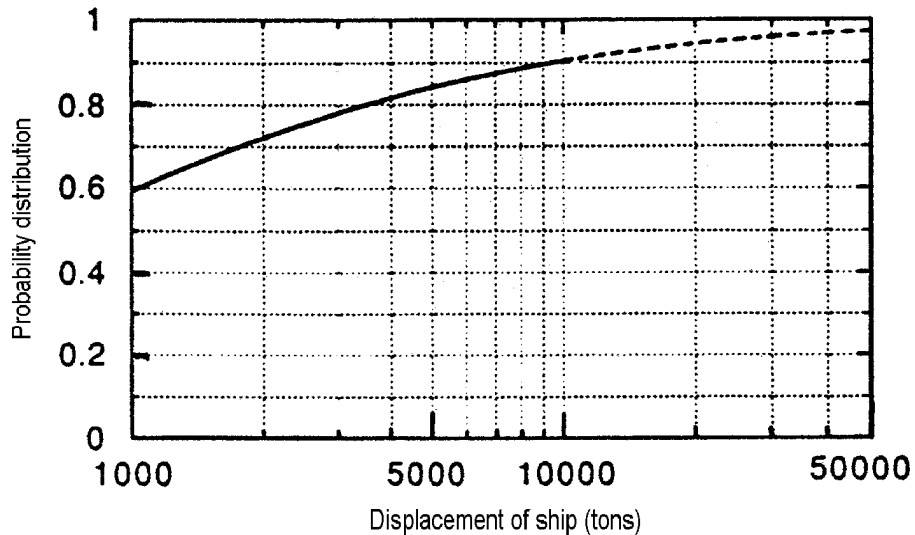
Fig. 4.51. Cumulative casualty probability of ship collisions around Japan
(Ito, 1994).

Fig. 4.51 shows that 90% of the collision accidents is less then 10,000 t displacement. Thus it may be concluded from Figs. 4.50 and 4.51 that the 293,000 dwt tanker may prevent oil pollution in the probability of 90% collision with other ships at a striking speed below 15.5 knots if this tanker sails on the sea around Japan.

4.5.4 Concluding Remark

In this section, the collision analysis of a 100,000 dwt double hull oil tanker struck by a raked bow is performed. The second example is a 293,000 dwt double hull tanker struck by a 50,000 t container ship. The critical collision speed is calculated. In order to consider the deformation of the striking bow, a simple empirical formula is used for calculating the energy absorbed by the striking bow. The results show that the 293,000 dwt tanker has about 90% probability of no oil spillage in all possible collisions if this tanker sails on the sea around Japan.

This page is intentionally left blank.

Chapter 5

Absorbed Energy versus Damaged Material Volume

5.1 Introduction

The most well-known empirical approach to collision analysis was made by Minorsky (1959), who analysed 26 collision cases of full-scale ship accidents and developed the formula $E(MJ) = 47.2 \cdot R_T(m^3) + 32.7$, which relates the absorbed energy (E) to the destroyed material volume (R_T). This empirical formula has been widely used in ship collision and grounding analyses because of its simplicity.

Minorsky's empirical formula indicates that the energy absorption by a ship during a collision is simply proportional to the volume of the destroyed material. That is, if we want to design a ship with a high capability to resist collision, we should use more building material. This is not entirely true, since the energy absorption efficiency of structures is different from structure to structure. It depends on the arrangement of the structure, the materials properties, and the damage mode.

Therefore, to investigate further the relationship between the absorbed energy and the volume of destroyed material could still be an interesting task.

Thus, the purpose of this chapter is to establish a method which can be used as a rough, but simple design tool for analysing ship collisions and grounding. Very simple expressions for the relation between the absorbed energy and the destroyed material volume are developed, which take into account the structural arrangement, the materials properties and the damage modes.

The present method is validated against a large number of the existing experimental results and numerical simulations. Application examples of full-scale accidents and bottom raking damage to tankers and damage distribution of high-speed vessels are

carried out. The proposed method may be considered as an alternative approach to the Minorsky method.

5.2 The Method

5.2.1 Prediction Methodology

The analysis of structural damage caused by ship collisions and grounding is very complex. The impact response is highly non-linear, involving continuous changes in the geometry of the ship structures. However, the observed failure modes from ship accidents reveal that the primary energy absorbing mechanisms are: crushing of decks, tearing of bottom plating, folding of web frames and stretching of shell plating.
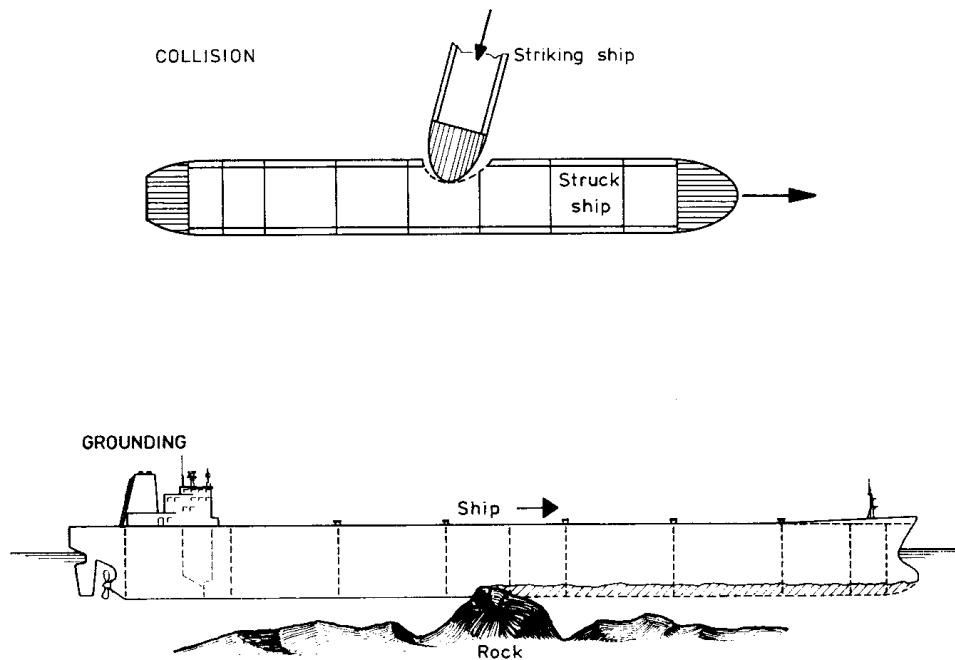
Fig. 5.1. Scenarios of ship collisions and grounding.

Based on the characteristics of the structural arrangement and the above mentioned failure modes in collision and grounding events, the ship structure is divided into a number of plated components. The damage modes of some of the basic structural elements are illustrated in Fig. 5.2. Several authors, for example Amdahl (1983), Wierzbicki and Abramowicz (1983), Kierkegaard (1993a), Abramowicz (1994), Ohtsubo and Wang (1995), Paik and Pedersen (1995), Lu and Calladine (1990), Wierzbicki and Thomas (1993) and Simonsen (1998b), have investigated crushing, tearing or folding of the basic elements using simplified theoretical or experimental methods.
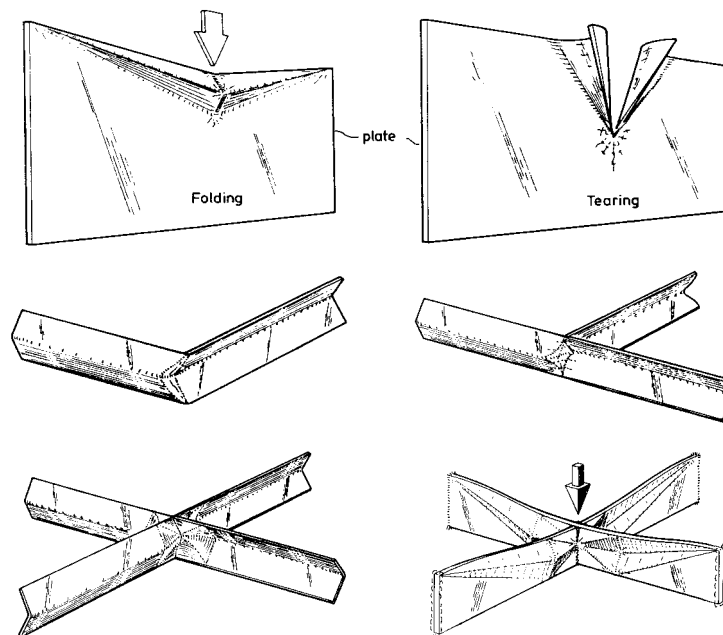
Fig. 5.2. Basic damage modes of structural units.

A comparison of the derived expressions for the different structural units with different failure modes (folding, tearing or crushing) shows that their mean resistance forces have some similarity. The mean resistance can be expressed as

$$F_m = D_1 \sigma_0 t^\alpha c^\beta$$

where σ_0 is the flow stress of the material, t is the thickness of the plate, c is the cross-sectional length of a unit or the tearing length, D_1 is a coefficient related to the actual crushing or tearing configuration, the exponent α is in the range $\alpha = 1.5 \sim 1.7$, the exponent β is in the range $\beta = 0.3 \sim 0.5$ and $\alpha + \beta = 2$. For a plate (such as a side shell) suffering lateral loading, its main behaviour is membrane tension. The relation of the resistance force F_p and the lateral indentation δ in this case can be written as

$$F_p = D_2 \sigma_0 t \delta$$

where D_2 is a coefficient related to the impact position and the plate size.

The actual damage in ship collisions and grounding is far more complicated than the damage to the basic elements. In fact, normally we cannot predict the exact damage mode during impact. It may be a mixed mode of crushing, folding, tearing and stretching. However, since the basic failure mechanisms have certain common relationships, it is possible to establish simple expressions to describe collision and grounding damages.

5.2.2   The Proposed Formulas

Three different energy absorption mechanisms have been identified. The first is the plastic tension deformation, such as indentation of the shell plating during a side collision. The second is the folding and crushing damage mode, such as crushing of a bow and folding and crushing of a deck. The third is the tearing damage mode, such as the raking damage in ship grounding. The proposed formulas for the relationship between the absorbed energy and the destroyed material volume are based on the theoretical work by Abramowicz (1994), Amdahl (1983), Wierzbicki and Thomas (1993) and the theory presented in Chapter 3 in the present thesis. The formulas are as follows:

(1). Energy absorption by the plastic tension damage mode

$$E = 0.77 \varepsilon_c \sigma_0 R_T \tag{5.1}$$

where E_1 is the absorbed energy, σ_0 is the flow stress of the material, ε_c is the critical rupture strain of the material, which is determined from $\varepsilon_c = 0.10(\varepsilon_f / 0.32)$ (see McDermott et al. 1974) where ε_f is the steel material ductility obtained in a tensile test, and R_T is the volume of tensioned and ruptured material.

(2). Energy absorption by the crushing and folding damage mode

$$E = 3.50 (\frac{t}{d})^{0.67} \sigma_0 R_T \tag{5.2}$$

where t is the average thickness of the crushed plates, d is the average width of the plates in the crushed cross-section, and R_T is the volume of crushed material (see details in the following examples).

(3). Energy absorption by the tearing damage mode

$$E = 3.21 (\frac{t}{l})^{0.6} \sigma_0 R_T \tag{5.3}$$

where t is the equivalent plate thickness, including longitudinal webs and stiffeners (in the tearing direction), and l is the critical tearing length where the steady tearing state has just been reached. If the steady state has not been reached, l is equal to the tearing length. R_T is the volume of torn material (see details in the following examples).

It is seen that these formulas have a simple form similar to the Minorsky formula. If we assume that the flow stress is $\sigma_0 = 260 N / mm^2$ and the ratio $t / d = 1 / 83$, then Eq. (5.2) gives $E = 47.0 R_T$, which is basically equal to the first term of Minorsky's formula. The second term in the Minorsky formula can be explained as the contribution from the shell

plating damage. This indicates that the present method to some extent includes the case of Minorsky's empirical expression. In the following section, detailed comparisons of results obtained by the present method and the existing experimental or numerical results are carried out. It is also illustrated how the proposed procedure can be used in practical applications.

5.3 Verification

5.3.1 Bow Crushing

(1). Comparison with Kierkegaard's Calculation of Bow Crushing

Kierkegaard (1993) carried out a numerical calculation of a 150,000 dwt bulk carrier colliding head-on with a rigid wall. The principal particulars of the ship are shown in Table 5.1.

Table 5.1. Principal particulars of a 150,000 dwt bulk carrier.

Length p.p.	274.0 m
Breadth moulded	47.0 m
Depth moulded	21.6 m
Max. draft	16.0 m
Displacement	174,850 t
Service speed	15.0 knots

The ship had a longitudinally stiffened bow. The plate thickness of the decks (forecastle deck, main deck and lower level decks) was 13.0 mm. The spacing of the longitudinals on decks was 800 mm. The flow stress of the steel material was 410 MPa. The volume of the damaged steel at an indentation of 16.3 m of the bow was approximately 55 m^3 (Kierkegaard, 1993). The dissipated energy obtained by the present method is calculated from

$$E = 3.50(\frac{t}{d})^{0.67} \sigma_0 R_T = 3.50 \cdot (\frac{13}{800})^{0.67} \cdot 410 \cdot 55 = 90.81 \cdot R_T = 4994(MJ)$$

The result given by Kierkegaard is 5453 MJ and by Minorsky's method it is 2629 MJ. The agreement between the present result and Kierkegaard's numerical result is quite good. Minorsky's method gives a lower result in this case. In fact, Minorsky's method was based on analyses where ships suffered heavy side damage. Therefore, the Minorsky method can not be expected to be useful in the case of bow crushing.

(2). Comparison with Woisin's Collision Tests

Woisin (1979) conducted a series of model collision tests. An example of the collision situation and the damaged bow after the collision test is presented in Fig. 5.3.
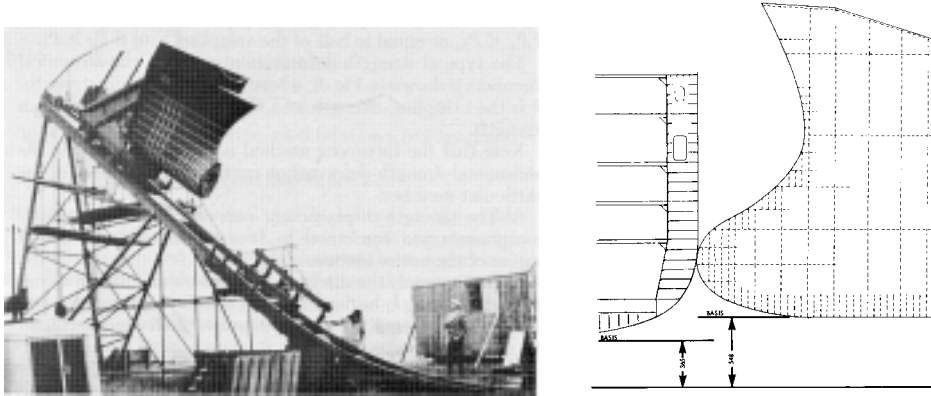
Fig. 5.3. Collision test model and damaged bow after the test (performed by Woisin).

The result of the collision tests showed that the bow suffered heavy damage. Damage to side structure is small. The average flow stress was (320+470)/2=395 MPa. The average thickness in the bow structure was 1.375 mm, the spacing of the horizontal deck was 135 mm. Therefore, the absorbed energy related to the destroyed material volume is expressed as

$$E = 3.50 \cdot (\frac{1.375}{135})^{0.67} \cdot 395 \cdot R_T = 64 \cdot R_T$$

The present result and Woisin's test result are compared and shown in Fig. 5.4. From the comparison it is seen that the correlation is good.
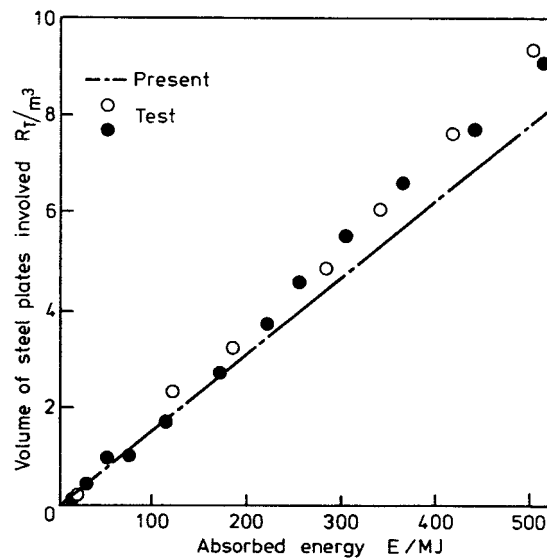
Fig. 5.4. Curves of the absorbed energy and the destroyed material volume obtained by the present calculation and Woisin's test result.

(3). Comparison with Amdahl's Bow Model Tests

Amdahl (1983) performed a series of model tests of bow crushing. Four test specimens are chosen here for comparison. The main dimensions and structural arrangements of the four models are shown in Fig. 5.5.

The models are made of 2.0 mm thick mild steel plates. Frames and stiffeners are made of 3.0 mm flat bars. The average flow stress of the material is (220+310)/2=265 MPa. The bow models are crushed progressively during the tests.
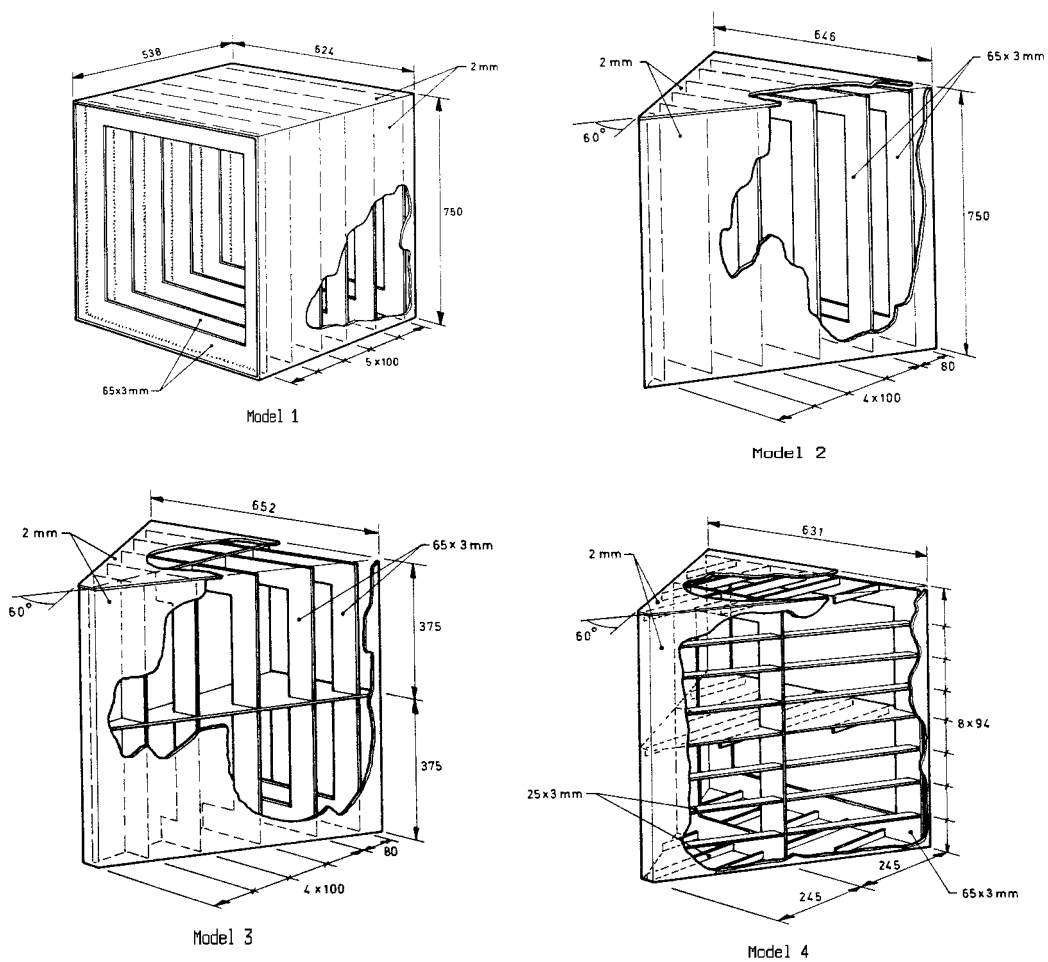
Fig. 5.5. Bow models tested by Amdahl (1983).

Model 1

Model 1 is a rectangular box with transverse frames. The thickness of the plating is $t = 2.0$ mm. The destroyed material volume at a damage length of 0.2 m is determined by

$$R_T = 2.17 \times 10^{-3} (m^3)$$

The average width d of the plates in the crushed cross-section is (750+624)/2=687 mm. Thus, the energy dissipated by Model 1 at the damage length of 0.2 m is found to be

$$E_{\text{mod } el1} = 3.50 \times (\frac{2}{687})^{0.67} \times 265 \times R_T = 18.55 \cdot R_T = 40.3(kJ)$$

Model 2

Model 2 is a wedge-shaped bow. The thickness of the plate is $t = 2.0$ mm. The destroyed material volume at the damage length of 0.2 m is calculated as

$$R_T = 1.37 \times 10^{-3} (m^3)$$

Since the width d is a linear function of the crushing distance, it is reasonable to use the mean value at half the considered damage length. Thus, the average width d is taken to be $750/2 + 100 \times \tan 30^0 = 432.7$ mm. Therefore, the energy dissipated by Model 2 at the damage length of 0.2 m is obtained as

$$E_{\text{mod } el2} = 3.50 \times (\frac{2}{432.7})^{0.67} \times 265 \times R_T = 25.28 \cdot R_T = 34.63(kJ)$$

Model 3

Model 3 is also a wedge-shaped bow but includes an additional deck and a longitudinal bulkhead. The thickness of the plate is $t = 2.0$ mm. The destroyed material volume at the damage length of 0.2 m is obtained as

$$R_T = 1.81 \times 10^{-3} (m^3)$$

The average width d is taken to be $(375 + 100 \times \tan 30^0)/2 = 216.4$ mm. Thus, the energy dissipated by Model 3 at the damage length of 0.2 m is calculated as

$$E_{\text{mod } el3} = 3.50 \times (\frac{2}{216.4})^{0.67} \times 265 \times R_T = 40.22 \cdot R_T = 72.79(kJ)$$

Model 4

Model 4 is also a wedge-shaped bow but includes longitudinal stiffeners on the shell. The thickness of the plate is $t = 2.0$ mm. The destroyed material volume at the damage length of 0.2 m is obtained as

$$R_T = 1.07 \times 10^{-3} (m^3)$$

The spacing of the longitudinal stiffeners is 94 mm. Thus, the average width d is taken to be 94 mm. The energy dissipated by Model 4 at the damage length of 0.2 m is found as

$$E_{\text{model4}} = 3.50 \times (\frac{2}{94})^{0.67} \times 265 \times R_T = 70.31 \cdot R_T = 75.23 (kJ)$$

In summary, the comparison of the absorbed energy obtained by the present method and test results at the damage length of 200 mm is shown in Table 5.2.

Table 5.2. Absorbed energy of the bow models at the crushing damage length of 0.2 m.

	Model 1	Model 2	Model 3	Model 4
Test result	48 kJ	27 kJ	70 kJ	90 kJ
Present calculation	40.3 kJ	34.6 kJ	72.8 kJ	75.2 kJ
Error	-16.0%	+28.1%	+4.0%	-16.4%

From the comparison in Table 5.2, it is seen that the general agreement between the present method and the test results is reasonable. The agreement for Model 3 is excellent. The difference for Model 2 is relatively large (+28%).

The other interesting result from the present calculation is that the energy absorption efficiency (E/R_T), which represents the absorbed energy per unit volume of destroyed material, is quite different for the four bow models. The results calculated by the present approach are listed in Table 5.3. It should be noted that Models 3 and 4 have relatively high efficiency of energy dissipation.

Table 5.3. Energy absorption efficiency of Amdahl's bow models.

	Model 1	Model 2	Model 3	Model 4
E/R_T (MJ/m^3)	18.55	25.28	40.22	70.31

5.3.2 Grounding

(1). Comparison with US Grounding Tests

A series of grounding tests was performed in the Naval Surface Warfare Center US (Rodd, 1997). The test facility is used to simulate grounding of a bottom of an oil tanker of 30,000 to 40,000 dwt on a scale of 1:5 on a pinnacle rock. Fig. 5.6 shows the test set-up.
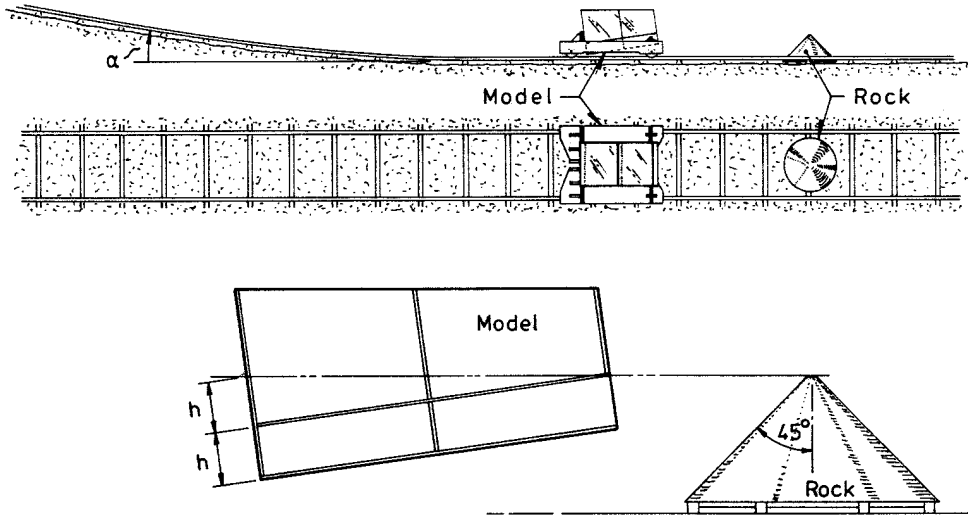
Fig. 5.6. Experimental set-up of grounding tests performed in the US.

Model 1 (CONV/PD328 is the number used in the test by Rodd, 1997) is a conventional double bottom design with transverse and longitudinal webs between the inner hull and the outer hull. Longitudinal stiffeners are attached to the inner and the outer bottom plates. This model is shown in Fig. 5.7.
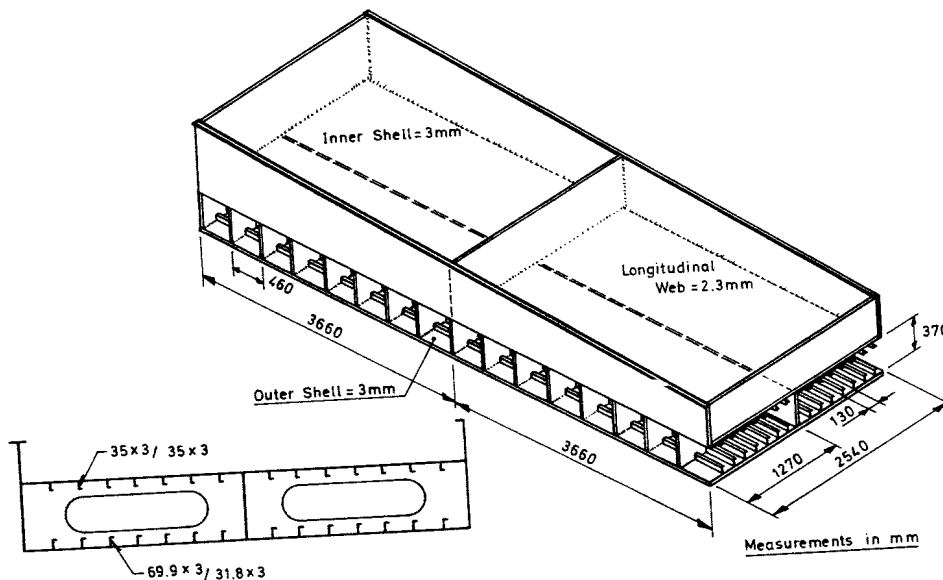
Fig. 5.7. Detailed parameters of Model 1 structure (CONV/PD328).

Model 2 (ADH/PB) is an advanced double hull construction. There are no transverse webs between the inner hull and the outer hull. It is shown in Fig. 5.8.
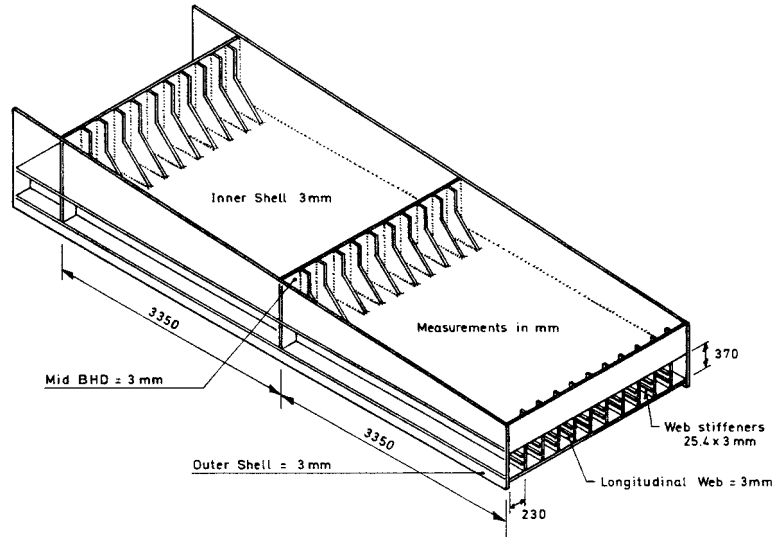
Fig. 5.8. Detailed parameters of Model 2 structure (ADH/PB).

Model 3 (ADH/PD328) is an advanced double hull construction with further tight spacing of longitudinal girders in comparison with Model 2. It is shown in Fig. 5.9.
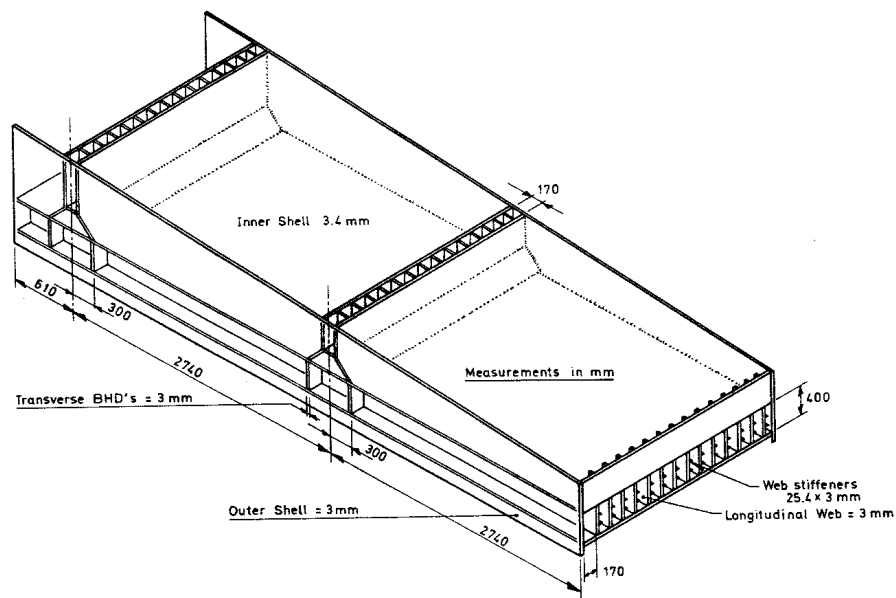
Fig. 5.9. Detailed parameters of Model 3 structure (ADH/PD328).

Model 4 is similar to Model 3 but it has no stiffeners on longitudinal webs. There is an increase of longitudinal web thickness from 3.0 mm in Model 3 to 3.4 mm.

The yield stress of the material is 283 MPa and the ultimate stress is 345 MPa. Thus, the average flow stress is (283+345)/2=314 MPa for all models. The absorbed energy of the destroyed bottom structures is by the present method calculated from

$$E = 3.21(\frac{t}{l})^{0.6}\sigma_0 R_T$$

In order to calculate the dissipated energy, we must determine the critical tearing length l and the volume of damaged material. According to the tearing experiments by Thomas (1992) and Wierzbicki and Thomas (1994), the steady tearing state will be reached when the tearing length is approximately equal to twice the wedge length. In the present case, the cone rock has a circular section in the horizontal plane, the length of the "wedge" can therefore be assumed to be the radius of the rock at the outer bottom plane. Thus, the critical tearing length is equal to twice the rock radius at the outer bottom level.

Fig. 5.10 shows a damaged section of Model 3 (ADH/PD328) after a grounding experiment (Rodd, 1997). It is seen that the damaged material in each position of the rock is just around the outer contour of the rock. It should be noted that the damage width in the outer bottom and in the inner bottom is similar. Therefore, it is assumed in the present calculation that the inner bottom and the outer bottom have the same damage width which equals the cone diameter at the outer bottom level. The detailed calculation procedure for each model is given in the following.
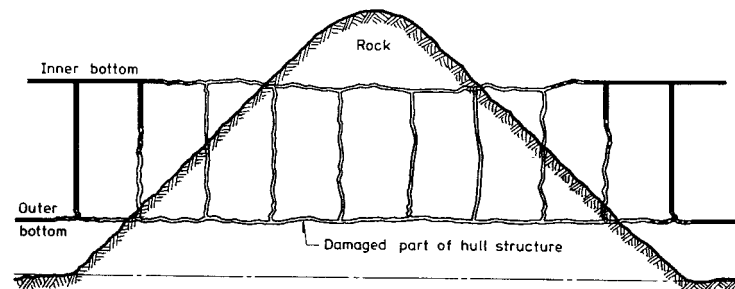
Fig. 5.10. Damage area of Model 3 (ADH/PD328) in grounding test (Rodd, 1997).

Model 1

The thickness of the outer bottom plating is 3.0 mm. Considering the longitudinal stiffeners on the outer hull, the equivalent thickness of the outer bottom is calculated from

$$t = 3.0 + \frac{(69.9 + 31.8) \times 3.0}{130} = 5.35(mm)$$

The semi-angle of the rock is 45 degrees. Therefore, the damage width at the penetration length of 5.46 m is obtained as 2(0.37+0.37(5.46/7.32)) =1.292 m, where 7.32 m is the total length of Model 1. Thus, the average damage width is (0.74+1.292)/2=1.016 m. The damaged material volume at the damage length of 5.46 m is approximately

$$R_T = 0.0687(m^3)$$

Then the energy dissipated by Model 1 at the damage length of 5.46 m is calculated from

$$E_{mod1} = 3.21 \times (\frac{5.35}{1016})^{0.6} \times 314 \times 0.0687 = 43.28 \cdot R_T = 2.97(MJ)$$

Model 2

The calculation procedure is similar to that of Model 1. The outer hull thickness is 3.0 mm. Considering the longitudinal girders on the outer hull, the equivalent thickness of the outer bottom is $t = 5.74$ mm.

The damage width at the penetration length of 5.46 m is obtained as 2(0.37+0.37(5.46/6.7)) =1.342 m, where 6.7 m is the total length of Model 2. Thus, the average damage width is (0.74+1.342)/2=1.041 m. The destroyed material volume at the damage length of 5.46 m is obtained approximately as $R_T = 0.0675$ m^3. Therefore, the energy dissipated by Model 2 at the damage length of 5.46 m is determined as

$$E_{mod2} = 3.21 \times (\frac{5.74}{1041})^{0.6} \times 314 \times 0.0675 = 44.50 \cdot R_T = 3.0(MJ)$$

Model 3

The outer hull thickness is again 3.0 mm. Considering the longitudinal girders on the outer hull, the equivalent thickness of the outer bottom is calculated as $t = 6.98$ mm.

The damage width at a penetration length of 5.46 m is obtained as 2(0.4+0.4(5.46/5.48)) =1.6 m, where 5.48 m is the total length of Model 3. Thus, the average damage width is (0.8+1.6)/2=1.2 m. The destroyed material volume at the damage length of 5.46 m is calculated as $R_T = 0.0967$ m^3. Therefore, the energy dissipated by Model 3 at the damage length of 5.46 m is found to be

$$E_{mod3} = 3.21 \times (\frac{6.98}{1200})^{0.6} \times 314 \times 0.0967 = 45.95 \cdot R_T = 4.45(MJ)$$

Model 4

The outer hull thickness is also 3.0 mm. Considering the longitudinal girders on the outer hull, the equivalent thickness of the outer bottom is calculated as $t = 7.0$ mm.

The damage width at the penetration length of 5.46 m is 2(0.4+0.4(5.46/5.48)) =1.6 m, where 5.48 m is the total length of Model 4. Thus, the average damage width is (0.8+1.6)/2=1.2 m. The destroyed material volume at the damage length of 5.46 m is found to be $R_T = 0.0969 \ m^3$. Then the energy absorbed by Model 4 at the damage length of 5.46 m is calculated from

$$E_{\mathrm{mod}4} = 3.21 \times (\frac{7}{1200})^{0.6} \times 314 \times 0.0969 = 46.03 \cdot R_T = 4.46 (MJ)$$

In summary, the comparison of the absorbed energy at a penetration length of 5.64 m obtained by the present method, experimental results and Simonsen's (1998b) is shown in Table 5.4.

Table 5.4. Comparison of absorbed energy obtained by different methods when the damage length is 5.46 m.

	Model 1	Model 2	Model 3	Model 4
Test result	3.25 MJ	2.65 MJ	5.34 MJ	6.03 MJ
Present calculation	2.97 MJ	3.00 MJ	4.45 MJ	4.46 MJ
Simonsen	3.0 MJ	2.8 MJ	5.6 MJ	5.9 MJ

The actual damage of the grounding tests is very complex. However, if the theoretical method catches the main mechanism of the complicated damage, then the results in Table 5.4 show that acceptable or even good agreement may be achieved by the present simple analysis.

The energy absorption efficiency of the four models calculated by the present method is shown in Table 5.5. It is seen that all the models have similar energy absorption efficiency in the grounding damage.

Table 5.5. Energy absorption efficiency of the four models in grounding damage.

	Model 1	Model 2	Model 3	Model 4
E / R_T (MJ / m^3)	43.28	44.50	45.95	46.03

(2). Comparison with ASIS Grounding Tests

From 1994 to 1995, a series of Japanese ASIS-sponsored grounding experiments was carried out. Some of the test results are presented by Wang, Ohtsubo and Liu (1997). The experiments were used to simulate grounding of a VLCC on the scale 1/4. The general test set-up is shown in Fig. 5.11. The model to be tested is fixed to a ship, which runs toward an artificial pinnacle rock.

The test models are double-bottom constructions. The thickness of the outer and the inner hull is 5.0 mm. The spacing of the transverse floors is 1250 mm with a thickness of 5.0 mm. The height of the double bottom is 750 mm. The spacing of the longitudinal stiffeners on the hull plates is 250 mm, the stiffeners are flat bars with a cross-section of 150 mm × 5.0 mm. The flow stress of the material is 340 MPa.
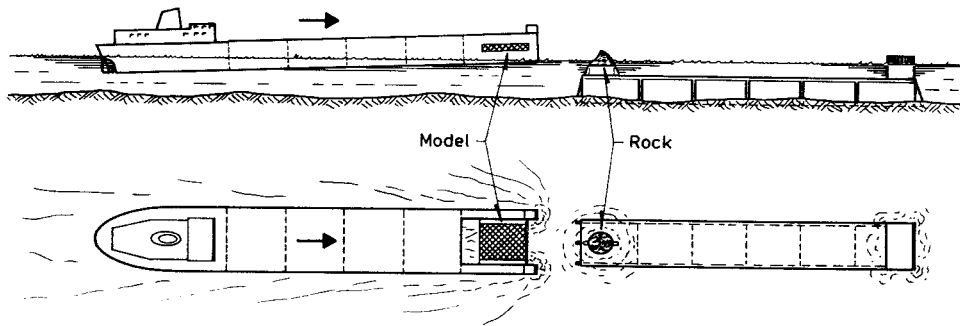
Fig. 5.11. ASIS grounding test set-up.

Test No. 1 was designed to simulate a minor grounding situation. Only the outer hull of the bottom was damaged, while the inner hull remained intact. The initial position of the top of the artificial rock was 180 mm below the inner hull. The test result revealed that the damage to the outer hull of the bottom was mainly confined within three times the spacing of the longitudinal stiffeners (i.e. 3×250 mm = 750 mm). The equivalent thickness of the outer hull plating including longitudinal stiffeners is calculated from

$$t = 5.0 + (150 \times 5.0) / 250 = 8.0 (mm)$$

The destroyed material volume at a penetration length of 5.0 m is found to be

$$R_T = 0.0356 (m^3)$$

Similar to the case of US grounding tests, the critical tearing length is assumed to be equal to the damage width, which is 750 mm in the present case. Thus, the absorbed energy at a penetration length of 5.0 m is calculated from

$$E = 3.21 \times (\frac{8}{750})^{0.6} \times 340 \times 0.0356 = 71.58 \cdot R_T = 2.55 (MJ)$$

The test result for the absorbed energy at the penetration length of 5.0 m is 2.20 MJ. The calculation result given by Wang et al. (1997) is 1.75 MJ. A comparison of the absorbed energy with various penetrations determined by the present method and the test result is shown in Fig. 5.12. The agreement is reasonable.
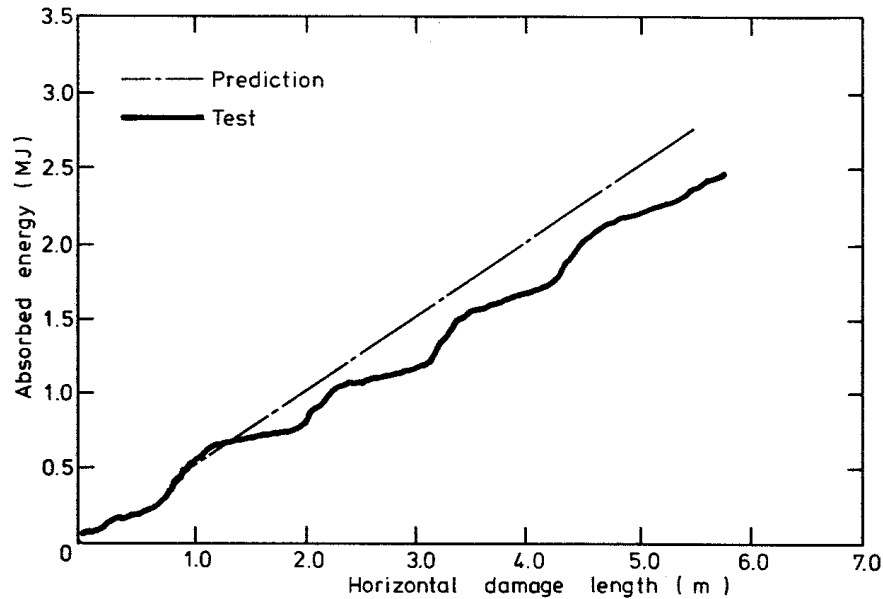
Fig. 5.12. Comparison of the absorbed energies obtained by the present method and the test result (Test No. 1).

Test No. 2 was designed to simulate a severe grounding accident. Both the outer and the inner hull of the bottom were damaged. The initial position of the top of the artificial rock was 540 mm above the inner hull. The test result revealed that the damage mode of the outer hull was very complex and that the inner hull suffered mainly tearing damage. The damage width in the transverse direction varied from 4 to 7 times the stiffener spacing in the outer hull and 3 to 5 times the stiffener spacing in the inner hull.

It is assumed that the average damage width in the outer hull and the inner hull of the bottom is four times the spacing of the longitudinal stiffeners (4×250 mm = 1000 mm). The destroyed material volume at a penetration length of 3.0 m is calculated as

$$R_T = 0.057(m^3)$$

Therefore, the absorbed energy at the penetration length of 3.0 m is determined by

$$E = 3.21 \cdot (\frac{8}{1000})^{0.6} \cdot 340 \cdot R_T = 60.23 \cdot R_T = 3.43(MJ)$$

The test result for the absorbed energy at a penetration of 3.0 m is 3.1 MJ. The result given by Wang et al. (1997) is 2.7 MJ. A comparison of the absorbed energy with various penetrations determined by the present method and the test result is shown in Fig. 5.13. Again, the agreement is good.
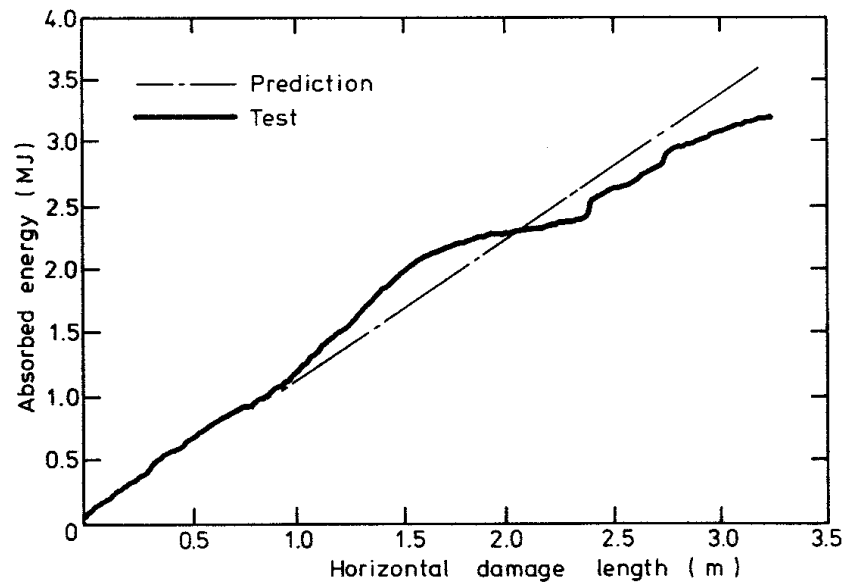
*Fig. 5.13. Comparison of the absorbed energies obtained by the present method
and the test result (Test No. 2).*

In summary, the absorbed energy for Tests No. 1 and No. 2 obtained by the present method and by test is listed in Table 5.6.

Table 5.6. Comparison of the dissipated energies obtained by different methods.

	Test No.1 at 5.0 m penetration	**Test No.2** at 3.0 m penetration
Test result	2.20 MJ	3.10 MJ
Present calculation	2.55 MJ	3.43 MJ
Error	+15.9%	+10.6%

(3). Comparison with Kitamura's Grounding Simulations

A comparative study on grounding damage to different bottom designs was carried out by Kitamura (1998). The considered three cases are standard single bottom, standard double bottom and unidirectional double bottom. The detailed structural parameters of the bottoms are given in Table 5.7. The grounding situation are shown in Fig. 5.14.

The yield stress of the material is 320 MPa and the ultimate stress is 600 MPa, thus, the average flow stress is (320+600)/2=460 MPa. The width of the rock at the outer bottom level is 8712 mm. The equivalent thicknesses of the outer bottom including longitudinals and longitudinal girders are 35.6 mm, 29.2 mm and 33 mm, respectively, for the standard single bottom, the standard double bottom and the unidirectional double bottom.

The results obtained by the present method and Kitamura's FEM simulation results for the energy absorption capacity per unit damage length are presented in Table 5.8.
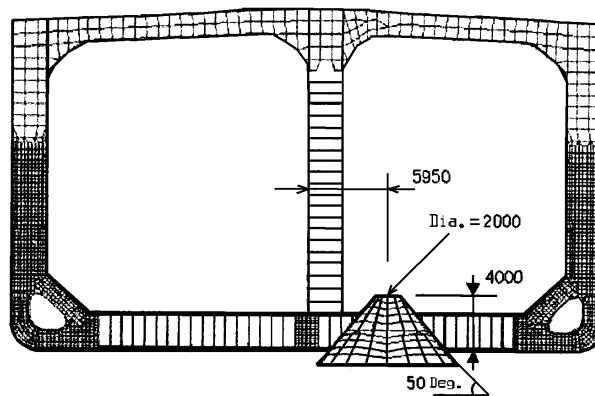
Fig. 5.14. Grounding simulation model used by Kitamura (1998).

Table 5.7. Dimensions of bottom structures of the three different designs.

	Standard single bottom	Standard double bottom	Unidirectional double bottom
Outer shell (mm)	18	19	19
Longitudinal of outer bottom	660*13.5+150*25	400*11+150*18	*
Inner shell	*	18.5	18.5
Longitudinal of inner bottom	*	400*11+150*20	*
Longitudinal spacing	860	860	*
Height of double bottom	*	2500	2500
Girder spacing	11900	16150	860
Girder web	14	21	16
Transverse spacing	5065	3640	18200
Transverse web	13	14.5	17

Table 5.8. Comparison of the present calculations and Kitamura's FEM simulations.

	Energy absorption capacity per unit length (MJ/m)		Error
	Kitamura	Present	
Single bottom	19.40	19.95	+3.8%
Double bottom	33.50	28.53	-14.8%
Unidi. Double bottom	23.50	30.70	+30.6%

It is seen from the comparison that the agreement between the present calculations and Kitamura's FEM calculations for the standard single bottom and the standard double bottom is good. But the difference for the unidirectional double bottom is high (+30.6%). Kitamura's results indicate that the unidirectional double bottom has lower capacity of energy absorption than the standard single bottom and the standard double bottom. But our result is that both of the double designs have similar energy absorption capacity.

5.3.3 Side Collision

(1). Comparison with Amdahl's Test of Double Hull Structures

Amdahl and Kavlie (1992) conducted model tests of double hull structures indented by a rigid object. The test was quasi-static. The original purpose of the test was to simulate grounding. But the experiment may also be treated as a collision for double hull side. The models and their scantlings are shown in Fig. 5.15. The flow stress of the shell plating is 385.5 N/mm^2, and the flow stress of the webs is 408.8 N/mm^2. The critical strain of the shell plating is assumed to be 7% as Paik and Pedersen used (1996).

Model No. 1.

The equivalent thickness of the shell plating including the attached stiffeners is found to be 4.83 mm. The destroyed material volume of shell plating up to an indentation of 200 mm is obtained as $4 \times (0.54 \times 0.54 \times 4.83 \times 10^{-3}) = 5.63 \times 10^{-3}$ m^3. Thus, the energy absorbed by the shell plating is

$$E_1 = 0.77 \varepsilon_c \sigma_0 R_T = 0.77 \times 0.07 \times 385.5 \times 5.634 = 116.5(kJ)$$

The damaged material volume of the webs at the indentation of 200 mm is obtained as $4 \times (0.54 \times 0.2 \times 0.003) = 1.3 \times 10^{-3}$ m^3. The energy dissipated by the webs is calculated from

$$E_2 = 3.50(\frac{t}{d})^{0.67} \sigma_0 R_T = 3.5 \times (\frac{3}{540})^{0.67} \times 408.8 \times 1.3 = 57.3(kJ)$$

Thus, the total absorbed energy at the indentation of 0.2 m is calculated as $E = E_1 + E_2 = 173.8 kJ$. The test result of Model No. 1 is $158 \, kJ$. The error is 10%.

Model No. 2.

The equivalent thickness of the shell plating including the attached stiffeners is calculated as 5.32 mm. The damaged material volume of the shell plating before the indenter just direct contacts the inner shell plating is approximated as $1.53 \times 1.08 \times 5.32 \times 10^{-3} = 8.79 \times 10^{-3}$ m^3. Therefor, the energy absorbed by the outer shell plating is

$$E_1 = 0.77 \times 0.07 \times 385.5 \times 8.79 = 182.7(kJ)$$

The damaged material volume of a floor is obtained as $1.53 \times 0.5 \times 0.0037 = 2.84 \times 10^{-3}$ m^3. The energy dissipated by the floor is calculated from

$$E_2 = 3.5 \times (\frac{3}{170})^{0.67} \times 408.8 \times 2.84 = 271.8(kJ)$$
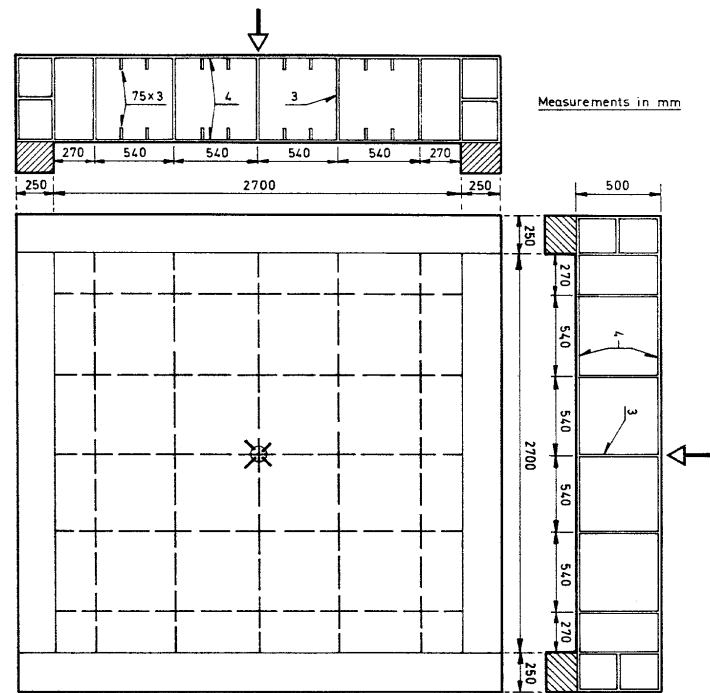
Model No. 1
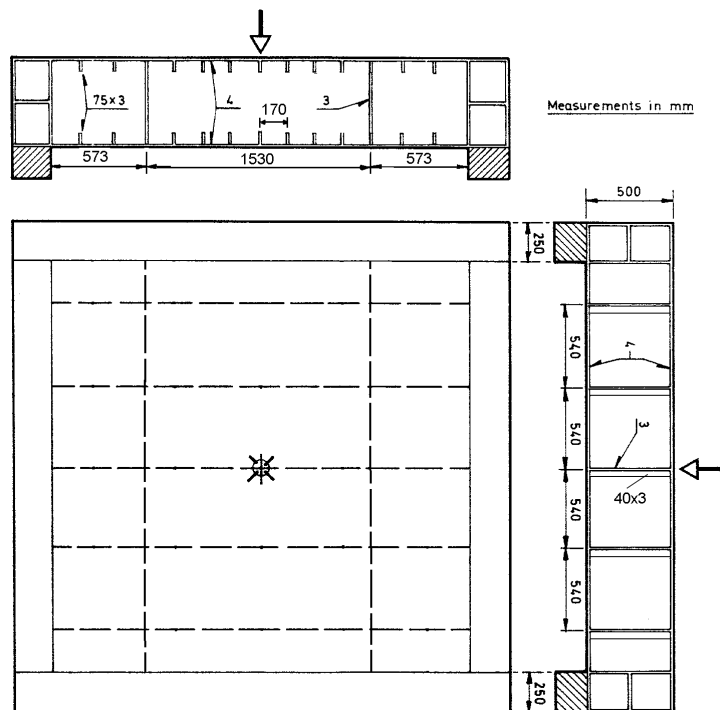
Model No. 2

Fig. 5.15. Models of the double hull structure tested by Amdahl and Kavlie (1992).

Thus, the total absorbed energy at the indentation before the indenter direct contacts the inner shell plating is calculated as $E = E_1 + E_2 = 454.5 kJ$. The test result of Model No. 2 is $500 kJ$. Good correlation is found.

(2). Comparison with Melton's Test for a Double Hull Model

Fig. 5.16 shows a double hull structure, which was the model in tests performed by Melton et al. (1994).
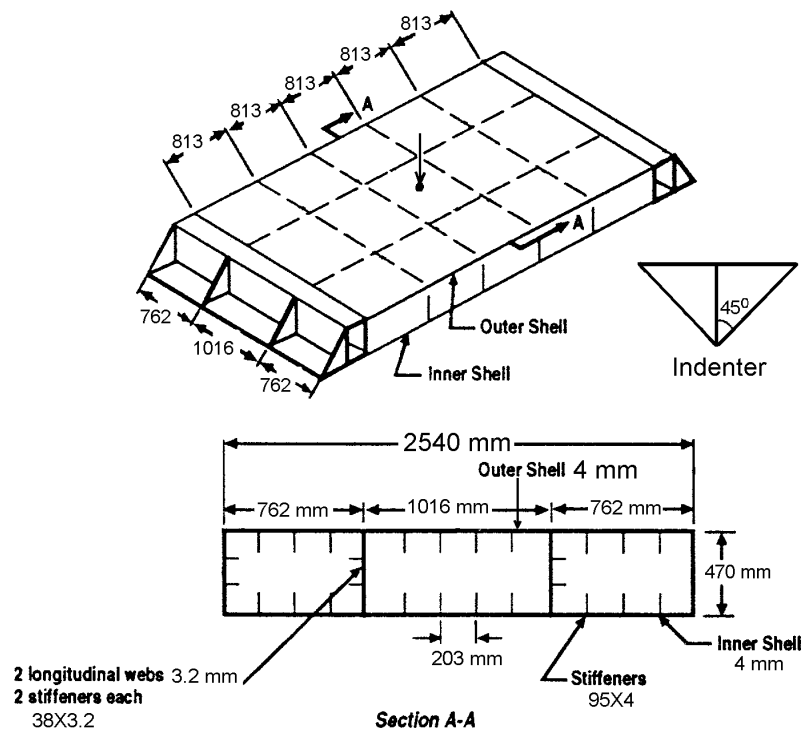
Fig. 5.16. Test model of the double hull structure (Melton et al., 1994).

A 90-degree rigid cone indents into the double hull structure at the central point quasi-statically (see Fig. 5.16). The flow stress of the material of the double hull structure is 320 N/mm^2, and the critical rupture strain is 7.5%.

Up to rupture of the inner shell at an indentation of 762 mm, and the damaged material volume of the outer shell plating is calculated from $2.54 \times 2.44 \times 0.00587 = 36.38 \times 10^{-3}$ m^3, and the damaged material volume of the inner shell plating is calculated from $1.016 \times 0.813 \times 0.00587 = 4.85 \times 10^{-3}$ m^3. The total damaged volume of the shell plating is obtained as 41.23×10^{-3} m^3. Thus, the energy absorbed by the shell plating is calculated as

$$E_1 = 0.77 \times 0.075 \times 320 \times 41.23 = 761.9(kJ)$$

The damaged material volume of the webs at rupture of the inner shell at an indentation of 762 mm is calculated from $(2 \times 2.54 + 2 \times 2.44) \times 0.3 \times 0.00372 = 11.11 \times 10^{-3}$ m^3. The average spacing of webs is taken to be $(1016 + 813)/2 = 914.5$ mm. The energy absorbed by the webs is found to be

$$E_2 = 3.5 \times (\frac{3}{914.5})^{0.67} \times 320 \times 11.11 = 269.5(kJ)$$

The total energy dissipated by the double hull structure at rupture of the inner shell is found to be $E = E_1 + E_2 = 1031.4$ kJ. The result obtained by experiments is 1047.6 kJ. The agreement is excellent.

(3). Comparison with Arita's Test for a Double Hull Model

Arita and Aoki (1985) conducted a model test of a double hull structure. Fig. 5.17 shows the tested model. A 90-degree rigid cone indents into the double hull structure at the central point quasi-statically as shown Fig. 5.17. The flow stress of the material of the double hull structure is 367.5 N/mm^2, and the critical rupture strain is 13.5%.
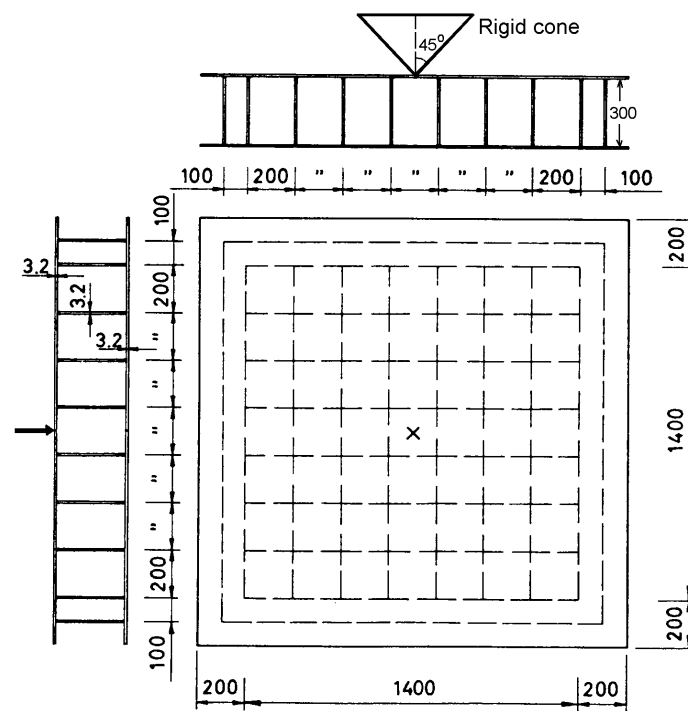
Fig. 5.17. Double hull model tested by Arita and Aoki (1985).

At penetration of 200 mm, the damaged material volume of the outer shell plating is obtained from $0.6 \times 0.6 \times 0.0032 = 1.152 \times 10^{-3}$ m^3. Thus, the energy absorbed by the outer shell plating is calculated as

$$E_1 = 0.77 \times 0.135 \times 367.5 \times 1.152 = 44.0(kJ)$$

The related damaged material volume of the webs at the penetration of 200 mm is calculated from $4 \times (0.6 \times 0.1 \times 0.0032) = 0.768 \times 10^{-3}$ m^3. The energy absorbed by the webs is found to be

$$E_2 = 3.5 \times (\frac{3.2}{200})^{0.67} \times 367.5 \times 0.768 = 61.87(kJ)$$

The total energy dissipated by the double hull structure at the penetration of 200 mm is found to be $E = E_1 + E_2 = 106$ kJ. The result obtained by experiments is 125 kJ. The error is −15%.

(4). Comparison with Paik & Pedersen's Calculation of VLCC Collision

Paik and Pedersen (1995) studied a collision between the bow of a container ship of 40,000 dwt and the side structure of a double hull VLCC of 300,000 dwt by using the idealised structural unit method (ISUM). The rigid bow strikes the side of the VLCC at a transverse web. The detailed scantlings of the striking bow, the side structure of the struck ship and the location of the collision are presented in Fig. 5.18. The average flow stress is $\sigma_0 = (315 + 441)/2 = 378$ MPa. The critical rupture strain of the material was selected to be 5% by Paik and Pedersen (1995).
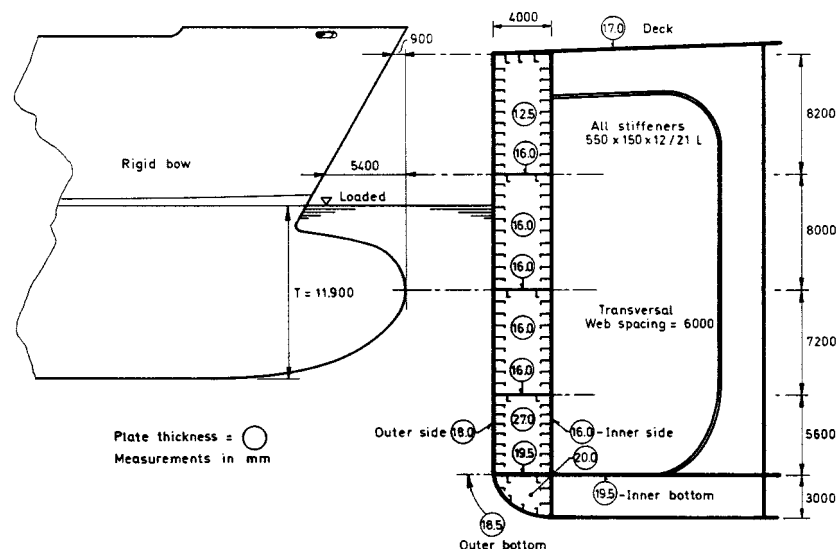
Fig. 5.18. Collision situation between the 40,000 dwt container ship and the 300,000 dwt double hull VLCC (Paik and Pedersen, 1995).

The side damage caused by the striking bow is confined to twice the transverse web spacing in the longitudinal direction (2×6 m = 12 m). The damage height is 7.2+8+8.2=23.4 m (see Fig. 5.18). Up to the rupture of the inner shell plating, the destroyed volume of the outer shell and inner shell including the attached longitudinal stiffeners is calculated as $R_1 = 13.6 \ m^3$. Thus, the energy dissipated by the shell plating is determined by

$$E_1 = 0.77 \times 0.05 \times 378 \times R_1 = 14.55 R_1 = 197.9 (MJ)$$

The damaged volume of the transverse webs and the longitudinal stringers is obtained as $R_2 = 3.82 \ m^3$. The thickness of the transverse webs and the longitudinal stringers is $t = 16$ mm, the average spacing of the transverse webs and the longitudinal stringers is taken to be $d = 7200$ mm. Thus, the absorbed energy by crushing of the transverse webs and the longitudinal stringers is calculated from

$$E_2 = 3.5 \times (\frac{16}{7200})^{0.67} \times 378 \times R_2 = 22.1 R_2 = 84.4 (MJ)$$

After the transverse webs and the longitudinal stringers have been totally compressed, the energy absorption with the further deformation can be approximated as tension deformation. They will further absorb energy up to rupture of the inner shell:

$$E_3 = 0.77 \varepsilon_c \sigma_0 R_T = 14.55 R_2 = 55.6 (MJ).$$

Thus, the total energy dissipated by the side structure up to rupture of the inner shell plating is $E = E_1 + E_2 + E_3 = 337.9$ MJ. The result calculated by Paik and Pedersen is 314.0 MJ. Again good agreement is achieved.

(5). Calculation Example for a Newly Designed Ferry

In Section 4.2.3, a collision analysis for a newly designed ferry was presented. Here we recalculate an example by using the method presented in this chapter. The collision situation is that a 6,000 t ship with a conventional bow strikes the side of a Ro-Ro ferry perpendicularly when the Ro-Ro ferry is at a standstill. The detailed structural dimensions of the Ro-Ro ferry at the midship are shown in Fig. 4.20 (Section 4.2.3). The entry angle of the striking bow is 80 degrees, the stem angle of the striking bow is 70 degrees, the height of the uppermost deck is 16.3 m. The collision position is shown in Fig. 5.19. The flow stress of the material is 305.5 N/mm^2, and the critical strain is 5%.

At a penetration of 5.0 m, we get the total damaged material volume of the shell plating: $R_1 = 1.633$ m^3. Thus, the energy dissipated by the shell plating is

$$E_1 = 0.77 \times 0.05 \times 305.5 \times R_1 = 11.76 \times 1.633 = 19.20 (MJ)$$
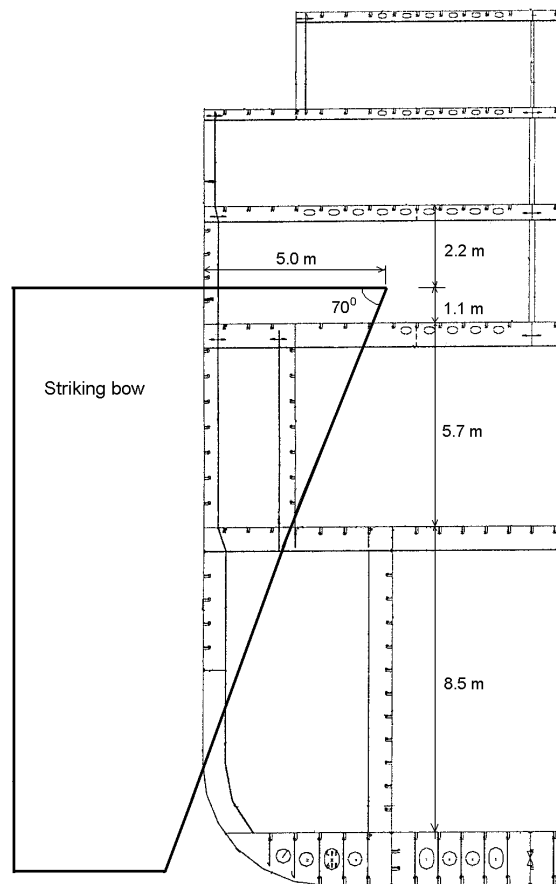
Fig. 5.19. Collision position for a conventional ship striking a Ro-Ro ferry.

The damaged material volume of the first crushed deck is obtained as 0.212m^3 and it is 0.073 m^3 for the second crushed deck. Hence the total damaged material volume of the two crushed decks is $R_2 = 0.285 \text{ m}^3$. The average width of the cross section of the crushed plate is $b = (2400+680+160)/3 = 1080$ mm. The thickness of the deck plate is $t = 8$ mm. Therefore, the energy absorbed by the deck crushing is calculated from

$$E_2 = 3.5 \times (\frac{8}{1080})^{0.67} \times 305.5 \times R_2 = 39.97 \times 0.285 = 11.39 (MJ)$$

Similarly, the damaged material volumes of the transverse frames and the longitudinal stringers are 0.201 m^3 and 0.047 m^3 respectively. Hence the energies absorbed by the damaged frames and the damaged stringers are $E_3 = 2.82$ MJ and $E_4 = 1.44$ MJ. Thus the total dissipated energy at the penetration of 5.0m is $E = E_1 + E_2 + E_3 + E_4 = 34.85$ MJ. The result obtained by a detailed calculation in Section 4.2.3 is 39.3 MJ. The correlation is good.

5.4   Application

5.4.1   Application to a Full-scale Grounding Accident

In 1975, a one-year-old single hull tanker ran aground at a speed of 11.5 knots on the coast of Singapore. More than 10,000t oil was spilled. The main particulars of the tanker are shown in Table 5.9. The grounding situation is presented in Fig. 5.20.

Table 5.9. Main particulars of the single hull oil tanker.

Length between perpendiculars	304.0 m
Breadth moulded	52.4 m
Depth moulded	25.7 m
Draught	19.8 m
Displacement	237,000 t
Grounding speed	11.5 knots
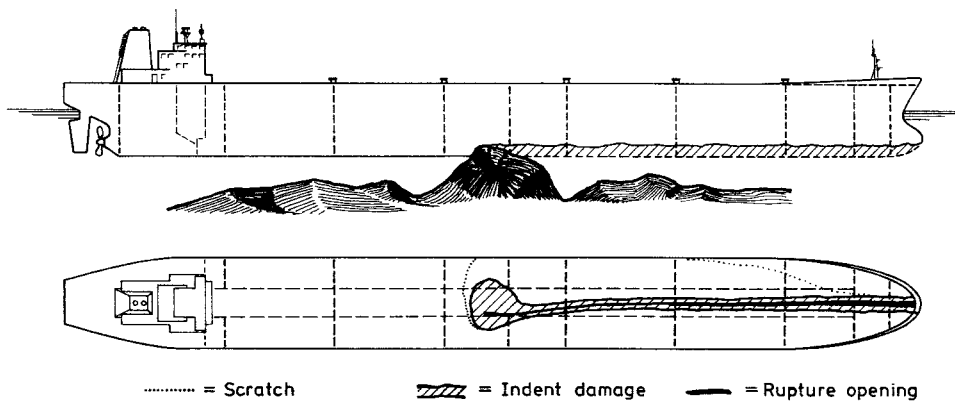
Fig. 5.20. Grounding accident and the resulting damage.

Kuroiwa (1996), Wang et al. (1997) and Simonsen (1998b) analysed this grounding accident. Good correlation between prediction and accidental damage was found on certain assumptions. Here the present method is used to analyse the same grounding event.

The thickness of the single-bottom plating is 28.5 mm. After considering the longitudinal stiffeners etc, the equivalent thickness of the bottom is 56.5 mm (see Wang et al. 1997). The flow stress of the material is 320 MPa. The damage width in the transverse direction is approximately 7 m to 8 m. The average damage width in the present calculation is taken to be 7.5 m. Thus, the destroyed material volume at a damage length L_{dam} is determined by

$$R_T = L_{dam} \times 7.5 \times 56.5 / 1000 = 0.424 L_{dam} \, (m^3)$$

The initial kinetic energy of the tanker including the 5% of added mass effect is calculated from

$$E_0 = \frac{1}{2} M (1 + 0.05) V^2 = 4354 (MJ)$$

It is assumed that all the initial kinetic energy of the tanker is dissipated by destroying the bottom structure. Thus, the damage length for the grounding accident is calculated by

$$L_{dam} = \frac{4354}{3.21 \cdot (\frac{56.5}{7500})^{0.6} \cdot 320 \cdot 0.424} = 187.8 (m)$$

The actual damage length of the accident is about 180 m. Considering the complexity of the phenomenon, such agreement is very satisfactory.

5.4.2   Bottom Damage to an 82,000 t Tanker and a 264,500 t VLCC

Encouraged by the above example, the bottom-raking damage to two tankers is further investigated in this section. One is an 82,000 t tanker and the other is a 264,500 t VLCC. Both ships are double-hull design. The principal dimensions and the scantlings of the bottom structures of the two tankers are shown in Table 5.10.

It is assumed that a rock is high enough to penetrate the inner bottom of the ships and that the damage widths in the inner and the outer bottom are equal. As previously, the critical tearing length is set to be the damage width. By use of the data of Table 5.10, the equivalent thickness (t) of the outer bottom, including longitudinal webs and longitudinal stiffeners for the 82,000 t tanker is obtained as 27.2 mm, and for the 264,500 t VLCC it is 37.3 mm.

The ratio between the damage length and the ship length is calculated for the two ships at full service speed and half service speed, respectively. The results are shown in Figs. 5.21 and 5.22. In the present calculation, the damage width is assumed to vary within 5% and 35% of the ship breadth.

The results show that the damage length is above 45% ~ 60% of the ship length if the ships sail at full service speed. The rock may cut the bottom through all the ship length if the rock is relatively narrow. On other hand, if the ships sail at half service speed, the damage length is within 12% ~22% of the ship length for the 82,000 t tanker and 18% ~35% of the ship length for the 264,500 t VLCC.

Table 5.10. Main parameters and bottom structures of 82,000 t tanker and 264,500 t VLCC.

	82,000 t tanker	264,500 t VLCC
Length Lpp (m)	218.7	327.0
Breadth (m)	32.0	56.0
Depth (m)	21.6	30.4
Draught (m)	16.0	19.8
Mass (t)	82,000	264,500
Service speed (m/s)	6.7	7.46
Material	Mild steel $\sigma_0 = 305MPa$ Double bottom	Mild steel $\sigma_0 = 305MPa$ Double bottom
Outer shell thickness (mm)	18.5	20.5
Inner bottom thickness (mm)	18.5	20.0
Double bottom height (m)	2.15	3.2
Spacing of transverse webs (m)	2.7	5.32
Equival. thickness of floor (mm)	12.0	18.5
Spacing of girders (m)	3.4	10.0
Equival. thickness of girder (mm)	12.3	21.3
Spacing of longitudinals (mm)	850	1000
Web height of longitudinals (mm)	340	600
Web thickness of longi. (mm)	12.0	13.0
Flange width of longi. (mm)	*	225
Flange thickness of longi. (mm)	*	25.0
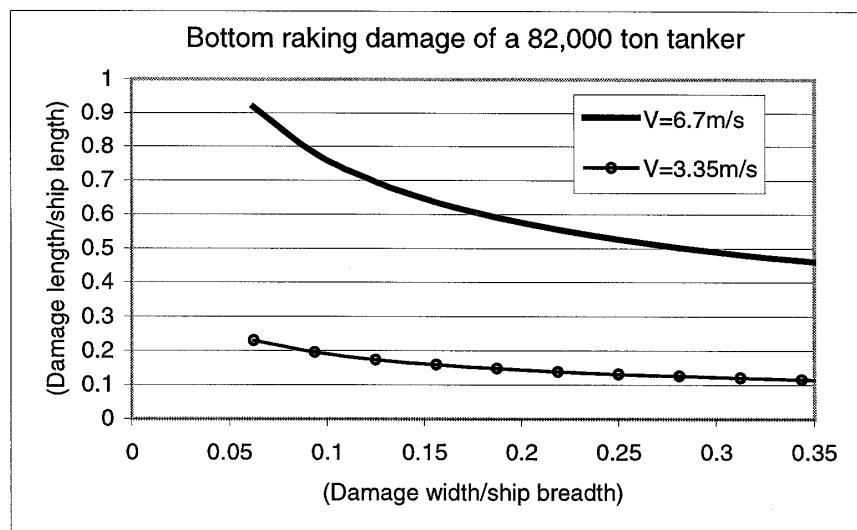
Fig. 5.21. Relative raking damage to the bottom of an 82,000 ton tanker at full service speed (V=6.7 m/s) and half service speed (V=3.35 m/s), respectively.
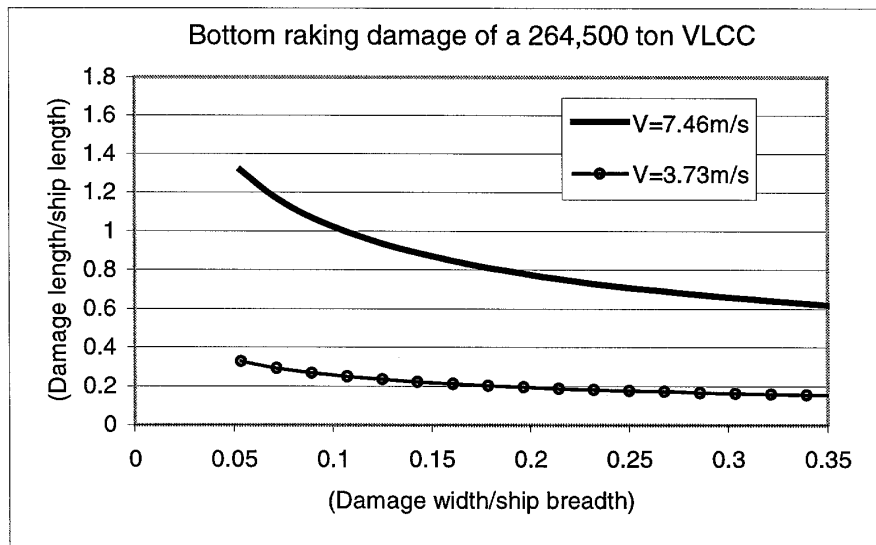
Fig. 5.22. Relative raking damage of the bottom to a 264,500 t VLCC at full service speed (V=7.46 m/s) and half service speed (V=3.73 m/s), respectively.

5.5 Prediction of Bottom Damage Distributions for High-speed Vessels

5.5.1 The Prediction Method

In May 1994, the International Maritime Organization (IMO, 1995a) adopted the Code of Safety for High Speed Craft (HSC). The Code states that "the longitudinal extent of damage should be 0.1L or 3 m+0.03L or 11 m, whichever is the least and the assumed damage should be increased by 50% in the case of damage in the forward 0.5L of the craft". L is the length of the craft.

After several years of use, it was found that the Code for the damage length was inadequate. In 1996, several European countries submitted revision to the IMO. They suggested that the longitudinal extent of damage should be for the full underwater length of the craft.

Recently, Simonsen (1998a) proposed an interesting procedure for analysis of the bottom raking damage distribution to a high-speed craft. Simonsen used the existing bottom damage distribution of conventional ships (such as IMO damage statistics) to predict the damage distribution of new high-speed craft. The parameter used to describe bottom damage is the ratio between the damage length and the ship length (L_{dam}/L). Based on a balance of energy, the following relation for two different ships can be established:

$$\frac{(L_{dam} / L)_1}{(L_{dam} / L)_2} = \frac{M_1}{M_2} \cdot (\frac{V_1}{V_2})^2 \cdot \frac{L_2}{L_1} \cdot \frac{P_2}{P_1} \tag{5.4}$$

where (L_{dam} / L) is the ratio between the damage length and the ship length, M is the ship mass, L is the ship length, V is the ship speed and P is the horizontal grounding force.

For comparison between various ship classes, the Froude number $F_n = V / \sqrt{gL}$ can be used instead of the ship velocity. Thus, Eq. (5.4) becomes

$$\frac{(L_{dam} / L)_1}{(L_{dam} / L)_2} = \frac{M_1}{M_2} \cdot (\frac{F_{n1}}{F_{n2}})^2 \cdot \frac{P_2}{P_1} \tag{5.5}$$

Eq. (5.4) or Eq. (5.5) indicates that if we know the damage distribution $(L_{dam} / L)_1$ for one ship, then the damage distribution $(L_{dam} / L)_2$ for the other ship can be determined.

As Simonsen discussed, the major challenge of this procedure is to determine the horizontal grounding forces P_1 and P_2. They depend on many factors, such as rock shape, bottom structure and material and indentation depth. Simonsen (1997) established a numerical method implemented in a computer program to analyse the grounding force. Here we apply our simple method for analysing the problem.

By use of Eq. (5.3) the energy balance for a ship grounding on a rock can be expressed as

$$3.21(\frac{t}{l})^{0.6} \sigma_0 R_T = \frac{1}{2} M \cdot V^2 \tag{5.6}$$

The volume of the destroyed material in the bottom raking damage is approximately calculated from $R_T = L_{dam} \cdot B_{dam} \cdot t_{eq}$, where L_{dam} is the damage length, B_{dam} is the damage width, and t_{eq} is the equivalent thickness of the whole bottom including transverse and longitudinal webs and stiffeners. t is the equivalent thickness of the outer bottom including longitudinal webs and longitudinal stiffeners only. As discussed previously, the critical tearing length is taken to be equal to the damage width, which is $l = B_{dam}$.

Therefore, the relationship of the relative damage between two different ships is expressed as

$$\frac{(L_{dam} / L)_1}{(L_{dam} / L)_2} = \frac{M_1}{M_2} \cdot (\frac{F_{n1}}{F_{n2}})^2 \cdot [\frac{\sigma_2}{\sigma_1} \cdot \frac{t_{eq2}}{t_{eq1}} \cdot (\frac{t_2}{t_1})^{0.6} \cdot (\frac{B_{dam2}}{B_{dam1}})^{0.4}] \tag{5.7}$$

From the right-hand side of Eq. (5.7) it is seen that all the parameters, except the damage width (B_{dam}), are known for two given ships. The damage width is related to ship size and colliding obstacle. Simonsen proposed that the vertical indentation of a rock into the ship bottom is proportional to the ship draught. This means that the ship with larger draught suffers larger vertical penetration. Therefore, the damage width will be increased with a larger draught of a ship. Thus, the ratio of the damage width between two ships is expressed as (T = the ship draught):

$$\frac{B_{dam2}}{B_{dam1}} = \frac{T_2}{T_1} \tag{5.8}$$

By substitution of Eq. (5.8) into Eq. (5.7), the final expression for the relative damage length between the two ships becomes

$$\frac{(L_{dam}/L)_1}{(L_{dam}/L)_2} = \frac{M_1}{M_2} \cdot (\frac{F_{n1}}{F_{n2}})^2 \cdot [\frac{\sigma_2}{\sigma_1} \cdot \frac{t_{eq2}}{t_{eq1}} \cdot (\frac{t_2}{t_1})^{0.6} \cdot (\frac{T_2}{T_1})^{0.4}] \tag{5.9}$$

If Eqs. (5.9) and (5.5) are compared, it is seen that a factor $K = \frac{\sigma_2}{\sigma_1} \cdot \frac{t_{eq2}}{t_{eq1}} \cdot (\frac{t_2}{t_1})^{0.6} \cdot (\frac{T_2}{T_1})^{0.4}$

is just the ratio of the horizontal grounding forces of the two ships.

5.5.2 Application to a High-speed Craft

Three different ships are analysed here. One is a conventional cargo ship, the second a medium-size Ro-Ro ferry and the third a high-speed craft (HSC). The main dimensions and the scantlings of the bottom structures of the three ships are presented in Table 5.11.

By use of the data from Table 5.11, the equivalent thickness t_{eq} of the whole bottom including the transverse and the longitudinal webs and stiffeners, and the equivalent thickness t of the outer bottom only including the longitudinal webs and the longitudinal stiffeners are calculated and shown in Table 5.12.

The factor K, representing the horizontal grounding force ratio between two ships, is determined as follows:

$$K_1 = \frac{C\arg o}{Ferry} = 1.96 , \quad K_2 = \frac{C\arg o}{HSC} = 5.23 , \quad K_3 = \frac{Ferry}{HSC} = 2.65$$

These results agree well with Simonsen's calculation results. The comparison of the present results and Simonsen's results for the force ratio between two ships is shown in Table 5.13.

Table 5.11. Main parameters and bottom structures of the three considered ships.

	Cargo ship	**Ferry**	**HSC**
Length Lpp (m)	122	128	63
Beam (m)	20.5	17.5	23.4
Depth (m)	12.2	12.4	10.7
Draught (m)	9.4	4.5	3.0
Mass (t)	18,000	6,300	910
Service speed (m/s)	8.0	9.5	19.5
Froude No. Fn	0.23	0.27	0.79
Material	Mild steel $\sigma_0 = 260 MPa$ Double bottom	Mild steel $\sigma_0 = 260 MPa$ Double bottom	Aluminum $\sigma_0 = 250 MPa$ Single bottom
Outer shell thickness (mm)	19.0	12.0	8.0
Inner bottom thickness (mm)	19.5	12.0	*
Double bottom height (m)	1.5	1.25	*
Spacing of transverse webs (m)	0.75	2.25	1.2
Equival. thickness of floor (mm)	6.5	9.0	8.0
Spacing of girders (m)	3.4	3.6	*
Equival. thickness of girder (mm)	14.5	10.0	*
Spacing of longitudinals (mm)	*	610	240
Web height of longitudinals (mm)	*	220	250
Web thickness of longi. (mm)	*	10	8
Flange width of longi. (mm)	*	70	50
Flange thickness of longi. (mm)	*	15	10

Table 5.12. Equivalent thickness of the bottoms of the three ships.

	Cargo	Ferry	HSC
$t(mm)$	22.2	19.1	18.4
$t_{eq}(mm)$	57.9	43.2	20.4

Table 5.13. Comparison of the grounding force ratio between two ships.

	$K_1 = \dfrac{C\arg o}{Ferry}$	$K = \dfrac{C\arg o}{HSC}$	$K_3 = \dfrac{Ferry}{HSC}$
Present	1.96	5.23	2.65
Simonsen	2.5	6.5	2.6

By application of Eq. (5.9), the relative damage ratio between two ships is given as

$$\frac{(L_{dam}/L)_{Ferry}}{(L_{dam}/L)_{C\arg o}} = 0.95 , \quad \frac{(L_{dam}/L)_{HSC}}{(L_{dam}/L)_{C\arg o}} = 3.12 , \quad \frac{(L_{dam}/L)_{HSC}}{(L_{dam}/L)_{Ferry}} = 3.28$$

It is seen from the results that the damage length ratio for the high-speed craft is about three times the damage length ratio for the cargo ship and the conventional Ro-Ro ferry. When the bottom damage distribution for conventional ships is known, the bottom damage distribution for a high-speed craft or other new type of ship can be established quite easily by such damage results.

Let us assume that the damage length ratio between a high-speed craft and the conventional vessel is approximately equal to 3.0. Based on this ratio, a predicted damage density distribution function of the longitudinal extent for the high-speed craft converted from the IMO density distribution function (IMO, 1995) for conventional ships is shown in Fig. 5.23.

In this translation, we have assumed that in the IMO damage distribution the raking damage is represented by a constant density distribution equal to 0.5 for damage lengths between 0 and 80% of the ship length. The reason is that the raking damage is only a part of several types of grounding damages to ships. Other grounding damages are e.g. soft grounding, sideways stranding. But the damage lengths above 30% of the ship length in IMO damage distribution are all assumed to be caused by raking damage. On this assumption the constant density distribution of raking damage for the high-speed craft is simply equal to 0.5/3 = 0.17.

It is seen from Fig. 5.23 that the probability of full ship length damage for high-speed craft is 23%, while the probability of full ship length damage for conventional ships in the IMO statistics is zero. This means that the high-speed craft suffer significantly higher probability of large damage lengths than the conventional ships.
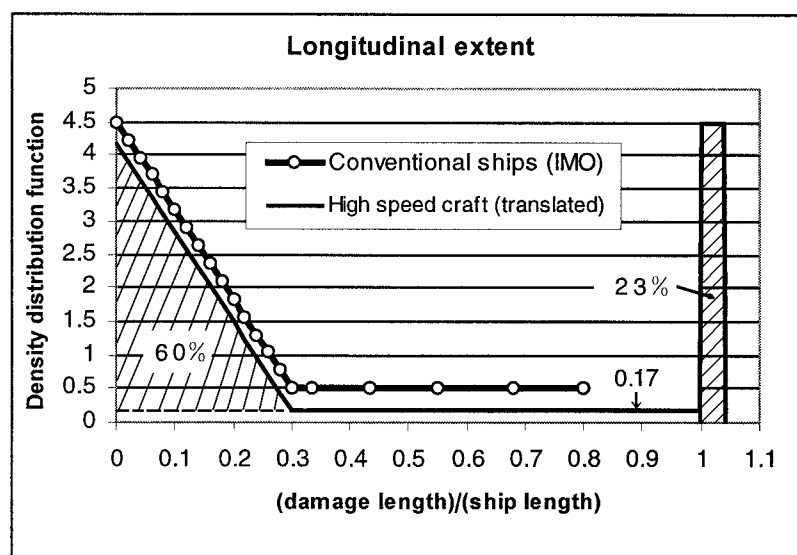
Fig. 5.23. Predicted bottom damage density distribution of high-speed craft translated from that of conventional vessels (IMO statistics).

5.5.3   Application to Newly Designed High-speed Ro-Ro Ferry

Ro-Ro vessels are key transport systems in many countries today. The safety of Ro-Ro ferries is identified as a key priority by the Commission of the European Countries. In this part, investigations of the bottom damage to a newly designed fast ferry are carried out. Damage to the new ferry is compared with that to old conventional ships. The newly designed fast ferry is shown in Fig. 5.24. The principal particulars and the bottom structures of the new ferry and the old conventional ships are presented in Table 5.14.
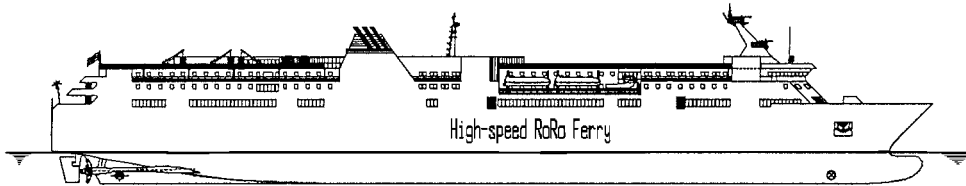
Fig. 5.24. A newly designed high-speed Ro-Ro ferry (V = 27 knots).

Table 5.14. Main particulars and bottom structures of the considered ships.

	New ferry	**Old ferry 1**	**Old ferry 2**	**Oil tanker**
Length Lpp (m)	173	128	158.5	219
Beam (m)	26.0	17.5	24.0	32.0
Depth (m)	15.7	12.4	14.0	21.6
Draught (m)	6.5	4.5	6.1	16.0
Mass (t)	16,073	6,300	15,000	82,000
Service speed (m/s)	14	9.5	11	6.7
Froude No. Fn	0.34	0.27	0.28	0.15
Material $\sigma_0 = 300 MPa$	Steel Double bottom	Steel Double bottom	Steel Double bottom	Steel Double bottom
Outer shell thickness (mm)	13.0	12.0	14.0	18.5
Inner bottom thickness	12.0	12.0	12.0	18.5
Double bottom height	1480	1250	2000	2150
Spacing of trans. webs	2400	2250	3000	2700
Equ. thickness of floor	10.0	9.0	10.0	12.0
Spacing of girders	3900	3600	3200	3400
Equ. thickness of girder	12.7	10.0	15.4	12.3
Spacing of longi.	650	610	800	850
Web height of longi.	180	220	260	340
Web thickness of longi.	10	10	11	12.0
Flange width of longi.	*	70	*	*
Flange thickness of longi.	*	15	*	*

The equivalent thickness t_{eq} of the whole bottom, including transverse and longitudinal webs and stiffeners, and the equivalent thickness t of the outer bottom, only including longitudinal webs and longitudinal stiffeners, are calculated and shown in Table 5.15.

Table 5.15. Equivalent thickness of the bottoms of the considered ships.

	New ferry	Old ferry (1)	Old ferry (2)	Oil tanker
t (mm)	18.2	19.1	22.3	27.2
t_{eq} (mm)	41.5	43.2	49.0	64.8

The factor K, representing the ratio of horizontal grounding resistance between two ships, is determined by

$$K = \frac{Old\ Ferry(1)}{New\ Ferry} = 0.92$$

$$K_2 = \frac{Old\ Ferry(2)}{New\ Ferry} = 1.30$$

$$K_3 = \frac{Oil\ Tanker}{New\ Ferry} = 2.85$$

The relative damage ratio between two different ships is calculated as

$$\frac{(L_{dam}/L)_{New}}{(L_{dam}/L)_{Old1}} = 3.73$$

$$\frac{(L_{dam}/L)_{New}}{(L_{dam}/L)_{Old2}} = 2.05$$

$$\frac{(L_{dam}/L)_{New}}{(L_{dam}/L)_{Tanker}} = 2.87$$

It is seen that the new fast ferry suffers larger grounding damage than the conventional ships if it happens. The non-dimensional damage length to the new ferry is more than twice the non-dimensional damage length to the conventional ships. Therefore, it is necessary for designers to reconsider the design of the new high-speed ferry in order to improve its safety in accidental situations.

5.6   Investigation of Grounding Damage Distributions in IMO Interim Guidelines

5.6.1   Introduction

In September 1995, the International Maritime Organization (IMO, 1995) adopted Interim Guidelines for Approval of Alternative Methods of Design and Construction of Oil Tankers under Regulation 13F(5) of Annex I of MARPOL 73/78. These guidelines give a probabilistic procedure for assessing the oil outflow performance of an oil tanker design in collision and grounding.

One of the important elements in the guidelines is the damage density distributions, which were derived from the actual damage data of 52 collisions and 63 grounding accidents of oil tankers, chemical tankers, OBOs and OROs of 30,000 tons deadweight and above, in the period form 1980 to 1990. This data was collected by classification societies including LR, ABS, DnV, ClassNK and RINA. Fig. 5.25 shows the probabilistic density distributions for longitudinal extent, vertical penetration and transverse extent for grounding in the IMO guidelines.

Since the publication of the IMO Interim Guidelines, many authors have used the IMO Guidelines to assess the environmental performance of oil tankers. For example Bockenhauer and Jost (1995) and Michel et al (1996). The Society of Naval Architects and Marine Engineers (SNAME) formed a special technical committee to make further assessment of the performance of oil tankers during 1995 to 1997 (Sirkar et al., 1997).

As discussed by Sirkar et al. (1997) and Rawson et al. (1998), a major shortcoming in the IMO guidelines is that they do not consider the effect of local structural design or crashworthiness on the damage extent and all tankers have the same damage distributions. Sirkar et al. (1997), Simonsen (1998) and Rawson et al. (1998) made theoretical calculations and established damage density distributions for grounding of a given ship. These calculations are based upon many assumptions, such as distributions of grounding speed, rock shape and rock elevation. This means that the validity of the density distributions obtained by such theoretical calculation needs further verification. Moreover, these calculations apply only to specific tankers. It is impossible to make such calculations for all tankers due to the wide variety of structural details and potential accident scenarios. Thus, it is difficult in this way to reach a general conclusion on the effect of structural design on the damage distributions.

Therefore, in this section, we do not intend to make a large number of calculations to establish damage density distributions. Instead, we shall analyse the influence of structural design on grounding damage distribution in general.
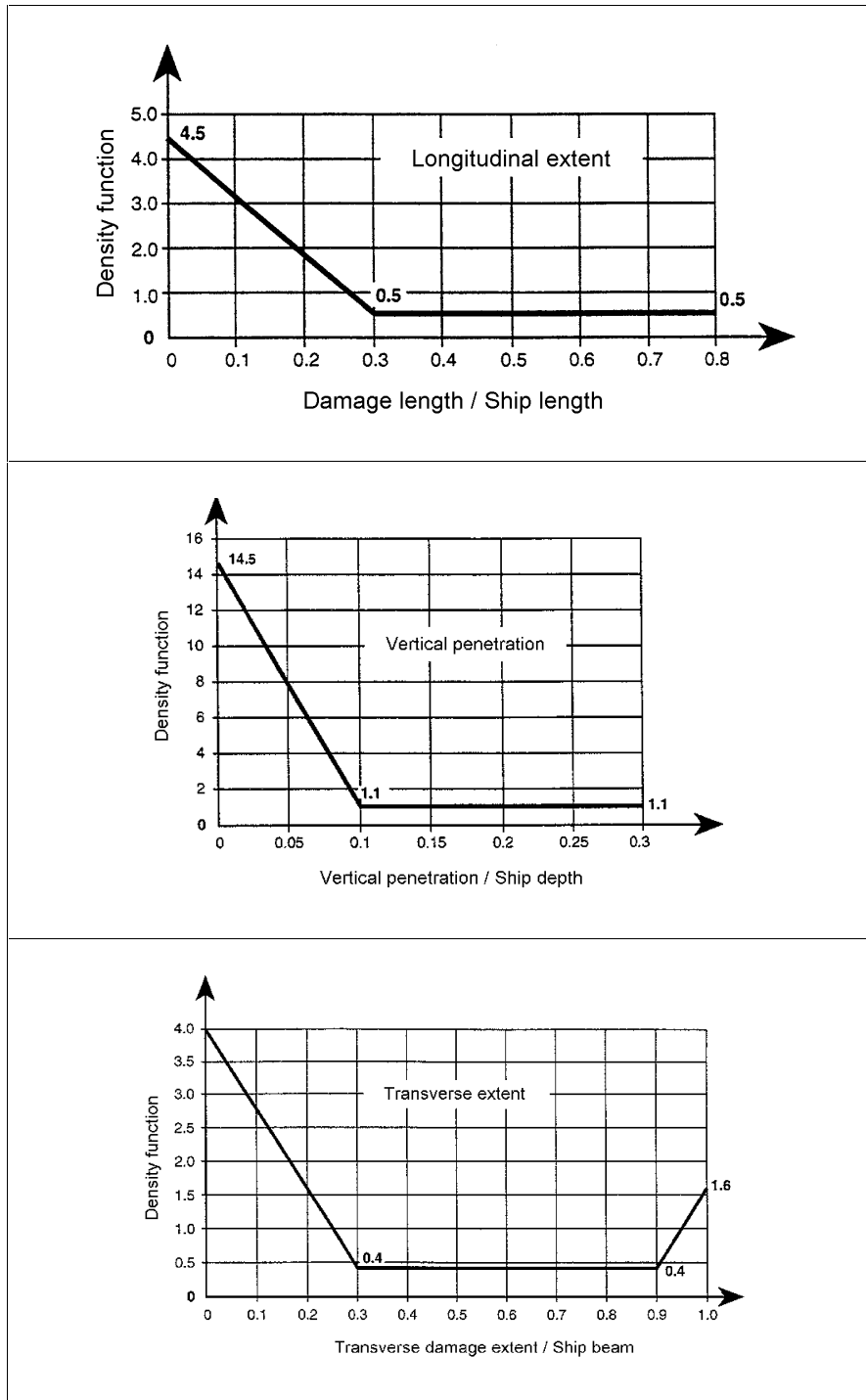
Fig.5.25. IMO density distributions for grounding damage (IMO, 1995).

5.6.2   Prediction of Relative Damage Extent in Grounding

As discussed previously, the relative damage length (L_{dam}/L) between two tankers can be determined from

$$\frac{(L_{dam}/L)_1}{(L_{dam}/L)_2} = \frac{M_1}{M_2} \cdot (\frac{V_1}{V_2})^2 \cdot \frac{L_2}{L_1} \cdot \frac{P_2}{P_1} \tag{5.10}$$

where

$$\frac{P_2}{P_1} = \frac{\sigma_2}{\sigma_1} \cdot \frac{t_{eq2}}{t_{eq1}} \cdot (\frac{t_2}{t_1})^{0.6} \cdot (\frac{T_2}{T_1})^{0.4}$$

In this formula, it has been assumed that the larger ship suffers larger vertical penetration and larger transverse damage extent. Obviously, the elevation of the rock above the baseline of the larger ship is greater than that of the smaller ship, as shown in Fig. 5.26. This means that the damage distribution for the vertical penetration and the transverse damage extent are assumed to be independent of the local structure.
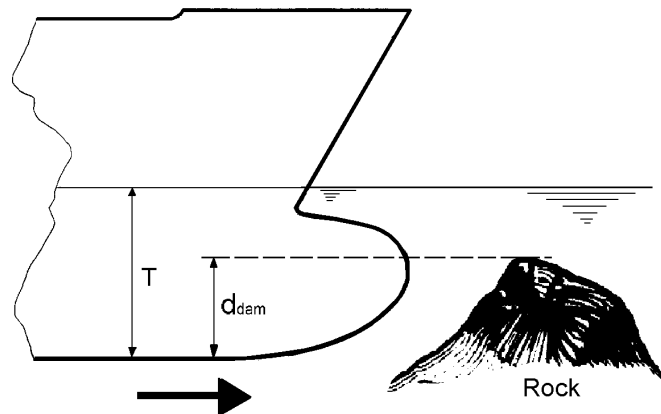
Fig. 5.26. Relation between the vertical penetration and the ship draught in grounding.

According to the design rules of the classification societies, the thickness of the bottom plating for same type of tankers may be approximated as

$$t_0 = k_0 \cdot L^\alpha / \sqrt{f} \tag{5.11}$$

where L is the ship length (m), t_0 is the bottom plating thickness (mm), k_0 and α are constant, $f = \sigma/235$ is a material factor, and σ is yield stress (N/mm^2). If k_0 is assumed to be **1.4,** and $f = 1$, $\alpha = 0.5$ the result for the bottom plating thickness with

various ship lengths from 160 m to 320 m is shown in Fig. 5.27. It is seen that the plating thickness varies from 18 mm to 25 mm for ship lengths from 160 m to 320 m. This result is reasonable for existing tankers.
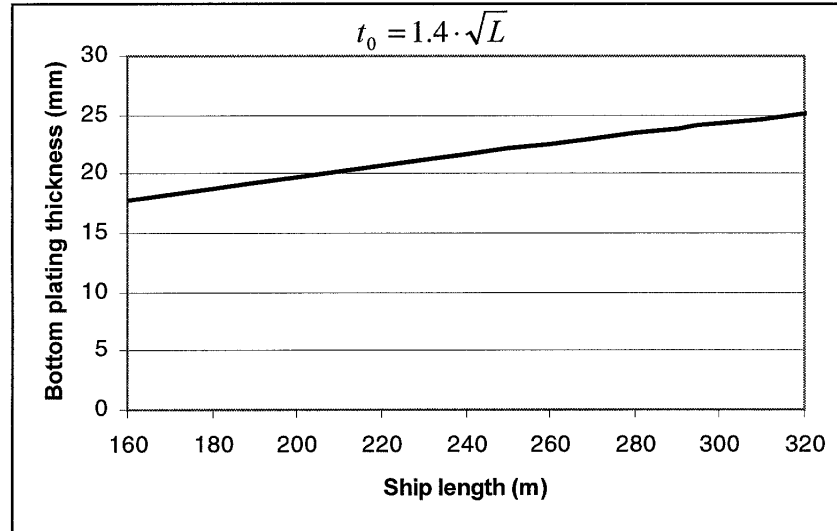
Fig. 5.27. Assumed relation for bottom plating thickness and tanker length.

Based on rough statistics and design rules, the equivalent thickness t of the outer bottom, including longitudinal webs and longitudinal stiffeners only, and the equivalent thickness t_{eq} of whole bottom, including longitudinal and transverse stiffeners are proportional to the thickness t_0 of the bottom plating. Therefore, the equivalent thicknesses t and t_{eq} for the same type of tankers may be determined approximately from

$$\begin{cases} t = k_1 \cdot t_0 \\ t_{eq} = k_2 \cdot t_0 \end{cases} \tag{5.12}$$

where k_1 and k_2 are constants. The relationship of the ship draught and the ship length is taken as:

$$T = k_3 \cdot L^{\beta} \tag{5.13}$$

where k_3 and β are constant. On the assumptions of Eqs. (5.11) to (5.13), the ratio of the horizontal grounding forces between two different tankers is obtained as

$$\frac{P_2}{P_1} = (\frac{\sigma_2}{\sigma_1})^{0.2} \cdot (\frac{L_2}{L_1})^{1.6\alpha + 0.4\beta} \tag{5.14}$$

Based on statistics and economic optimisation, the ship length can be approximated by (Schneekluth, 1987):

$$L = C \cdot \nabla^{0.3} V_0^{\,0.3} \tag{5.15}$$

where ∇ is the ship displacement in tonnes, V_0 is the design speed in knots, $C = 3.2$, L is the ship length in metres. By substituting Eqs. (5.14) and (5.15) into (5.10), we get the following relationship of the relative damage length between two different tankers:

$$\begin{cases} \dfrac{(L_{dam}/L)_1}{(L_{dam}/L)_2} = (\dfrac{\sigma_2}{\sigma_1})^{0.2} \cdot (\dfrac{L_1}{L_2})^{(2.333-1.6\alpha-0.4\beta)} \cdot (\dfrac{V_1}{V_2})^2 \cdot (\dfrac{V_{02}}{V_{01}}) \\ or \\ \dfrac{(L_{dam}/L)_1}{(L_{dam}/L)_2} = (\dfrac{\sigma_2}{\sigma_1})^{0.2} \cdot (\dfrac{\nabla_1}{\nabla_2})^{(0.7-0.48\alpha-0.12\beta)} \cdot (\dfrac{V_1}{V_2})^2 \cdot (\dfrac{V_{01}}{V_{02}})^{(0.3+0.48\alpha+0.12\beta)} \end{cases} \tag{5.16}$$

For most of oil tankers, the design speed is around 12 knots to 15 knots. The difference is not large. Therefore, it is assumed that the design speed for all oil tankers is similar. It is also reasonable to assume that the distribution of the grounding speed for all oil tankers is similar, that is

$$\begin{cases} \dfrac{V_1}{V_2} = 1 \\ \dfrac{V_{01}}{V_{02}} = 1 \end{cases}$$

Thus the expression for relative damage length between two different tankers is

$$\frac{(L_{dam}/L)_1}{(L_{dam}/L)_2} = (\frac{\sigma_2}{\sigma_1})^{0.2} \cdot (\frac{L_1}{L_2})^{(2.333-1.6\alpha-0.4\beta)} \tag{5.17}$$

Based on statistics and the classification rules, the constant α and β can be taken as $\alpha = 0.5$ and $\beta = 1$. Then Eq. (5.17) becomes

$$\frac{(L_{dam}/L)_1}{(L_{dam}/L)_2} = (\frac{\sigma_2}{\sigma_1})^{0.2} \cdot (\frac{L_1}{L_2})^{1.133} \tag{5.17}$$

It is seen from Eq. (5.18) that the distribution for the longitudinal damage length in grounding accidents depends on ship size. A large ship suffers a large relative damage length. This reflects the influence of structural design on the damage distribution of the longitudinal extent.

5.6.3 Calculation Example and Discussion

An example of the relative damage length between different ships (displacements from 30,000 t to 300,000 t is given in Fig. 5.28. The design speed is assumed to be 15 knots for all tankers.

From the result it is seen that the relative damage length of a 240,000 t tanker (ship length = 300 m) is **2** times that to a 30,000 t tanker (ship length = 160 m). Ship size influences the relative longitudinal damage length significantly in accidental grounding.

Fig. 5.28. The effect of ship size on relative damage length in grounding.

The damage density distributions in the IMO guidelines were derived from the actual damage data of ships of 30,000 dwt and above as mentioned previously. Here it is assumed that the mean value of displacements is 120,000 t in the IMO statistical data. It is assumed that the IMO damage distribution for the longitudinal extent is correct for a tanker of a size about 120,000 t displacement. By application of Eq. (5.18), the converted density distributions of longitudinal extent for tankers of 30,000 t and 300,000 t in displacement are shown in Fig. 5.29, and the cumulative probabilities are shown in Fig. 5.30.

In these translations, assumptions similar to those of the example of the high-speed craft are used (Section 5.4.3). That is we have assumed that in the IMO damage distribution the raking damage is represented by a constant density distribution equal to 0.5 for damage lengths between 0 and 80% of the ship length.

It is seen from Figs. 5.29 and 5.30 that the larger tanker suffers higher probability of larger relative damage length than that of the smaller tanker. For a damage length above 30% of a ship length, the probability is 29% for the 300,000 t tanker, and the probability is 16% for the 30,000 t tanker.
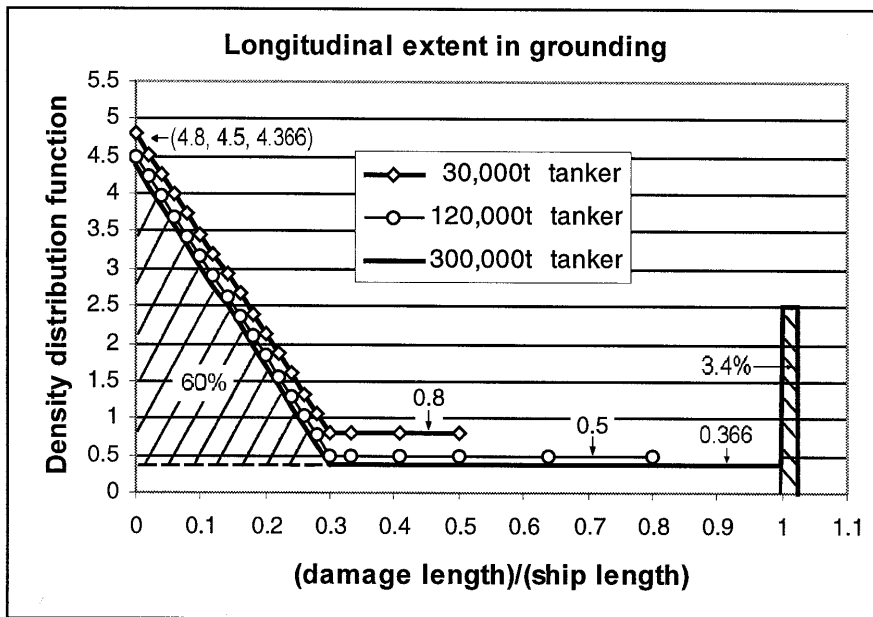
Fig. 5.29. The translated density distributions obtained by the present method for the longitudinal extent with different ship sizes in grounding.
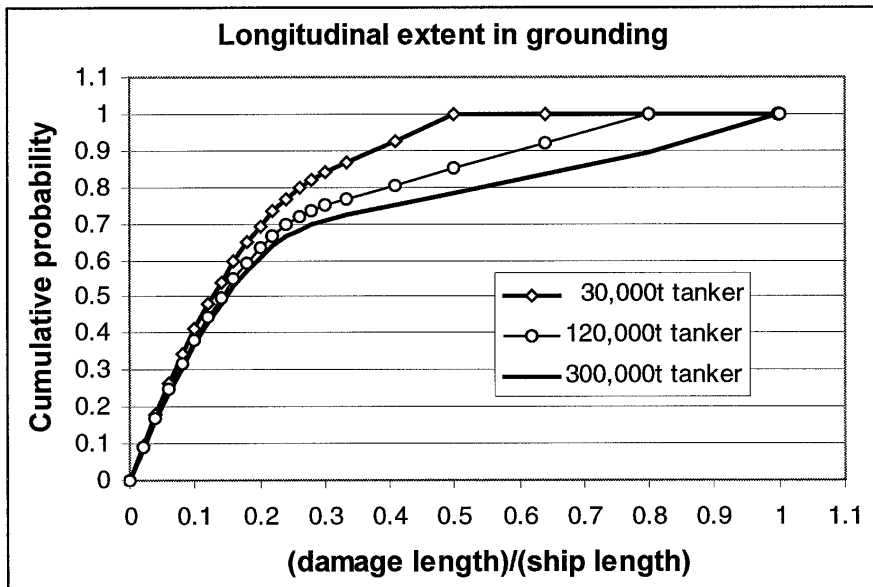
Fig. 5.30. The translated cumulative probabilities obtained by the present method for the longitudinal extent with different ship sizes in grounding.

The results obtained by the present method agree well with a statistical analysis of ship grounding accidents (Bjørneboe, 1999). The statistical results for bottom damage density distributions of the longitudinal extent are shown in Fig. 5.31, and the cumulative probabilities are shown in Fig. 5.32.
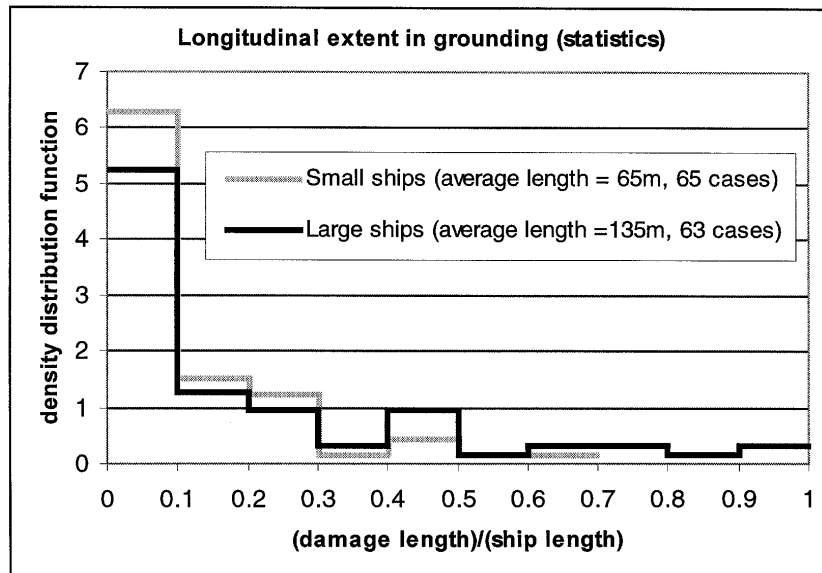
Fig. 5.31. Density distributions for the longitudinal extent with different ship sizes in grounding obtained by statistical data in the period of 1945 to 1965.
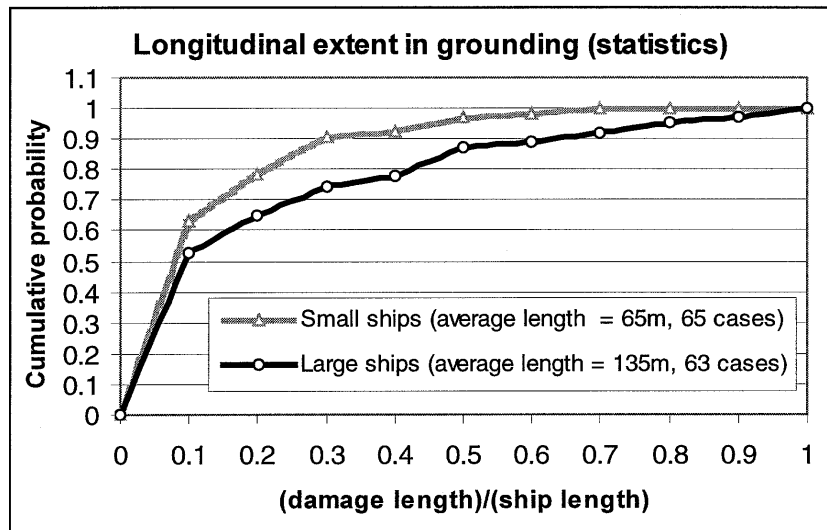
Fig. 5.32. Cumulative probabilities for the longitudinal extent with different ship sizes in grounding obtained by statistical data in the period of 1945 to 1965.

The distributions in Figs. 5.31 and 5.32 are based on 128 grounding accidents which happened in the period of 1945 to 1965 mainly involving various cargo ships. In order to investigate the effect of ship size on the damage distribution, the 128 grounding accidents are divided into two groups based on ship size. One group represents ship lengths less than 100 m (the average length is 65 m), in the other group, the ship lengths are larger than 100 m (the average length is 135 m). The small ship group contains 65 grounding cases, and the large ship group includes 63 cases.

It is seen clearly from the statistical results that the large ship group has high probability of large relative damage length. For the damage length above 30% of the ship length, the probability is 25.4% for the large ship group, and it is 9.2% for the small ship group.

In conclusion, the bottom damage distribution for the longitudinal extent depends on tanker size. A larger tanker suffers higher probability of a larger relative damage length than a smaller tanker.

5.7 Effect of Ship Size on Non-Dimensional Damage Size in Side Collisions

5.7.1 Introduction

The influence of ship size on the damage distribution of grounding has been studied in Section 5.6. The conclusion is that a larger ship suffers a higher probability of non-dimensional damage length than a smaller ship in grounding. In this section, we analyse the effect of ship size on the relative damage size of the side shell in ship-ship collisions.

5.7.2 Prediction of Relative Damage Size in Collisions

In Chapter 2, the energy loss to be dissipated by destroying the ship structure has been analysed. To simplify the analysis procedure, it is assumed that the striking ship impacts the midship of the struck ship perpendicularly where the struck ship is standstill before the collision. In this case, the energy loss is expressed as

$$E = \frac{M}{M + 0.6M_0} \cdot E_0 \qquad (5.19)$$

where M is the mass of the struck ship, the added mass coefficient for sway motion is taken as 0.66 and $E_0 = 0.5M_0U_0^{\,2}$ is the kinetic energy of the striking ship where M_0 is the mass of the striking ship, and U_0 is the speed of the striking ship.

In side collisions, the energy is absorbed mainly by crushing of the decks and stretching of the shell plating as shown in Fig. 5.33 (striking bow is assumed to be rigid). Thus, the absorbed energy can be calculated from

$$E = 0.77\varepsilon_c\sigma_0 R_1 + 3.50(\frac{t}{d})^{0.67}\sigma_0 R_2 \qquad (5.20)$$

where R_1 is the volume of the damaged shell plating, and R_2 is the volume of the crushed decks. From Fig. 5.33 it is seen that the damage length and the damage height in the side shell plating are proportional to the damage depth δ. Therefore, the volume of the damaged shell plating can be approximated by

$$R_1 = c_1\delta^2 t_1$$

where c_1 is a constant and t_1 is the equivalent thickness of the side shell plating. Similarly, the volume of the crushed decks is determined by:

$$R_2 = c_2\delta^2 t_2$$

where c_2 is a constant and t_2 is the equivalent thickness of the deck.
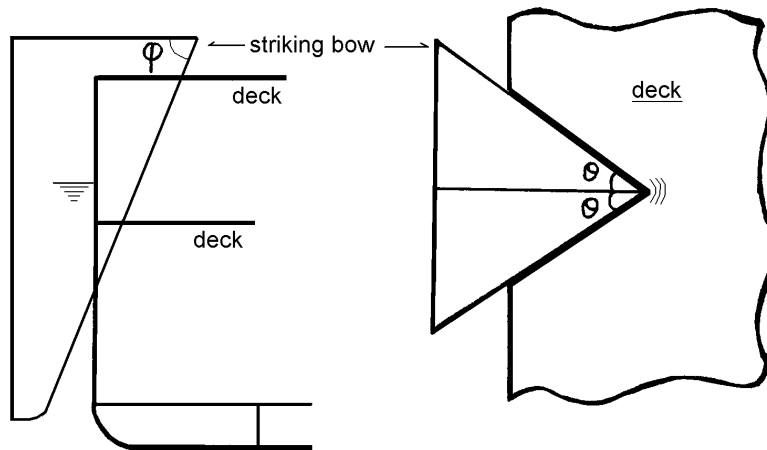
Fig. 5.33. A rigid bow penetrating into the side structure of a cargo ship.

Based on the design rules of the classification societies, the equivalent thickness of the side shell plating t and the equivalent thickness of the deck t_2 can be approximated by

$$t_1 = k_1 \cdot L^\alpha / \sqrt{f}$$

$$t_2 = k_2 \cdot L^\alpha / \sqrt{f}$$

where L is the ship length, $f = \sigma / 235$ is a material factor, k_1, k_2 and α are constant. It is assumed that the ratio t / d between the deck plate thickness and the spacing of the transverse stiffeners on the decks is independent on the ship size for the same type of ships. Therefore, Eq. (5.20) is further simplified as

$$E = C_3 \sigma_0^{0.5} L^\alpha L_{dam}^{\ 2}$$

where C_3 is a constant, L_{dam} is the damage length which is proportional to the damage depth δ. The non-dimensional damage length between the damage length and the ship length is expressed as

$$\frac{L_{dam}}{L} = \frac{E^{0.5}}{\sqrt{C_3} \sigma_0^{\ 0.25} L^{1+0.5\alpha}} \tag{5.21}$$

Substituting Eq. (5.19) into Eq. (5.21), the ratio of non-dimensional damage length between two struck ships can be determined from

$$\frac{(L_{dam} / L)_1}{(L_{dam} / L)_2} = (\frac{\sigma_2}{\sigma_1})^{0.25} \cdot (\frac{L_2}{L_1})^{(1+0.5\alpha)} \cdot (\frac{M_1}{M_2} \frac{M_2 + 0.6M_{02}}{M_1 + 0.6M_{01}})^{0.5} \cdot (\frac{E_{01}}{E_{02}})^{0.5} \tag{5.22}$$

Using Eq. (5.15) and assuming all the ships have similar design speed V_0, Eq. (5.22) becomes

$$\frac{(L_{dam} / L)_1}{(L_{dam} / L)_2} = (\frac{\sigma_2}{\sigma_1})^{0.25} \cdot (\frac{L_1}{L_2})^{(0.667-0.5\alpha)} \cdot (\frac{L_2^{\ 3.33} + 0.6L_{02}^{\ 3.33}}{L_1^{\ 3.33} + 0.6L_{01}^{\ 3.33}})^{0.5} \cdot (\frac{E_{01}}{E_{02}})^{0.5} \tag{5.23}$$

If it is assumed that a same striking ship impacts with two different struck ships and the constant α to be 0.5, the ratio of non-dimensional damage length between the two struck ships is simplified as

$$\frac{(L_{dam} / L)_1}{(L_{dam} / L)_2} = (\frac{\sigma_2}{\sigma_1})^{0.25} \cdot (\frac{L_1}{L_2})^{0.417} \cdot (\frac{L_2^{\ 3.33} + 0.6L_0^{\ 3.33}}{L_1^{\ 3.33} + 0.6L_0^{\ 3.33}})^{0.5} \tag{5.24}$$

From this equation it is seen that the ratio of non-dimensional damage length between two different struck ships not only depends on the two struck ships, but also depends on the size of the striking ship.

5.7.3 Analysis Examples and Discussions

It is assumed that a striking ship impacts with two different struck ships. The length of the struck ship No. 1 is $L_1 = 135$ m, and the length of the struck ship No. 2 is $L_2 = 65$ m. The length of the striking ship varies from 60 m to 140 m. The ratios of the non-dimensional damage length of the two struck ships obtained by Eq. (5.24) are shown in Fig. 5.34.

It is seen from Fig. 5.34 that the ratios between the two struck ships depend on the striking ship length. When the striking ship is small, the difference of the relative damage length between the two struck ships is large. When the striking ship is large, the difference becomes smaller. The result in this example varies between 0.48 to 0.92.
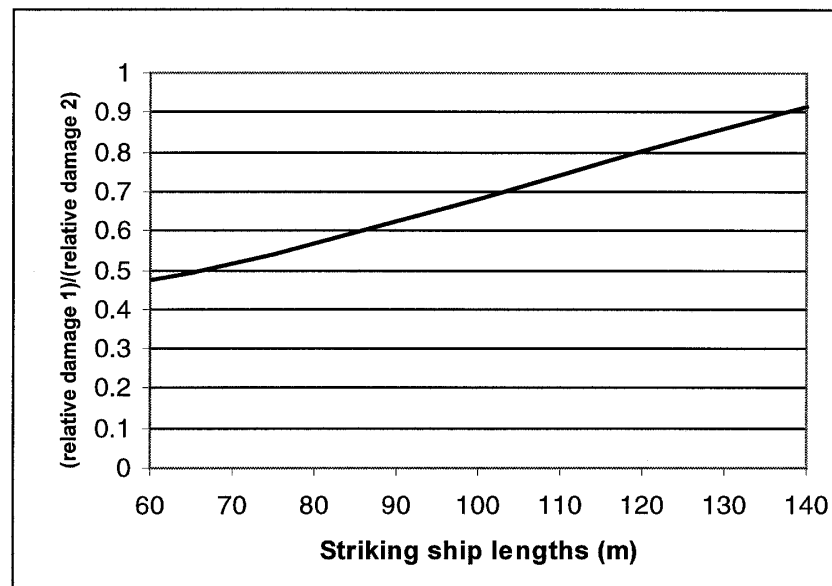
Fig. 5.34. Ratios of the relative damage length between the struck ship No. 1 (L_1 =135m) and the struck ship No. 2 (L_2 =65m) colliding with different striking ships.

It is assumed that an 100 m striking ship impacts different struck ships in length of 60 m to 140 m. The results of the relative damage length between different struck ships are shown in Fig. 5.35. It is shown that the relative damage size of a large struck ship is smaller than that of a small struck ship.

Therefore, one conclusion may be drawn from the example. That is the large struck ship suffers smaller relative damage length than that of the small struck ship.
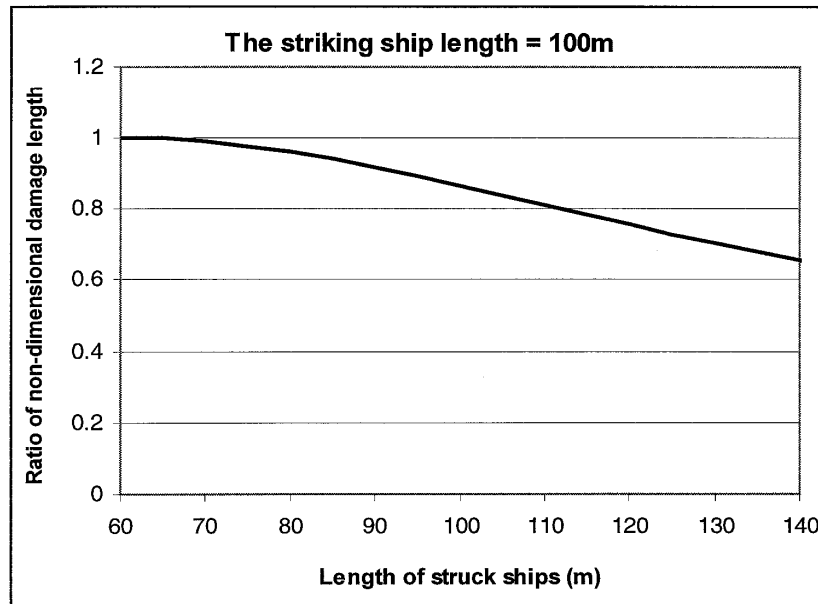
Fig. 5.35. Relative damage length between different struck ships where the striking ship length is 100 m.

This result correlates with the IMO statistical analysis from 291 collision cases occurred during the period of 1945 to 1965. The regression line for the non-dimensional damage length between different ships is show in Fig. 5.36. The statistical results show that the non-dimensional damage length of a large ship is smaller than that of a small ship. But the difference is not large.
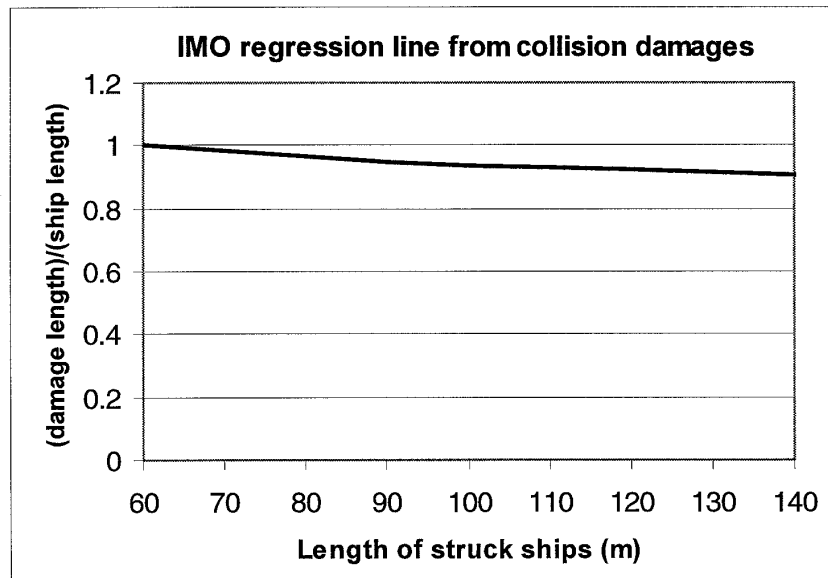
Fig. 5.36. The IMO statistical results on relative damage length between different struck ships obtained from collision damages in the period of 1945 to 1965.

To investigate further the effect of ship size on the damage distribution, the IMO accidental ships are divided into two groups. One group represents larger ships where the length is above 100 m, and the other group represents smaller ships where the length is less than 100 m. The average length of the large ship group is 135 m (including 139 collision cases) and the average length of the small ship group is 65 m (including 131 collision cases). The statistical results of the probabilistic density distribution, and the cumulative probabilities are shown in Figs. 5.37 and 5.38.
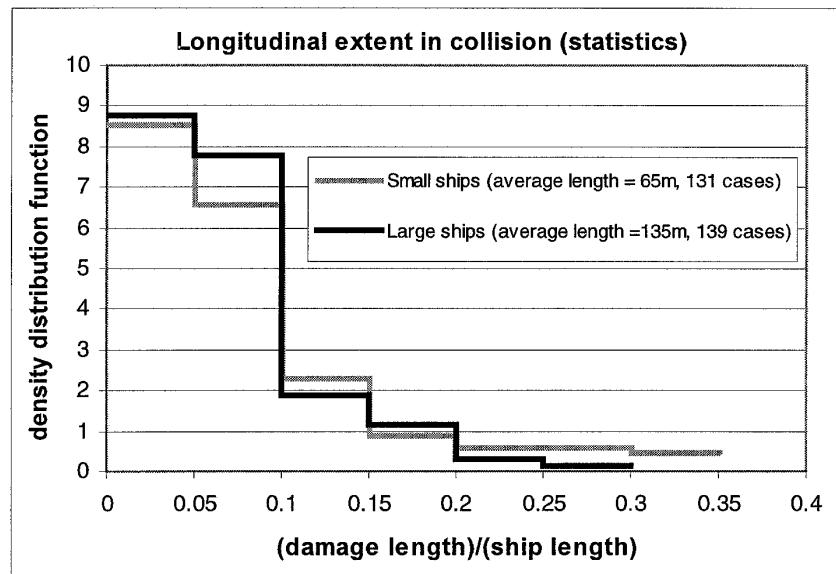
Fog. 5.37. Density function of damage length with different ship sizes in collisions found from statistical data in the period of 1945 to 1965.
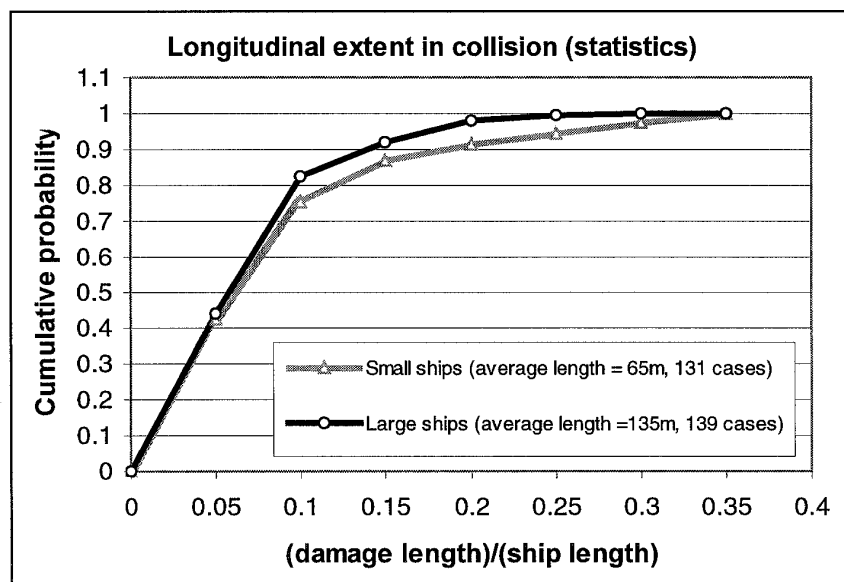
Fog. 5.38. Cumulative probabilities of damage length with different ship sizes in collisions found from statistical data in the period of 1945 to 1965.

The statistical results show that the group of the small ship has higher probability of larger non-dimensional damage length than that of the group of the large ship. For a damage length above 15% of the ship length, the probability is 25% for the small ship group, and it is 17% for the large ship group.

Pedersen et al (1996) carried out a probabilistic analysis of damage distributions for RoRo ferry collisions. A cumulative probabilities of non-dimensional damage length for a large ferry (the ship length = 180 m) and a small ferry (the ship length = 95 m) are shown in Fig. 5.39. This analysis results also show that the small ferry has higher probability of larger non-dimensional damage length than that of the large ferry.

The conclusion of this analysis is that the non-dimensional damage length of a larger ship is smaller than that of a smaller ship in collision damages. This result has been confirmed by statistical results and numerical analyses.

It is noted that this result of collision damage is just opposite to the result of grounding damage.
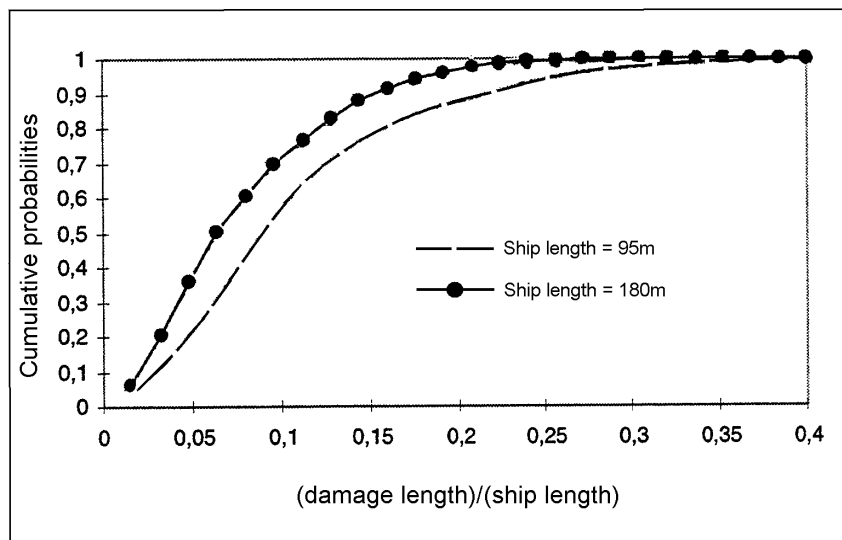
Fig. 5.39. Cumulative probabilities of non-dimensional damage length for a large ferry and a small ferry (Pedersen et al., 1996).

However, for ship-ship collisions, further studies are needed to include collision angles and collision positions etc.

5.8 Concluding Remarks

In this chapter, simple expressions for the relationship between the absorbed energy and the destroyed material volume are presented for analysis of ship collisions and grounding. Expressions (5.1) to (5.3) represent energy absorption by plastic tension, by crushing and folding and by tearing. It has been demonstrated that a high-energy structural damage may be represented by a sum of these energy terms. The formulas are simple to use and have forms similar to Minorsky's empirical expression. The proposed method overcomes the major drawback of Minorsky's classical method as it takes into account the structural arrangement, the materials properties, and the damage pattern.

A large number of comparisons between the present method and existing experimental and numerical results indicate that the present method can give reasonable predictions. It may therefore be considered as an improved approach to Minorsky's method for analysing ship collisions and grounding.

The study shows that the energy absorption efficiency, which represents the absorbed energy per unit volume of destroyed material, varies strongly from structure to structure. It depends on the structural arrangement, the materials properties and the failure mode. The range of the energy absorption efficiency, determined from the present examples, is $20 \sim 90 \ MJ/m^3$, while Minorsky's result is always a constant of $47.2 \ MJ/m^3$.

It is demonstrated how the proposed method can be used to translate grounding damage distribution from conventional vessels to new types of ships such as high-speed vessels. The examples show that the high-speed craft and the new fast ferry suffer larger grounding damage than the conventional ships.

Finally, an investigation of the effect of ship size on damage distributions is carried out. The results show that the damage density distribution for the longitudinal extent depends on ship size. A larger ship has higher probability of a larger relative damage length than that of a smaller ship in grounding, but the result of ship collisions is just opposite to the result of ship grounding.

This page is intentionally left blank.

Chapter 6

Conclusions

The analyses of ship collisions in this thesis include four main parts:

- External dynamics of ship collisions. Analytical procedures for the energy loss to be dissipated by destroying ship structures are developed.

- Internal mechanics of ship collisions. The upper-bound method is used to calculate structural plastic deformation and energy dissipation under extreme loading.

- Analyses of full-scale ship collisions. Calculation examples of damage in collisions are performed.

- Revised Minorsky's method for structural damage analysis. Relationships between the absorbed energy and the destroyed material volume are established for analysis of collisions and grounding.

1. In the external dynamics of collisions, analytical procedures for the energy loss and the impact impulse are developed for ship-ship collisions, ships colliding with rigid walls and ships colliding with offshore platforms. The energy loss in collisions is expressed in a closed form. The analysis results show that the energy loss is mainly determined by the following parameters:

   - Masses of the striking ship and the struck ship
   - Velocities of the involved ships
   - Collision location
   - Collision angle

The study of ship collisions indicates that the energy released for crushing is larger in the fore part than in the aft part of the struck ship. This is in accordance with IMO (1992) damage statistics. The study of an impact where a supply vessel drifts against the leg of a jack-up rig shows that a significant reduction of the severity of the collision can be

obtained by letting the supply vessel approach the rig from its aft or forward part, so that the probability of a midship collision is reduced.

2. In the internal analyses, a literature review is presented and a series of damage analyses for basic structural components is carried out by using the upper-bound method:

    • Formulas for load-penetration relations and energy-penetration relations in large plastic deformations of shell plating subjected to various loadings are derived.

    • Folding and crushing of frames are studied. A new formula for concertina tearing is derived. Comparison of the present method and existing experimental results shows that the agreement is good.

    • Denting of intersections is analyzed. Damage modes for basic elements, such as L-, T- and X- intersections, are constructed. Comparison shows that the results obtained by the present method agree well with FEM simulation results.

    • A theoretical model for cutting of bare plates is established. The critical rupture strain enters the solutions of the cutting force and the absorbed energy. The validity of the present method for both thin plates and thick plates is verified by comparing the present calculations with experimental results and some existing formulas.

    • Folding and crushing of stiffened decks or bottoms are analysed.

3. Several examples for analysis of full-scale ship collisions are presented:

    • A study on the impact strength of high-speed craft colliding with floating objects and dropped objects impacting plates is presented. The classification rule for the minimum thickness requirement of aluminium craft and FRP single-skin craft is converted into critical impact energy or critical object mass. The comparisons show that an acceptable agreement between the present results and experimental results is found. For a high-speed craft colliding with floating slender objects, the shell plating is most easily ruptured when the slender object is orientated in the sailing direction of the ship.

    • Calculations for collisions where Ro-Ro vessels are struck by other ships are carried out. The present calculation results are compared with existing results and acceptable agreement is achieved. The analysis procedure is also used to calculate the damage to a newly designed fast ferry. It is shown that the damage to the struck ship is larger when the struck ship has a forward speed than when the struck ship has zero speed.

• Analysis of collisions where unidirectional double-hull tankers are struck by other ships is performed. A comparison of the present calculation results with model test results shows that good agreement is found. The unidirectional double-hull design (ADH) has a high capability to resist grounding with its relatively tight spacing of longitudinal girders (Rodd, 1997). But due to the relatively small girder spacing, it may cause early rupture of the shell plating in side collisions.

• Collision analysis of a double-hull oil tanker is performed. In order to consider the deformation of the striking bow, a simple empirical formula is used for calculating the energy absorbed by the striking bow. Calculation examples show that the striking bow may absorb about 20% ~30% of the total collision energy depending on the ratio of strength of the striking bow and the struck side. The results also show that double oil tankers have good capability to prevent oil outflow in accidental situations.

4. Finally, relations for the absorbed energy and the destroyed material volume and their applications have been presented:

• Simple expressions for the relationship between the absorbed energy and the destroyed material volume are developed for analysis of ship collisions and grounding. The expressions represent energy absorption by plastic tension, by crushing and folding and by tearing. It is demonstrated that a high-energy structural damage can be represented by a sum of these energy terms. The formulas are simple to use and have forms similar to Minorsky's empirical expression. The proposed method overcomes the major drawback of Minorsky's classical method as it takes into account structural arrangement, materials properties, and damage patterns. The method may be considered as an alternative approach to Minorsky's method for analysing ship collisions and grounding.

• The validity of the proposed method is verified against a large number of the existing experimental results and numerical simulations. Applications to a full-scale grounding accident and bottom damage to large oil tankers are made. Very good correlation is found between the prediction and the actual damage.

• The study shows that the energy absorption efficiency, which represents the absorbed energy per unit volume of destroyed material, varies strongly from structure to structure. It depends on the structural arrangement, the materials properties and the failure modes. The range of the energy absorption efficiency, determined from the present examples, is $20 \sim 90$ MJ/m^3, while Minorsky's result is always a constant of 47.2 MJ/m^3.

• The proposed method has been used to translate grounding damage distribution from conventional vessels to new types of ships such as high-speed vessels. The examples show that the high-speed craft and the new fast ferry suffer larger grounding damage than the conventional ships.

- The proposed method has also been used to investigate the effect of ship size on damage distributions. The study shows that the damage density distribution for the longitudinal extent depends on the tanker size. A larger tanker has higher probability of a larger relative damage length than a smaller tanker in grounding. The result for ship collisions is just opposite to the result for ship grounding. This result has been verified by statistical results and numerical results.

References

A

(1) Aamlid O. and Antonsen G. A. (1997): "Oblique Impact Testing of Single Skin-Aramid Fiber Reinforced Plastic Panels", DNV Report No. 97-2000, Oslo, Norway.

(2) Aamlid O. (1995): "Oblique Impact Testing of Aluminum and Composite Panels ", DNV Report No. 95-2042, Oslo, Norway.

(3) Abramowicz W. and Jones N. (1997): "Transition from Initial Global Bending to Progressive Buckling of Tubes Loaded Statically and Dynamically", Int. J. Impact Engineering, Vol. 19, Nos. 5-6, 1997, pp. 415-437.

(4) Abramowicz W. (1994): "Crushing Resistance of T, Y, and X Sections", MIT-Industry Joint Program on Tanker Safety, Massachusetts Institute of Technology, USA, Report No. 24.

(5) Abramowicz W. and Wierzbicki T. (1989): "Axial Crushing of Multi-Corner Sheet Metal Columns", J. of Appl. Mech. Vol. 56, No. 1, pp. 113-120.

(6) Abramowicz W. and Jones N. (1986): "Dynamic Progressive Buckling of Circular and Square Tubes", Int. J. of Impact Engineering, Vol. 4, No. 4, pp. 243-270.

(7) Abramowicz W. (1983): "The Effective Crushing Distance in Axially Compressed Thin-Walled Metal Columns", Int. J. Impact Engineering, Vol. 1, No. 3, pp. 309-317.

(8) American Bureau of Shipping (ABS: 1990): "Rules for Building and Classing Steel Ships".

(9) Akita Y., Ando N., Fujita Y. and Kitamura K. (1972): "Studies on Collision-Protective Structures in Nuclear Powered Ships", Nuclear Engineering Design, No. 19.

(10) Akita Y. and Kitamura K. (1982): "A Study on Collision by an Elastic Stem to a Side Structure of Ships", J. of Naval Arch. of Japan, No. 131, 1982, pp. 307-317.

(11) Amdahl J. (1983): "Energy Absorption in Ship-Platform Impact", Norwegian Institute of Technology, Report No. UR-83-34.

(12)   Amdahl J. and Kavlie D. (1995): "Tanker Grounding Resistance", PRADS' 95.

(13)   Amdahl J. (1995): "Side Collision", 22nd WEGEMT Graduate School, Technical University of Denmark.

(14)   Amdahl J. and Kavlie D. (1992): "Experimental and Numerical Simulation of Double Hull Stranding", DNV-MIT Work Shop on Mechanics of Ship Collision and Grounding, DNV, Norway.

(15)   Amdahl J. and Eberg E. (1993): "Ship Collision with Offshore Structures", Structural Dynamics EURODYN'93, Trondheim, Norway.

(16)   Ammerman D. J. and Daidola J. C. (1996): "A Comparison of Methods for Evaluating Structure during Ship Collisions", International Conference on Design and Methodologies for Collision and Grounding Protection of Ships, San Francisco, California, USA, August 22-23.

(17)   Arita K. and Aoki G. (1985): "Strength of Ship Bottom Grounding", 1st report, J. of Naval Arch. of Japan, Vol. 158.

(18)   Astrup O. (1994): "Cutting of Thick Plates by a Wedge – an Experimental Study", MIT-Industry Joint Program on Tanker Safety, Massachusetts Institute of Technology, USA, Report No. 27.

(19)   ASIS (1998): "Research on the Methodology for the Prediction of Accidental Damage to Tanker Structure in Case of Collision or Grounding and Development of New Hull Design with Improved Crashworthiness (1991-1997)", The Association for Structural Improvement of the Shipbuilding Industry of Japan.

B

(20)   Bai Y. and Pedersen P. T. (1991): "Earthquake Response of Offshore Structures", Proceedings of the International Conference on Offshore Mechanics and Arctic Engineering, Bokk No. G00611-1991.

(21)   Bai Y. and Pedersen P. T. (1993): "Elastic-Plastic Behavior of Offshore Steel Structures under Impact Loads", Int. J. Impact Engng. Vol. 13, No. 1, pp. 99-115.

(22)   Bai Y., Bendiksen E., and Pedersen P. T. (1993): "Collapse Analysis of Ship Hulls", Marine Structures, No. 6, pp. 485-507.

(23)   Bishop R. E. D. and Price W. G. (1979): "Hydroelasticity of Ships", Cambridge University Press.

(24)   Bjørnebo N. (1999): "Statistical Analysis of Ship Grounding Accidents", Master thesis, Department of Naval Architecture and Offshore Engineering, Technical University of Denmark.

(25)   Bleich F. (1952): "Buckling Strength of Metal Structures", Mc.Graw-hill Book Company, INC.

(26)   Bockenhauer M. and Jost A. (1995): "Guidance for the Assessment of Alternative Tanker Designs", 22nd WEGEMT Graduate School, Technical University of Denmark.

(27)   Brach R. M. (1993): "Classical Planar Impact Theory and the Tip Impact of a Slender Rod", Int. J. Impact Engineering, Vol. 13, No. 1, pp. 21-33.

(28)   Bracco M. D. and Wierzbicki T. (1997): "Tearing Resistance of Advanced Double Hulls", J. of Ship Research, Vol. 41, No. 1, pp. 69-80.

(29)   Bracco M. D. (1994): "Grounding Resistance of Longitudinally Stiffened Single and Double Hull", MIT-Industry Joint Program on Tanker Safety, Massachusetts Institute of Technology, USA, Report No. 30.

C

(30)   Chang P. Y., Seibold F. and Thasanatorn C. (1980): "A Rational Methodology for the Prediction of Structural Response Due to Collisions of Ships", SNAME Transactions, Vol. 88, pp. 173-193.

(31)   Card J. C. (1975): "Effectiveness of Double Bottoms in Preventing Oil Outflow from Tanker Bottom Incidents", Marine Technology, January 1975.

(32)   Che J. and Jang G. (1995): "Numerical Simulation of Structural Response of D/H VLCC in Collision", PRADS'95.

(33)   Chen W. F. and Han D. J. (1988): Plasticity for Structural Engineers, Springer-Verlag.

(34)   Choi S. K., Wierzbicki T. and Culbertson-Driscoll J. (1994): "Crushing Strength of a Web Girder", MIT-Industry Joint Program on Tanker Safety, Massachusetts Institute of Technology, USA, Report No. 23.

(35)   Choqueuse D., Baizeau R. and Davies P. (1997): "Experimental Studies on Impact of Marine Composites", Int. Conf. on Advances in Marine Structures III, Rosyth, UK.

(36)   Curry R. (1996): "Merchant Ship Losses 1934-1993: An Overview", Transactions of the Royal Institution of Naval Architects, Part A, Vol. 138, pp. 1-20.

D

(37)   Daidola J. C. (1995): "Tanker Structure Behavior during Collision and Grounding", Marine Technology, Vol. 32, No. 1, pp. 20-32.

(38)   Det Norske Veritas (DnV, 1988): "Design Guidance for Offshore Steel Structures Exposed to Accidental Loads", DNV Report No. 88-3172, Oslo, Norway.

(39)   Det Norske Veritas (DnV, 1993): "Rules for Classification of High-Speed Light Craft", DNV, Oslo, Norway.

(40)   Det Norske Veritas (DnV, 1991): "Rules for Classification -- Steel Ships".

E

(41)   Edinberg D.L. and Mater P. R. (1981): "A Comparison of the Collision Resistance of Membrane Tank-type and Spherical Tank-type LNG Tankers", GASTECH'81, Hamburg, Germany.

(42)   Egge E. D. and Bochengauer M. (1989): "Calculation of the Collision Resistance of Ships and Its Assessment for Classification Purposes", Marine Structures, Vol. 4, No. 4, pp. 35-56.

(43)   Ellinas C. P. and Valsgard S. (1985): "Collision and Damage of Offshore Structures a State-of-the Art", 4th Int. Symposium on Offshore Mechanics and Arctic Engineering, Dallas, Texas, February 17-22.

F

G

(44)   Gerard G. (1958): "The Crippling Strength of Compression Element", J. of the Aeronautical Science.

(45)   Goksoyr (1994): "Crushing Resistance of Web Girders in Unidirectional Stiffened Double Hull ", MIT-Industry Joint Program on Tanker Safety, Massachusetts Institute of Technology, USA, Report No. 20.

H

(46)   Hagiwara K., Takanabe H. and Kawano H. (1983): "A Proposed Method of Predicting Ship Collision Damage", Int. J. of Impact Engineering, Vol. 1, No. 3.

(47)   Hanhirova H. (1995): "External Collision Model, Safety of Passenger/RoRo Vessels", Helsinki University of Technology, Ship Laboratory, Oct. 1995.

(48)   Haywood J. H. (1971): "A Note for Collision Estimates for LNG Carriers", Naval Construction Research Establishment, S. Leonard's Hill, Fife.

(49)   Hildebrand M. (1994): "The Effect of Raw-material Related Parameters on the Impact Strength of Sandwich Boat-laminates", Technical Research Center of Finland, VTT publication No. 211.

(50)   Hu C. et al. (1998): "Risk Analysis for Shuttle Tankers and Mitigating Measures", 17th OMAE.

(51)   Hysing T. (1993): "Oil Spill from Tankers in Collisions and Grounding --- Damage Statistics", Technical Report No. 93-0518, Det Norske Veritas.

(52)   Hysing T. (1995): "Damage and Penetration Analysis-safety of Passenger/RoRo Vessels", DNV Report No. 95-0419, Norway.

I

(53)   International Maritime Organization (IMO, 1995a): "International Code of Safety for High-Speed Craft (HSC Code)", Resolution MSC.36(63), London.

(54)   International Maritime Organization (IMO, 1995b): "Interim Guidelines for Approval of Alternative Methods of Design and Construction of Oil Tankers under Regulation 13F(5) of Annex I of MARPOL 73/78. Technical Report, Resolution MEPC. 66 (37), pp. 1-40.

(55)   International Maritime Organization (IMO, 1992): IMO Resolution A.684(17).

(56)   ISSC (1967): "Plastic and Limit Design", Proc. 3rd Int. Ship Structures Congress, Hamburg.

(57)   ISSC (1997): "Specialist Panel V.4 -- Structural Design against Collision and Grounding", 13th International Ship and Offshore Structures Congress, 18-22 August, Trondheim, Norway, Vol. 2, pp. 83-116.

(58)   Ito H., Kondo K., Yoshimura N. and Kawashima M. (1984): "A Simplified Method to Analysis the Strength of Double Hulled Structures in Collision", 1st report, J. of Naval Arch. of Japan.

(59)   Ito H., Kondo K., Yoshimura N. and Kawashima M. (1985): "A Simplified Method to Analysis the Strength of Double Hulled Structures in Collision", 2nd report, J. of Naval Arch. of Japan.

(60)   Ito H., Kondo K., Yoshimura N. and Kawashima M. (1986): "A Simplified Method to Analysis the Strength of Double Hulled Structures in Collision", 3rd Report, J. of Naval Arch. of Japan.

(61)   Ito H., Hayashi K. and Kitano K. (1994): "A Design-Oriented Investigation into the Collision Strength of Double-Hulled Structures", 1994 OMAE-Volume I, Offshore Technology, ASME.

(62)   Ishiyama S., Nishimura T. and Tsuchiya Y. (1983): "Impact Response of Thin-Walled Plane Frame Structures", Int. J. Impact Engng. Vol. 1, No. 3, pp. 227-247.

J

(63)   Jensen J. J., Baatrup J. and Andersen P. (1995): "Collision Damage Statistics and Probabilistic Damage Stability Calculation in Preliminary Ship Design", 22nd WEGEMT Workshop on Damage Stability of Ships, Technical University of Denmark.

(64)   Jensen J. J. (1995): "Probabilistic Damage Stability Calculations for Ships", 22nd WEGEMT Graduate School, Technical University of Denmark.

(65)   Jones N. (1976): "On the Collision Protection of Ships", Nuclear Engineering and Design, 38, 1976, pp. 229-240, North-Holland Publishing Company.

(66)   Jones N. (1979): "A Literature Survey on the Collision and Grounding Protection of Ships", Ship Structures Committee Report, SSC-283.

(67)   Jones N. and Jouri W. S. (1987): "A Study of Plate Tearing for Ship Collision and Grounding Damage", Journal of Ship Research, Vol. 31, No. 4, pp. 253-268.

(68)   Jones N. (1997): "Dynamic Plastic Behavior of Ship and Ocean Structures", The Royal Institute of Naval Architects.

(69)   Jones N. (1989): Structural Impact, Cambridge University Press.

(70)   Jones N. and Wierzbicki T. (edited, 1983): Structural Crashworthiness, Butterworth & Co. (Publishers) Ltd.

(71)   Jones N. and Wierzbicki T. (edited, 1993): Structural Crashworthiness and Failure, Elsevier Applied Science.

(72)   Jones N. (1994): "Some Comments on the Scaling of Inelastic Structures Loaded Dynamically", Proceedings of the International Union of Theoretical and Applied Mechanics (IUTAM), Symposium on Size-scale Effects in Failure Mechanisms of Materials and Structures, Turin, Italy, October.

(73)   Jones N., Kim S. and Li Q. (1997): "Response and Failure of Ductile Circular Plates Struck by a Mass", Transactions of the ASME, Vol. 119, August 1997.

K

(74)   Kaminishi K. and Taneda M. (1992): "Crack Initiation and Extension under Penetration of Thin Metal Sheet", JSME Int. Journal, Vol. 35, No. 4.

(75)   Karagiozova D. and Jones N. (1997): "Strain-rate Effects in the Dynamic Buckling of a Simple Elastic-plastic Model", J. of Applied Mechanics, Vol. 64, March 1997.

(76)   Kawano S. and Kaminishi K. (1988): "Energy-absorbing Capacity of Ductile Thin Metal Sheet under Quasi-static Penetration by Conical Punch", JSME Int. Journal, Vol. 31, No. 1.

(77)   Kierkegaard H. (1993a): "Ship Collision with Icebergs", Technical University of Denmark, Ph.D. thesis.

(78)   Kierkegaard H. (1993b): "Ship Bow Response in High Energy Collisions", Marine Structures, No. 6.

(79)   Kinkead A. N. (1980): "A Method for Analyzing Cargo Protection Afforded by Ship Structures in Collision and Its Application to an LNG Carrier", RINA Transactions, pp. 299-323.

(80)   Kitamura O. and Kusuba S. (1997): "A Study on the Crashworthiness of Double Side Structure of VLCC", OMAE.

(81)   Kitamura O. (1997): "Comparative Study on Collision Resistance of Side Structure", International Conference on Design and Methodologies for Collision and Grounding Protection of Ships, San Francisco, California, USA, August 22-23, 1996. Also in "Marine Technology", Vol. 34, No. 4, pp. 293-308.

(82)   Kitamura O. and Kuroiwa T. et al. (1998): "A Study on the Improved Tanker Structure against Collision and Grounding Damage", The Seventh International Symposium on Practical Design of Ships and Mobile Units, PRADS' 98, The Hague, the Netherlands, September 20-25.

(83)   Kuroiwa T. (1996): "Numerical Simulation of Actual Collision & Grounding Accidents", International Conference on Design and Methodologies for Collision and Grounding Protection of Ships, San Francisco, California, USA, August 22-23.

L
(84)   Langseth M., Hopperstad O. S. and Berstad T. (1997): "Impact Loading of Plates--Validation of Numerical Simulations by Testing", Int. J. of Offshore and Polar Engineering.

(85)   Lee J. W. and Hong S. J. (1997): "A Study on the Dissipation Energy of Plate Due to Cutting", J. of Ship & Ocean Technology, Vol. 1, No. 1, pp. 48-56.

(86)   Lehman E. and Yu X. (1998): "Inner Dynamics of Bow Collision to Bridge Piers", International Symposium Advances in Bridge Aerodynamics-Ship Collisions Analysis-Operation and Maintenance, Lyngby, Denmark.

(87)   Lehman E. and Yu X. (1995): "Progressive Folding of Bulbous Bows", PRADS'95.

(88)   Lemmen P. M., Vredeveldt W. and Pinkster J. A. (1996): "Design Analysis for Grounding Experiments", International Conference on Design and Methodologies for Collision and Grounding Protection of Ships, San Francisco, California, USA, August 22-23.

(89)   Lenselink H. and Thung K. G. (1992): "Numerical Simulations of Ship Collisions", Pro. Of the Second Int. Offshore and Polar Engineering Conference, San Francisco, USA, June 14-19.

(90)   Lloyd's Register of Shipping (LR, 1996-97): "Register of Ships".

(91)   Lloyd's Register of Shipping (LR, 1997): "Rules and Regulations for the Classification of Ships".

(92)   Lu G. and Callidine C. R. (1990): "On the Cutting of a Plate by a Wedge", Int. J. of Mechanical Sciences, Vol. 32, No. 4, pp. 293-313.

(93)   Lubliner J. (1990): "Plasticity Theory", Macmillan Publishing Company.

(94)   Lützen M. (1998): "Dimensionering for Mindre Kontaktskader", Master thesis (in Danish), Dept. of Naval Architecture and Offshore Engineering, Technical University of Denmark.

M
(95)   Manolakos D. E. and Mamalis A. G. (1985): "On Ship Collisions: the Plastic Collapse of Longitudinally Framed Shell Plating Subjected to Oblique Loading", Int. J. Impact Engng. Vol. 3, No. 1, pp. 41-55.

(96)   Maxwell L. M. (1993): "Effect of Rock Geometry in the Failure Mode of Plates and the Forces in Grounding Experiments", MIT-Industry Joint Program on Tanker Safety, Report No. 15.

(97)   McDermott J., Kline R., Jones E., Maniar N. and Chiang W. (1974): "Tanker Structural Analysis for Minor Collisions", SNAME Transactions.

(98)   Melton W. et al. (1994): "Advanced Double Hull Research and Development for Naval and Commercial Ship Application", SNAME Transactions, Vol. 102, pp. 259-323.

(99)   Michel K., Moore C. and Tagg R. (1996): "A Simplified Methodology for Evaluating Alternative Tanker Configurations", Journal of Marine Science and Technology, Vol. 4, No. 1, pp. 209-219.

(100)   Michel K. (1998): "Oil Outflow Analysis for a Series of Double Hull Tankers", Report, Herbert Engineering Corp., prepared for the U.S. Coast Guard.

(101) Michel K., Moore C. and Tagg R. (1996): "A Simplified Methodology for Evaluating Alternative Tanker Configurations", Journal of Marine Science and Technology, Vol. 4, No. 1, pp. 209-219.

(102) Minorsky V.U. (1959): "An Analysis of Ship Collision with Reference to Protection of Nuclear Power Ships", J. of Ship Research, Vol. 3, No. 2, pp. 1-4.

(103) Minorsky V. U. (1975): "Ship Collision Study-Present Situation Survey", U. S. Maritime Administration.

(104) Motora S. et al. (1971): "Equivalent Added Mass of Ships in Collisions", Selected Papers from J. Soci. Nav. Arch. Japan, Vol. 7, pp. 138-128.

(105) Munro-Smith R. (1975): "Elements of Ship Design", published by Marine Media Management Ltd., London.

N

(106) Nagasawa H., Arita K., Tani M. and Oka S. (1975): "A Study on the Collapse of Ship Structure in Collision with Bridge Piers", J. of Naval Arch. of Japan, Vol. 142.

(107) Nakamura T. and Kuroiwa T. (1995): "Experimental Study on Failure of Ship Side Structure", International Conference on Technologies for Marine Environment Preservation, MARIENV'95, Vol. 1, Tokyo, Japan, September 24-29.

(108) Nielsen L. P. (1995): "Traffic and Route Data—Safety of Passenger RoRo Vessels", Dept. of Ocean Engineering, Technical University of Denmark.

(109) Nippon Kaiji Kyokai (ClassNK, 1997): "Rules and Regulations".

O

(110) Ohtsubo H. and Suzuki K. (1995): "The Crushing Mechanics of Bow Structures and Its Optimal Design against Head on Collision", PRADS'95.

(111) Ohtsubo H., Suzuki K. and Yonesato N. (1995): "Prediction of Collision Strength of Side Structures", J. of Naval Arch. of Japan, Vol. 178.

(112) Ohtsubo H. and Wang G. (1995): "An Upper-Bound Solution to the Problem of Plate Tearing", J. of Marine Science and Technology, No. 1, pp. 46-51.

(113) Ohtsubo H. and Wang G. (1997): "Damage of Ship Structures in Collision and Grounding Accidents", Int. Conf. on Advances in Marine Structures III, DERA, ROSYTH, UK.

P

(114) Paik J. K. (1996): "On Quasi-static Crushing of a Stiffened Square Tube", J. of Ship Research, Vol. 40, No. 3, pp. 258-267.

(115)   Paik J. K. (1994): "Cutting of a Longitudinally Stiffened Plate by a Wedge", J. of Ship Research, Vol. 38, No. 4, pp. 340-348.

(116)   Paik J. K. and Pedersen P. T. (1995a): "Ultimate and Crushing Strength of Plated Structures", J. of Ship Research, Vol. 39, No. 3, pp. 250-261.

(117)   Paik J. K. and Pedersen P. T. (1995b): "On Design of Double Hull Tankers against Collisions", PRADS'95.

(118)   Paik J. K and Wierzbicki T. (1997): "A Benchmark Study on Crushing and Cutting of Plated Structures", Journal of Ship Research, Vol. 41, No. 2, pp. 147-160.

(119)   Pakstys M. P. (1977): "Ship Collision Dynamics and the Prediction of the Shock Environment for Colliding Ships", Ph.D. dissertation, University of Rhode Island, USA.

(120)   Papka S. D. and Kyriakides S. (1998): "In Plane Crushing of a Polycarbonate Honeycomb", Int. J. Solids Structures, Vol. 35, Nos. 3-4, pp. 239-267.

(121)   Pawlowski M. (1995): "Energy Loss in Ship's Collisions", Centrum Techniki Okretowej, Poland.

(122)   Pedersen P. T. and Simonsen B. C. (1995): "Dynamics of Ships Running Aground", Journal of Marine Science and Technology, No. 1, pp. 37-45.

(123)   Pedersen P. Terndrup, Hansen P. F. and Nielsen, L. P. (1996): "Collision Risk and Damage after Collision", RINA International Conference on the Safety of Passenger RoRo Vessels".

(124)   Pedersen P. Terndrup (1995): "Outer Dynamics of Ship Collisions", 22nd WEGEMT Graduate School, Technical University of Denmark.

(125)   Pedersen P. T. and Jensen J. J. (1991): "Ship Impact Analysis for Bottom Supported Offshore Structures", Advances in Marine Structures II, Elsevier Applied Sciences.

(126)   Pedersen P. T. (1994): "Ship Grounding and Hull-girder Strength", Marine Structures, No. 7, pp. 1-29.

(127)   Pedersen P. T., Valsgaard S., Olsen D. and Spangenberg S. (1993): "Ship Impacts: Bow Collisions", Int. J. of Impact Engineering, Vol. 13, No. 2, pp. 163-187.

(128)   Pedersen P. T. (1998): "Ship Crushing Load Studies", Chapter 3.6, East Bridge, The Storebælt Publications, Editor Niels Gimsing, pp. 44-57.

(129)   Pedersen P. T. and Zhang Shengming (1998a): "The Mechanics of Ship Impacts against Bridges", International Symposium Advances in Bridge Aerodynamics-Ship Collisions Analysis-Operation and Maintenance, Lyngby, Denmark, published by A. A. Balkema, Rotterdam, pp. 41-52.

(130)   Pedersen P. T. and Zhang Shengming (1998b): "Minimum Plate Thickness in High-Speed Craft", PRADS'98, September, The Hague, the Netherlands, Elsevier Publisher, pp. 959-966.

(131)   Petersen M. J. (1982): "Dynamics of Ship Collision", Ocean Engineering, Vol. 9, No. 4, pp. 295-329.

(132)   Petersen M. J. and Pedersen P. T. (1981): "Collision between Ships and Offshore Platforms", Offshore Technology Conference, Houston, USA, Paper OTC 4134.

(133)   Petersen E. and Valsgard S. (1983): "Collision Resistance of Marine Structures", Chapter 12 in Structural Crashworthiness edited by Jones N and Wierzbicki T, Butterworth & Co Ltd.

(134)   Pianic (1984): Permanent International Association of Navigation Congress Report of the International Commission for Improving the Design of Fender Systems, Supplement to Bulletin No. 45 (1984), Brussels, Belgium.

Q

(135)   Qvist, S., Nielsen K. B., Schmidt M. H. and Madsen S. H. (1995): "Ship Collision- Experimental and Numerical Analysis of Double Hull Models", 9th DYMAT Technical Conference.

R

(136)   Rawson C., Crake K. and Brown A. (1998): "Assessing the Environmental Performance of Tankers in Accidental Grounding and Collision", SNAME Annual Meeting 1998, San Diego, USA.

(137)   Reardon P. C. and Sprung, J. L. (1996): "Validation of Minorsky's Ship Collision Model and Use of the Model to Estimate the Probability of Damaging a Radioactive Material Transportation Cask during a Ship Collision", Proceedings of International Conference on Design and Methodologies for Collision and Grounding Protection of Ships, San Francisco, California, August 22-23.

(138)   Reckling K. A. (1983): "Mechanics of Minor Ship Collisions", Int. J. Impact Engineering, Vol. 1, No. 3, pp. 281-299

(139)   Rodd J. L. (1997): "Frame Design Effects in the Rupture of Oil Tanks during Grounding Accidents", Int. Conf. on Advances in Marine Structures III, DERA, ROSYTH, UK.

S

(140) Samuelides E and Frieze P. A. (1989): "Fluid-structure Interaction in Ship Collisions", Marine Structures, Vol. 2, pp. 65-88.

(141) Sano A., Muragishi O. and Yoshikawa T. (1996): "Strength Analysis of a New Double Hull Structure for VLCC in Collision", International Conference on Design and Methodologies for Collision and Grounding Protection of Ships, San Francisco, California, USA, August 22-23.

(142) Sirkar J., Ameer P., Brown et al. (1997): "A Framework for Assessing the Environmental Performance of Tankers in Accidental Groundings and Collisions", Report of SNAME T&R Ad Hoc Panel on the Environmental Performance of Tankers, 1997.

(143) Scharrer M. and Ostergaard C. (1996): "Safety of Passenger/RoRo Vessels-Analysis of Collision Energies and Hole Sizes", GERMANISCHER LLOYD, Report No. FL96.009, Hamburg.

(144) Schneekluth H. (1987): "Ship Design for Efficiency and Economy", Butterworth & Co. (Publishers) Ltd.

(145) Simonsen B. C. and Ocakli H. (1999): "Experiments and Theory on Deck and Girder Crushing", Dept. of Naval Architecture and Offshore Engineering, Technical University of Denmark.

(146) Simonsen B. C. (1998a): "Bottom Raking Damage to High-Speed Craft", Technical University of Denmark (to be published).

(147) Simonsen B. C. (1998b): "Ship Grounding on Rock, Theory and Validation", Marine Structures, 10(7), pp. 519-584.

(148) Simonsen B. C. (1997): "The Mechanics of Ship Grounding", Technical University of Denmark, Ph.D. thesis.

(149) Simonsen B. C. and Wierzbicki T. (1996): "Grounding Bottom Damage and Ship Motion over a Rock", Int. J. of Offshore and Polar Engineering, Vol. 6, No. 3.

(150) Simonsen B. C. and Pedersen P. T. (1997): "On Grounding of Fast Ships", Int. Conf. on Advances in Marine Structures III, DERA, ROSYTH, UK.

(151) Simonsen B. C. and Wierzbicki T. (1997): "Plasticity, Fracture and Friction in Steady-state Plate Cutting", Int. J. of Impact Engineering, Vol. 19, No. 8, pp. 667-692.

T

(152) Thunes R. (1994): "Development of Analytical Models of Wedge Indentation into Unidirectional Stiffened and Orthogonal Stiffened Double Hull ", MIT-Industry Joint Program on Tanker Safety, Report No. 21.

(153) Thomas P. F. (1992): "Application of Plate Cutting Mechanics to Damage Prediction in Ship Grounding", MIT-Industry Joint Program on Tanker Safety, Report No. 8.

U

(154) Ueda Y. and Murakawa H. (1995): "Strength Estimation Method of Ship Structures Subjected to Hard Bow Collision", J. of Naval Arch. of Japan, Vol. 178.

V

(155) Vaughan H. (1978): "Bending and Tearing of Plate with Application to Ship-Bottom Damage", Naval Architects, Vol. 3, pp. 97-99.

(156) Vaughan H. (1980): "The tearing Strength of Mild Steel Plate", J. of Ship Research, Vol. 24, No. 2, pp. 96-100.

(157) Vredeveldt A. W., Wevers L. J. and Lemmen, P. P. M. (1993): "Full Scale Ship Collision Tests", Third International Symposium on Structural Crashworthiness and Failure, Liverpool, April 14-16, edited by Jones and Wierzbicki.

W

(158) Wang G. (1995): "Structural Analysis of Ship Collision and Grounding", Ph.D. thesis, University of Tokyo.

(159) Wang G. and Ohtsubo H. (1997): "Deformation of Ship Plate Subjected to Very Large Load", OMAE.

(160) Wang G., Ohtsubo H. and Liu D. (1997): "A Simple Method for Predicting the Grounding Strength of Ships", J. of Ship Research, Vol. 41, No. 3, pp. 241-247.

(161) Wen H. M and Jones N. (1993): "Experimental Investigation of the Scaling Laws for Metal Plates Struck by Large Masses", Int. J. Impact Engineering, Vol. 13, No. 3, pp. 485-505.

(162) Wierzbicki T. and Abramowicz W. (1983): "On the Crushing Mechanics of Thin-Walled Structures", Journal of Applied Mechanics, Vol. 50.

(163) Wierzbicki T. and Thomas P. (1993): "Closed-Form Solution for Wedge Cutting Force through Thin Metal Sheets", Int. J. Mech. Sci. Vol. 35, No. 3/4, pp. 209-229.

(164) Wierzbicki T., Rady E., Peer D. B. and Shin J. G. (1990): "Damage Estimates in High Energy Grounding of Ships", Joint MIT-Industry Project on Tanker Safety, Report No. 1.

(165)   Wierzbicki T. (1994): "Concertina Tearing of Metal Plates-Improved Solution and Comparison", Joint MIT-Industry Project on Tanker Safety, Report No. 22.

(166)   Wierzbicki T. and Simonsen B. C. (1996): "Global Structural Model of Bow Indentation into Ship Side", MIT Rupture Analysis of Oil Tankers in Side Collision, Report No. 2.

(167)   Woisin G. (1979): "Design against Collision", Schiff & Hafen, Vol. 31, No. 2, pp. 1059-1069, Germany.

(168)   Woisin G. (1982): "Comments on Vaughan: The Tearing Strength of Mild Steel Plate", J. of Ship Research, Vol. 26, No. 1, pp. 50-52.

(169)   Woisin G. (1988): "Instantaneous Loss of Energy with Unsymmetrical Ship Collisions", Schiff & Hafen, Vol. 40, No. 1, pp. 50-55.

X

Y

(170)   Yahiaoui M., Bracco M., Little P. and Trauth A. T. (1994): "Experimental Study on Scale Models for Grounding", MIT-Industry Joint Program on Tanker Safety, Report No. 18.

(171)   Yang P. D. C and Caldwell J. B. (1988): "Collision Energy Absorption of Ship Bow Structures", Int. J. Impact Engineering, Vol. 7, No. 2, pp. 181-196.

(172)   Yu Xing (1996): "Strukturverhalten mit grober Verformung bis zum Brucheintritt und mit dynamischer Zusammenfaltung", Dr. Ing. Dissertation, Universitat Hamburg, Germany.

Z

(173)   Zheng Z. and Wierzbicki T. (1996): "A Theoretical Study of a Steady-State Wedge Cutting through Metal Plates", Int. J. of Fracture, 78, pp. 45-66.

(174)   Zhu L. and Faulkner D. (1994): "Dynamic Behavior of Plates in Minor Ship Collision", Int. J. of Impact Engineering, Vol. 15, No. 2, pp. 165-178.

(175)   Zhu L. and Atkins A. G. (1998): "Failure Criteria for Ship Collision and Grounding", The Seventh International Symposium on Practical Design of Ships and Mobile Units, PRADS' 98, The Hague, the Netherlands, pp. 141-147.

Ph.d. Theses
Department of Naval Architecture and Offshore Engineering, DTU

1961   **Strøm-Tejsen, J.:** "Damage Stability Calculations on the Computer DASK."

1963   **Silovic, V.:** "A Five Hole Spherical Pilot Tube for three Dimensional Wake Measurements."

1964   **Chomchuenchit, V.:** "Determination of the Weight Distribution of Ship Models".

1965   **Chislett, M.S.:** "A Planar Motion Mechanism".

1965   **Nicordhanon, P.:** "A Phase Changer in the HyA Planar Motion Mechanism and Calculation of Phase Angle".

1966   **Jensen, B**.: "Anvendelse af statistiske metoder til kontrol af forskellige eksisterende tilnærmelsesformler og udarbejdelse af nye til bestemmelse af skibes tonnage og stabilitet".

1968   **Aage, C.:** "Eksperimentel og beregningsmæssig bestemmelse af vindkræfter på skibe".

1972   **Prytz, K.:** "Datamatorienterede studier af planende bådes fremdrivningsforhold".

1977   **Hee, J.M.:** "Store sideportes indflydelse på langskibs styrke".

1977   **Madsen, N.F.:** "Vibrations in Ships".

1978   **Andersen, P.:** "Bølgeinducerede bevægelser og belastninger for skib på lægt vand".

1978   **Römeling, J.U.:** "Buling af afstivede pladepaneler".

1978   **Sørensen, H.H.:** "Sammenkobling af rotations-symmetriske og generelle tre-dimensionale konstruktioner i elementmetode-beregninger".

1980   **Fabian, O.:** "Elastic-Plastic Collapse of Long Tubes under Combined Bending and Pressure Load".

1980   **Petersen, M.J.:** "Ship Collisions".

1981   **Gong, J.:** "A Rational Approach to Automatic Design of Ship Sections".

1982   **Nielsen, K.:** "Bølgeenergimaskiner".

1984   **Rishøj Nielsen, N.J.:** "Structural Optimization of Ship Structures".

1984   **Liebst, J.:** "Torsion of Container Ships".

1985   **Gjersøe-Fog, N.:** "Mathematical Definition of Ship Hull Surfaces using B-splines".

1985   **Jensen, P.S.:** "Stationære skibsbølger".

1986   **Nedergaard, H.:** "Collapse of Offshore Platforms".

1986   **Junqui, Y.:** "3-D Analysis of Pipelines during Laying".

1987   **Holt-Madsen, A.:** "A Quadratic Theory for the Fatigue Life Estimation of Offshore Structures".

1989   **Vogt Andersen, S.:** "Numerical Treatment of the Design-Analysis Problem of Ship Propellers using Vortex Latttice Methods".

1989   **Rasmussen, J.:** "Structural Design of Sandwich Structures".

1990   **Baatrup, J.:** "Structural Analysis of Marine Structures."

1990   **Wedel-Heinen, J.:** "Vibration Analysis of Imperfect Elements in Marine Structures".

1991   **Almlund, J.** "Life Cycle Model for Offshore Installations for Use in Prospect Evaluation".

1991   **Back-Pedersen, A.:** "Analysis of Slender Marine Structures"**.**

1992   **Bendiksen, E.:** "Hull Girder Collapse".

1992   **Buus Petersen, J.:** "Non-Linear Strip Theories for Ship Response in Waves".

1992   **Schalck, S.:** "Ship Design Using B-spline Patches".

1993   **Kierkegaard, H.:** "Ship Collisions with Icebergs".

1994   **Pedersen, B.:** "A Free-Surface Analysis of a Two-Dimensional Moving Surface-Piercing Body".

1994   **Friis Hansen, P.:** "Reliability Analysis of a Midship Section".

1994   **Michelsen, J.:** "A Free-Form Geometric Modelling Approach with Ship Design Applications".

1995   **Melchior Hansen, A.: "**Reliability Methods for the Longitudinal Strength of Ships".

1995   **Branner, K.: "**Capacity and Lifetime of Foam Core Sandwich Structures".

1995   **Schack, C.:** "Skrogudvikling af hurtiggående færger med henblik på sødygtighed og lav modstand".

1997   **Cerup Simonsen, B.:** "Mechanics of Ship Grounding".

1997   **Riber, H.J.:** "Response Analysis of Dynamically Loaded Composite Panels".

1998   **Andersen, M. Rye:** "Fatigue Crack Initiation and Growth in Ship Structures".

1998- **Olesen, N. Anker:** "Turbulent Flow (Not printed yet)

1999- **Nielsen, L.P.:** "Structural Capacity of the Hull Girder"